

ALMA MATER STUDIORUM  
UNIVERSITA' DI BOLOGNA

SCHOOL OF ENGINEERING AND ARCHITECTURE  
Forlì Campus

Second Cycle Degree in  
INGEGNERIA AEROSPAZIALE/ AEROSPACE ENGINEERING  
Class LM-20

*THESIS*

*in Aerospace Structures*

**Analysis of aircraft load spectrum by means of  
flight simulator**

CANDIDATE

*Dario Donati*

SUPERVISOR

*Enrico Troiani*

Academic Year 2014/2015

Session II

# Dedication

---

*To my Father and Mother to whom  
I'll be forever indebted.*

# Table of Contents

---

1	INTRODUCTION .....	10
	What is fatigue? .....	10
	Fatigue process .....	11
	Main purposes of this work .....	13
2	EVOLUTION OF AIRCRAFT FATIGUE DESIGN .....	16
	Safe-life philosophy.....	16
	Fail-Safe philosophy .....	20
	Damage Tolerance philosophy.....	22
	Aircraft design philosophy .....	26
	Input for Damage Tolerance Analysis .....	28
3	FRACTURE MECHANISM .....	30
	Historical Overview .....	30
	The use of fracture mechanism and its main objectives .....	33
	Basic Fracture mechanism concepts.....	40
	Crack growth model for variable amplitude load .....	69
4	LOAD SPECTRA.....	81
	Processing load spectrum .....	83
	Stress history generation .....	97
	Load Spectrum generation.....	101
	The born of our idea, first concepts.....	105
5	FLIGHT DYNAMIC MODEL .....	109
	Basic Flight Dynamic concepts .....	110
	DIGITAL DATCOM.....	125

Navigation and Control system.....	129
6 NUMERICAL METHODOLOGY FOR DAMAGE TOLERANCE DESIGN ANALYSIS .....	154
Objective of the developed methodology .....	154
Main assumptions and inputs determination for crack growth analysis .....	155
Stress history generation .....	159
Process of load spectrum generation .....	177
Crack growth analysis algorithm.....	189
Fracture control .....	204
Summary of the developed methodology .....	217
7 COMMENTS AND FUTURE WORK .....	219
Principal sources of errors .....	219
Future Work.....	222
Comments on achieved results.....	237

# Table of Figures

---

Figure 1: Typical S-N curve.....	10
Figure 2:Cyclic slip leads to crack nucleation.....	12
Figure 3: Fatigue life periods.....	13
Figure 4: Parameters for design against fatigue .....	16
Figure 5: Design on the edge of failure concept.....	17
Figure 6: Safe-life approach design.....	18
Figure 7:De Hallivand Comet, fuselage explosion .....	19
Figure 8:Example of fail-safe designed structure .....	20
Figure 9:Rear spar top chord failure under fail-safe design approach.....	22
Figure 10:Potential of infinite life of a structure designed under Damage tolerance approach .....	23
Figure 11: Damage tolerance inspection periods .....	24
Figure 12: Typical damage tolerance diagram: crack growth and residual strength diagram .....	24
Figure 13:Safe-life VS Damage tolerance design approach .....	25
Figure 14: Damage tolerance inputs and outputs .....	26
Figure 15: Aircraft design philosophy .....	27
Figure 16: Crack growth curve of a multiple path structure.....	27
Figure 17: Minimum detectable and critical crack length .....	28
Figure 18: Elliptical hole in a flat plate.....	31
Figure 19: Example of Residual strength diagram with Feddersen interpolation .....	36
Figure 20: Maximum permissible crack length on residual strength diagram .....	36
Figure 21: Typical crack growth curve with design life H .....	37
Figure 22: Fracture mechanism concepts for Damage Tolerance analysis .....	39
Figure 23: Crack opening modes.....	40
Figure 24: Stress concentration factor concept.....	42
Figure 25: Stress concentration factor for different geometry notches .....	42
Figure 26: Infinite element at the crack tip .....	43
Figure 27: CTS specimen typically used for fracture toughness experiment test .....	48
Figure 28: Geometry factor curve.....	48
Figure 29: Fracture collapse VS plastic collapse .....	51
Figure 30: Feddersen interpolation .....	53

Figure 31: Cyclic stress intensity factor.....	54
Figure 32: Fatigue crack growth regions.....	55
Figure 33: Crack growth prediction based on similarity principle .....	59
Figure 34: Elber's experiment results about crack closure phenomenon .....	62
Figure 35: Effective stress range .....	63
Figure 36: Crack tip opening .....	65
Figure 37: Crack growth retardation phenomenon .....	66
Figure 38: Thickness effect on retardation phenomena .....	66
Figure 39: Material Yield strength effect on retardation phenomena .....	67
Figure 40: Simple VA load sequence .....	67
Figure 41: Crack growth retardation due to overload .....	68
Figure 42: Yield zone model concept.....	72
Figure 43: Humps formation on crack surface due to overloads .....	76
Figure 44: Load sequence considered in PERFFAS model .....	78
Figure 45: Dugdale model .....	80
Figure 46: Equivalent schematization to Dugdale model .....	80
Figure 47: Rule of load spectrum in fatigue analysis procedure .....	81
Figure 48: Typical wing load spectrum per flight.....	82
Figure 49: Regular and symmetrical load history .....	84
Figure 50: Regular not-symmetric load history .....	85
Figure 51: Irregular load history .....	86
Figure 52: Level cross counting method .....	86
Figure 53: Typical exceedance diagram .....	87
Figure 54: Number of peaks per interval .....	87
Figure 55: Exceedance diagram for a non-symmetric load history .....	88
Figure 56: Difference between flat and steep load spectrum .....	89
Figure 57: 1D range counting method procedure .....	91
Figure 58: Typical 2D range counting matrix .....	92
Figure 59: Simple load sequence .....	93
Figure 60: Effect of intermedia small range.....	93
Figure 61: Cyclic plasticity loop.....	94
Figure 62: Up range Rainflow decomposition .....	95

Figure 63: Down range Rainflow decomposition.....	95
Figure 64: Basic idea behind the Endo Rainflow algorithm .....	96
Figure 65: Endo algorithm concept.....	96
Figure 66: Typical Semi-Random load sequence .....	98
Figure 67: Semi random Stress History generation .....	100
Figure 68: Accuracy variation with different number of load levels .....	101
Figure 69: FALSTAFF standardized loading sequence.....	103
Figure 70: TWIST standardized load sequence .....	104
Figure 71: Boeing C-17 Globemaster III .....	107
Figure 72: Euler and Aerodynamic angles .....	112
Figure 73: 3D Digital Datcom output .....	128
Figure 74: Typical outputs of Digital Datcom software .....	129
Figure 75: Root locus coming from design procedure used .....	139
Figure 76: General overview of the 6DOF flight dynamic model in Simulink environment.....	142
Figure 77: Non-linear equation of motion subsystem.....	143
Figure 78: ISA atmospheric model Simulink block.....	145
Figure 79: Gravity model Simulink block .....	146
Figure 80: Pitot tube representation for airspeed measurements .....	146
Figure 81: Barometric altimeter simulation for altitude measurements .....	147
Figure 82: Speed Variation.....	149
Figure 83: Altitude variation .....	149
Figure 84: Pitch angle comparison.....	149
Figure 85: Bank angle comparison.....	150
Figure 86: 2D trajectory tracked .....	150
Figure 87: 3D trajectory tracked .....	150
Figure 88: Automatic 2D trajectory tracked with RNP constrinments .....	151
Figure 89: 2D Trajectory tracked .....	151
Figure 90: 3D Trajectory tracked with RNP constrains .....	151
Figure 91: Cross track errors .....	152
Figure 92: Along track errors .....	152
Figure 93: Altitude error .....	152
Figure 94: Aircraft 1DOF force schematization.....	155

Figure 95: Schematic wing representation .....	156
Figure 96: Simple wing schematization .....	157
Figure 97: Inertial force time history .....	158
Figure 98: Lift force spectrum.....	159
Figure 99: Volume and contact forces on a generic body .....	160
Figure 100: Body interactions .....	163
Figure 101: Infinitesimal 3D material portion of tetrahedral shape .....	164
Figure 102: 2D infinitesimal material portion of tetraedic shape .....	165
Figure 103: Beam loads characteristic distributions.....	172
Figure 104: Double T section dimensions .....	174
Figure 105: Generated stress history.....	175
Figure 106: Stress history generated divided in levels .....	178
Figure 107: Exceedance diagram of the obtained stress history.....	180
Figure 108: Histogram representing number of peaks per interval .....	180
Figure 109: Summary table of the processed load spectrum.....	182
Figure 110: 2D Rainflow counting matrix .....	185
Figure 111: Testing constant amplitude load sequence .....	186
Figure 112: Testing damping load sequence .....	186
Figure 113: 2D Rainflow 2D counting matrix for CA testing loading sequence.....	187
Figure 114: Rainflow 2D counting matrix for damping testing load sequence .....	187
Figure 115: Critical locations for crack development .....	194
Figure 116: Residual strength diagram with Feddersen interpolation.....	195
Figure 117: Crack growth results from non-interaction model.....	199
Figure 118: Crack growth results from Yield zone model.....	201
Figure 119: Crack growth results from crack closure model .....	203
Figure 120: Time period H to reach critical crack length .....	205
Figure 121: Probability of detection curve .....	206
Figure 122: Different fracture control procedure.....	208
Figure 123: Fracture control for different crack growth process .....	209
Figure 124: Fracture control inspection interval prescribed .....	213
Figure 125: Different fracture control plan .....	214
Figure 126: Cost of fracture control.....	215



Figure 127: More detailed Inertial force and Lift distribution .....	223
Figure 128: Load characteristics related with elliptical lift distribution .....	225
Figure 129: Load characteristics related with triangular inertial force distribution .....	225
Figure 130: Part through crack and through crack .....	226
Figure 131: Semi-elliptical initial flaw extension .....	227
Figure 132: Stress intensity factor variation on the crack front of a semi-elliptical crack .....	229
Figure 133: Part through crack shape variation during crack extension .....	230
Figure 134: Different crack growth prediction model .....	233

# 1 INTRODUCTION

## What is fatigue?

Fatigue failures in metallic structures are a well-known phenomenon. The failures were already observed in 19<sup>th</sup> century, and the first investigation on fatigue were carried out in that time by August Wohler. He recognized that, a single load application, far from the static strength of the structure, did not do any damage to the structure. However, if the same load was repeated many times, it could induce a complete failure. This observation conduced him to develop his famous S-N curve where the maximum applicable repeated stress as a function of the number of times that it can be applied before failure is represented.

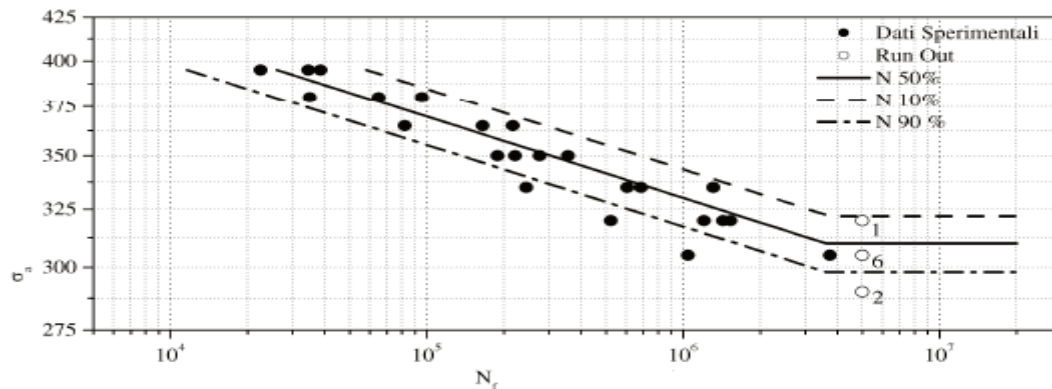


Figure 1: Typical S-N curve

In the 19<sup>th</sup> fatigue was thought to be a mysterious phenomenon in the materials because fatigue damage could not be seen. Failures apparently occurred without any previous warning. In the 20<sup>th</sup> was learned that repeated load applications can start a fatigue mechanism in the material leading to nucleation of a microcrack, crack growth and ultimately to complete, failure of the structure. Understanding of the fatigue mechanism is essential for considering various technical conditions which affect fatigue life and fatigue crack growth. In fact, fatigue prediction methods can only be

evaluated if fatigue is understood as a crack initiation process followed by a crack growth period. For this reason, fatigue life is generally split in two different periods: *crack initiation period* and *crack growth period*.

## Fatigue process

The initiation period is supposed to include some microcracks growth but the fatigue cracks are still too small to be visible by eyes. In the second period, the crack is growing until complete failure.

It is of significantly importance to split the fatigue life of a structural component in these two different periods and treat them separately. In fact, several practical conditions have a large influence on crack initiation period but only limited or, no influence at all, on crack growth period. Moreover, fatigue prediction methods are also different for the two periods. The stress concentration factor  $K_t$  (Chapter 3) is the important parameter for predictions on crack initiation. On the other hand, stress intensity factor  $K$  (chapter 3) is the most important parameter to predict crack growth.

Nucleation of microcracks generally occurs very early in the fatigue life. It takes place almost immediately in the fatigue. However, fatigue failure does not occur if the applied loads are below the so called *fatigue limit* whose value is a function of the selected material and the applied mean stress. In spite of early crack nucleation, microcrack remains invisible for a considerable part of the total fatigue life. After a microcrack has been nucleated, crack growth can still be a slow and erratic process, due to the effects of the micro structure such as grain boundary. Deeper details about microscopic effects are out of the purpose of this work and for this reason they will not be described here in deep. More details about the fatigue process can be found in [1] Anyway, what is important to underline here, is that, once some microcrack growth has occurred away from the nucleation site, a more regular crack growth process is observed. This is the beginning of the second period introduced before. In few words, the crack initiation period and crack growth period can be described as follow:

1. Crack initiation period

Fatigue crack initiation, is a consequence of cyclic slip in slip bands. These cyclic slip requires cyclic shear stress. In particular, on a microscopic level, these shear stresses are not homogeneously

distributed through the material. In some grains at the material surface, especially due to the lower containment that is present because of at one side environment is present, condition for cyclic slip are more favourable. If a slip occurs in a surface grain, a slip step will be created at the material surface. It implies that a rim of new material is exposed to the environment. An important aspect, that probably is the key point of the fatigue process, is that, slip during the increase of the load also implies a strain hardening in the slip band. The consequence is that, upon unloading a larger shear stress, in the reverse direction, will be needed on the same slip band. For this reason reverse slip does not occur on the same slip band but on a parallel one. In fact, if cyclic slip would be a fully reversible process, fatigue phenomenon would not exist.

The following figure intends to summarize the general fatigue process during this first period:

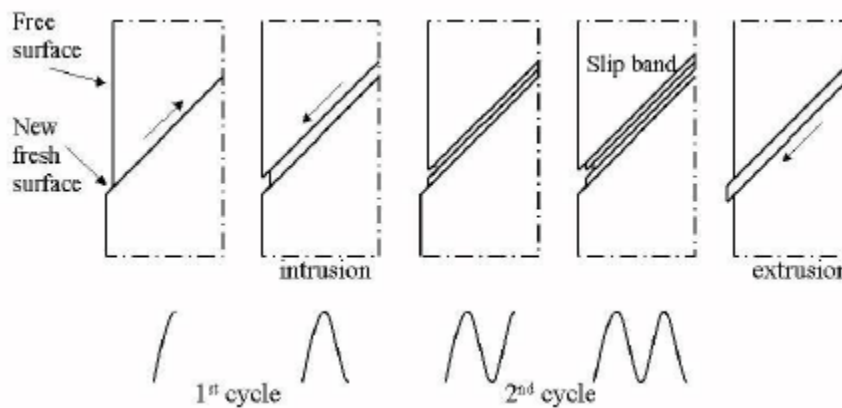


Figure 2: Cyclic slip leads to crack nucleation

As already mentioned, initiation period is a material surface phenomena.

## 2. Crack growth

This second period, related with a crack already propagated inside the material, is no longer a surface phenomenon but it is considered to be a bulk property of the material. In fact as will be introduced in following chapter, crack growth resistance is a characteristic of the typical material considered. How fast the crack will grow inside the material depends on the crack growth resistance of the material itself. It is generally expressed in term of crack growth rate, the crack length increment per cycle.

This quick introduction done up to now on the general fatigue process, can be summarized by the following figure.

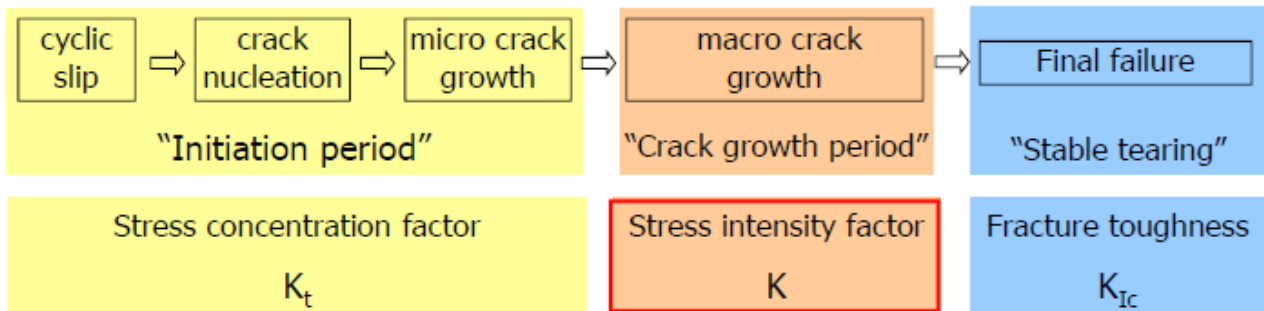


Figure 3: Fatigue life periods

The second period is that one on which our work is focused. As will be discussed later on, crack growth relations are described by the so called fracture mechanism concepts. All these concepts and their importance on modern design approach against fatigue failure will be presented later on in this thesis. Relations on which these concepts are based will not be mathematically derived in deep. In fact, a predicting engineering does not care about it, but it is accepted that it can be done. The real concern is what it means for the solution of practical problems.

### Main purposes of this work

Design offices prefer standardized calculation procedures for predictions on fatigue strength, fatigue life, crack growth and residual strength. Standardized procedures can be useful, but it should be realized that such procedures may imply a considerable risk of unconservative or overconservative results. The main reason is that, such calculation procedures, start from some generalized conditions, which are not really similar to that of the problem. It then requires understanding, experience and engineering judgment to evaluate the significance of the calculated result. In case of some doubts about calculated predictions, it is useful to perform supporting fatigue tests. Some people in fact consider experiment as highly superior than theoretical calculation saying that "Experiment never fails". It could be considered true but however, must be recognized that experiments can provide results applicable to the condition of the experiment only. This was not realized in the past and many accidents happened for this

reason. Also experiments require question about test condition and realistic service simulated condition so that they need understanding, experience and engineering judgment. In other words, all these observations are to say that, whether design against fatigue failure is done by analysis, calculation or experiments, it requires a profound knowledge of the fatigue phenomenon in a structure, material and the large variety of condition that can affect fatigue.

On the basis of this observation, the work developed on this thesis has the purpose to reduce standardized procedures used to design an aircraft against fatigue failure. As will be clear in the following, one important parameter needed to perform analysis about crack growth rate, on which modern design approach are based, is represented by service load spectrum. Service load spectrum for the structure to be used should be as much as possible similar to the real one at which the designed structure will be subjected. Today, in aeronautical design approach, standardized load sequences that will be introduced in Chapter 2 are one of the most common used methods to represent service load spectrum for the airplane to be designed. They are used because provide a quite economical way in term of money and time to proceed. However, these standardized load sequences could be in some case too much general for the specific design to be carried out. For this reason, the central focus of this work is the development of a numerical methodology to design an aircraft, against fatigue failure that, using load spectrum derived from an appositely designed flight simulator allowing to represent closely typical missions, providing the most important results of the modern damage tolerance approach using concepts provided by fracture mechanism. This way to proceed should provide results less general with respect those coming out from damage tolerance design approach using the standardized load sequences mentioned before.

The following of this thesis will be structured as follow: in chapter 2 the main approaches developed in the history of the design against fatigue are presented. Doing this will be pointed out many different accidents that were the starting point to improve current methodology to arrive at the modern damage tolerance approach. The basic concept on which this new design approach is based will be here in this chapter introduced. The basic one is represented by fracture mechanism. The main relation supporting fracture mechanism theory will be introduced and described in Chapter 3, they are fundamental to understand the different steps on which the numerical approach developed is based. In Chapter 4 the importance of load spectrum and how they can be processed will be described in deep. Here a description of the main standardized sequence commonly used today in aeronautical approach will be also described. Chapter 5 deals with the

designed flight dynamic simulator. Within this chapter the principal concepts needed to understand and use this one to produce specific load spectrum will be introduced in deep starting from the dynamic equation needed to represent forces and moments up to the control system used to manually and automatically flight the aircraft along predefined trajectories. Moreover all the principal blocks developed in Matlab/Simulink environment will be described. All the previous concepts will be then used in Chapter 6 to explain step by step the points followed to develop our methodology. The intent of our work is the development of a first methodology providing damage tolerance approach. For this reason in doing this, many assumptions have been introduced to simplify the problem. In this chapter all the assumptions introduced are described and explained so that, once this methodology has been tested and verified they can be removed to produce more real results.

In the final Chapter 7, comments on obtained results and possible future works will be provided.

## 2 EVOLUTION OF AIRCRAFT FATIGUE DESIGN

Over time, subjected to repeated service loading, the residual strength of the structure will decrease. The objective of designing against fatigue is to ensure that the residual strength remains above the design limit load for the useful life of the structure, through design or prescribed inspections.

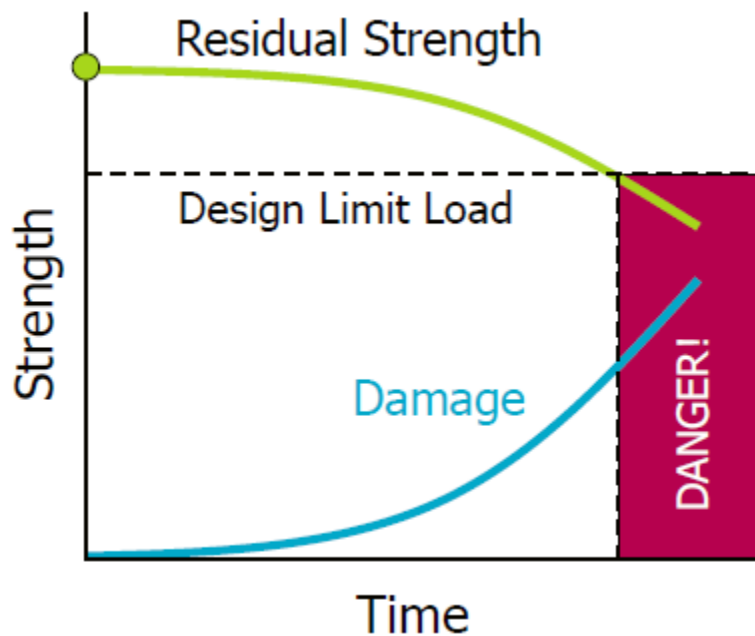


Figure 4: Parameters for design against fatigue

### Safe-life philosophy

In this type of approach, practise is to establish a finite life (safe life) based upon empirical data on the life of the structure until failure. In other words, the safe-life design products are designed to survive a specific “design life” with a chosen reserve. The *infinite-life* design, is a subset of the safe-life methodology where, operational stresses, are set to be below the fatigue limit of the material. This type of approach to design against fatigue failure, is generally employed in critical systems which are either, very difficult to repair or may cause severe damage to life and property. These types of systems are designed to work for years without requirement of any repairs.



Designing under this approach, the basic instrument to be used is the S-N curves generated for the specific element that we are going to design or coming out from tests on coupon elements of the same material but with different geometry. In fact, generally the S-N curves, are provided for a specific material but considering a simple rotating bending coupon (constant amplitude).

Especially in this second case, in which the S-N curve is based on coupons and not on samples of the structure, many different observations are needed before to use this one. Typical important questions that must be carried out designing under this approach are:

- How representative is the load on the coupon with respect to the load acting on the real structure in service?
- How comparable are the surface condition of the coupon and the real structure?
- Which are the environmental conditions used to make the tests on the coupon?

The answers at each of these questions are extremely important because, learning from the past, each of these parameters can strongly affect the fatigue life of a component in service.

For all these reasons (and many others!) a large amount of scatter is typically present in an S-N curve. Using safe-life design approach, scatter and uncertainties must be taken into account by using safety factor which could increase the weight of the structure without any need of this.

Starting from these observations one can understand how, the principal drawback of structural elements designed under safe-life approach, is the fact that they are generally over-built with respect what is needed, which may be uneconomical. Of course, it is especially true in case where, an infinite-life design approach is used. This explains why, this particular design approach, is not practical for aerospace purpose. The following figure (figure 5) explains a quite clear concept about the problem of designing against fatigue in aerospace field.

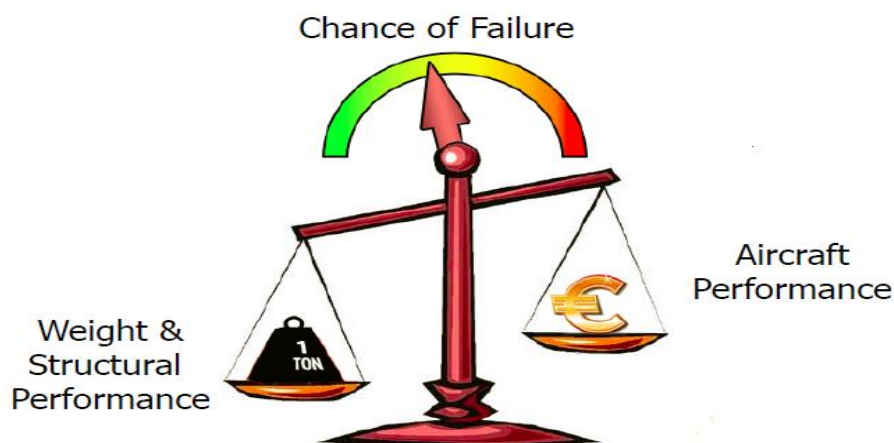
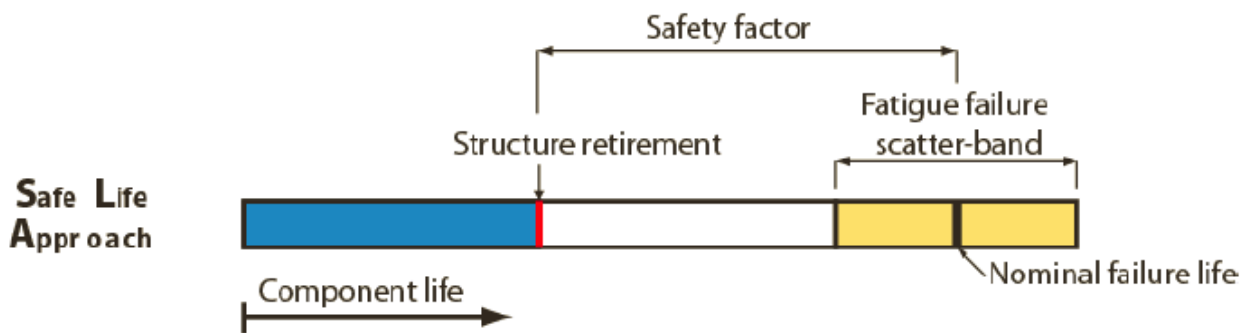


Figure 5: Design on the edge of failure concept

This figure summarizes the needed to design on the edge of failure, typical of the aerospace field. Another drawback, designing under safe-life approach is that, once the design life is reached, the component must be substituted to maintain the designed safety even if it may still have a considerable life ahead. A schematic visualization of the Safe-life design approach is available in the following figure.



**Figure 6: Safe-life approach design**

Safe-life design approach, also called finite-life design approach, has been applied in aerospace industry starting from the early 1950. Regulations, at that time, to design under this approach can be simply summarized as follow:

*“The structure should be designed in so far as practicable, to avoid point of stress concentration where variable stresses above the fatigue design limit are likely to occur in normal service”*

Summarizing, the two main tasks of a designer applying this methodology are:

1. Design so that stress levels are below the endurance limit everywhere in the structure
2. Retire the structure prior to the fatigue life

For this reason the main instrument needed to apply this methodology are:

- Wohler curve (or only fatigue limit in case of infinite-life approach)
- Load spectrum
- Miner rule

Regarding to aerospace industry, the first failure of airplanes designed under this approach happened in 1954 at the *De Hallivand Comet*. Here the inconvenient was related with a problem not detected during fatigue tests because of an unfortunate load sequence creating a retardation

effect (plasticity at the tip of the crack creating the so called crack closure phenomena) ,not known at that time, that was not present in the real structure because of a smaller load sequence. In particular, failure happens for explosive decompression of the fuselage. Fuselage was designed to maintain pressure of 8000ft at 40000ft. Safe-life approach used a design limit of 16000 flights or 10 years. However, as mentioned, the problem here was related with the load sequence used during fatigue test producing a plasticity effect (Chapter 3) beneficial from a fatigue life point of view. The front section of the fuselage was tested to 11psi while overpressure valve in service was set to 8.5psi. Plastic deformation at defects ( n particular failure happened from defects at rivet hole) reduced stress raiser, resulting in 18000 cycles fatigue life. This problem was not known before.

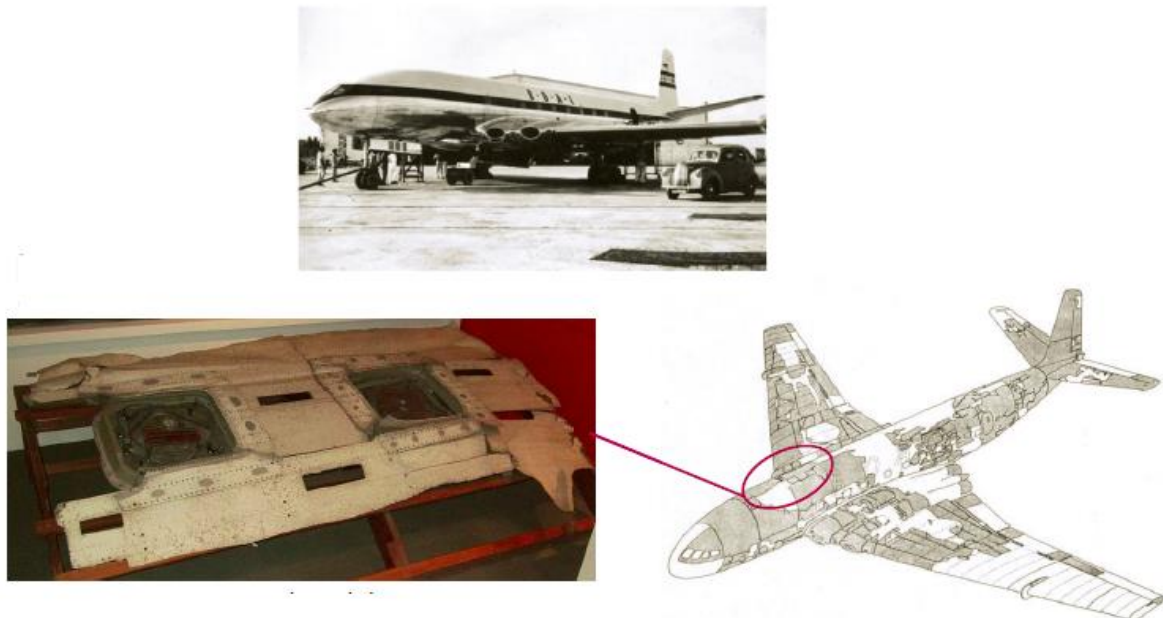


Figure 7:De Hallivand Comet, fuselage explosion

Starting from 1959 Safe-life design approach was substitute by a newer approach, the so called *Fail-safe approach*. However, Safe-life approach continues to be an option for particular elements. Especially on helicopters, engines and undercarriages this design approach is still used in combination with fail-safe approach.

## Fail-Safe philosophy

Here, the main concept is to ensure that, redundancies in a structure are present such that obvious partial failure can be sustained. Designing under fail-safe approach means, in other words, design under a multiple stiffening elements concept. In this way, if one element fails, the load is redistributed and structure is still capable to carry loads safely. Anyway, redistribution of loads, once one element fails needs to be calculated in each case/failure. An example of a fail-safe system is reported in figure. It is a good example to understand the importance of recalculating the load distribution in each possible case/failure. In fact, as can be expected, loads redistribution on the system will be different in the case where the steel beam or the bronze beam fails.

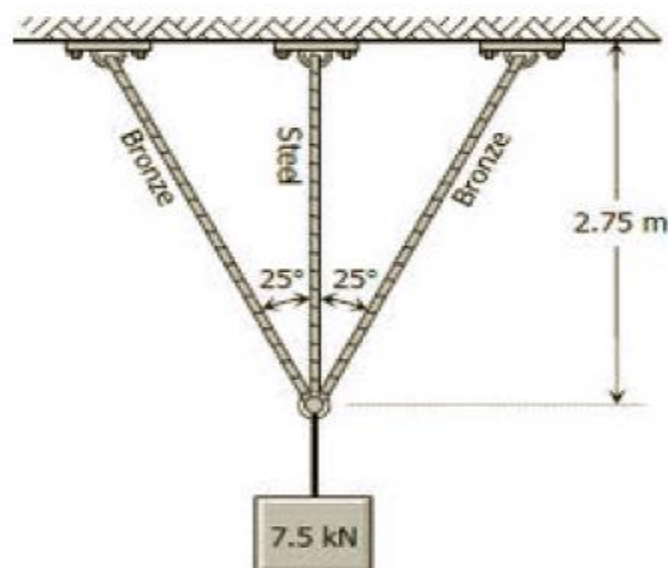


Figure 8: Example of fail-safe designed structure

Significantly, a system's being "fail safe", does not mean that failure is impossible/improbable to occur but rather that, system's design, prevents or mitigate unsafe consequence of the system's failure. That is, if and when a "fail safe" system fails, it is safe or at least no less safe than when it is operating correctly.

A key concept of this approach is that, a failure of a stiffeners, is easily detected and can be easily repaired or substituted. In fact, in fail-safe design approach is assumed that a complete element failure or partial failure would be obvious during a general area inspection and would be corrected within a very short time. The probability of detecting damage during routine inspections before it

could progress to catastrophic limits is very high. In other words, fail-safe design can be firstly seen as a safe-life design. In fact, also in this case, initially the structure is design to achieve a satisfactory life with no significance damage. Then, in addition to the previous approach, structure is also designed to be inspectable in service and able to sustain significant and easily detectable damage before safety is compromised.

In aerospace industry, fail-safe approach has been applied starting from 1959. What is important to observe at this point is that, Paris relation (basic relation used today to design against fatigue as will be described in the following of this thesis) has been developed in 1960. It is an important observation because it underlines that, fail-safe design approach is not based on crack growth propagation. In fact, the previous mentioned inspections, on which this methodology is based, are not *prescribed inspections* but, on the other hand, they are simple *routine inspections* in which failure has an high probability to be discovered.

Regulation prescribed to design under fail-safe approach can be summarized as follow:

*“It shall be shown by analysis/tests that catastrophic failure or excessive structural deformations are not probable after fatigue failure or obvious partial failure of Principle Structural elements (PSE). After such a failure, the remaining structure shall be capable of withstanding static loads corresponding with certain prescribed flight loading condition”*

Principal Structural Elements (PSE), named in this sentence, are defined as those elements which significantly contribute to carry flight, ground, and pressurization loads and whose failure could result in a catastrophic failure of the airplane.

The first failure of an airplane designed under this approach happened in 1977. It was a Boeing 707 who lost its right horizontal stabilizer due to a fatigue failure of the rear spar top chord after 47600 hours of flight and 16670 landing even if the Design Service Goal (DSG) of the designed airplane, i.e. the flight cycles or flight hours used in the design was 60000 flight hours and 20 years.

The aircraft had been maintained correctly to an approved maintenance program but inspections methods and maintenance programs prescribed by the fail-safe design approach were inadequate to detect partial cracks. Following failure of the rear spar top chord, structure could not sustain loads long enough to enable detection of failure through inspections.

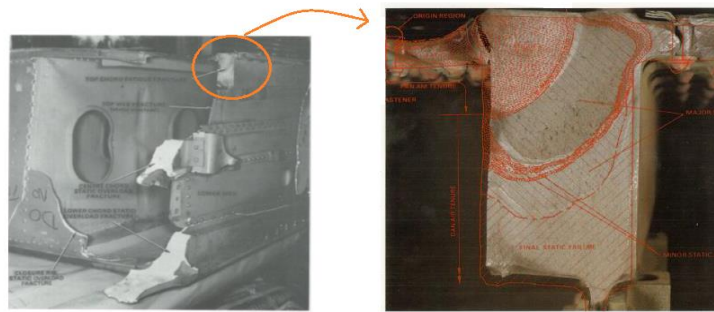


Figure 9:Rear spar top chord failure under fail-safe design approach

After this accident in 1978 there was the introduction of an additional regulation prescribing the increment of inspections for ageing aircraft

## Damage Tolerance philosophy

Starting from 1980 recommendation for damage tolerance for large civil airplane was introduced.

Damage tolerance can be seen as an extension of the concept of fail-safe.

The damage tolerance philosophy can be described as:

*“The ability of structure to sustain anticipated loads in the presence of fatigue, corrosion or accidental damage until such damage is detected, through inspections or malfunctions, and repaired.”*

Hence, the most important innovation, introduced by damage tolerance philosophy is that, during the design phase, damage is considered to occur and this damage will be associated with a reduction of strength over time. For this reason, a detection window, based on damage growth prediction, need to be define. This is the commonly used approach in aerospace engineering to manage the extension of cracks in a structure applying principles of fracture mechanism. This philosophy became the prevailing engineering philosophy after 1980, when a deeper knowledge about fracture mechanism was available. Before this time, redundancy approach, required by a fail-safe design, as described in the previous paragraph, was the prevalent method.

In a general way, the main task, designing under this design philosophy is to show that catastrophic failure, due to fatigue corrosion or accidental damage, will be avoided throughout the

operational life of the structure. In particular, this type of evaluation must be conducted for each part which could contribute to catastrophic failure such as wing, empennage, control surface and their systems, fuselage, landing gear and their primary structural elements (PSE). Each evaluation must include:

- Typical loading spectra, temperature and humidity expected during the operational life of the structure
- Identification of critical points (primary structural elements and detail design point), the failure of which, will cause a catastrophic failure of the aircraft
- Service history of airplanes with similar structures must be used in the evaluation

A structure can be considered damage tolerant if a maintenance program has been implemented. It will result in the detection and repair of accidental damage, corrosion and fatigue cracking before such damage reduces the residual strength of the structure below an acceptable limit.

Damage tolerance philosophy, relies on three important capabilities that are the basic concepts of the fracture mechanism theory:

- Residual strength prediction
- Damage growth prediction
- Damage detection limits

The basic idea behind this philosophy is that, when damage has been detected, it can be repaired and then, a new damage tolerance analysis must be performed to prescribe a new inspection window. Hence, inspections must be established as necessary to prevent catastrophic failure. Starting from this basic idea, this approach has the potential for an infinite life of the structure as shown in figure 10.

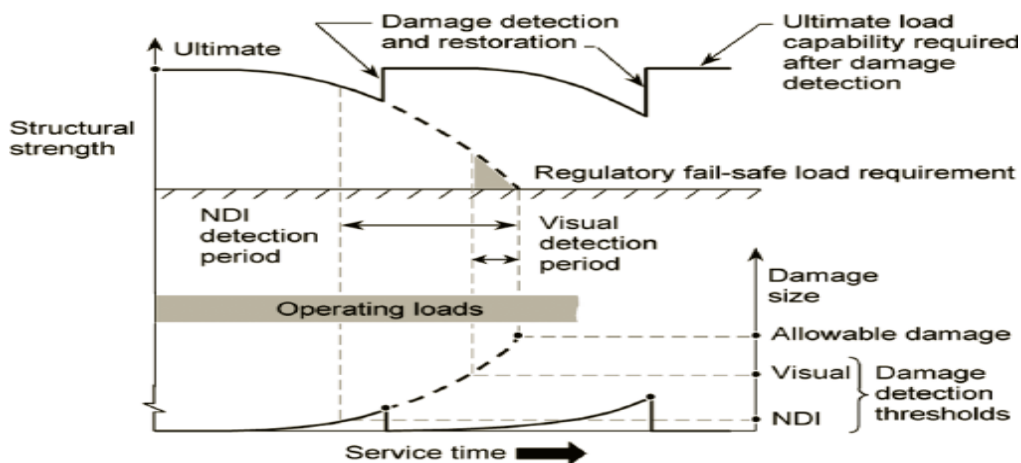


Figure 10: Potential of infinite life of a structure designed under Damage tolerance approach

From performed damage tolerance analysis, designer can be able to determine an inspection threshold that can be considered as a *safe-life for inspection*, i.e. no inspections should be done during this period because crack is not visible (initiation period) . However, a detection interval must be prescribed before detection limit is reached. Within these inspection intervals, inspections must be performed to monitor crack growth. The following figures (11,12) summarize all the concepts introduced up to know.

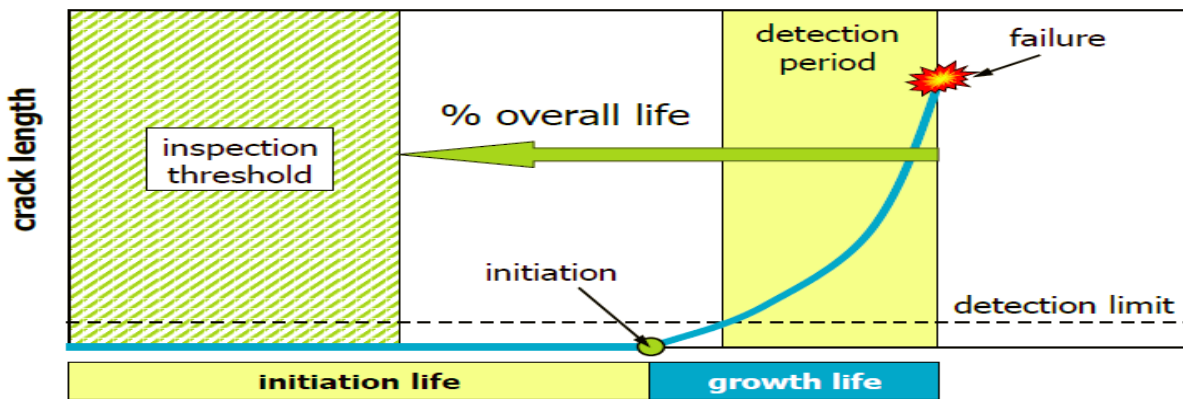


Figure 11: Damage tolerance inspection periods

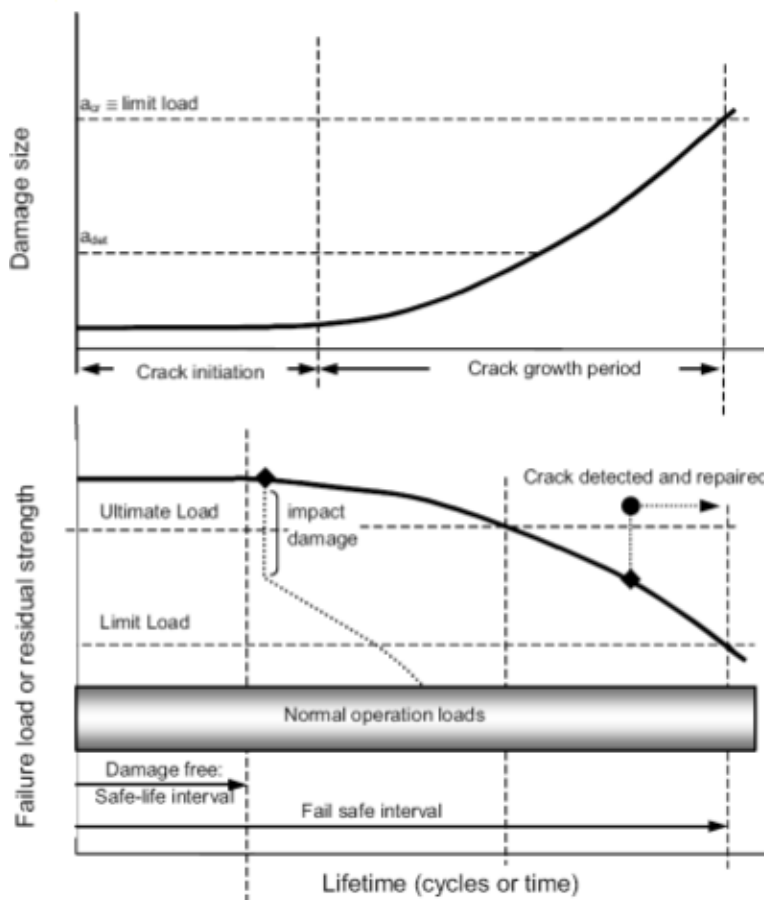


Figure 12: Typical damage tolerance diagram: crack growth and residual strength diagram



Crack growth curve represented in figures above has been determined using the fracture mechanism analysis concepts which, as will be shown in the next chapter, are based on some material constants and a given service load spectrum coming out from structures already in service, working in a similar operational environment.

The following figure 13 makes more clear the improvement introduced by damage tolerance philosophy with respect to the first explained safe-life approach.

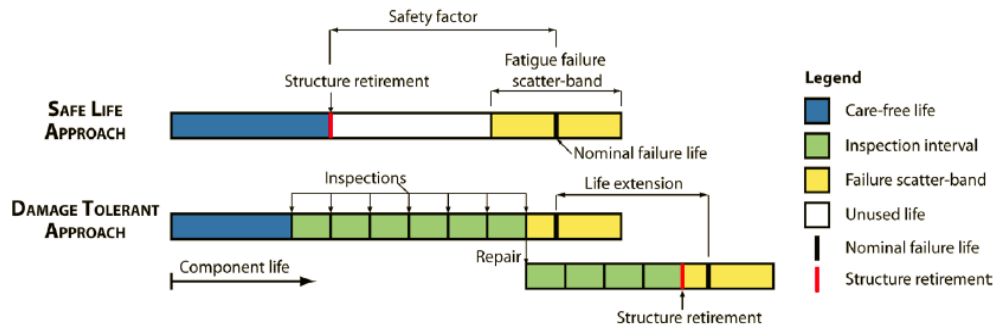


Figure 13: Safe-life VS Damage tolerance design approach

Again this figure shows how, during the initial life period of the component, no inspections are needed. Here, can also be seen clearer the fact that, in damage tolerance analysis, not only one inspection should be performed but many inspection intervals must be prescribed so that, when the crack is detected, structure is repaired with the positive consequence of increasing its operation life ahead respect to its initial nominal life. As will be described in Chapter 6, inspection interval are prescribed using fracture control methods based on probability of detection. All the observations did up to now, make clear how this type of approach is beneficial from an economical point of view.

With regard to the difference between Damage Tolerance philosophy and fail-safe approach, it can be explained in term of inspections required. In fact, while fail-safe as described before does not prescribe additional inspections to those of routine, confiding on a failure easily visible. On the other hand, Damage tolerance does not require consideration of complete failure or obvious partial element failure but it requires an inspection program tailored to the crack propagation characteristics of the particular part when subjected to the loading spectrum expected in service. This inspection program must be provided to ensure that cracks are detected before they reach a critical length (figure 12). Damage Tolerance places a much higher emphasis on inspections

needed to detect cracks before they progress to unsafe limits. Anyway as we will see in the following paragraph, fail-safe features may be included in structure designed to satisfy damage tolerance requirements.

The following figure, schematically represents all the input needed and the output achievable with a computer software performing damage tolerance analysis.

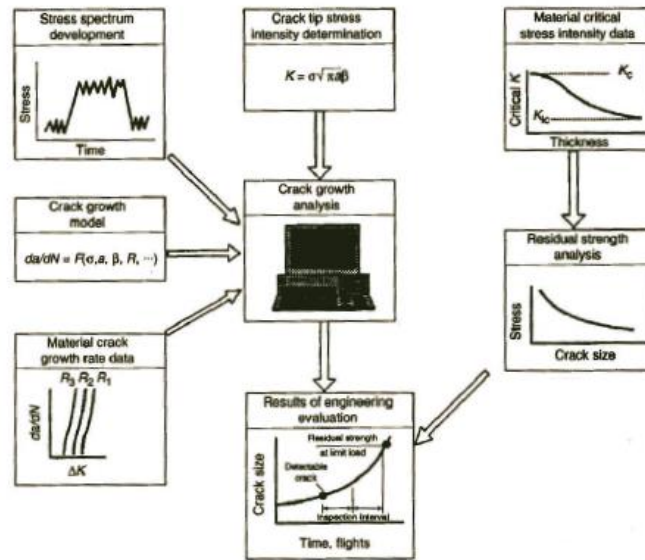


Figure 14: Damage tolerance inputs and outputs

This figure will result extremely useful in the following. In fact, it can be considered as a good visual summary of inputs and outputs of the methodology for the computer software damage tolerance analysis developed in our work. Details of how these inputs and outputs are obtained and their meaning is described in the next chapters of this thesis

### Aircraft design philosophy

Today, designing an aircraft, all three methodologies described before are used. In particular, fail-safe approach is now used as a combination of pure fail-safe and damage tolerance approach. It means that even if the structure is designed with a multiple path load approach, damage growth and inspections are still considered.

The following figure 15 shows a flow-chart representing the idea behind the use of all these methodologies to design an airplane.

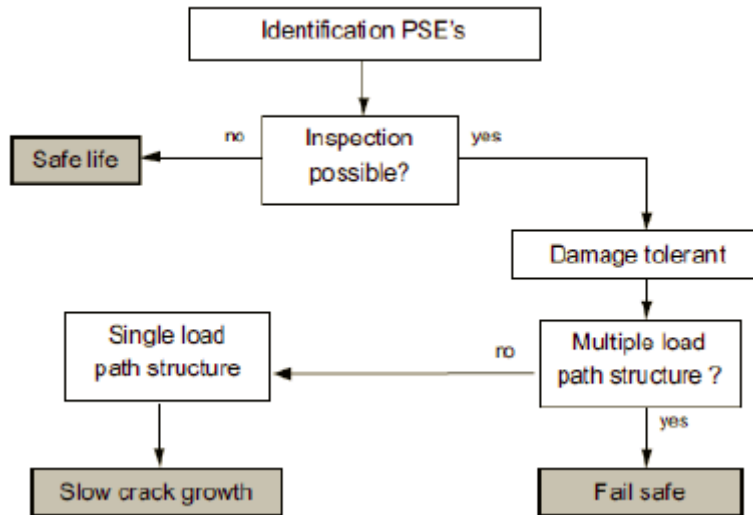


Figure 15: Aircraft design philosophy

As can be expected from the introduction done up to now about each of these methodologies, the key question to distinguish when a safe-life or a fail-safe/damage-tolerance approach should be used is: Are inspections possible? Of course, cases in which inspections are not possible a safe-life approach must be used in spite of all its drawbacks introduced before. On the other hand, if inspections are possible, fail-safe/damage-tolerance approach must be used. Under this condition, difference between multiple load path structure and single load path structure must be considered. In the first case the influence of the failure of each path on the crack growth on the others must be considered, in particular a reduction of the crack growth life (CGL) or, in the same way, an increase in the crack growth rate must be accounted for. A typical behaviour of the variation of the crack growth in a multiple load path structure when a path fails is represented in figure 16.

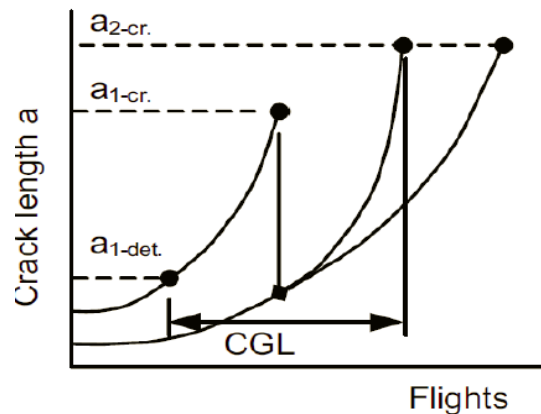
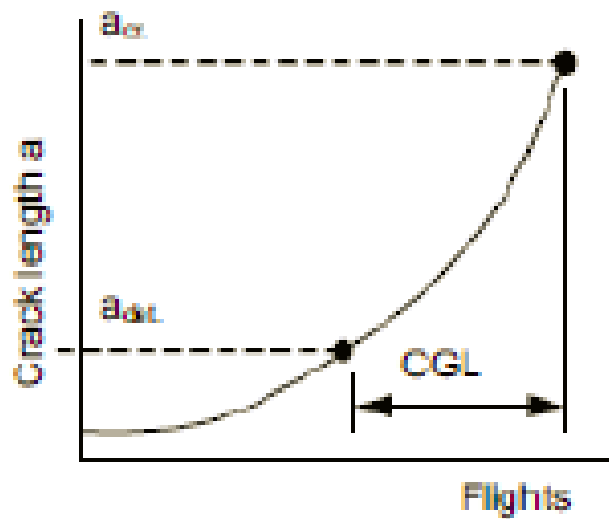


Figure 16: Crack growth curve of a multiple path structure

On the other hand, in case where a single path load structures is selected as design choice, a threshold should be based on crack growth analysis assuming maximum manufacturing defect size (Figure 17). Generally this type of parameter is provided in term of minimum allowable residual strength. Then, starting from this value, using fracture mechanism concepts and other consideration related with plastic collapse the value of the critical crack length can be obtained. The way to proceed to get this value will be deeply described in the following of this thesis.



**Figure 17: Minimum detectable and critical crack length**

**Input for Damage Tolerance Analysis**

Before to introduce a list of the main inputs needed for damage tolerance analysis, which will be analysed in deeper detail in the following paragraphs, we need firstly to summarize which are the main assumptions and capabilities required for a damage tolerance analysis. They are a logic consequence of the basic concepts on which this type of philosophy is based.

A first important assumption is that, a significant proportion of the fatigue life up to failure is occupied by crack growth (remembering that as pointed out in Chapter 1, fatigue life of a structure can be divided in two periods: initialization period and crack growth period).

A second important consideration is that, we need to be sure about damage detection and monitoring techniques which must have accuracy compatible with the rates of damage growth and damage influence on residual strength. It is a key point to be sure that detection can be

performed as it is prescribed. On the other hand, these detection techniques are based on the assumption that, predictive capability of damage growth rates and damage extent, are accurate enough to accurately calculate residual strength of damaged structure. Moreover, on the basis of production process, damage tolerance analysis relies on the ability to fabricate structures resistant to damage initiation and damage growth.

The list of inputs mentioned before, needed for the damage tolerance analysis, can be summarized with the following points:

- Service load spectrum for anticipated service environment. This spectrum must be typical of anticipated used. Today TWIST or MINITWIST (for transport aircraft) and FALSTAFF or short FALSTAFF (for military aircraft) are the standard spectrum used to initiate the damage tolerance analysis of the new structure to be designed. The effort of this thesis is to improve this point; generating more informative load spectra for the structure currently designed using an appositely developed flight simulator.
- Stress analysis measured relating with stresses to stresses at the crack site. Important will be consider here effect load sequence on crack growth (Chapter 3).
- Stress intensity factor from start defect size to failure
- Material crack growth rate data for selected material coming from handbook
- Predictive models for crack growth process.

Following of this thesis treats each of these points in deeper detail. In addition, in Chapter 6, they will be used to develop a methodology that, starting from data coming out from the already mentioned flight simulator (whose design is described in Chapter 5 ), used to get typical load spectrum, is able to perform a damage tolerance analysis.

## 3 FRACTURE MECHANISM

### Historical Overview

Several structure failures can be associated with the fracture of one or more of the components making the structure. When such events occur, they are mostly unexpected, sudden and unfortunate, and it is natural to focus attention on minimizing the undesired consequences when designing and analysing modern-day structures. The study of crack behaviour, prevention and analysis of fracture of materials is known as *fracture mechanism*.

In other word fracture mechanism can be also defined as:

*“The study of mechanical behaviour of cracked material subjected to an applied load”*

In every discipline, including fracture mechanism, it is of critical importance to examine the historical antecedents. This is the reason why in the previous chapter, describing the history of the design approaches against fatigue, we did some examples of accidents occurred in aerospace field in the past years. People who tend to ignore the past are more prone to repeat mistake. Development in fracture mechanism concepts is quite a new idea.

By the end of the 19<sup>th</sup> century, the influence of crack on structure strength was widely appreciated but its nature and influence was still unknown. The first study was carried out by an Inglies, a research who observed that, the corner of an elliptical hole in a plate (Figure 18) feels the highest stress and, as the ellipse gets longer and thinner the stresses at the corner become even larger. From his studies we got an estimation of the stress concentration factor at the tip of the corner that can be expressed as:

$$K_t = \frac{\sigma_{peak}}{\sigma_{nom}} = 1 + 2 \frac{a}{b} = 1 + 2 \sqrt{\frac{a}{\rho}} \quad (eq. 1)$$

Where  $a$  and  $b$  are the semi-major and semi-minor axes respectively and  $\rho$  is the root radius at the tip of the ellipse. Deeper details on this relation and its influence in fracture mechanism will be analysed later on in this thesis.

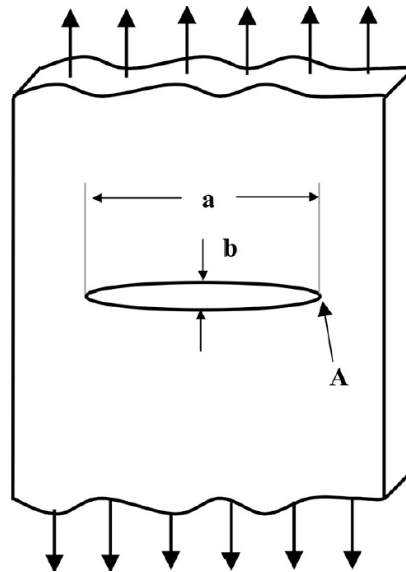


Figure 18: Elliptical hole in a flat plate

Inglis evaluated various hole geometries and he realized that, it is not really the shape of the hole that matters but the length of hole perpendicular to the load and the curvature at the end of the hole.

The basic ideas leading to the start of the modern fracture mechanism can be attributed to a theory of fracture strength of a glass, which was published by A.A Griffith in 1920. Using Inglis' work as foundation, Griffith proposed an energy balanced approach to study the fracture phenomenon in cracked bodies. A great contribution to the ideas about breaking strength of materials emerged when Griffith suggested that the weakening of material by a crack could be treated as an equilibrium problem. He proposed that the reduction in strain energy of a body when the crack propagates could be equated to the increase in surface energy due to the increase in surface area. The Griffith theory assumed that the fracture strength was limited by existence of initial cracks and that brittle materials contain elliptical microcracks, which introduce high stress concentration near their tips. He developed a relationship between crack length ( $a$ ), surface energy connected with traction free crack surface ( $\gamma$ ) and applied stress, which is given by:

$$\sigma^2 = \frac{2\gamma E}{\pi a}$$

Plasticity effects in metals limited the theorem and it was not discovered until Irwin's work in 1948, when a modification was made to Griffith's model to make it applicable to metals. Irwin's first major contribution was to extend the Griffith approach to metals including their energy dissipated by local plasticity flow.

It is an interesting fact and perhaps relevant to point out that scientific curiosity towards fracture mechanism became significantly important engineering discipline after the unfortunate failures of Liberty ships during World War II. The Liberty ships were built used a new construction method for mass production in which the hull was welded instead of riveted. The Liberty ship program was an astounding success until 1943, when a Liberty ship broke completely in two while sailing in the North Pacific. An investigation into Liberty ship failures pointed out poor toughness of steel and transition from ductile to brittle behaviour at the service temperatures that ship experienced. It was noticed that the fractures initiated at the square hatched corners on the deck where there was a local stress concentration and the sharp corners acted like starter crack. Research into this problem was led by George Rankine Irwin. It was the research during this period that resulted in the development and definition of what we now refer to as Linear-Elastic-fracture-mechanism (LEFM). A major step ahead, occurred in 1950 when Irwin provided the extension of Griffith theory for an arbitrary crack and proposed the criteria for the growth of this crack. The criterion was that the *strain energy release rate* ( $G$ ) must be larger than the critical work ( $G_c$ ), which is required to create a new unit crack area. Irwin also related strain energy release rate to the stress field at the crack tip. In particular Irwin showed that the stress field in the area of the crack tip is completely determined by a quantity  $K$  called the *Stress Intensity Factor*  $K$ . In particular Irwin presented a relation between the energy release rate and the stress intensity factor as:

$$\sigma_{ij} = \frac{K f_{ij}(\theta)}{\sqrt{2\pi r}} \quad (\text{eq. 2})$$

$$K^2 = EG \quad (\text{eq. 3})$$

Other scenarios of failures that were experienced during that period was that of the De Hallivand "Comet" commercial aircraft, already introduced in the previous chapter as a key point to pass from the safe-life design approach to a life-safe design approach against fatigue. The failure of this airplane was at that time analysed using the basic concept available of fracture mechanism. In particular, the equilibrium concept showed that the comparison between the critical energy



release rate and the energy release rate has not been large enough to prevent crack propagation in the failure of the commercial aircraft.

In 1960, a significant contribution to the development of LEFM was put forth when Paris advanced an idea to apply fracture mechanism principles to fatigue crack growth. Although he provides convincing experimental and theoretical arguments for his approach, the initial resistance to his work was intense and he could not find a peer-reviewed technical journal to publish his manuscript. He finally opts to publish his work in a University of Washington periodical entitled "The Trend in Engineering".

The Paris's work was a landmark in the fatigue aspects of fracture mechanism and yields the equation:

$$\frac{da}{dN} = C\Delta K^m \quad (\text{eq. 4})$$

Where C and m are material constant parameters fitting the experimental curve results. This is the basic equation on which modern crack growth model used for damage tolerance analysis are based.

Linear elastic fracture mechanism is not valid when significant plastic deformation precedes failure.

### **The use of fracture mechanism and its main objectives**

Fracture control of structures is the concerted effort by designers, metallurgist, production and maintenance engineers and inspectors to ensure safe operations without catastrophic fracture failures. Of the various structural failure modes (buckling, fracture, excessive plastic deformation) fracture is only one. Very often a fracture occurs due to an unforeseen overload on the undamaged structure. Usually, it is caused by a structural flaw or a crack: due to repeated or sustained "normal " service loads a crack may develop (starting from a flaw or stress concentration) and grow slowly in size, due to the service loading. Cracks and defects impair the strength. Thus, during the continuing development of the considered crack, structural strength decreases until it becomes so low that the service load cannot be carried any more, and fracture

happens. Fracture control is intended to prevent fracture due to defects and cracks at the maximum load experienced during operation service.

If fracture is to be prevented, the strength should not drop below a certain safe value. This means that cracks must be prevented from growing to a size at which the strength would drop below the acceptable limit. In order to determine which size of crack is admissible, one must be able to calculate how the structural strength is affected by cracks especially as a function of their size. For this reason, one must first identify locations where cracks could develop. Analysis then must provide information on crack growth times and on structural strength as a function of crack size. These are the main purposes of this type of analysis called damage tolerance analysis.

As introduced in previous chapter, damage tolerance can be defined as the property of a structure to sustain defects or cracks. Elimination can be affected by repair or replacing of the cracked structure or component. In the design stage, one still has the options to select a more crack resistance material or improve the structural design to ensure that cracks will not become dangerous during the projection economic service life (Safe-life design approach). Alternatively, periodic inspections may be scheduled, so that, crack can be repaired or components replaced when cracks are detected. Either, the time for replacement or the inspections interval and type of inspection, must follow from the crack growth diagram calculated in the damage tolerance analysis.

Inspections can be performed by a number of non-destructive techniques, provided the structure is inspectable and accessible. Fracture control (Chapter 6) is a combination of measures such as described above, including analysis, to prevent fracture due to cracks during operation. It may include all or some of these measures, namely damage tolerance analysis, material selection, design improvement, possibly structural testing and maintenance/inspections/replacement schedules. The extent of the fracture control measures depends upon the critically of the component, upon the economic consequences of the structure being out of service, and last but not least, the consequential damage caused by a potential fracture failure. For example fracture control of a hammer may be as simple as selecting a material with sufficient fracture resistance but, on the other hand, fracture control of an airplane, includes damage tolerance analysis, tests and subsequent inspections and repair/replacement plans. Deeper observations on fracture control procedure will be introduced in Chapter 6.

Damage tolerance analysis and its results, as introduced in the previous chapter, form the basis of the fracture control plans. In fact, inspections, repairs and replacements must be scheduled based

on results coming out from a damage tolerance analysis. Mathematical tools employed in the damage tolerance analysis are *fracture mechanism* concepts. They provide equations used to determine how cracks grow and how crack affect the strength of the structure. These concepts and equations will be introduced in a deeper detail in the following paragraphs.

During the last 25 years fracture mechanism has evolved into a practical engineering tool. It is not perfect but no engineering analysis is. As an example of this imperfection, we can consider the relation used to determine bending stress

$$\sigma = \frac{M}{I} \quad (\text{eq.5})$$

This relation, used also in our methodology, will be derivate in the following of this thesis but for the moment, what is interesting to note is that it is rather in error when used to calculated structural strength, because it ignores plastic deformation. Anyway it has been successfully used in fracture mechanism analysis in past years. In fact, what must be considered rather than the inadequacy of the concepts is the inaccuracies of the inputs, they have a large influence on the obtained results (Chapter 7). A deeper discussion about fracture mechanism will be carried out in the following of this chapter.

Naturally, results of damage tolerance analysis must be used judiciously, but this can be said of any other engineering analysis as well.

The observations introduced up to now, are just an introduction underlining the importance of fracture mechanism concepts, especially in the new design approach based on damage tolerance analysis. In particular, what comes out from all these considerations is that, the establishment of a fracture control plan requires knowledge of the structural strength, particularly as it is affected by cracks and time involved for cracks to grow to a dangerous size. Thus, fracture mechanism, that provides results for damage tolerance analysis, has two objectives:

- Determination of the effects of crack growth on strength (margin against fracture)
- Determination of crack growth as a function of time

Following figure (Figure 20) shows a general way of how the crack length affects the residual strength of the material. As will be well explained later on, this plot has been created considering the so called Feddersen interpolation needed to get physical results. In fact, results must consider

that the strength of the new free-crack structure has a finite (and not infinite!) residual strength (equal to the ultimate strength) and the residual strength, when the crack length is equal to the width of the structure, must be equal to zero.

These observations will be readdressed in detail later on in this thesis.

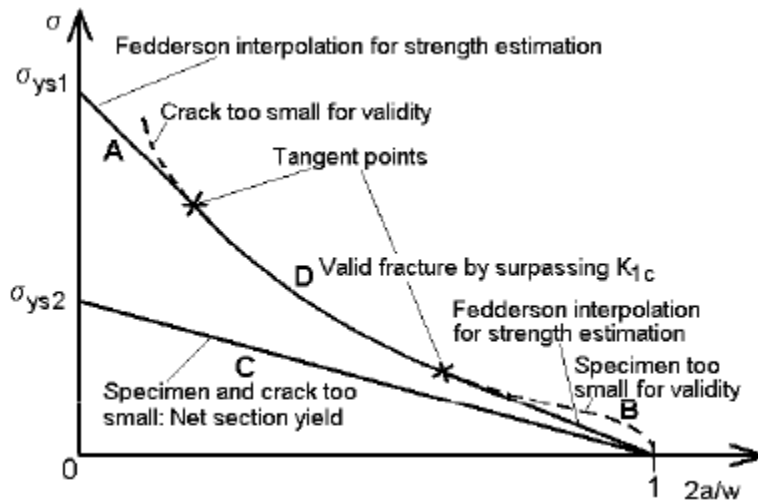


Figure 19: Example of Residual strength diagram with Feddersen interpolation

Due to continual growth, crack becomes longer and residual strength reduces. Probability of fracture will be higher. If nothing is done and the structure remains in service, residual strength at a certain point will become smaller than what is allowable so that fracture will occur. This is what must be prevented: crack should not be allowed from becoming so large that fracture occurs at service loads. Hence the structure or component must be replaced before the crack becomes dangerous, or the crack must be detected and repaired before such time. In other words it means that some decision must be made to set the minimum permissible residual strength, so that, the maximum permissible crack size  $a_p$  can be determined from the residual strength diagram.

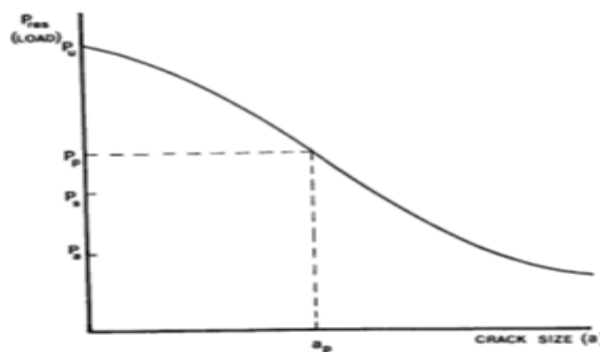


Figure 20: Maximum permissible crack length on residual strength diagram

Assuming that, minimum residual strength is provided, the maximum allowable crack size can be determined from a plot like that one in Figure 21. Even if the value of the minimum allowable residual strength is provided and from here the maximum allowable crack size can be directly determined, generally the calculation of the entire residual strength diagram is preferable. The residual strength diagram will be different not only for different structural components but it also depends on crack locations. It means that different maximum permissible crack size will be expected as well.

The maximum permissible crack size is generally called *critical crack size*. A critical crack is that one would cause fracture in service. Based on this definition, a crack will be critical only in the event that a stress larger than the minimum residual strength occur.

Anyway knowing that the crack may not exceed  $a_p$  is of little help. For this reason, second objective of the fracture mechanism is to provide a crack growth curve representing the behaviour of crack length in time, generally expressed as number of cycles. A general crack growth curve is reported in Figure 21.

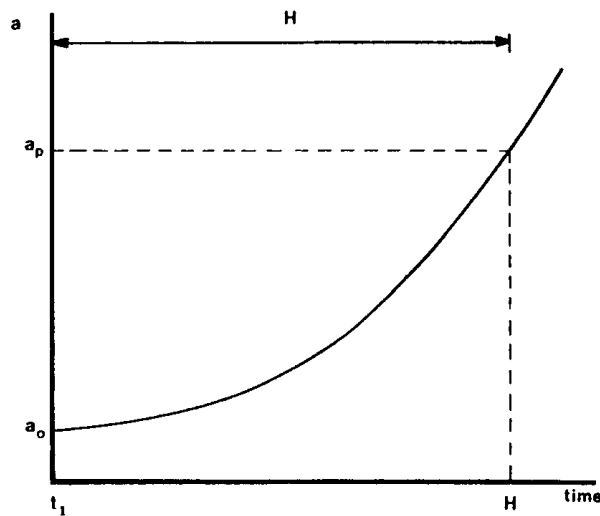


Figure 21: Typical crack growth curve with design life H

Under the action of normal service loading, cracks grow by fatigue, stress corrosion or creep. Starting at some crack size ( $a_0$ ) crack will grow in size during time with a typical behaviour reported in Figure 22. The permissible crack, is also plotted in a graph like that one before (Figure 22).

Still considering Figure 22, if  $a_0$  is for example an assumed initial defect, component or structure must be replaced after a certain time (expressed in number of cycle, hours or number of flight) named  $H$ . Since crack growth is not allowed beyond  $a_p$ , the crack must be detected and repaired or otherwise eliminated before the time  $H$  has expired. Therefore, time between inspections must be less than  $H$ . For example doing an inspection at time  $t_1$  the crack will be missing being this one smaller than the minimum detection limit. So if the next inspection will be programmed  $H$  hours (or cycles or flights) later the crack would be reach the critical length  $a_p$  already which is not permitted. For this reason a general inspection interval could be equal to  $H/2$ .

In any case the value of  $H$  comes out from damage tolerance analysis which also provides the residual strength diagram.

Fracture mechanism, as all engineering mechanism, uses stress rather than loads. Thus the residual strength diagram is generally expressed in term of stress and it represents the stress that the structure can sustain before fracture occurs. Residual strength should not be confused with residual stress that is the stress is rising in a structure while there are no loads applied. Also these types of stresses have a strong influence in fatigue life of the considered component but their meaning is completely different.

Stress can be used as the basis for the analysis if there is a relationship between the applied stress and the process taking place at the crack tip. As the crack tip events are governed by the local stresses at the crack tip, it is required that the local crack tip stress be described as a function of the applied stress.

To get a better idea about all the concepts introduced up to know, regarding the application of the fracture mechanism concepts that will be deeper considered later on, the following flow-chart (Figure 18) can be used to summarize visually the main steps needed to perform this analysis

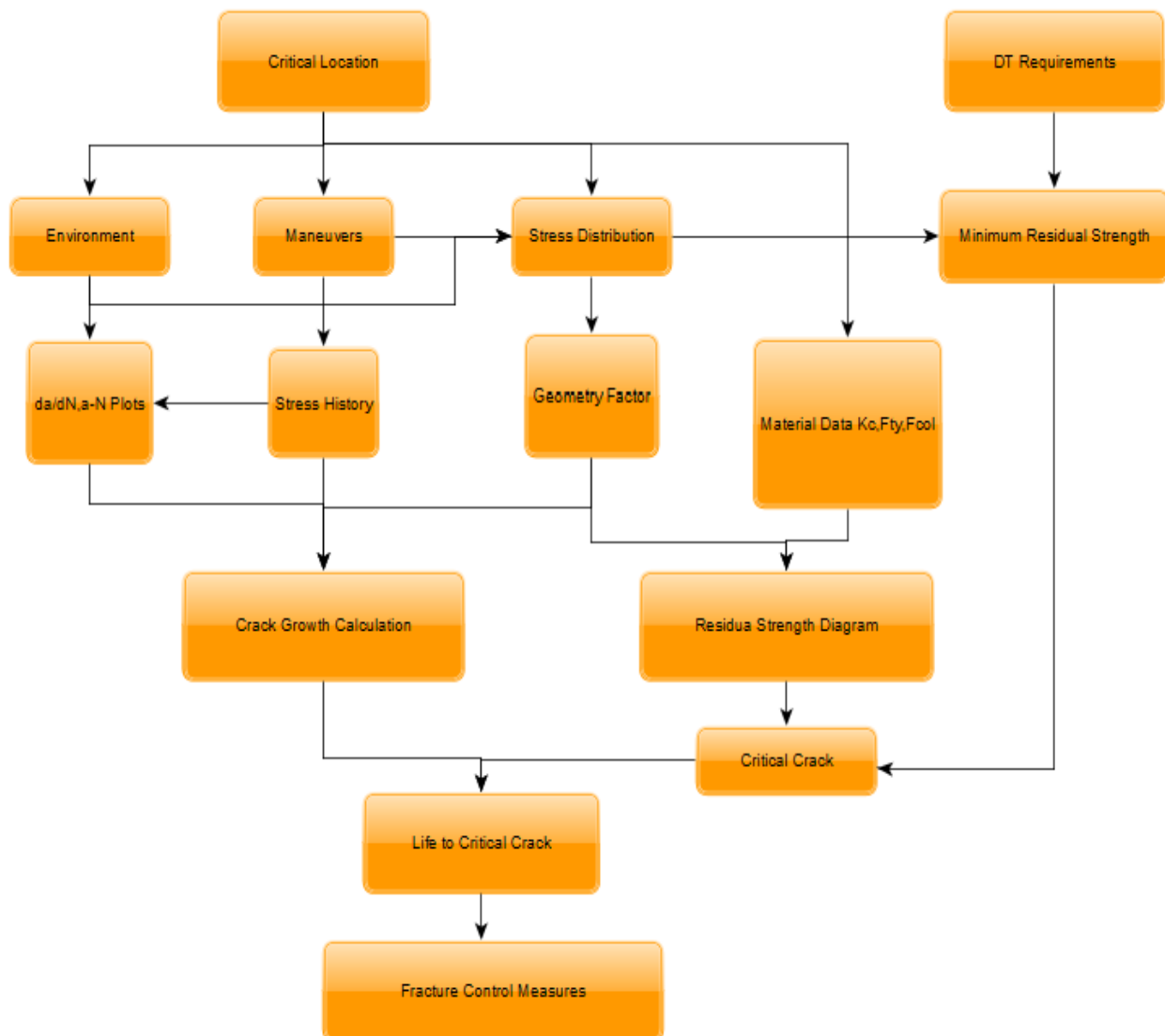


Figure 22: Fracture mechanism concepts for Damage Tolerance analysis

Two of the most important concepts needed to track each of the charts of the previous flow chart are:

- Basic concepts and equations of the fracture mechanism
- Load spectrum

For this reason, before to deal with this flow chart, describing step-by-step the developed methodology to get a numerical damage tolerance analysis starting from load sequence generated using a developed flight simulator, the basic concepts and equations of fracture mechanism and the principal aspects of load spectrum and how they can be obtained to perform analysis must be quickly introduced so that the developed methodology will result more clear. Anyway what is

important to underline at this level of detail is that to derive these relationships one must distinguish between 3 modes of loading. They are shown in the following figure (Figure 24).

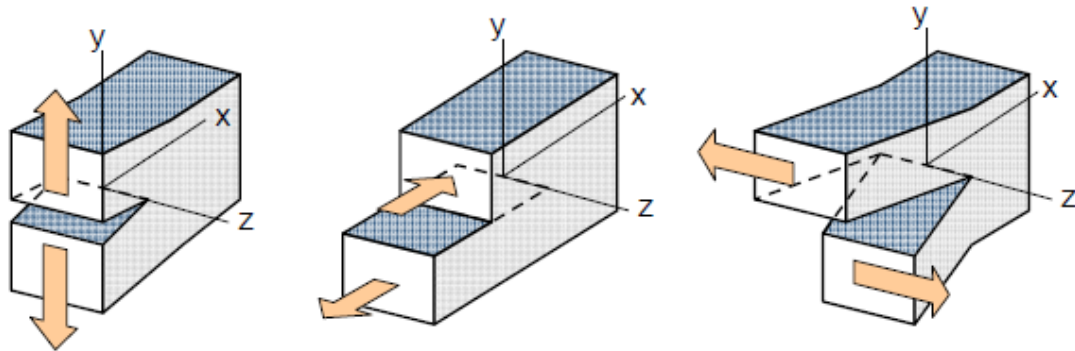


Figure 23: Crack opening modes

These modes of loading (no modes of cracking) are usually simply referred by Roman numerals as I,II,III. In a deeper detail they can be called as:

- Mode I: tension mode
- Mode II: in-plane shear mode
- Mode III: out-plane shear mode.

The crack tip stress equations are very similar for each of the modes and consequently the fracture and crack growth analysis. It is the reason why in the following of this thesis we will refer only to mode I (Tensile mode) being also the most common one. Note that, however, in reality, these modes do not occur individually but they generally occur in combination. This consideration will be reconsidered in Chapter 7. In the following paragraphs a list of the main concepts of fracture mechanism with a short explanation on their importance is reported. For deeper details, not useful for the purpose of our work, information can be found in [2]

## Basic Fracture mechanism concepts

In this chapter we are going to introduce quickly each of the basic concepts of fracture mechanism needed for fracture analysis developed in our work. In fact, using these concepts will be possible to obtain the two important diagram, objects of damage tolerance analysis, as introduced in the previous paragraph:

1. The residual strength diagram
2. Crack growth life



### Stress concentration factor

This parameter is not directly straightforward in damage tolerance analysis and in addition, it is not a real fracture mechanism concept. By the way, its knowledge and so its introduction here, is fundamental to determine location of the critical point from a fatigue point of view. As can be seen from the previous flow-chart, determination of this critical location, represents the starting point for the subsequent analysis. This is the reason why in this chapter, introducing all the main concepts to develop a fracture control strategy this concept has been considered.

Importance of this parameter comes out due to the fact that, in a structure, the presence of a notch like for example a geometrical hole or a geometrical section variation cannot be avoided. They are causing inhomogeneous stress distribution with a stress concentration at the root of the notch itself.

For this reason, a Stress Concentration Factor  $K_t$ , defined as the ratio between the peak stress at the root of the notch and the nominal stress which would be present if a stress concentration did not occur (Figure 24) is needed to determine the maximum stress acting in a critical location.

$$K_t = \frac{\sigma_{peak}}{\sigma_{nom}} \quad (eq. 6)$$

A quite accurate analytical solution for the strip with a hole has been obtained. In particular the exact solution is available for an infinite sheet with an elliptical hole. For this particular case the  $K_t$  value can be obtained using the relation already introduced in a previous paragraph that is here reported for simplicity:

$$K_t = 1 + 2 \frac{a}{b} = 1 + 2 \sqrt{\frac{a}{\rho}} \quad (eq. 7)$$

Looking at this relation some important observations about stress concentration can be done:

- A small notch root radius will give an higher  $K_t$
- Larger is the dimension of the notch in the direction perpendicular to the applied stress and larger is the  $K_t$  value

- Larger is the dimension of the notch in a direction parallel to the applied load and smaller is the  $K_t$  value

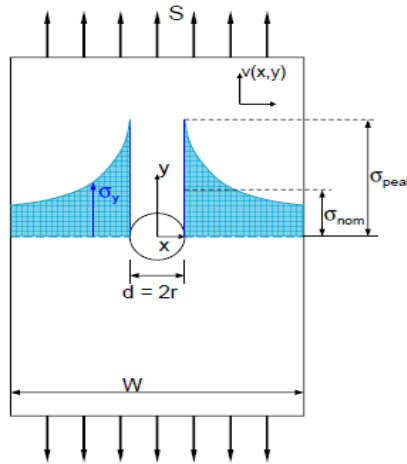


Figure 24: Stress concentration factor concept

The stress concentration factor, named  $K_t$ , is an elastic concept. It gives a direct indication of the severity of the stress concentration, because it is an amplification factor of the stress level which is nominally present in the net section of the notch. The smallest value of  $K_t$  that we could have is 1 and it happens when a homogeneous stress distribution is present.

In other words the stress concentration factor can be also defined as a parameter that gives information about how much homogenous are the stress distribution inside a structure. This second definition can be probably better understood considering the following figure:

Notch	Geometry	$K_t$
Single hole		2.25
Triple holes		1.81
Ellipse		1.24

Figure 25: Stress concentration factor for different geometry notches

Looking at this figure, reduction in  $K_t$  values can be expected passing from a circular hole to an elliptical also considering its first definition. On the other hand, reduction of  $K_t$  with a series of hole is quite unexpected: it is related with the reduction of inhomogeneity of the stress inside the material in this configuration as prescribed by the second definition given for the stress concentration factor

$K_t$  values can be obtained with different methods:

- By calculation: analytical methods, finite element methods (FEM)
- By measurements: strain gage ,measurements, photo-elastic measurements

The severity of the stress concentration and so the intensity of the stress concentration factor is depending on the geometry of the notch configuration. This is why designers should always reduce stress concentrations as much as possible in order to avoid fatigue problems

### Stress intensity factor

In a different way with respect the previous one, this parameter is the key one in fracture mechanism.

Let us consider a body of arbitrary shape with a crack of arbitrary size, subjected to arbitrary stress: tension, bending or both. Material will be considered elastic and so following the Hooke's law. In this particular case, the elasticity theory can be used to calculate stress field around crack tip.

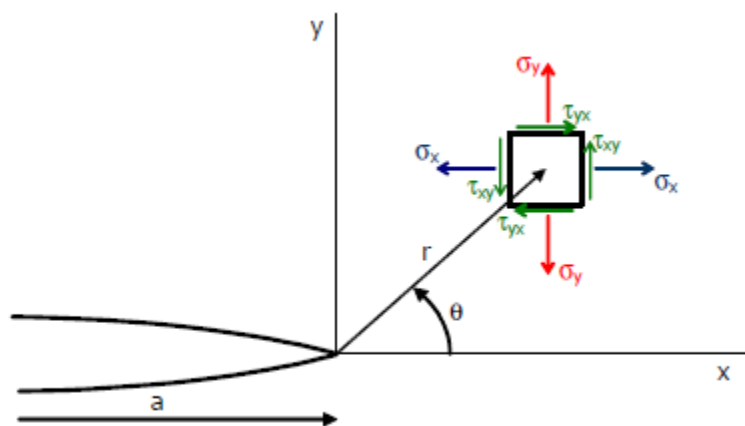


Figure 26: Infinite element at the crack tip

Stresses  $\sigma_x, \sigma_y, \tau_{xy}$  can be obtained. Details on how they are derived can be found in reference [2]. What we are going to consider here are just the solution and an explanation of them.

Stress on a material element around the tip of the crack can be described by the following set of equations:

$$\begin{aligned}\sigma_x &= \frac{S\sqrt{\pi a}}{\sqrt{2\pi r}} \cos \frac{\theta}{2} \left(1 - \sin \frac{\theta}{2} \sin \frac{3\theta}{2}\right) - S \\ \sigma_y &= \frac{S\sqrt{\pi a}}{\sqrt{2\pi r}} \cos \frac{\theta}{2} \left(1 + \sin \frac{\theta}{2} \sin \frac{3\theta}{2}\right) \\ \tau_{xy} &= \frac{S\sqrt{\pi a}}{\sqrt{2\pi r}} \cos \frac{\theta}{2} \left(\sin \frac{\theta}{2} \sin \frac{3\theta}{2}\right)\end{aligned}\quad (eq. 8)$$

Where S is the applied stress and other terms are clear looking at Figure 26.

These relations can be summarized as:

$$\sigma_{ij} = \frac{K}{\sqrt{2\pi r}} f_{ij}(\theta) \quad (eq. 9)$$

Where:

$$K = S\sqrt{\pi a} \quad (eq. 10)$$

is the so called *Stress Intensity Factor* which represents the severity of the stress at the tip of the crack.

What we can be observed from these relations is that, stresses at the tip depend upon the distance x from the crack tip and in particular they are greater at smaller distance.

These relations appear to be quite simple and it can be applied to describe the stress at each crack tip in every elastic body. The stress intensity factor K appears in each solution but its definition is different for different modes. As a consequence, stress intensity factor is often labelled in accordance with the mode of loading. Since equations before are true for all cracks problem as mentioned, there is no objection against selecting a simple familiar geometry to provide some

important conclusion about the results. For this purpose let us consider a very large (infinite) panel, subjected to uniform uniaxial loading with a nominal stress  $\sigma$  and a central crack. The size of the crack is called  $2a$ . This is a convention because in fracture mechanism all cracks with two tips are called in this way. Considering this simple case as example, is now possible to examine in deep the significance of the stress intensity factor,  $K$ , and relation between stress and crack length. An important observation that must be done considering an elastic body is that the stresses are proportional to the applied load everywhere. Starting from this observation one can conclude that crack tip stress must be proportional to the applied stress  $\sigma$ :

$$\sigma_y \div \frac{\sigma}{\sqrt{2\pi r}} \quad (\text{eq. 11})$$

Looking at the unit of these two quantities (right left hand side of the relation) we can easily understand that another parameter needed is a length. What can be thought is that the crack tip stresses are related with the crack size. In particular the stress will be certainly higher when the crack length  $a$  is larger and it confirms that length dimension must appear at the numerator of the relation above. So considering again that both sides of the equations must have the same units there is only one way in which the crack length  $a$  can be considered in the numerator. In fact in order to cancel the square root of the denominator the crack size must appear in the numerator as square root of  $a$  so that:

$$\sigma_y \div \frac{\sigma\sqrt{a}}{\sqrt{2\pi r}} \quad (\text{eq. 12})$$

This relation still contains a proportionality sign instead of an equal sign because of dimensional analysis does not show whether there is a dimensionless number involved. Calling this dimensionless number  $C$ , one finally arrives at an equation

$$\sigma_y = \frac{C\sigma\sqrt{a}}{\sqrt{2\pi r}} \quad (\text{eq. 13})$$

A formal solution would be necessary to obtain the actual value of  $C$ . It turns out that  $C = \sqrt{\pi}$ .

So that in case of infinite plate:

$$\sigma_y = \frac{\sigma\sqrt{\pi a}}{\sqrt{2\pi r}} \quad (eq. 14)$$

Where:

$$K = \sigma\sqrt{\pi a} \quad (eq. 15)$$

Anyway these relations are true only for an infinite plate. Being real plate of finite dimension, now we need to find a general form for these equations even in case of real finite plate. In fact, it should be expected that the size of the plate also will affect the stress at the tip of the crack. In particular the stresses at the tip of the crack will increase when the width  $W$  of the considered plate is shorter. Anyway considering all the previous found relationships, the only way in which the dimension  $W$  of the plate can affect the stress at the tip of the crack is changing the parameter  $C$ . Hence,  $C$  must be a function of the width of the plate  $W$ . In particular, it will be a function of the ratio between the crack length  $a$  and the width of the plate, considering that it must be a dimensionless quantities. However, to maintain the validity of the previously determined equation for an infinite plate, once  $W$  is very large or the crack length is very small the value of  $C$  will tend to  $\sqrt{\pi}$  as in the case of infinite sheet.

Now becomes clear that for any configuration the crack tip stress will be always

$$\sigma_y = \frac{C\left(\frac{a}{W}\right)\sigma\sqrt{a}}{\sqrt{2\pi r}} \quad (eq. 16)$$

And the stress intensity factor is always:

$$K = C\left(\frac{a}{W}\right)\sigma\sqrt{a} \quad (eq. 17)$$

In practical use, in the equations all  $C$ 's are divided by  $\sqrt{\pi}$  and  $\sqrt{\pi a}$  is then substitute to  $\sqrt{a}$ . The function

$$\beta = \frac{C\left(\frac{a}{W}\right)}{\sqrt{\pi}} \quad (\text{eq. 18})$$

is generally named  $\beta$  and it is called *Geometry Factor* and take into account that in reality we have a finite plate. In case of infinite plate the value of this parameter, as mentioned, is equal to 1.

$$\sigma_y = \frac{\beta\sigma\sqrt{\pi a}}{\sqrt{2\pi r}} \quad (\text{eq. 19})$$

$$K = \beta\left(\frac{a}{W}\right)\sigma\sqrt{\pi a} \quad (\text{eq. 20})$$

These relations represent the crack tip stresses and stress intensity factor for all crack problems even if it has been derived for an arbitrary crack in an arbitrary body with arbitrary loading mode (mode I). In fact for any crack in any practical problem, only the function  $\beta$  needs to be derived. However, for many configurations the function beta has already been calculated.

### Toughness

Several difficulties will arise with the direct use of the equations introduced at the previous paragraph and these may have serious consequence. Anyway the practical use of these equations for fracture problems can be used in a first analysis.

Fracture will occur when the stresses at the crack tip becomes too high for the material to bear. As the stress intensity factor defined before determines the entire crack tip stress field, the above statement is equivalent to say: fracture will occur when K becomes too high for the material. How high the stress intensity factor can be, depends upon the selected material. It must be determined from test providing material data. These types of tests can be carried out for example on tensile machine with apposite sample like the so called *centre tensile specimen* (CTS) reported in figure that is generally preferred to the *centre cracked specimen* (CCS).

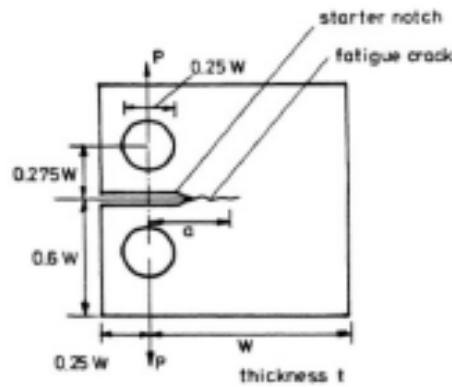


Figure 27: CTS specimen typically used for fracture toughness experiment test

The reason why the CTS is generally preferred to the CCS for this type of test can be easily understood looking at the following figure.

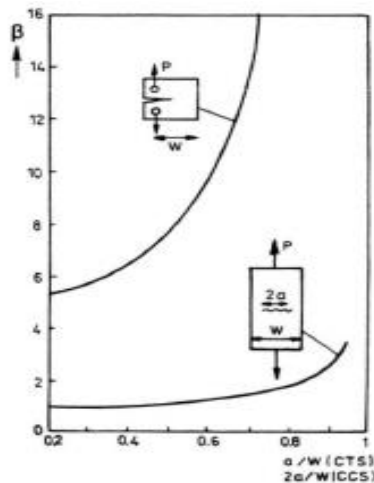


Figure 28: Geometry factor curve

This figure shows a different behaviour of the geometry factor  $\beta$  previously introduced. Remembering the meaning of  $\beta$  in the stress tip relation derived above, and observing from this figure how in case of CTS a larger value is present at the same crack length and with  $W$ , a smaller applied stress will be required. It is something that could be extremely important when testing material with high fracture toughness due to limited capacity of the testing machine.

The material data of interest is then simply obtained by calculating the stress intensity factor with the relation provided in the previous paragraph and considering a given crack length and the load



leading to failure. In fact, apparently, when  $K$  reaches the so calculated value the stresses at the crack tip were too high for the material and fractured ensued. This value of  $K$  is called the “toughness” of the material. Hence, the toughness of a material can be defined as the highest stress intensity that can be supported by a cracked component made of that material or in the same way, Toughness is the value of the stress intensity at which fracture occurs in the case of cracked material.

The unit of the toughness is the same of that of the stress intensity factor that is  $MPa\sqrt{mm}$ .

Once toughness of a material has been measured in a test, its value can be recorded in a data sheet or data handbook as for the Yield strength  $F_{ty}$ . With the definition given of toughness we can schematically write:

$$\text{Fracture if: } a_{critic} = \frac{1}{\pi} \left( \frac{K_c}{\beta \sigma_{02}} \right)^2$$

The nominal stress at which fracture takes place will be denoted as  $\sigma_{fr}$ . So follows from equation above:

$$\sigma_{fr} = \frac{K_c}{\beta \sqrt{\pi a}} \quad (eq. 21)$$

The fracture stress  $\sigma_{fr}$  is the residual strength, i.e. the remaining stress under the presence of crack. Using equation before, one can calculate the residual strength of a certain material for different crack size. Then, if these results are plotted the *residual strength diagram* is obtained.

Must be observed that, fracture stress  $\sigma_{fr}$  would indeed be the residual strength unless failure by collapse prevails. This is the reason why  $\sigma_{fr}$  is not yet called  $\sigma_{res}$ .

However as can be seen looking at the previous relation, the fracture strength of a material is strictly related with the measured fracture toughness of the material itself. Even if generally, the fracture toughness is considered as a material property, it is a function of many different factors that should be considered when carrying out design. The most important ones are:

- Thickness
- Yield strength (different heat treatment could cause different Yield strength for the same material)

When using material data coming from handbook or experimental test one should always consider at which specific material they are referred.

### Plastic collapse

Not only may the high local stress cause cracks by fatigue or stress corrosion which may eventually lead to a fracture, they also may cause fracture to proceed immediately from the notch, particularly when the notch is sharp (high stress at the tip of the notch described by the stress concentration factor parameter  $K_t$  previously introduced). In fact, alternatively, failure can occur by plastic collapse which is always followed by fracture. With the given stress-strain curve, without work hardening, the cross section with the notch, cannot carry any more load once the entire cross section is yielding because yielding will continue uninhibited until fracture results. This is called plastic collapse. Thus the maximum carrying capability in this case can be described as:

$$\sigma_{fc} = \frac{W - a}{W} F_{ty} \quad (\text{eq. 22})$$

Where  $a$  is the notch depth or crack length and  $W$  is the total width. The failure load is called the collapse load or limit load.

This is the equation of a straight line as a function of the notch/crack depth. Also in this case, the failure stress is plotted as a function of the crack length.

If the fracture will occur as a consequence of the collapse the strength  $\sigma_{fc}$  will be the residual strength.

Anyway if the material work hardens, the notched cross section can carry a higher load. In any case the failure can never occur when all the section is subjected to the same stress equal to the tensile stress. It can be realized considering that strains are not uniform along the section but they will be always higher at the root of the notch.

What can be said is that, for a not work hardening material, collapse strength is equal to the yield strength  $F_{col} = F_{ty}$  while for a work hardening material it will be something higher but always less than the ultimate tensile stress. Anyway, as it is not very well possible to determine the values of the yield strength and the ultimate strength with a tensile test, similarly it is not very well possible to determine the values of  $F_{col}$  other than by a tensile test on a notched sample.

It follows that for a work hardening material, equation before becomes:

$$\sigma_{fc} = \frac{W - a}{W} F_{col} \quad (eq. 23)$$

This is also a straight line as a function of the crack length.

These types of relations represent the highest load carrying capability: at collapse plastic deformation becomes unbounded and fracture follows regardless of the toughness. Hence failure by collapse happen before K reaches the toughness  $K_c$ .

**Competition of fracture failure and plastic collapse**

As a result of the previous paragraph, it is clear that fracture can happen for different reasons. If the fracture toughness is high, it will predict, using the relation introduced before, a very high residual strength and this may be higher than the stress for failure by collapse. In this particular case the failure by collapse will prevail.

In a more general way, we can say that, of two competing failure modes, that one which first becomes possible will prevail or in other words, the lower of the two possible residual strength introduced, will prevail.

Generally speaking, and as it is also clear looking at the relation of the residual strength modes, there are three possible condition in which a collapse failure could prevail:

- Toughness is very high
- Crack is very small
- The width W is very small

The following plots in Figure 29 summarize these different possibilities.

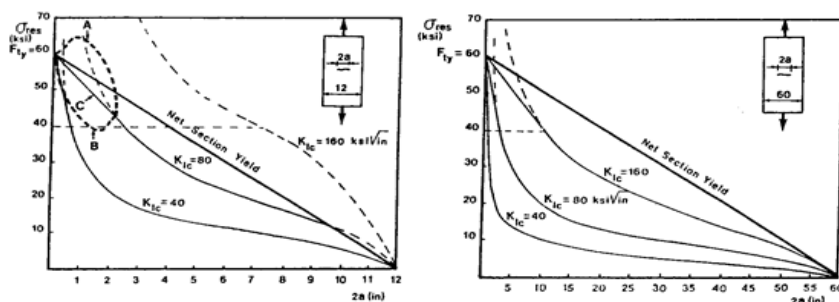


Figure 29: Fracture collapse VS plastic collapse

To determine correct residual strength of a material, some correction factors need to be introduced. It is particularly obvious considering that, stress intensity factor as derived before is an elastic concept and it is not still valid in case of significant plasticity.

In particular, when we have small cracks length the plastic zone has a significant behaviour and, in the same way, when the crack length is very large (near to  $W$ ), all the un-cracked material is plasticized. Particularly in these two conditions the residual strength reduction provided by crack growth analysis are somewhat unrealistic. In fact considering the relation:

$$\sigma_{fr} = \frac{K_c}{\beta\sqrt{\pi a}} \quad (\text{eq. 24})$$

We can see that:

- For  $a \rightarrow 0$   $\sigma_{fr} \rightarrow$  infinite
- For  $a \rightarrow W$   $\sigma_{fr} \rightarrow$  constant

Of course these two conditions are physically unrealizable considering that, when the crack length is zero residual strength must be equal or less to the Ultimate strength and, when the crack length is equal to the width of the plate residual strength must be equal to zero. For this reason a solution at this problem has been found using the so called *Feddersen Interpolation*. Using Feddersen Interpolation, residual strength diagram of the material can be divided in three different portion that, starting from small crack length can be described as:

1. Linear interpolation between  $F_{ty}$  (Yield strength) at “no crack” condition and curve according to  $K$  at a point where  $\sigma_{res} = \frac{2}{3}F_{ty}$
2. Strength can be calculated using the concept of fracture toughness
3. Linear interpolation between zero strength when the crack length is equal to the width of the plate and the curve according to  $K$  at a point for which the crack length is equal to  $\frac{1}{3}W$ .

A visual representation of how this interpolation is carried out is reported in Figure 30.

After this discussion, another consideration that must be underlined here is that, two different plates of the same material could fail one by collapse and the other by fracture. This is an important point to be taken into account especially doing test to determine fracture toughness of a certain material: we must be sure that the coupon is failed due to fracture and not due to

collapse. This possible mistake is a consequence of the previous mentioned dependence of fracture toughness by the thickness and heat treatment at which material has been subjected.

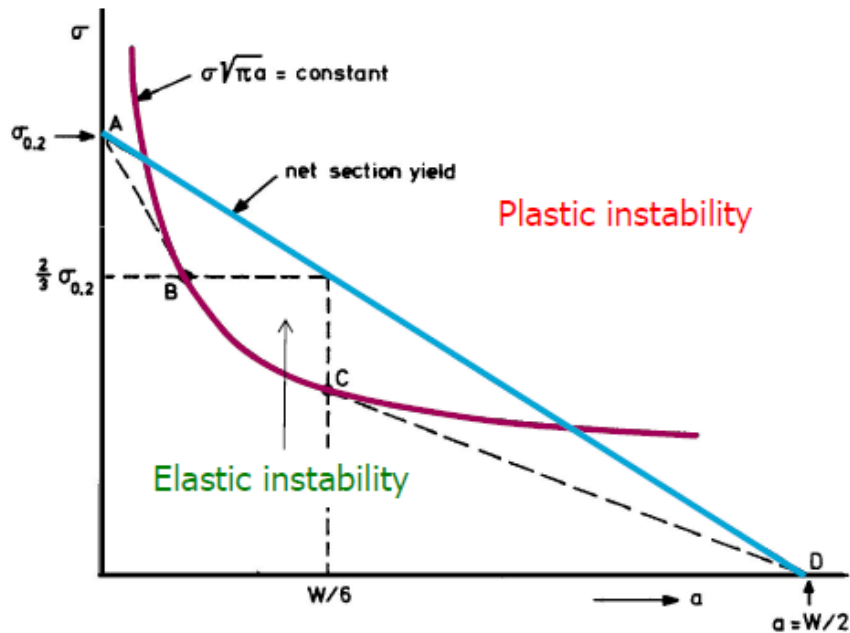


Figure 30: Feddersen interpolation

### Crack growth rate relation

As mentioned before, one of the two key points in damage tolerance analysis is represented by the calculation of the crack growth life. Results of this type of calculation can be presented in two different types of curves:

- Crack growth curve (a-N)
- Crack growth rate curve (da/dN-a)

To obtain such types of results, introduction of cyclic stress intensity factor concept is needed. As introduced before, stress intensity factor  $K$  is a measure of the stress distribution around the tip of the crack. A fatigue load on a cracked specimen, introduces a cyclic stress intensity factor at the tip of the crack varying between a  $K_{max}$  and a  $K_{min}$ :

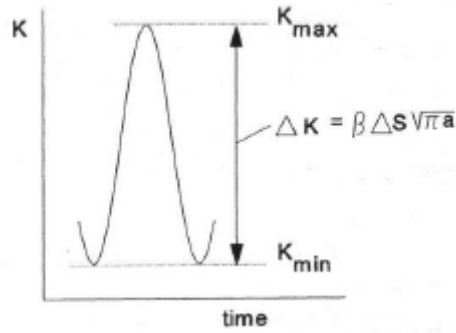


Figure 31: Cyclic stress intensity factor

So that

$$K_{max} = \beta S_{max} \sqrt{\pi a} \quad (eq. 25)$$

$$K_{min} = \beta S_{min} \sqrt{\pi a} \quad (eq. 26)$$

$$\Delta K = K_{max} - K_{min} \quad (eq. 27)$$

A cyclic stress defined by  $K_{max}$  and  $K_{min}$  can be also defined by the stress ratio R defined as

$$R = \frac{\sigma_{min}}{\sigma_{max}} \quad (eq. 28)$$

And the cyclic stress intensity factor  $\Delta K$ .

In fact, considering that, for each crack length the stress intensity range can be obtained using the relations introduced above, results can also be plotted in term of  $\frac{da}{dN} - \Delta K$

It appears to be fully correct if the crack growth rate, which is the crack extension in one cycle, is assumed to be a function of  $K_{max}$  and  $K_{min}$  or in the same way of  $\Delta K$  and R so that:

$$\frac{da}{dN} = f(K_{max}, K_{min}) = f(\Delta K, R) \quad (eq. 29)$$

Experiments show that the general behaviour of this function is more or less that one represented in figure. In fact, scatter in material data must always be considered as will be also remembered later in Chapter 7.

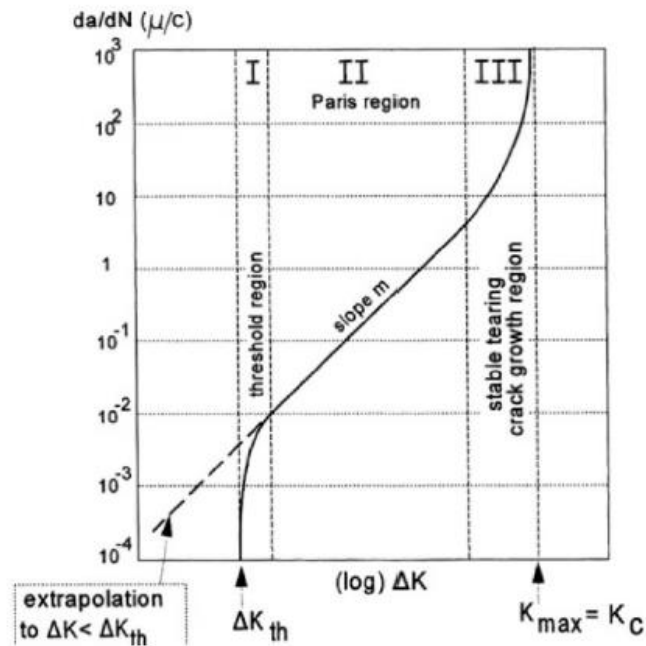


Figure 32: Fatigue crack growth regions

From here can be noted how this general curve can be divided in three different regions generally called *fatigue crack growth regions*.

- 1. Threshold region:** This region is characterized by the relation  $\Delta K < \Delta K_{th}$ . It means that stresses on the crack front are smaller than a certain lower limit whose value depends on the particular material considered. Attention should be placed to avoid confusion between this region and with the nucleation phase described in Chapter 1. In fact these results are applied at macrocracks that due to these small loads are not able to propagate. A standard rule prescribes that crack growth can be neglected if  $da/dN$  value is lower than  $10^{-10} mm/cycle$
- 2. Paris region:** This is a region where the curve is linear in a double logarithmic plot like that one before. This is the only region considered by Paris to develop his famous relation (eq.4) representing the basic one in fracture mechanism analysis
- 3. Stable tearing crack growth region:** In this last region an asymptote is present due to the fact that  $K_{max}$  is becoming closer and closer to  $K_{critical}$ . Here the crack growth rate is quite high and for this reason the time in which the crack is inside this region is not so interesting from an engineer and fracture control point of view. However this region is important because the fracture toughness introduced in the previous paragraph can be observed. In fact material will fail when the maximum stress intensity factor reaches this value.

However, what is important to underline is that eq.29 is considered to be a material property and it represents the fatigue crack growth resistance of this material subjected to a specified  $\Delta K$  and R. In other words, if crack growth is considered on another specimen or another structure, crack growth can be predicted based on the similarity concept which says:

*“Similar cyclic condition ( $\Delta K, R$ ) applied to fatigue cracks in different specimens or structures of the same material should have similar consequence that means similar crack extension per cycle and so the same  $da/dN$ ”*

This principle will be particularly important for experimental tests because it does not require tests on a specified structure to evaluate the crack growth but it only require the same materials for structure to be designed and coupon component. Anyway, this principle is just a general relation. In fact, there are many considerations that should be considered to make it fully correct. First of all, must be considered that plasticity at the tip of the crack can affect crack growth rate. In particular, plastic zone at the tip of the crack presents different size in case of plane stress (thin component) or plane strain (thick component). Considering that plastic zone in case of plane stress is larger, a larger crack growth rate in thick component will occur. This phenomenon is also called thickness effect and it is the same that influence values of fracture toughness.

After this observation, can be understood how similarity conditions in reality are no so obvious as said by the previously introduced similarity principle. Hence, must be here underline that same material is not anymore the only condition needed to get same results in term of crack growth in two different components.

A relation between the crack growth rate  $da/dN$  and the stress intensity factor range  $\Delta K$ , summarizing the previously introduced general relation (eq.29) was found by Paris around 1960. It has been already introduced before (eq.4) and it is repeated here for simplicity:

$$\frac{da}{dN} = C \Delta K^m$$

C and m are material constants. Substituting eq.20 , this relation can also be written as:



$$\frac{da}{dN} = C(\beta\Delta S\sqrt{\pi a})^m \quad (\text{eq. 30})$$

Useful indication can be obtained from Paris equation if the constant  $C$  and the exponent  $m$  are known from material data information. As appears from this relation, if stress level is changed the value  $C(\beta\sqrt{\pi a})^m$  remains the same because it depends on the crack length only but the crack growth is changed proportionally to  $\Delta S^m$ . In particular, because it is true for any crack length, what can be pointed out is that: crack growth life is inversely proportional to  $\Delta S^m$ .

However, directly applying this relation some errors will be introduced in the prediction. For this reason, shortcomings that must be considered when using this relation and possible alternatives will be introduced in Chapter 7 where an algorithm useful to compare all these ones will be also presented.

For the moment considering Paris relation, can appear clear what already said before, that is, to make prediction on fatigue crack growth two different type of information are required:

- Material data
- Stress intensity factor (Knowledge of load and geometry)

The incremental number of cycle  $\Delta N$  required for an increment in crack length  $\Delta a$  can be obtained as:

$$\Delta N = \frac{\Delta a}{\frac{da}{dN}} \quad (\text{eq. 31})$$

Where, the crack growth rate should follow from the Paris equation as well.

The number of cycle to growth from  $a_0$  to  $a_p$  is then obtained as:

$$\Delta N = \int_{a_0}^{a_f} C (\beta\Delta S\sqrt{\pi a})^m da \quad (\text{eq. 32})$$

This integral must be generally solved numerically because the parameter  $\beta$  (geometry factor), as defined before, is also a function of the crack length  $a$ . Moreover, from this relation results clear

how the crack growth life  $N$  is inversely proportional to  $\Delta S^m$  independently from the value of the integral.

What is important to consider at this point, is that all these relations for crack growth prediction are applicable only in case of constant load CA. How this relations need to be modified in the more real case of variable amplitude load will be discussed later on. For the moment is interesting to make some important observations based on the simple relations introduced above for CA loading. Starting from these simple observations in fact, the basic concepts affecting crack growth prediction can be derived and their knowledge will be useful in the application of our methodology. Using relation for the crack growth life  $N(a)$ , it can be calculated for three different ranges of  $a_0$ - $a_f$ .

Results are summarized in table

$a_0(mm)$	$a_f(mm)$	$N(Kc)$	Ratio of $N$
5	50	382	1
5	100	419	1.1
1	50	3781	10

Looking at results reported in this table, the following important observations can be done:

- Increasing the final crack length from 50 to 100 only increase the life  $N$  about 10 percent. It means that the increment in life is really small and it is due to the fact that for these crack lengths the crack growth rate is quite high
- Reducing the initial crack from 5 to 1 the life  $N$  is increased about 10 times

These considerations have a great practical interest and confirm that the major portion of the crack growth life is consumed by the growth of a small and practically invisible crack. These observations are particularly important also considering that, generally, doing numerical prediction on crack growth the initial crack length value is an arbitrary choice. So, in selecting this parameter, these concepts are extremely important to be considered. In addition, an important consideration can be derived: if we want to be conservative in our analysis we have to consider a quite large initial crack length.

Other important observations come out from experiments related to what happen when the crack is very small. Here similarity principle and Paris relation are not anymore supported by experimental data because of at a microscopic level crack growth is dependent on the grain size and characterized by an inhomogeneous stress distribution. These results underline how the meaning of the stress intensity factor for small crack (crack initiation period) is rather limited. A question, consequence of these considerations is:

How large should be the crack to allow application of the similarity principle and Paris relation? There is no a general answer at this question but, the minimum crack length for which these relations are applicable is a function of the type of material considered.

Prediction according to the similarity principle occurs in few steps (Figure 33):

- Consider a certain initial crack length  $a_0$
- Read the  $\Delta K$  value for the specific geometry considered
- For this  $\Delta K$  calculate the corresponding  $da/dN$
- Plot  $da/dN$  as a function of  $a$
- Obtain  $a-N$  curve as integration of  $da/dN$ - $a$  curve

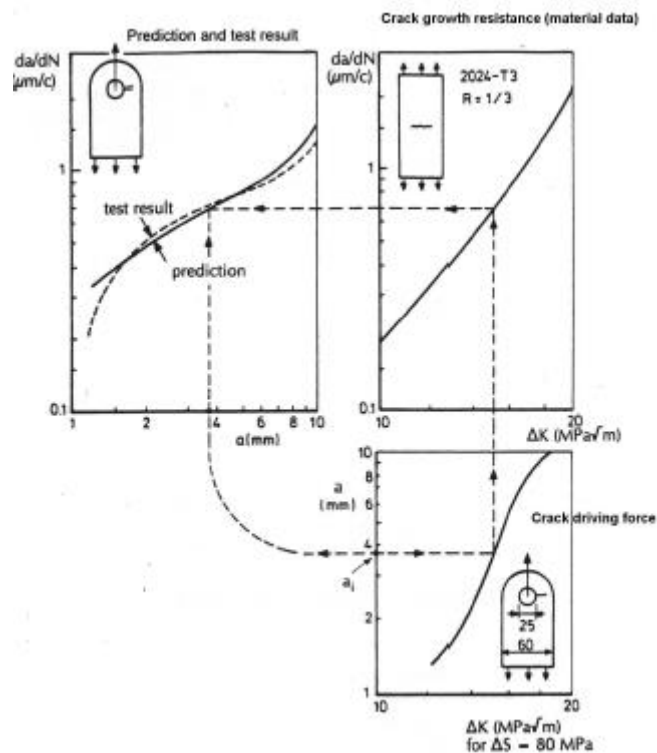


Figure 33: Crack growth prediction based on similarity principle

As mentioned before, all the previously introduced relations for predictions can be used when a CA loading sequence is applied. Anyway, generally, in real case, structure will be subjected to a variable amplitude loading sequence (VA). In this case, stress range, stress ratio and stress intensity range must be defined for each cycle:

$$\Delta K_k = \beta_k \Delta S_k \sqrt{\pi a_{k-1}} \quad (eq. 33)$$

$$\left(\frac{da}{dN}\right)_k = C \Delta K_k^m \quad (eq. 34)$$

Then for each k (number of cycle considered) these values can be used as described before. The only difference, is that now the calculation of the life N cannot come out as before from an integral that is a "fixed" relation. In this case will be necessary to consider a summation being, not priori known, the growth of the crack per each cycle. In other words it means that the effect of each cycle must be considered separately:

$$\Delta N = a_0 + \sum_{k=1}^N C \Delta K_k^m = a_0 + \sum_{k=1}^N C (\beta_k \Delta S_k \sqrt{\pi a_{k-1}})^m \quad (eq. 35)$$

Where, a possible assumption is that the value of  $\beta$  is constant for the crack growth in one cycle. In any case, crack growth under variable amplitude loading is a much more complex phenomena to be analysed with respect a constant amplitude loading case, not only for the difference between an integral and a summation to determine crack length after a certain number of cycle but particularly due to a significant interaction effect and sequence effect that must be taken into account doing prediction on crack growth. In particular there are three important aspects to be considered. They are:

- Crack tip plasticity
- Crack closure
- Cycle with low  $\Delta K$

Before to analyze in deeper detail the developed models to account for these phenomena in crack growth prediction let us introduce quickly the concept of crack closure introduced by Elber in 1970.

### Crack closure

A tension stress on a cracked specimen will open the crack. In particular, according with equations for displacement, based on elastic material behaviour, crack opening displacement return to zero when the tension stress on the specimen is removed. Theoretically, a compressive stress should introduce negative displacement but it is physically impossible. What we have instead, is that, crack will be closed under compressive stress and the compressive stress can be transmitted through the cracked are. It means that in a different way with respect a tension stress a compressive stress is not a *crack driving force*.

Anyway, in spite of these considerations, has been discovered that, a fatigue crack under a tension load, could be already closed during unloading before the tension stress becomes zero. It implies that crack tip is closed at positive tension stress. This last observation has a significant consequence in fatigue crack growth predictions.

Now, to get a better idea about this phenomenon, let us consider a centre cracked specimen. During cyclic loading, plastic deformation occurs at the crack tip. Even if it is a small scale, it implies that a plastic zone is created when the stress goes from  $S_{min}$  to  $S_{max}$ . In particular, as already mentioned before, the plastic zone size at the crack tip depends on the type of stress: Plane stress, Plane strain.

$$r_p = \frac{1}{\pi} \left( \frac{K_{max}}{\sigma_{02}} \right)^2 \quad (\text{plane stress}) \quad (\text{eq. 36})$$

$$r_p = \frac{1}{3\pi} \left( \frac{K_{max}}{\sigma_{02}} \right)^2 \quad (\text{plane strain}) \quad (\text{eq. 37})$$

In any case, plastic zone size is proportional to  $\left( \frac{K_c}{\sigma_{02}} \right)^2$ .

Should be considered that this plastic zone will be elongated along the loading direction. As a consequence, plastic zone will be loaded in compression during unloading so that, some reversed plasticity occurs at the crack tip. This is the result of the elastic unloading that tends to put in compression that deformed material.

What must be observed now is that, plasticity at the tip of the crack, occurs at each cycle and the crack is thus growing through plastic zones of the previous cycles. As a result, plastic zone will be left in the wake of the crack. Then, considering that as said before, the material in the plastic wake field is elongated in the loading direction, we can explain why crack can be closed during unloading while the specimen is still under tension load. This phenomenon is known as “*plasticity induced crack closure*” and was observed firstly by Elber which measured the crack opening displacement at the centre of the cracked specimen as a function of the applied stress (Figure 34). The important point to be observed here is that, the slope of the curve of this plot is representative of the stiffness of the material. In deep, larger slope means a larger stiffness.

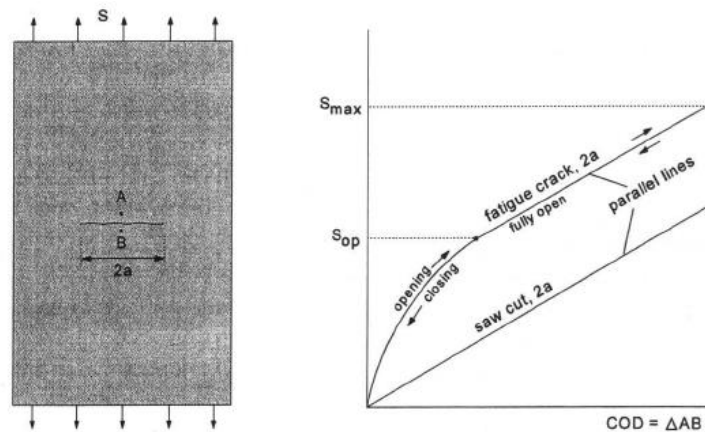


Figure 34: Elber's experiment results about crack closure phenomenon

Important results can be obtained comparing the curve of a fatigue crack and a saw cut. The principal difference between these two types of cracks is at the tip: in the saw cut, plasticity is not present because it does not come out from a fatigue process.

Comparing results of these two cracks, comes out how fatigue crack must be fully opened during the linear part of the COD-S record. Instead, for  $S < S_{op}$ , the slope becomes larger so that, as said, the stiffness will be higher and the specimen behaves as if the crack is shorter. This is the result of the crack closure phenomena, i.e the crack is partially closed due to the excess of plastically elongated material in the wake of the crack.

What can be pointed out at this point is that, during cyclic loading, crack closure (i.e the crack closed under tension) is present if  $S_{min} < S_{op}$  while the crack will be partially or fully opened at  $S = S_{op}$  and it then remains opened up to  $S = S_{max}$ . Upon unloading the crack will be opened until crack closure starts again at the crack tip.

Now, it is important to recognize that, stress singularity at the crack tip, defined by the stress intensity factor  $K$ , is present as long as the crack tip is open, while as soon as the tip is closed the stress singularity is no longer present at the tip of the crack. This is an extremely important observation for fatigue crack growth prediction in which we are directly interested for the proceeding of this work. In fact, in other words, it means that the large stress variation at the crack tip, occurs when the crack is fully opened while it does not occur anymore as soon as the crack tip is closed.

This concept is the key point in crack growth prediction. In particular, it makes plasticity at the tip of the crack, a beneficial effect in terms of crack growth rate (reduced due to this effect).

Once this observation has been understood an *effective stress range*  $\Delta S_{eff}$  was defined by Elber to predict crack growth taking into account this phenomenon. He proposed that, load variation on the specimen, will contribute to crack extension only if the crack tip is open. This is the reason why a definition of effective stress range is needed (Figure 35):

$$\Delta S_{eff} = S_{max} - S_{op} \quad (eq. 38)$$

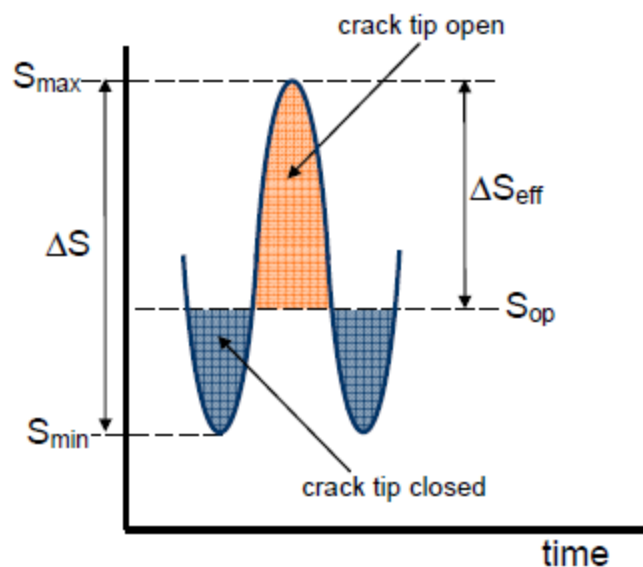


Figure 35: Effective stress range

Starting from this given definition of effective stress range, an effective stress intensity factor can be also defined:

$$\Delta K_{eff} = \beta \Delta S_{eff} \sqrt{\pi a} \quad (eq. 39)$$

According with the Elber's concept, fatigue crack growth rate relation becomes:

$$\frac{da}{dN} = f(\Delta K_{eff}) \quad (eq. 40)$$

Note that this relation already includes the effect of the R-ratio in fact, the reversed crack tip plasticity depends upon  $S_{min}$  and as a consequence the plastic wake field depends on R.

As can be understood from the above introduced relation, in order to apply Elber's concept in crack growth prediction, the key point is represented by the determination of the opening stress level  $S_{op}$ . For this purpose, Elber demonstrated that the  $S_{op}$  value is independent from the crack length  $a$  but it only depends on the stress ratio R of the current cyclic stress. To determine this key parameter for prediction, what can be defined is a new parameter U, function of the R- and determined empirically, that can be used to estimate the percentage of  $\Delta K$  during which the crack tip is opened.

$$U = \frac{\Delta K_{eff}}{\Delta K} = \frac{\Delta S_{eff}}{\Delta S} \quad (eq. 41)$$

Where the function U can be empirically considered, for  $-0.1 < R < 0.7$ , to be:

$$U = 0.55 + 0.33R + 0.12R^2 \quad (eq. 42)$$

A problem of this relation is that it cannot be used for value of R smaller than -0.1 because it predict an increase of  $S_{op}$  that is physically impossible. For this reason many other empirical relations of this type have been developed from many researchers (Figure 36).



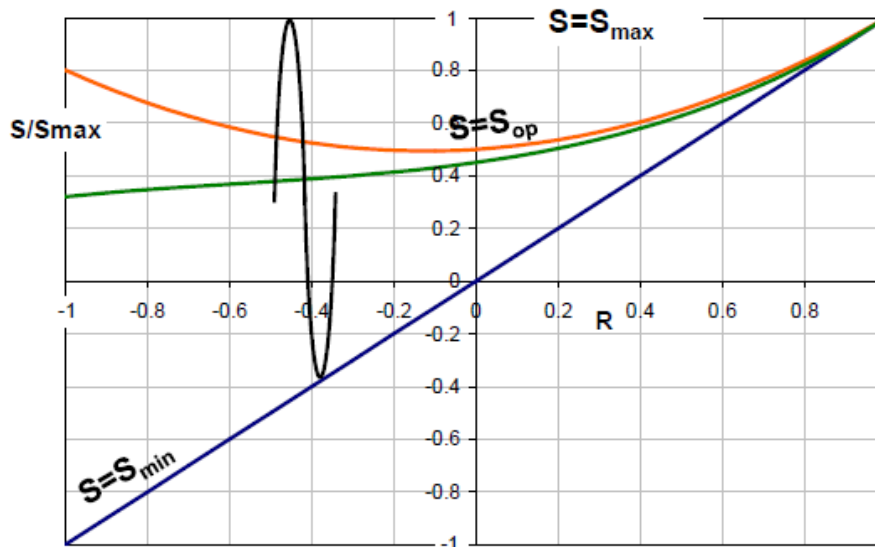


Figure 36: Crack tip opening

Now that a crack closure phenomenon has been introduced, retardation effect on crack growth can be described.

### Retardation phenomenon

Retardation phenomena, is one of the most important consequence of interaction effect related with load sequence. This type of phenomena occurs as a consequence of the presence of an overload in the load history. In fact, after this load occurs a very slow crack growth for some cycles is observed. This phenomenon is due to plasticity induced crack closure described in the previous paragraph. Crack growth retardation is a consequence of plastically elongated material left in the wake of the crack previously created at the crack tip plastics zone. This phenomenon induces crack closure at a positive stress. A load cycle with a large maximum stress will cause a relatively large plastic zone, leaving more plastic deformation in the wake of the crack later on. As explained, it increases the crack tip opening stress level  $S_{op}$  reducing the effective stress intensity factor range  $\Delta K_{eff}$ . This lower  $\Delta K_{eff}$  explains the crack growth retardation phenomenon. These observations are summarized in the following figure (Figure 37):

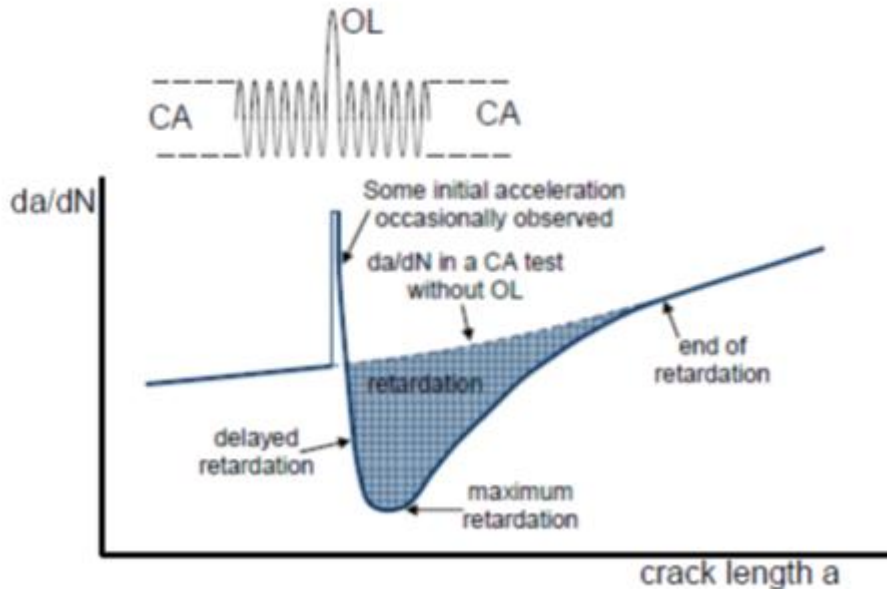


Figure 37: Crack growth retardation phenomenon

From this figure, another important observation can be carried out. Immediately after the application of an overload, the opening stress  $S_{op}$  is drastically reduced due to the fact that the overload itself when applied tends to open the crack. This phenomenon is generally referred as “*delay crack growth retardation*”. Then, after some cycles experiments show a significantly increase in  $S_{op}$  that creates the previous defined retardation effect. Anyway, real phenomenon is even more complex. In fact, retardation will be different if a positive overload is followed by a negative one. In this particular case retardation effect on crack growth is reduced. In addition, there are also others parameters that influence this positive effect from a crack growth rate point of view. In particular, there are different conditions that influence the number of cycle in which crack growth rate is smaller ( $N_D$ ). The two most important ones are:

- Thickness effect: Smaller is the thickness and larger is the retardation effect (Figure 38)

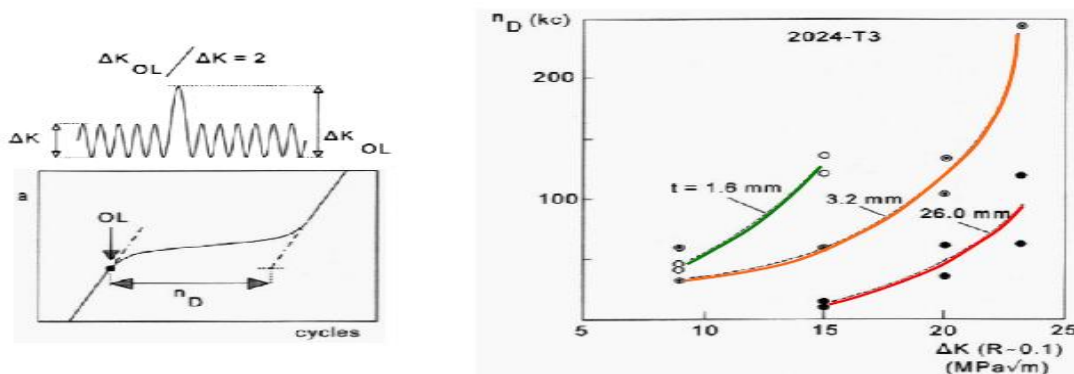


Figure 38: Thickness effect on retardation phenomena

- Material Yield Strength: The reduction of crack growth rate due to retardation phenomena created by an overload is larger for material with a lower yield strength (Figure 39)

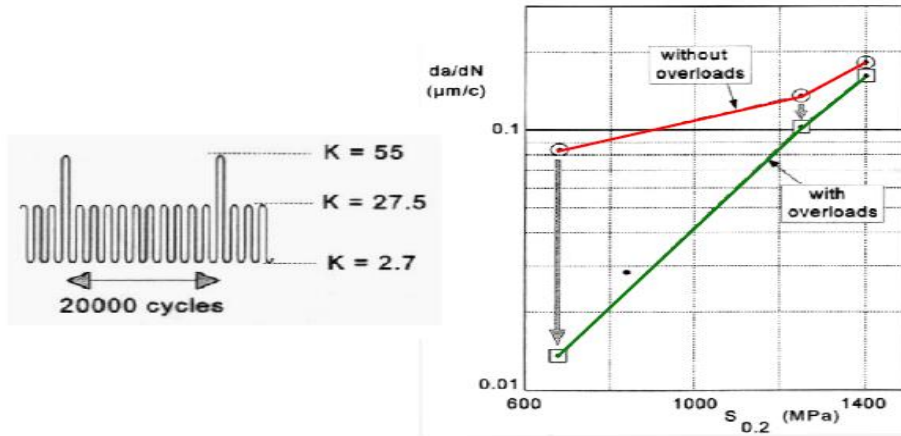


Figure 39: Material Yield strength effect on retardation phenomena

Due to retardation phenomena, a Variable amplitude load cannot be treated as a simple constant amplitude load. Anyway, just to get an idea on how retardation effect can influence crack growth rate, let us consider a very simple variable load sequence composed of two main blocks of constant amplitude load: a high load block and a low load block. Considering the previous discussion about retardation effect, induced by created plasticity at the tip of the crack, what can be expected is different crack growths if the first block is characterized by high load with respect the case in which the first block would be characterized by the lower one.

Let us consider, for example, a case in which the load sequence is characterized by a high load block followed by a lower one as shown in figure (Figure 40).

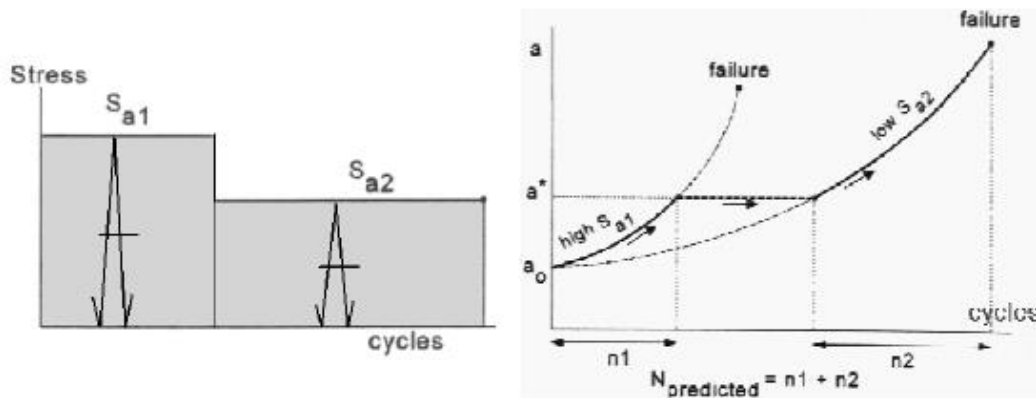


Figure 40: Simple VA load sequence

Fatigue crack growth under high cycle stress amplitude, named  $S_{a1}$ , starts from an initial crack length  $a_0$  until a crack  $a^*$  is obtained. At this point the stress amplitude is reduced from  $S_{a1}$  to  $S_{a2}$  and the test is continued until failure. If the crack growth due to the second amplitude load block is not influenced by how the crack has grown up to  $a^*$  the initial crack growth along curve 1 (due to higher loads) is continued along curve 2 as reported in figure (Figure 40).

If this is assumed to be correct real crack growth behaviour, then the total crack growth life is given by the sum of the crack growth life of the two block so that:

$$N = n_1 + n_2 \quad (eq. 43)$$

This type of prediction implies that  $n_1$  and  $n_2$  are predicted in the same way as it is done for CA loading. Unfortunately, as can be expected considering all the previous discussion about crack closure and retardation effect, real crack growth under VA loading, even if simple like that one considered on this example, is different. In particular, crack growth in the second (lower) load block, is influenced by the crack growth in the first block. For this reason, before to calculate the crack growth of the second block by simply applying the relation already introduced before for constant amplitude loads, a certain period where crack growth is reduced (because of retardation phenomenon) must be considered. Taking in mind this observation and considering a CA load sequence with overloads at some points the crack growth, can be understood how the expected behaviour is somewhat like that reported in figure.

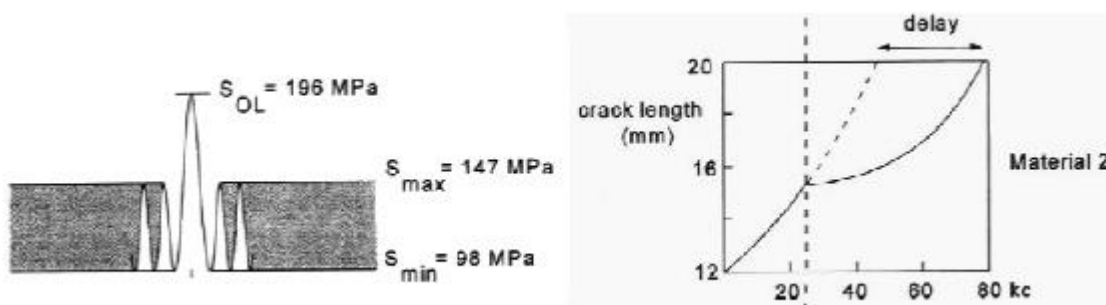


Figure 41: Crack growth retardation due to overload

Now that the importance of retardation phenomena in the crack growth under VA loading has been introduced, a quick introduction of the most important models developed to analyse crack growth rate under variable amplitude loading and taking into account all these effects can be

considered. However, should be realized that the simple load histories, like those used to explain these concepts, are significantly different from real ones acting on a structure. In fact, a real load sequence will be generally not divided in block of constant loads but they will be characterized by a much more random behaviour. Description of different types of load sequence but and how they can be processed to get inputs needed for the application of the crack growth models will be carried out in the following of this thesis (Chapter 4).

Following paragraph of this chapter introduce crack growth models for VA loading case. The key point that differentiates a model from another is represented by how crack growth retardation is predicted.

### **Crack growth model for variable amplitude load**

At a general level, these models can be divided in *global analysis* and *cycle-by-cycle analysis* [3]. The global analysis concept predicts fatigue crack growth considering the average of the applied loading cycle. The cycle by cycle analysis, on the other hand, evaluates the crack growth for each load cycle and determines the crack growth life by accumulation.

Cycle by cycle analysis can be performed with or without involving interaction effects, i.e the effect of load cycle on crack growth in later cycles like for example the retardation effect.

A comparison between not interaction and interaction effect models is necessary to see if significant load sequence interaction occurs. This type of comparison has been carried out in the final part of this thesis where results are reported and described (Chapter 6). In particular, in that chapter will be shown how, as expected, non-interaction prediction model leads to a larger predicted crack length after the same number of cycles respect prediction coming out from an interaction model. Occurrences of this difference, significantly indicates presence of load interaction effect.

### **Linear damage non-interaction effects models**

As pointed out in a previous paragraph, fatigue crack growth under VA loading, would be simple if crack growth in every cycle is dependent on the severity of the current load cycle only and not on

the load history. In fact under this assumption the simple crack growth prediction of CA loading case can be applied.

The linear damage accumulation method is simply a summation of calculated crack growth increments. As a result, it is the simplest model to predict the crack growth rate under VA loading. In general this rule can be presented mathematically as:

$$a_n = a_0 + \sum_{i=1}^N \Delta a_i \quad (\text{eq. 44})$$

Where  $\Delta a_i$  is simply obtained cycle-by-cycle using the Paris Relation introduced before (eq.4).

This is a simple but, at the same time, unrealistic non interaction model. Considering all the previous observations done about loads interaction effect, this prediction model can be categorized as a conservative model. In other words, applying non-interaction model like this, a shorter crack growth life is expected or, in the same way, for a given crack growth life the final crack length will be larger. Again, how much conservative it is with respect interaction models, will be considered at the end of this thesis when results coming out from the application of both model will be shown (Chapter 6).

Anyway, presence of interaction effect is always a key parameter in crack growth analysis under VA loading and hence the simple linear damage accumulation rule described is physically unrealistic.

### *Interaction effect models for crack growth analysis*

Presence of loads interaction effects is not just a pure theoretical concept but it is evident also from experiments carried out on specimens subjected to VA loading. These effects always alter the crack growth rate under the application of VA loading as previously described. In order to correctly predict crack growth under VA loading is necessary involve interaction effects while developing a certain prediction model. There are a lot of models developed to predict crack growth taking into account interaction effects.

Here below there is a description of the most important interaction models starting from the simplest one to arrive at the more advanced model.

In particular, models taking into account these effects can be generally divided into three main categories:

1. Yield Zone models: it is the first developed type of model. They are promoted by considerations on the size of the plastic zone at the crack tip as created by high peak loads. Plastically induced crack closure is not considered in these models.
2. Crack Closure Models: In these types of models crack closure effect is also considered and it can be seen as an improvement of the more primitive Yield Zone models. However here, relations used to include crack closure in the model, i.e. relation used to estimate the value of the opening stress  $S_{op}$  are empirically determined. These models are not able to predict delay of retardation.
3. Strip Yield Models: These are the most sophisticated models taking into account crack closure phenomena by using experimentally determined relation. Moreover, the effect of delay of retardation can be here estimated.

### ***YIELD ZONE MODELS***

These types of models, try to explain interaction effect by considering condition in front of the crack tip where a plastic zone region, with a dimension depending from the applied load history is present. Two important Yield Zone Models have been developed.

#### 1. Wheeler

The Wheeler prediction model is based on the simple linear damage accumulation relation introduced in the previous paragraph modified by a retardation factor parameter named  $C_p$ .

$$\left(\frac{da}{dN}\right)_{VA} = C_p \left(\frac{da}{dN}\right)_{CA} \quad (eq. 45)$$

$C_p$  varies from 0 to 1 depending on the location of the crack tip in a previously created larger plastic zone ( $r_p$ ) and on the plastic zone of the current load cycle  $r_i$ . The value of  $C_p$  is calculated using the following relation:

$$C_p = \left(\frac{r_i}{r_p}\right)^m \quad \text{if } r_i < r_p$$

$$C_p = 1 \quad \text{if } r_i \geq r_p \quad (\text{eq. 46})$$

Where the exponent  $m$  is an experimentally calculated parameter depending on the applied stress level, cracks shape as well as the load spectrum. Then  $r_i$  is the current plastic zone size its which meaning is reported in figure (Figure 42), can be calculated as:

$$r_p = (a_{OL} + r_{OL}) - a_i \quad (\text{eq. 47})$$

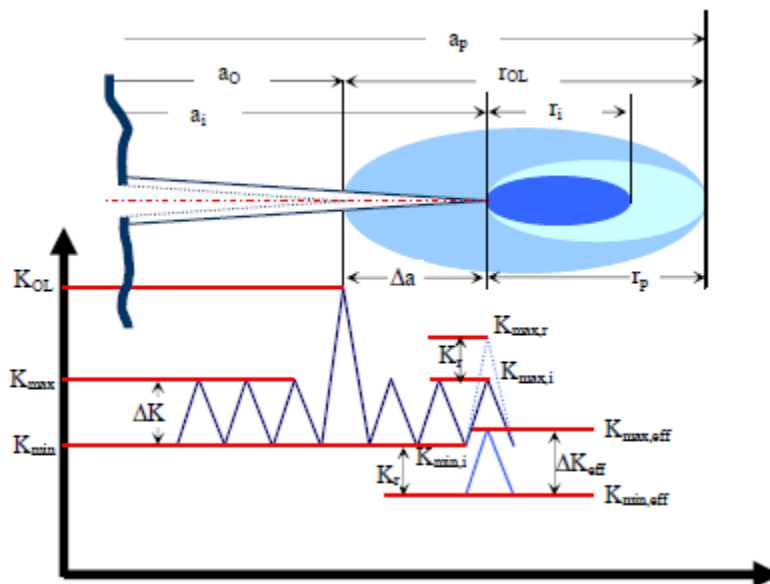


Figure 42: Yield zone model concept

Using this model should be considered that its accuracy strongly depend on the definition of the parameter  $m$ .

However the wheeler model, being a Yield Zone Model, does not consider crack closure phenomena. Moreover, this model can only consider crack growth retardation but not acceleration making it unable to predict the occurrence of the delay retardation phenomena being CP, for its definition, only larger than 1. After an overload, maximum retardation is considered to occur immediately, i.e. delayed retardation is not predicted. Actually, the model assumes a very



simple crack growth behaviour, even if, as shown before (Figure 37) immediately after the application of peak loads the phenomenon is very complex.

## 2. Willemborg

In this case, crack growth retardation is assumed to be a function of the stress intensity factor required to cancel the effect of plastic zone created by an overload. In this model, a required maximum stress intensity factor  $K_{max,req}$  is introduced. It is defined as the stress intensity factor producing a plastic zone just large enough to touch the border of the plastic zone created by an overload. Moreover, Willemborg assumes the occurrence of a residual compressive stress ( $S_{res}$ ), caused by the overload, which reduces the effective stress at the crack tip. The values of  $K_{max,i}$  and  $K_{min,i}$  of the current cycle are then reduced by  $K_{red}$  to obtain the effective values. Finally, the effective stress intensity factor and the effective load ratio, were used to determine the crack growth rate for current cycle  $i$ . If  $a_i + r_i \geq a_p$  (Figure 42) then the residual stress as well as the retardation effect are ignored.

This model should be preferred to the Wheeler model described before because avoid the use of the empirically calculated, and tuned, parameter  $m$  that significantly influence the results obtained with that model. However as that one before it does not consider delayed retardation.

## **CRACK CLOSURE MODEL**

The occurrence of crack closure at a positive tensile stress level after removing the load on the specimen is a physical reality. In order to be accurate, this phenomenon should be an essential element in a crack growth prediction model. Its importance has already been pointed out in the previous paragraph.

Many models were developed to take into account crack closure effect on crack growth prediction. Some of these were very accurate but, due to their complexity, they required a long computational time so that they were impractical in reality to be used. For this reason, many other simple analytical crack closure models have been developed.

Crack closure models, for Variable Amplitude load (VA), require a cycle by cycle calculation of the crack opening stress level  $S_{op}$ , and the corresponding  $K_{op}$ . In particular, the current value of the opening stress level depends on the preceding fatigue crack growth and corresponding wake field of the fatigue crack. The most important point in crack closure models is how the variation of  $S_{op}$  is predicted for a VA load history. In particular, the variation of  $S_{op}$  during the load history, as we will see analysing each of the most important crack closure models in the following, is dependent on the load history itself. In other words, it means that information on the load history must be stored in a memory file. These information are associated with the larger positive and negative load peaks being these ones those that introduce a significant plastic zone and reversed plasticity respectively. Hence they are those that tend to increase or decrease  $S_{op}$  of following cycles.

The three main models, which are based on Elber's crack closure assumption, were primarily developed to predict fatigue crack growth under flight simulation loading.

Now let's see quickly the main concepts on which each of them is based.

### 1. ONERA MODEL

The Onera model is a simple model based on Elber mechanism as it is a stress history dependent concept of crack growth threshold. It assumes that the crack opening level is limited by two extreme conditions, i.e CA loading and single overload. In case of VA loading, it is assumed to be in between, depending on a defined load spectrum parameter  $\alpha$ .

The ONERA model is based on the comparison of current plastic zone size and stress intensity factor to the equivalent plastic zone size and stress intensity factor. In case of an overload, a new monotonic plastic zone will be created, having a size greater than the equivalent size of the last plastic zone. In case of absence of monotonic plasticity the equivalent stress intensity  $K_{max,eq}$  becomes smaller when the crack is growing because the equivalent plastic zone size becomes smaller.

In the ONERA model, the crack opening  $K_{op}$  can be expressed as:

$$K_{op,i} = K_{max,eq,i}(\alpha f_1(R_{eq,i} + (1 - \alpha)f_2 R_{eq,i})) \quad (eq. 48)$$

Where  $R_{eq,i}$  is the equivalent stress intensity ratio factor,  $\alpha$  is a loading parameter varying from 0 to 1 and  $f_1, f_2$  are material dependent empirical function. The loading parameter  $\alpha$  varies from 0 in case of CA loading to 1 in case of single overload cycle. Generally for MINITWIST spectrum  $\alpha=0.5$  while for FALSTAFF  $\alpha=0.65$ .

Hence, in order to calculate the crack growth rate  $da/dN$  for each cycle, is necessary to determine the material data i.e.  $f_1, f_2$  and Paris relation constant  $C$  and  $m$ .

The crack growth relation used in ONERA model utilizes a modified version of the Paris equation that can be expressed as:

$$\frac{da}{dN} = C_0 K_{max}^n \left[ \frac{1 - f_2(R)}{1 - f_2(0)} \right]^m \quad (eq. 49)$$

The Elber's  $U(R)$  defined in the ONERA model is:

$$U(R) = \frac{\Delta K_{eff}}{\Delta K} = \frac{0.9}{1.9 - 0.9R} \quad (eq. 50)$$

Some short comings of this model are:

1. It is not able to fully predict the interaction effects as well as transient phenomena (Initial fast crack growth)
2. For simple VA loads sequences, a significant difference was predicted by the model between periodic underload-overload and overload-underload sequences which was not observed in reality tests.
3. The state of stress (plane stress, plane strain) influences predictions. Plane strain leads to a shorter predicted life, whereas plane stress leads to a longer predicted life
4. The accuracy of input data and empirical relation is important to give accurate prediction. A different  $R$  value adopted in CA tests result in a different material parameter
5. The multiple overload effect is still not predicted in the ONERA model

## 2. CORPUS MODEL

The CORPUS model was proposed by De Koning in 1981. The CORPUS model is based on the hump mechanism, i.e the crack closure is visualized by the hump formation on crack surfaces. As it is shown in figure (Figure 43).

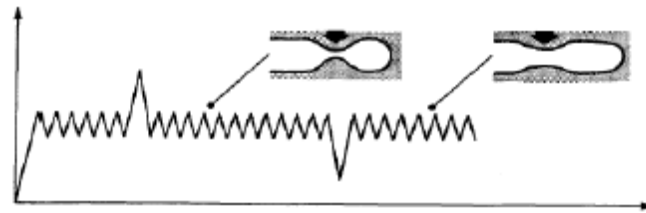


Figure 43: Humps formation on crack surface due to overloads

There is no evidence in supporting the formation of humps on the crack surface presented in literature. However, only schematics are available to understand the hump creation and flattening. In case of an overload, a larger hump will be created and then will be flattened by a later compressive load in the spectrum as represented in the figure above. In every cycle, a hump is created with associated  $S_{op}$  level, and for the estimation of the opening stress  $S_{op}$  a cycle by cycle calculation is required, since  $S_{op}$  is essential for CORPUS model.

This model, introduces few new concepts in crack growth analysis. These are related with the concepts of primary plastic zones (plastic zone developed in a virgin material) and secondary plastic zones (plastic zone developed in an already plastically deformed material) and multiple overload effect. Anyway, even if concepts behind the model are quite simple, the mathematical interpretation of the model appears to be fairly complex.

In order to describe hump behaviour after the application of an overload-underload combination, a form similar to Elber's function has been determined empirically for alluminum alloys 2024 and 7075.

$$U = (-0.4R^4 + 0.9R^3 - 0.15R^2 + 0.2R + 0.45) \quad \text{if } R > 0 \quad (\text{eq. 51})$$

$$U = (-0.1R^2 + 0.2R + 0.45) \quad \text{if } -0.5 \leq R \leq 0 \quad (\text{eq. 52})$$

Using Finite Element Analysis, has been demonstrated how the value of  $S_{op}$  depends on  $S_{max}$ ,  $S_{min}$  and  $\sigma_{max}$  in comparison with the yield strength. In order to incorporate influence of high load level with in this model a correction factor  $h$  for the  $S_{op}$  values is defined. This correction factor was obtained by a curve fitting procedure of results coming out from finite element analysis.

An overload is playing a major role in creating the hump while, an underload will reduce the hump and happening stresses. A lower underload decreases the  $S_{op}$  level of the previous cycle while an overload higher than the previous overload cycles increases the  $S_{op}$  level.

As mentioned, CORPUS model introduces also the concept of primary (PPZ) and secondary (SPZ) plastic zone. In particular, is considered that, interaction of an overload with an overlapping PPZ causes an increase of the crack opening levels, which will give more crack growth retardation. This effect plays an important role in the CORPUS model. The hump opening stress that can be obtained from equations before is valid for a single overload combined with an underload. If a series of overloads are applied the model assumes that  $S_{op}$  will reach a stationary upper bound level defined by:

$$1 + m_{st} \left[ \frac{1}{U} - 1 \right]$$

Where  $m_{st}$  is a stationary parameter which depends on the crack growth increment  $\Delta a$  between the overloads and the plastic zone size  $\Delta n$  of the overload. For the CA loading case, the ratio between  $\Delta a$  and  $\Delta n$  goes to zero and the value of  $m_{st}$  becomes 0.1. Finally, if the crack is grown through the overload plastic zone  $\Delta a/\Delta n > 1$  and the overload interaction is ignored and the equation before is used to calculate  $\Delta K_{eff}$  for the Paris relation.

Considering what is reported in literature about comparison between analytical results of this model and test results we can say:

- Crack growth in most severe flights was under estimated
- The CORPUS model gives much more importance to a rarely occurring negative load if that load is more compressive that the frequently occurring ground stress level
- The CORPUS model predict an higher crack growth rate for a lower yield stress if the other material constants are not changed.

3. PREFFAS MODEL

The PREFFAS model was proposed with the objective to produce a simple model with a few crack growth calibration tests to characterize the material response and its sensitivity to overload effects.

The load history will be considered as cycles of stress intensity factor  $K$  (Figure 44).

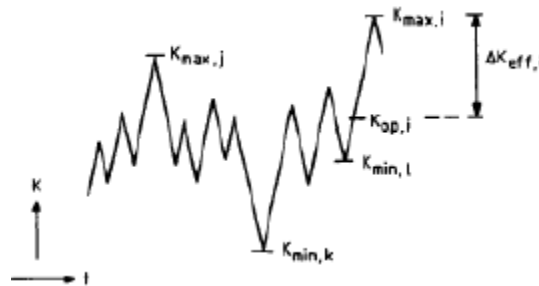


Figure 44: Load sequence considered in PREFFAS model

Each cycle is supposed to start with a maximum  $K_{max}$  followed by a minimum  $K_{min}$ .  $K_{op}$  is calculated for each cycle using the corresponding  $K_{max}$  and  $K_{min}$ . Maximum reversed plasticity, which occurs at  $K_{min,k}$  (the absolute minimum), should be considered.  $K_{max,i}$  (The maximum peak up to the current point) and  $K_{min,i}$  (the absolute minimum up to the current point) must be considered to calculate  $K_{op}$  (the next needed). According to the PREFFAS model the maximum  $K_{op}$  should be used for cycle  $i$ . According with this model, way we found a value for the current cycle that is affected by the previous load sequence.

$$K_{max,j} - K_{op,i,j} = U(K_{max,j} - K_{min,k}) \quad (eq. 53)$$

Where:

$$U = A + BR = A + B \left( \frac{K_{min,k}}{K_{max,j}} \right) \quad (eq. 54)$$

For calculation of  $K_{op}$  at the present cycle a limited number of  $K_{max}$  and  $K_{min}$  must be stored in memory. So at this point, instead of considering the maximum  $K_{max,i}$  of the current cycle and the minimum  $K_{min,i}$  of the current cycle we are going to consider as relevant parameter  $K_{max,i}$  of the current cycle and  $K_{op,i,j}$ . This is a logical consequence of the crack closure concept.

In this model there are four parameters i.e.  $C, m, A, B$  that must be determined. As already known,  $C$  and  $m$  are the parameters needed in Paris relation depending on the material considered. On the other hand  $A$  and  $B$  are the parameters needed to determine the function  $U$  introduced to estimate  $K_{op,i,j}$ . Experience shows that the relation  $A + B = 1$  can be considered for Aluminium and Steels used for aircraft structures. In particular, we should note that a large value of  $B$  implies more crack closure and so, as consequence, more retardation effect. The values assumed by these parameters also include the thickness effect in this model. Typical value for parameter  $B$  in case of Alluminium 2024 and 7075 structure are:

- Thickness  $1 < t < 15\text{mm}$   $B = 0.45 - 0.35$  Al2024
- Thickness  $1 < t < 15\text{mm}$   $B = 0.35 - 0.33$  Al7075

Then the value of parameter  $A$  can be easily determined considering relation above.

In short, the PREFFAS model is a simple model based on the Elber crack closure concept. The crack closure is calculated with a cycle by cycle approach.

The model is characterized by few limitations that can be summarized in the following points:

1. In this model compressive stress are truncated at zero ( $S=0$ ). In reality, the ground-air-ground cycle in the compressive range has a systematic effect on crack growth.
2. In the most of the prediction model the plastic zone size calculations are an important issue. This aspect is not explicit described in PREFFAS model.

### **STRIP YIELD MODEL**

The previous crack closure models are based on the occurrence of crack closure which, instead, is not considered in the Yield zone models. However, assumptions had to be made to account for crack closure under variable amplitude loading and plastic deformation in the crack wake is not calculated.

Strip Yield models are based on Dugdale model. The Dugdale model was used to estimate the size of the plastic zone  $r_p$  at the tip of the crack.

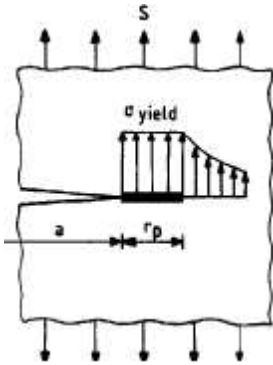


Figure 45: Dugdale model

Dugdale, assumes that yielding occurs in a narrow strip ahead of the crack tip as shown in figure. The material response to plastic deformation is rigid-perfectly plastic, which leads to a constant stress (yield stress) in the plastic zone. Dugdale assumes that this situation could be considered as equivalent to that represented in the figure below where, a larger fictitious crack length  $a^* = a + r_p$  is present with crack edge loading between  $a$  and  $a^*$  with stress  $\sigma = \sigma_y$ . The equivalence also requires that the stress at the

fictitious tip is non-singular. The strip yield model is initially proposed to solve the elastic-plastic crack problems approximately for the plane stress state. The crack opening

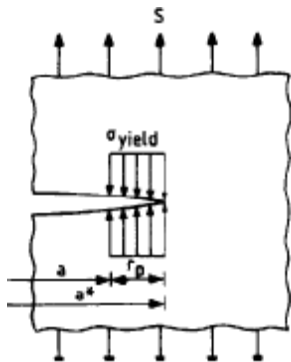


Figure 46: Equivalent schematization to Dugdale model

depends on the remote applied load and the yield stress applied in the plastic zone on the fictitious crack tip. Because crack grows into the plastic zone, a plastic wake field is created which can induce crack closure at a positive stress level. Reversed plastic deformation can also occur when the crack is closed and locally under compression. What is done in this model is a calculation of stresses and displacement per strip.

This is the more complex developed model for crack growth prediction under VA loading but, at the same time, it is also that one able to provide the best

results. Important improvements with respect the other models introduced before are:

- Empirical calculation of crack closure level are replaced by calculation of  $S_{op}$  as a function of the previous plastic deformation
- Delayed retardation can now be predicted



# 4 LOAD SPECTRA

Load spectrum is generally the term used to refer to fatigue loads act on a structure or structural component during its operational life in terms of amplitude, number of cycles and sequence of variable loads. In other words, the load spectrum should give information about the load time history defined as the variation of load as a function of time  $P(t)$ . The present knowledge of the fatigue process clearly indicates that, the significant point of this load history  $P(t)$ , are the maxima and minima generally named  $P_{max}$ ,  $P_{min}$ . In fact, at these load levels reversal of cyclic slip occurs in the material, either at the material surface and in the crack tip zone.

Without information about the anticipated load spectra, fatigue prediction analysis, described in the previous chapters, are impossible to be performed. Designers must know the loads. If the load spectrum is unknown it must be estimated considering the expected usage (using FEM, CFD, etc.) of the structure in service and validate it using physical measuring. These measures are generally carried out one time only and on first production products using strain gage applied in the most critical location. However as we will also see in deeper detail in the following, especially for aircraft, the load sequence are mandated by certification authorities.

Then, as already pointed out before, validation test are needed to support these analysis. The following figure gives an idea about the important rule played by load spectra in fatigue analysis process.

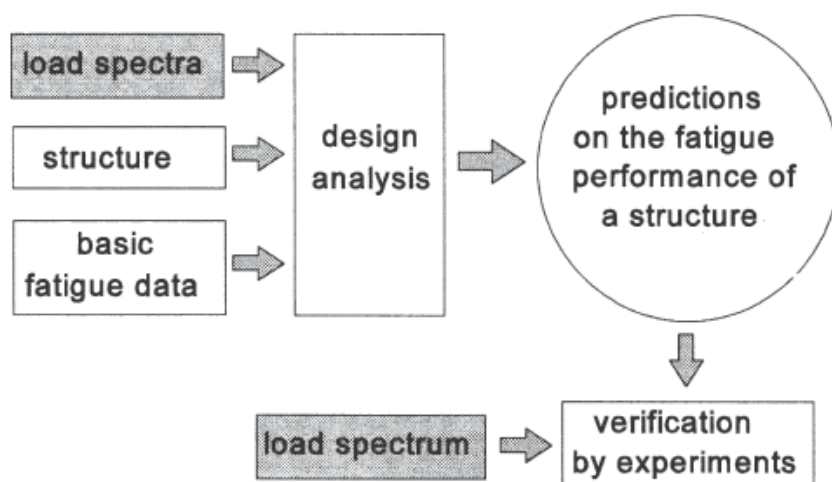


Figure 47: Rule of load spectrum in fatigue analysis procedure

There are various questions that should be carried out when dealing with load spectrum.

However, the two most important ones, needed to start in developing analysis are:

- Is the load history which a structure will experience in service known?
- How can the load history be described to present all the relevant information?

Of course the load acting on a structure in service depends on its usage. For example if we consider the wing of an airplane, that is also our case of study, the aerodynamic lift can be supposed (neglecting the small quantities of lift created by the fuselage) to carry the weight of the airplane. This distributed load exerts a bending moment on the wing with a maximum at the root of the wing itself. When the aircraft is on the ground, the lift is zero and the aircraft is supported by the undercarriage. Each flight thus implies a cycle of the bending moment on the wing that is represented by the heavy line in Figure 48. This is a very slow load cycle that can be considered to be a quasi-static load (it happens once per flight).

On the other hand, wing is also subjected to much faster load sequences. These cycles are caused by turbulent air and are predominately especially during climb and descent at low altitude.

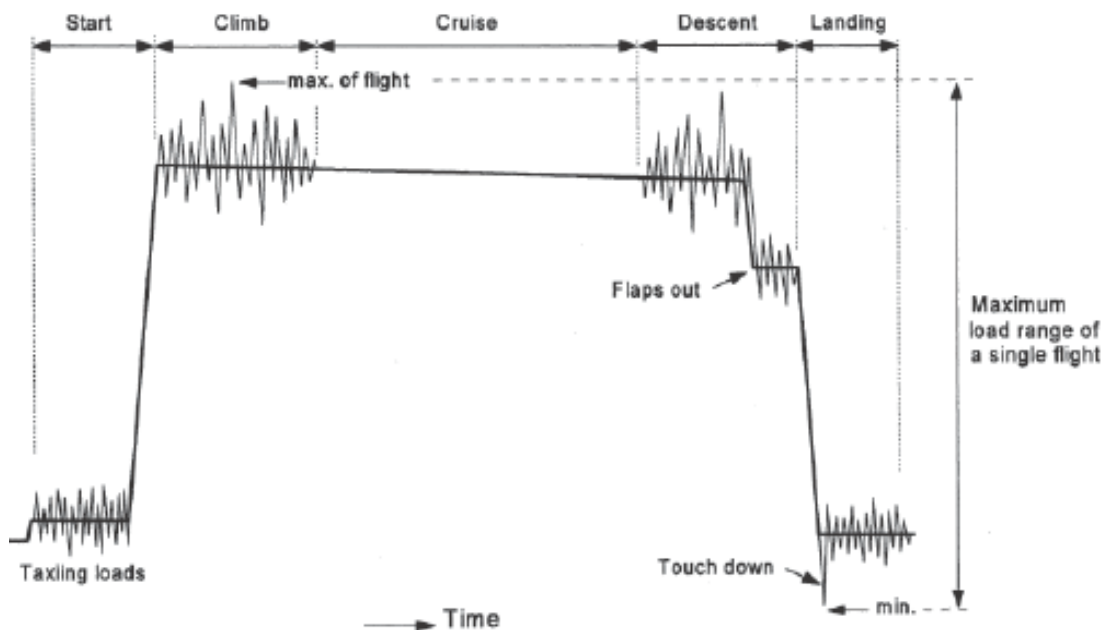


Figure 48: Typical wing load spectrum per flight

Bending of the wing introduces tension in the lower portion of the wing structure that is well recognized as the critical point for fatigue. Anyway in addition to bending, torsion moment should also be considered for a much more complete analysis.

As can be understood from this example, the load acting on a structure in service can be divided in two different categories of loads:

- *Deterministic loads*: A load is considered to be deterministic if it can be defined as a specific occurrence from which it is known that it will occur with a certain magnitude and frequency. This type of loads followed by the planned use of the structure.
- *Stochastic loads*: These loads are characterized by an essentially statistical nature. Contrary to the deterministic ones, they cannot be predicted to occur with a certain magnitude at a given time. A description of stochastic loads can only be given using a statistical approach.

Deterministic and stochastic loads can also happen together and the real problem in fatigue analysis evaluations is represented by how these loads can be combined and processed. In fact, superimposed loads make more severe the load spectrum itself because they increase the maximum load and at the same time reduce the minimum one.

## Processing load spectrum

Once the load spectrum has been obtained it must be processed in order to obtain the most relevant characteristics. These characteristics are those needed to perform fatigue analysis using relations and methods introduced in previous chapters. Two different families of methods can be used to process a spectrum. They are the so called:

- Level crossing count method
- Range counting method

Processing the spectrum is an essential step to generate input for fatigue analysis software. In particular, one of the important tasks of the processing methods is getting a data reduction. It is needed in order to save memory (especially in case of wireless transfer data) and also to enable a reduction of operational measurement. However preserve essential signal characteristic like peaks, valley and ranges is a key point, especially for more irregular load spectrum. However what is important to underline here is the fact that, as will be much more clear later on, with the usage of these methods the load sequence is often lost.

Now, before to describe in deeper detail how do these two mentioned methods work let us introduce a definition of different types of load spectrum.

### Definition of different load spectrum

In a general way a load spectrum could be also describe as a load history defined by a sequence of maxima and minima if the time dependant phenomena are not considered. Then, as we will see this sequence is usually reduced to a statistical representation in order to have a useful survey of the fatigue loads. However, in order to understand why a statistical representation is really useful a definition of different load history should be introduced.

#### 1. Regular and symmetric load history

A load history like this one is represented in Figure 49. As can be seen from this figure, symmetry in the load history is present around a certain level, named *reference level*. This level is generally indicated as *level 0*. In particular, in a spectrum like this, the same number of maxima (peak above the reference) and minima (valley below the reference) with the same amplitude are present. Looking at this spectrum appears clear that, to process histories like these, only information about load above the reference level are needed. In fact, information of minima can be obtained simply by mirroring these results below level 0.

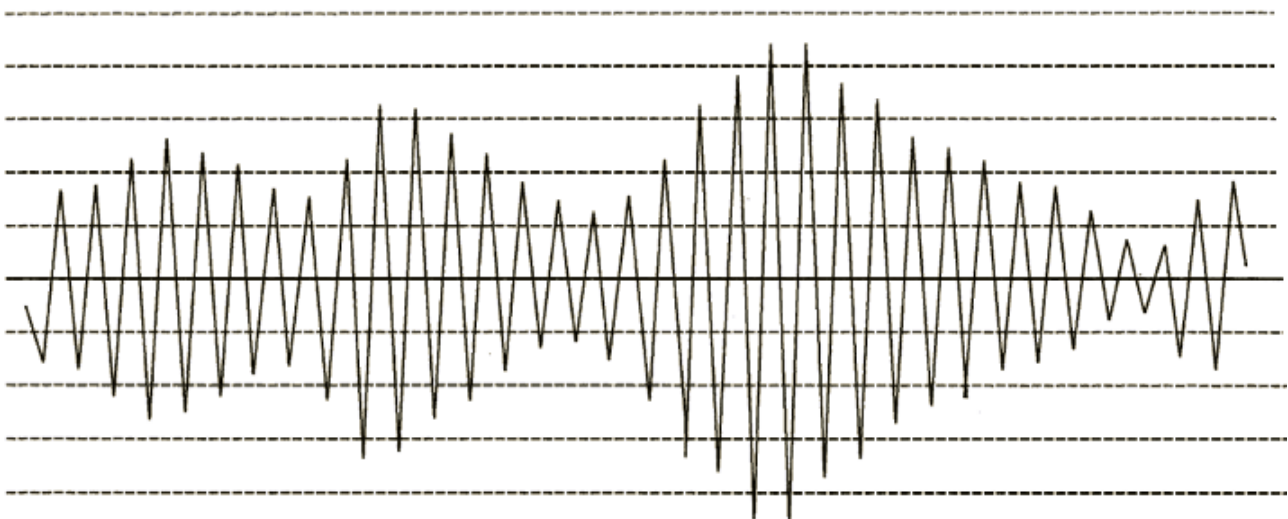


Figure 49: Regular and symmetrical load history

### 2. Regular not symmetric spectrum

A load history like this is reported in Figure 50. The most important difference with respect the previous one is that now maxima and minima are not characterized by the same intensity. However, histories like these are still regular because for each maxima above the reference level we have a minimum below. Differently with respect the regular and symmetric spectrum, to process these types of loads we need information not only on the load above the reference level but also information about load below.

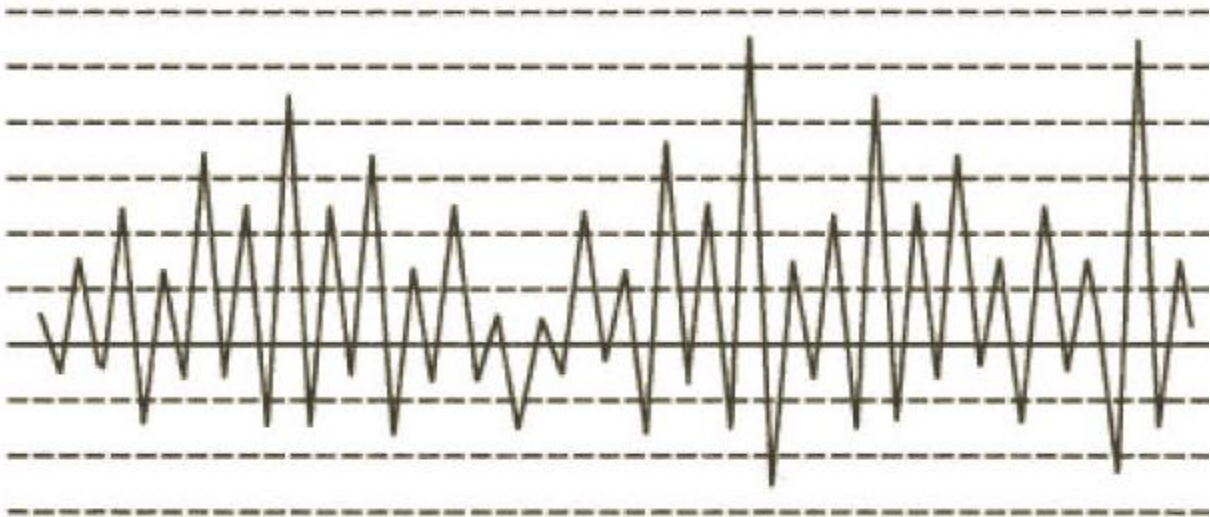


Figure 50: Regular not-symmetric load history

### 3. Irregular spectrum

A load history like this is reported in Figure 51. Here in a difference way with respect what happen in the other cases for each maximum we do not have a minima and vice-versa but we could have more peaks above the reference level than peaks below. Then, again, as in the previous one, maximum and minima are not characterized by the same intensity. As can be understood, these types of load histories are more difficult to be analysed. In particular to get a much more clear idea about the irregularity of the load history an irregularity factor  $k$  can be defined as:

$$k = \frac{N^\circ \text{ of peaks above a certain level}}{N^\circ \text{ of time that a certain level is cross}} \quad (\text{eq. 55})$$

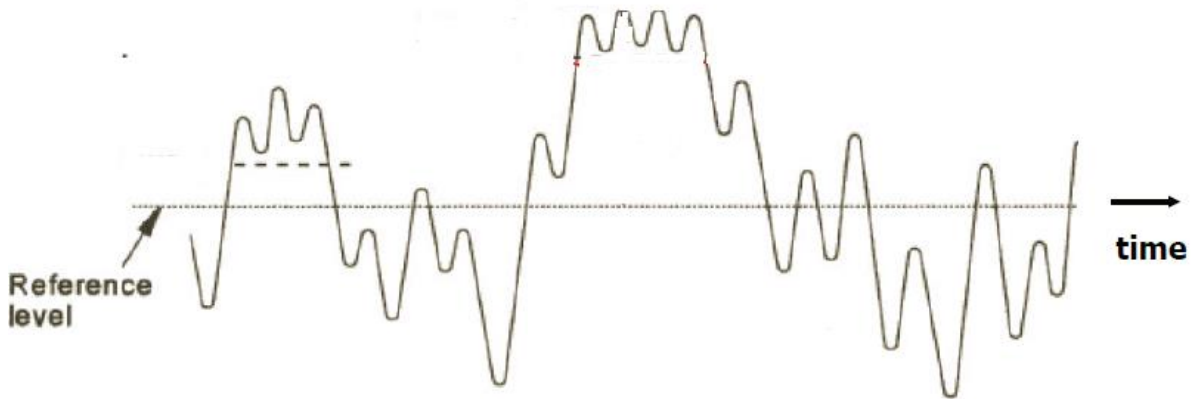


Figure 51: Irregular load history

In words it can be defined as the ratio between the number of peak values above the reference level and the number of level crossing this reference level itself.

The irregularity factor is equal to 1 for regular load history (first category of load histories).

Now that the main types of load history that can be encountered in reality have been introduced, the previously two processing methods mentioned can be analysed.

### Level cross counting method

The first thing is dividing the spectrum into load levels and determines: the number of times that a load level is exceeded and the number of time that a peak is present in a certain interval defined by two different levels. An example is reported in Figure 52.

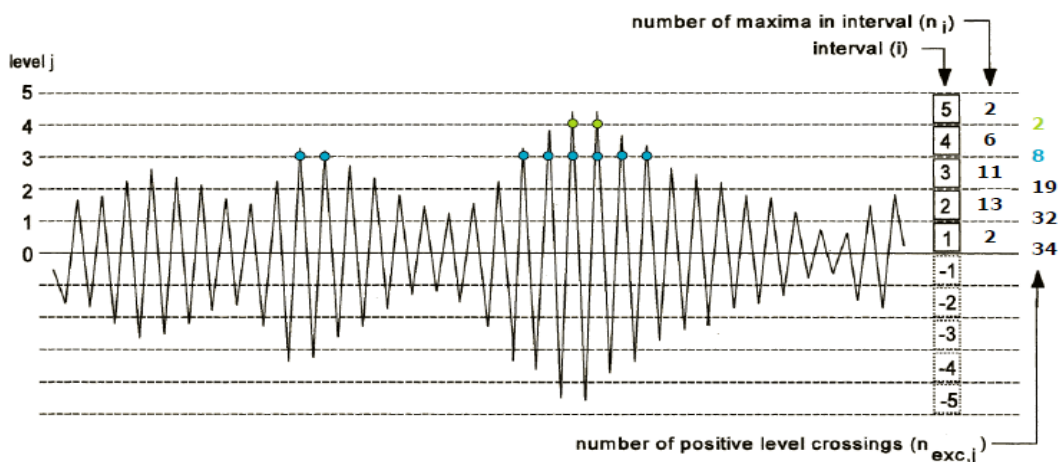


Figure 52: Level cross counting method

In this way, a load history can be presented as the number of peaks values above a certain load level J denoted as  $n_{exe,j}$  or, as the number of peaks in a certain interval i named  $n_{peak,i}$  that can be obtained using the following simple relation:

$$n_{peak,i} = n_{exe,j-1} - n_{exe,j} \quad (eq.56)$$

At this point these numbers are used to create histograms which can be represented as:

- Number of peak above a certain interval i

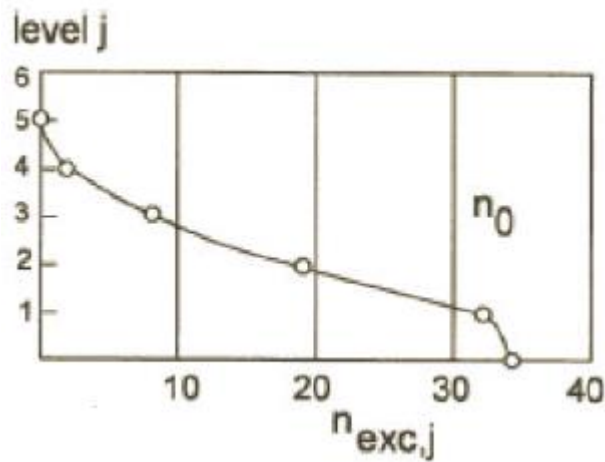


Figure 53: Typical exceedance diagram

In statistical term this bar chart can be seen as associated with the *Probability density function* of the number of peaks

- Number of peak per interval

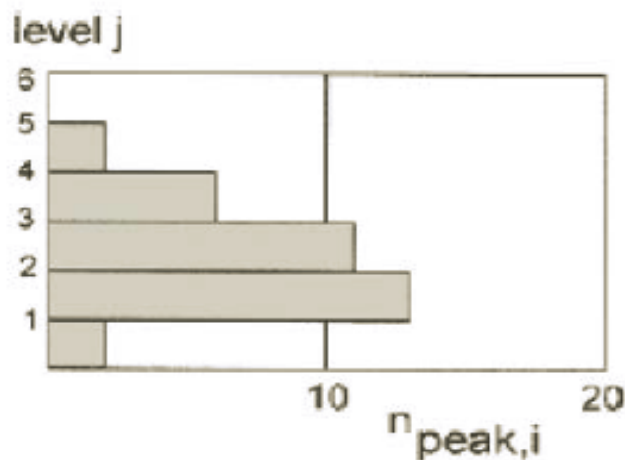


Figure 54: Number of peaks per interval

This last curve, in statistical term can be seen as an estimation of the *Probability function* of the occurrence of peak values.

These diagrams are also referred in literature as “*exceedance diagram*”.

However as mentioned before, giving the definition of the different load histories, a representation like these, where only peaks above the reference level are considered, provide enough information only in cases where a regular and symmetric load histories is present. On the other hand, in case where the load sequence is no longer symmetric, information on peak below the reference level are needed. They can be obtained proceeding in the same way but rotating the spectrum of 180°. In this case, the histogram plot becomes something like that reported in Figure 55.

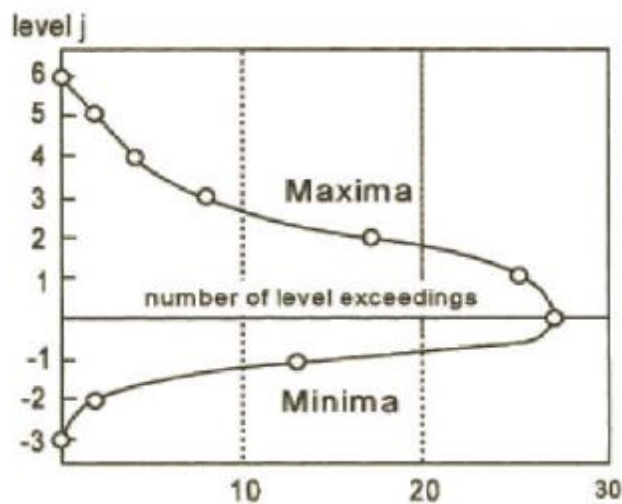


Figure 55: Exceedance diagram for a non-symmetric load history

Obviously, in case of symmetric load history, where as defined before a reference level can be defined, the number of maxima above level 0 and minima below level 0 must be the same.

In case of irregular load histories plot like these are no longer meaningful due to the fact that, in this case, even small load variations like those reported in Figure 51 are considered like maxima and so as large load variation. Anyway, they can still be draw to get a first evaluation about the severity of the spectrum but also to comparing severity of different spectrum. In fact representation of the load history in these ways can be useful to distinguish if a load spectrum can be categorized as *flat* or *steep* (Figure 56).



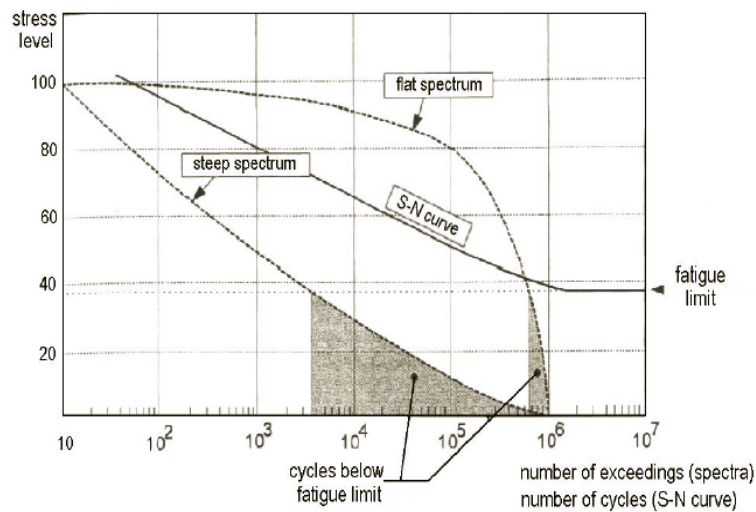


Figure 56: Difference between flat and steep load spectrum

A *steep* spectrum is characterized by a small number of high loads and a large number of small loads. On the other hand, a *flat* spectrum is characterized by a large number of high loads. Hence, plot like these can be useful also to reduce the number of loads by applying the so called truncation and omission procedure.

**Truncation levels:** Due to retardation effects described in Chapter 3, high loads can have a beneficial effect on fatigue damage accumulation in metallic materials. From measurement or calculations, the highest load levels (extreme values) expected in service will be known. But due to the usage variability, not all structures in service will experience the same high loads. To adjust for this, truncation of high loads in a loading standard may avoid unconservative test results. However, truncation does not affect fatigue damage accumulation in a very straightforward way, but the effect will depend on spectrum shape. In a general way, can be said, if the same truncation level has been selected for a flat and steep spectrum it will strongly affect the last one. In other words, truncating a relatively flat spectrum will less drastically lead to more conservative test results.

Another important aspect in doing this is the considered material. Retardation effect of high loads is known to exist in metals due to the formation of a plastic region at the tip of the crack that reduce the crack growth of the subsequent cycle. Attention must be placed in considering that a quite different behaviour is true in case of composite material where, an infrequent high load may

cause a sudden damage growth. It means that truncation is conservative in metals but it will be unconservative for composites.

Omission level: Large reduction of testing time can be obtained by omitting low-amplitude cycles from spectrum. The acceptable degree of reduction will depend on the spectrum type. In a general way, can be said we that, a steeper spectrum shows a lower sensitivity to load omission.

However with the level crossing count method described up to now we are able to get useful information about severity of the spectrum but, at the same time, they are not so useful for fatigue analysis. In fact, number of exceedances is not directly used in prediction methods but what we need to perform these analyses are load amplitudes which cannot be determined using this type of method. This is the reason way, the range counting method described in the following paragraph is much more useful from a fatigue analysis point of view.

### ***Range Counting method***

First of all we have to consider that a fatigue cycle can be divided as:

- Peak, valley, peak
- Valley, peak, valley

Even more important is to consider that a cycle can be split in two half cycle:

- Up range
- Down range

This difference is extremely important considering that up ranges are more dangerous. This types of ranges in fact, are those that tend to open the crack. Range counting methods involve in counting up the amplitude of all ranges and the number of times that certain amplitude range is repeated.

In particular, range counting method can be divided in:

1. Simple 1D range counting method
2. 2D range counting methods

1D Range counting method

In this method first of all, load history is divided in ranges. Each up range and down range counts as half cycle. Then, the amplitude of each range is recorded. In the following figure (Figure 57) there is an example of the application of this method to a simple load sequence.

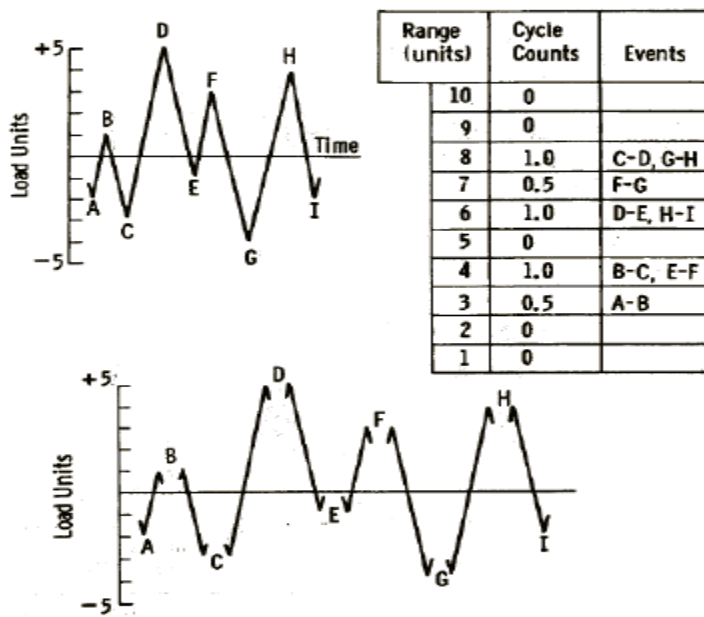


Figure 57: 1D range counting method procedure

The important observation here is that, being this method a 1D method, only amplitude of ranges is recorded but, information on mean stress and so on the R-ratio are not considered. This problem is related with the facts that applying this type of range counting method, there are no information about where each cycle starts and finish. This explains way a simple 1D counting method is generally replaced by a more complete 2D counting method.

2D Range counting method

Different types of 2D counting methods, has been developed in the past years. Here, just two of them are described:

- *Simple 2D counting method:* in this case all range are simply counted as they occur
- *Rainflow counting method:* this method will be deeper described in the following of this paragraph

Being these methods 2D, rather than recording only amplitude as before, start and end level of each cycle is recorded so that, in this case, information about mean stress and R-ratio can be obtained. Results of 2D counting methods are typically stored in a matrix like that reported in figure (Figure 58).

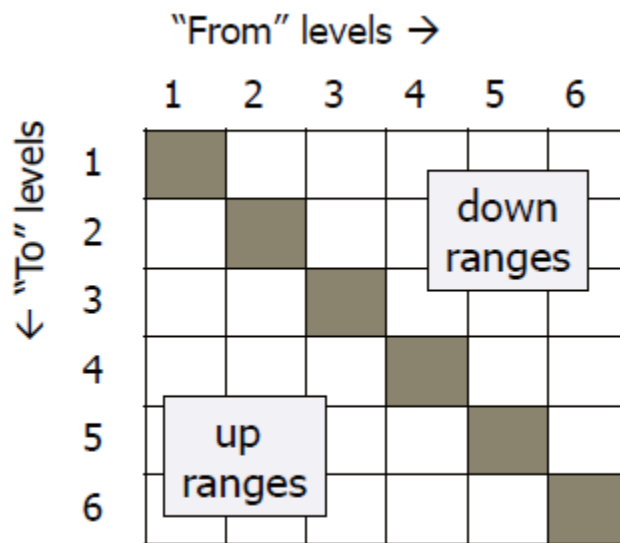


Figure 58: Typical 2D range counting matrix

In this matrix each range is counted as coming from a certain initial interval and going to a certain final interval. Positive ranges (up ranges) are stored in the lower part of the matrix while negative ranges (down ranges) are stored in the upper part of the matrix.

Looking at the shape of the matrix, once it has been filled in, information about the severity of the spectrum can be obtained. In particular, more symmetric is the load spectrum and more similar to a diagonal matrix this matrix will.

Of course, the accuracy achievable with these methods is limited. In fact, counting of peak value, do not indicate exactly where the peak is inside the considered interval. For this reason, smaller will be the considered interval (larger will be the number of considered levels) and better will be the accuracy obtained. However the cost to pay for this larger accuracy is a larger computational time.

Rainflow counting method

The simple 2D counting method, as mentioned before, counts all successive load ranges. It means that also loads characterized by small amplitude and occurring between adjacent larger ranges are counted for. The Rainflow method, on the other hand, is based on the idea that this small load variations between two large peaks and valleys can be discarded because their contribution to damage is negligible or, at least, if they are considered the obtained result will be less conservative.. This idea is supported by the following consideration:

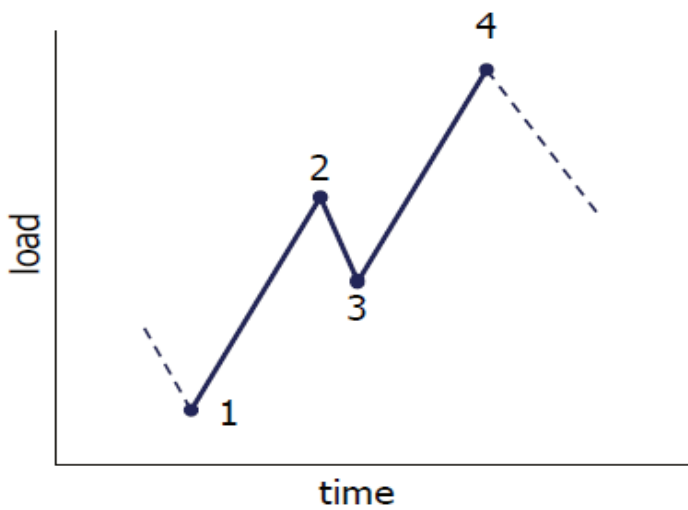
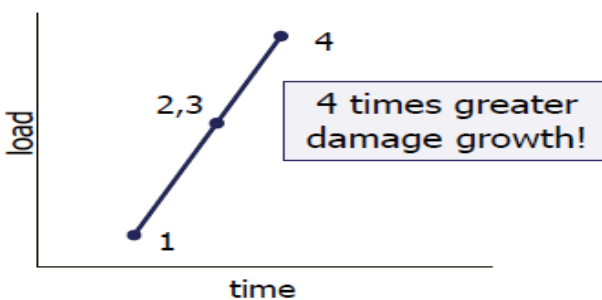
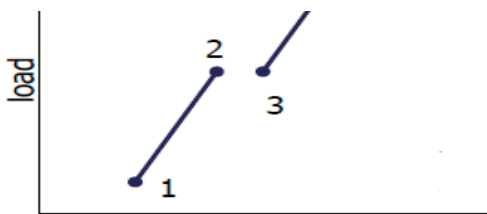


Figure 59: Simple load sequence

Let us consider this load sequence in figure (Figure 59). Moreover we assume that:

- Range 1-2 = Range 3-4
- Point 2 and 3 are coincident
- Paris relation with  $m=3$

$$\frac{da}{dN} = C(\Delta K)^3$$



$$\begin{aligned} \Delta a &= C(K_{2,3} - K_1)^3 + C(K_4 - K_{2,3})^3 \\ &= 2C\left(\frac{1}{2}(K_4 - K_1)\right)^3 = \frac{1}{4}C(K_4 - K_1)^3 \end{aligned}$$

As can be seen from previous simple calculations, an unique large cycle is more dangerous than a

Figure 60: Effect of intermedia small range

cycle with many shorter cycle inside.

The Rainflow counting method, based on this observation, provides a conservative counting method. In fact, the small range between a larger one is firstly eliminated so that the large range alone is counted as a real range of the sequence and then the small range is counted separately. Rainflow counting procedure, has found support also in considering cyclic plasticity. To explain this, a short load sequence with the corresponding plastic behaviour is represented in the following figure (Figure 61). This plastic behaviour could be applied to local plasticity at the material surface during the initiation period or at crack tip plasticity during the crack growth period.

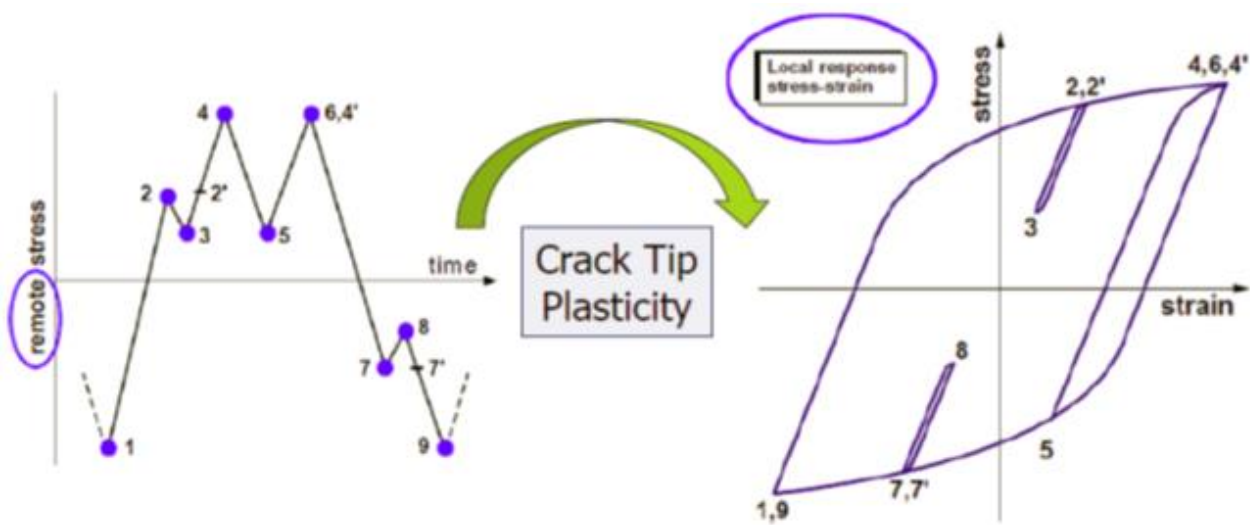


Figure 61: Cyclic plasticity loop

The intermedia loads are causing the hysteresis loops inside that one of the major cycle. It is assumed that the intermedia plasticity loops do not affect the major loop. This gives support to the rainflow counting method.

However, as can be understood from here, the key point of Rainflow method is in determining when and how a small range inside a larger one can be eliminated. In order to do this two different algorithm have been developed:

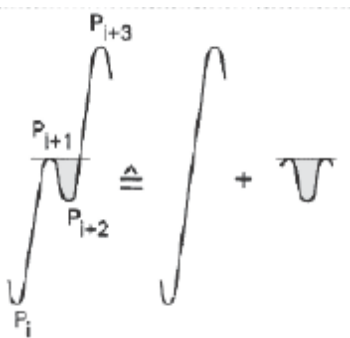
- The ASTM algorithm
- The Endo algorithm

1. ASTM algorithm

This algorithm can be realized as composed by the following three steps:

- Compare 3 consecutive ranges
- If the middle range is smaller than the bounding range extract this range otherwise move ahead one range
- Repeat

In particular, the second point, in term of mathematical relations, referring to Figure 62 can be expressed so that, the intermedia range can be removed if:

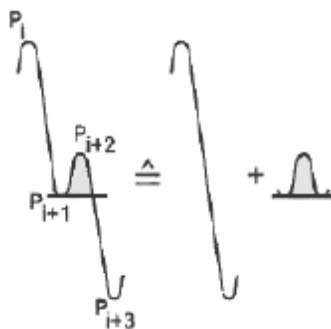


$$P_{i+2} > P_i$$

$$P_{i+3} > P_{i+1}$$

Figure 62: Up range Rainflow decomposition

Obviously the method can be used also if the intermedia load occurs in a descending load range. In this case we must consider:



$$P_{i+2} < P_i$$

$$P_{i+3} > P_{i+1}$$

Figure 63: Down range Rainflow decomposition

Then the range of the residue must be considered separately at the end and stored in the 2D matrix.

### 2. Endo Algotim

This algorithm has been developed by two Japanese researchers. The way in which they start to develop this method is quite curios and merit to be mentioned here. They note a flow of rain water on the roof of a Pagoda (Figure 64) which can be associated with a load sequence rotate of 90° as reported in figure.

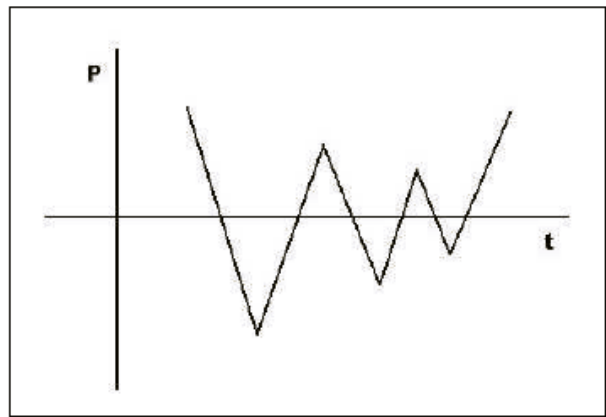


Figure 64: Basic idea behind the Endo Rainflow algorithm

The algorithm can then be described as follow. First of all we need to rotate of 90° the load sequence  $P(t)$  so that the time axis is downward. At this time we imagine that some water flow starts from each of the “pagoda roofs” as in figure (Figure 65). Then each of these flows will be stopped when:

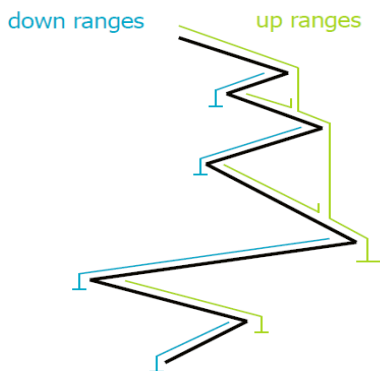


Figure 65: Endo algorithm concept

- Meet another flow coming from the pagoda roof above if this one has a minimum that is lower
- Arrive at a point at which meet a flow coming from above started from a pagoda roof with a lower minimum



Applying one of these algorithms, at the end, we will always obtain a reduced load sequence where the highest and lowest points are linked even if they are widely spread in the original load sequence.

The important thing to note here is that, at this point, the sequence in which the counts were made is lost by these counting procedures. In fact, the matrix introduced before, collects number of ranges between successive peaks but information about range sequence is lost. However, as we know from consideration introduced in Chapter 3, sequence is an important feature for fatigue damage and so, the way in which each of this counted range will be considered strongly affect final results obtained in term of crack growth applying one of the methods introduced in the previous chapter.

The loss of sequence is one of the most important difficulties in load spectrum analysis, especially because a new sequence must be generated to use these results in damage tolerance analysis.

## **Stress history generation**

No load experiences are available for a new structure. For this reason fatigue crack growth analysis must be based on past experience and then projected into the future, introducing uncertainties in crack growth prediction. Now, before to see in deeper detail how past experience are currently considered in damage tolerance analysis, let us try to understand how a stress history for a new structure under design is generally obtained.

Doing this, a particular rule is played by the exceedance diagram introduced before. These diagrams are obtained from similar structure in service (See following paragraph) and are given for a certain time period that can be expressed in terms of: hours, years, flights, etc.

As described above on these diagrams one can identify the number of time that a certain peak level is exceeded in a certain considered period. Once the exceedance diagram is known, positive and negative excursion must be combined and sequenced. Of course for a logical purpose, a down-gust must be followed by an up-gust of approximately equal magnitude, otherwise air would disappear in space. Hence, a priori, a combination of positive and negative excursion of the same frequency of occurrence is quite realistic, the content of the stress history is known but the sequence must still be determined.

In order to generate a sequence, different cases must be considered. First of all, if retardation phenomena do not have a so large influence on the crack growth, sequencing of stresses is rather irrelevant. In fact, if this phenomenon is not taken into account, fatigue crack growth analysis without load interaction can be considered using relation introduced in the previous chapter. Looking at that relation can be understood how the predicted crack growth is quite insensitive to load sequence. Of course, this type of conclusion is not anymore possible if load interaction is expected to play an important role in crack growth. In these cases, load sequences becomes of large importance. In many computers analysis, the load is simply applied in a random way. However, it actually does not provide a correct description of the real crack growth behaviour because, in reality, service loading is defined to be *semi-random*. In fact, as can be imaged, not all flights are of the same severity, so that an aircraft in its life will experience smooth flights and occasionally some more severe flights. For a transport aircraft, it is primary dependent from weather condition. This underline that, the loading sequence is no truly random but periods of high loads occur occasionally during the life of the structure. As a consequence of these observations, retardation effect will be much less. Fatigue crack growth analysis must account for these effects and so, a mixture of flights at different severity must be applied. This is the so called *semi-random* load sequences. In Figure 66 an example of semi-random sequence is reported.

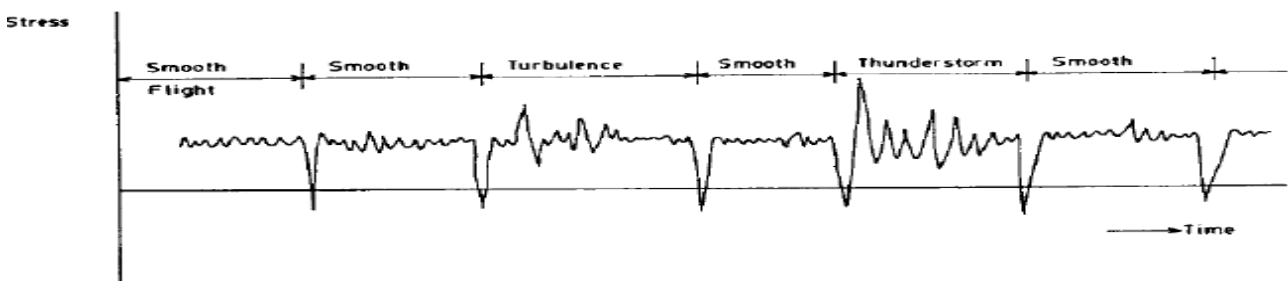


Figure 66: Typical Semi-Random load sequence

What should be done, in a computer analysis, is to apply periods of different severity in a random way whit range in each period applied randomly. Results obtained, will be extremely different from the application of random ranges from the first to the last cycle.

Now that the concept of semi-random sequence has been introduced the question is: how a semi-random load sequence can be generated?

First of all to answer at this question, let us consider what is currently done in aerospace field and then we will introduce observations that are possible considering our developed methodology of proceeding.

As mentioned before, considering that, today standardized load sequences (see following paragraph for deeper detail) expressed in term of exceedance diagram are used to design against fatigue applying damage tolerance concepts, an important rule is played by the exceedance diagram itself. In fact, mild and severe periods can be generated by observing that the exceedance diagram for each period is characterized by an exceedance diagram of the same shape of the total one but with a different slope that, for this reason is named *severity factor*. Of course, the theoretical sum of each of these considered exceedance diagram for each period must return the total exceedance diagram, i.e. that one containing the entire load period.

How we have to proceed to create an exceedance diagram for each period starting from the general one?

First of all the total number of periods and the total number of exceedance of the complete diagram must be considered. With these values the total number of exceedance for each period can be simply obtained:

$$Exceedance\ per\ Period = \frac{Total\ number\ of\ exceedance}{Number\ of\ periods} \quad (eq. 57)$$

Now, the way to proceed can be explained as follow. Knowing the total number of exceedance per period (result coming out from the previous relation) and the number of the highest level, the exceedance diagram for each period can be drawn. In detail, the number of time that the severest period occurs will be equal to the number of time that the highest level is exceeded. It is because each of the exceedance diagrams is characterized by only one peak exceeding the highest level. The exceedances for each of the other levels can be read from this diagram. Reading the number of time that the other levels are exceeded is extremely important because, the number of time that the second (in order of severity) diagram will be present, depend upon the difference between the total number of exceedance of these level in the total case and the number of times that this level has already been exceeded in the severest diagrams (those already drawn). Hence, the way to build up this second diagram is the same of that one before. Starting from the maximum number of exceedance per period and considering that we want only one peak above

the maximum level that, in this second case, is represented by the second (in absolute) highest load level. Proceeding in this way for each of the other level we can understand why each exceedance diagram is characterized by a different severity factor (slope). To get a better idea about the way to proceed to get different periods with different intensity in order to generate a semi-random load sequence, as described up to now, following figure (Figure 67) can be useful.

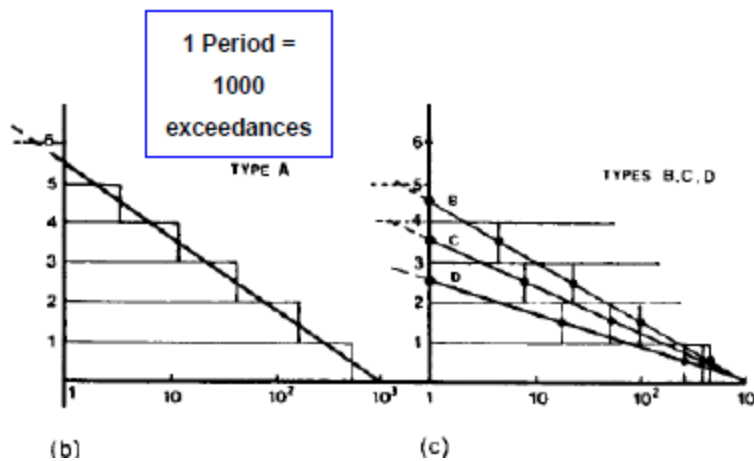


Figure 67: Semi random Stress History generation

Proceeding in this way, at the end, we will get a number of different flight types characterized by different severity that is equal to the number of level in which the spectrum has been divided to carry out the counting methods described before. Then, each of these flights types will be repeated a certain number of time depending on how many times the corresponding maximum level is exceeded in the total exceedance diagram.

Considering now our developed methodology based on parameters coming out from flight simulator (Chapter 5), the way to proceed to get a semi-random load sequence is easier. In fact, the flight dynamic simulator has been designed appositely to provide the possibility to self-simulate typical flights representing the operational life of the airplane to be designed. It means that load history of different severity can be already considered once the program of the flight to be simulated is programmed. Details on how this real semi-random load sequence is then generated are described in Chapter 6 where developed algorithms used are also reported. Here, what is interesting to note, is just how a first simplification on the entire process eliminating also strong assumption on the shape of the exceedance diagram, needed to obtain a semi-random load sequence performing the method described before, are achievable with the application of our methodology.

As introduced before and as it is more clear now that how the methods works has been described, larger is the number of levels, and higher will be the accuracy that can be obtained. In fact, higher is the number of level in which the spectrum has been divided and smaller will be the error in the position of the considered peak inside a certain interval. In deeper detail, regarding the accuracy has been demonstrated how, to get a sufficiently accurate result, a good choice for the number of levels lies in between 10 and 12. A larger number of levels increase the computational time required to perform the complete analysis without any large improvement in the achievable accuracy. This is also represented in the following figure (Figure68). Here accuracy is represented in term of fatigue life resulting from crack growth analysis. As can be seen, for a number of levels larger than 10, the difference in obtained fatigue life is not so large.

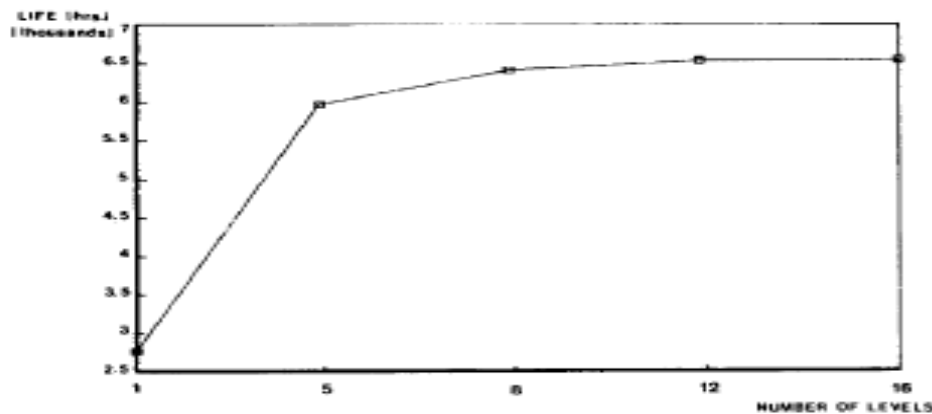


Figure 68: Accuracy variation with different number of load levels

### Load Spectrum generation

All the previous observations done about load spectrum, description and processing methods are based on the assumption that, the load spectrum itself, is provided to the designer and it is referred to a structure already in service, which is expected to undergo similar loads of that one to be designed. As said at the beginning of this chapter, the knowledge of the load spectrum is a key point to perform damage tolerance analysis. This type of information, can be obtained in different way like for example, from estimation of expected load or physical measurement on structure that are already in service. Physical measurements, considering the average life of an aircraft (20 years) can be extremely expensive not only from an economical point of view but also

in term of time needed for designing. However, due to the fact that the knowledge of the loading spectrum is needed for fatigue crack growth analysis and these loads must be as much as possible representative of the loading of the structure in service, at the presence time, it is generally accepted that fatigue test and, even more, analysis under constant amplitude or blocked loading insufficiently represent the interaction effects between individual load cycles of a more realistic loading sequence. Together with the development in data processing methods and testing capabilities, variable-amplitude loading is now widely appreciated in fatigue testing and analysis.

In order to produce reliable fatigue life or crack growth data for a specific structure, test loads are required to simulate the anticipated loading for that structure as accurately as possible. Anyway, if on the other hand, the aim is to evaluate materials, fabrication technique, design solutions, surface treatments, analytical prediction models etc., the demand for similarity between service loading and testing loading is not so stringent.

Since 20 years ago, all these observations related with service load sequence, were realized within some of the European aeronautical institutes, a number of international working groups have been acting, which has led to the definition of the so called loading standards so that, the economical and time costly operation to generate these load spectrum can be reduced. Moreover, we need to consider that, the definition of a load time history for a flight simulation test, as comes out also from all the previous observations, is not as simple as it is for a constant amplitude test. Load spectra and load sequences have to be specified. These are the reasons why the definition of loading standard has been carried out for:

1. Fighter Aircraft lower wing skins (FALSTAFF)
2. Transport Aircraft lower wing skins (TWIST, Mini-TWIST)
3. Helicopter rotor baled (Helix,Felix)
4. Tactical aircraft cold-end engine discs (Cold TURBINSTAN)
5. Tactical aircraft wing skin composites (ENSTAFF)

The FALSTAFF (Fighter Aircraft Loading standard For Fatigue) Loading sequence was developed to be representative of the stress in the lower wing surface in tactical aircraft and is based on load factor and strain measurement from five such aircrafts.

The ENDSTAFF (Environmental FALSTAFF) loading sequence was developed to be representative of the stresses and environmental condition expected to be experienced by composite structures in service in a modern fighter aircraft. It combines the FALSTAFF loading sequence with a series of

associated temperature cycles and a defined moisture content because as we know environmental concepts are particularly important when talking about composite materials.

Results are reported on an exceedance diagram expressed as a function of the load factor. An example of how these results are represented has been reported in figure (Figure 69).

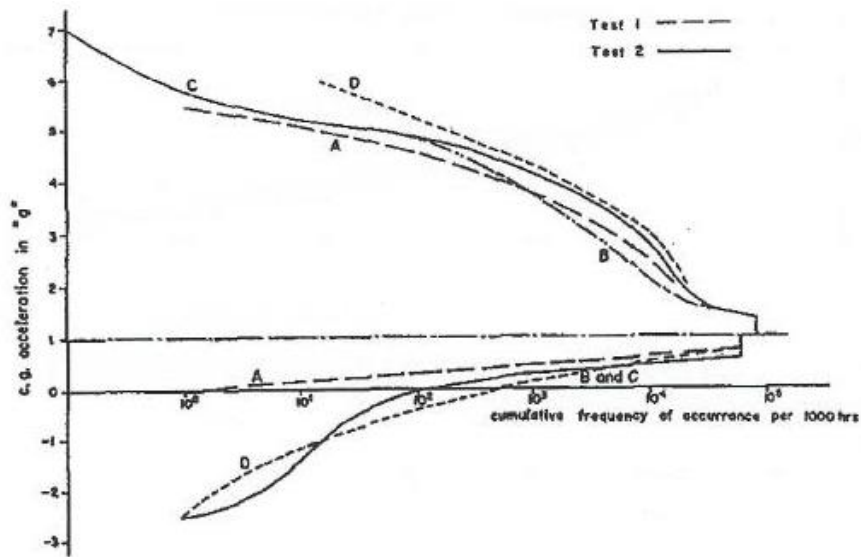


Figure 69: FALSTAFF standardized loading sequence

Helix and Felix are standard loading sequences for the main rotor of helicopters for hinged or free (semi-rigid) rotors respectively. They are based on the measurement of loads taken at the position of maximum flap-wise bending moment on the rotor. In the case of articulated rotors this has been found to be at approximately half rotor radius on the lower surface of the blade. In the case of semi-rigid rotor it has been found to be at the lower surface of the blade root

The standard load sequence TWIST (transport wing standard) has been developed by the National Lucht en Ruimtevaart Laboratorium. It is considered as a representative loads sequence for transport aircraft wing tension skins (lower wing skin) at the root of a transport aircraft, since this has been found to be typically the most critical location.

Anyway an important question of the development of a load sequence is the definition of the number of flights in the repetitive block defining the magnitude of the highest load included. A general rule could be to consider a number of flights equal to one tenth (if the number of level is ten) of the anticipated time life. For example if the design service objective value is 40.000 flights the repetitive block must be of 4.000 flights. The Design Service Objective (DSO) is defined as the minimum period of service during which primary structure is designed to be essentially free of detectable fatigue cracks, with a high degree of reliability and confidence.

The sequence TWIST includes 40000 different flights. There are ten types of flight, ranging from “stormy” (A) to “tranquil” (J) conditions. Ten different gust load levels are considered. It also means considering what previously pointed out the load spectrum to obtain this exceedance diagram has been divided into ten severity levels.

The TWIST spectrum is presented as a function of  $S/S_{mf}$  where  $S_{mf}$  is the mean stress pertaining to undisturbed flight at 1g. (Figure 70)

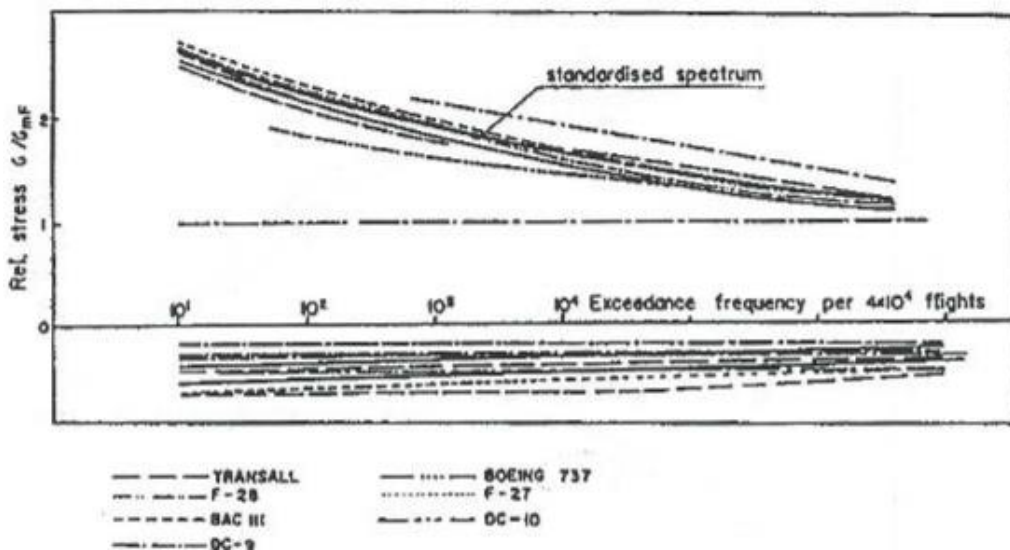


Figure 70: TWIST standardized load sequence

In a different way with respect FALSTAFF (standard exceedance diagram for fighter aircraft) in case of transport aircraft, the highest load cycles are associated not with manoeuvres but with the peak-to-peak ground-air –ground (GAG) cycles associated with severe gusts.

TWIST is generally used as basic load sequence and includes approximately 100 load cycles per flight. This is a relatively high number that can cause a long testing time. This is also the reason why new shortened version of TWIST indicated as mini-TWIST has been developed. The main difference is that Mini-TWIST contains considerably less load cycles of the smallest amplitude resulting in approximately 15 loads per cycle. So Mini-TWIST is a shorter version of TWIST for use where limited testing time prohibits the use of the full TWIST. However, small loads are removed also from FALSTAFF load history which leads to Short-FALSTAFF.

On the other hand, always with the purpose of reducing the testing time these sequences can also be reduced applying a certain truncation process whose meaning has been already defined before. In general, a good choice as truncation level could be that level exceeded on an average of 10



times in an aircraft life time. Anyway it is just a reasonable choice but still remains an arbitrary choice. Truncation of high-amplitude cycles was applied to the TWIST and Mini-TWIST load history. In literature, coming from experimental results, can be found many observations about standardized load sequences that have been introduced. The most important ones can be summarized as follow:

1. In most case the fatigue life, both crack initiation and macro-crack growth, under MiniTWIST loading was considerably larger than for TWIST. Life ratio's is in the range of 1-3. So apparently low amplitude cycles can contribute significantly to fatigue damage.
2. In most cases the fatigue life, both for crack initiation and macro-crack growth, under short FALSTAFF were approximately the same as for FALSTAFF. It means that contrary to what happen for Transport aircraft, small load cycles do not significantly affect crack growth.
3. Some exceptions to conclusions of the previous two points were found and can be attributed to plasticity and crack closure effects. Anyway conclusions before reflect the general trend.
4. Truncation of the TWIST and Mini-TWIST load spectrum at lower amplitude level implied a significantly slower crack growth due to significant crack growth retardation introduced by severe flights
5. The previous conclusion seems to be applicable also to other load spectrum history with similar shape. It means that these conclusions can be believed relevant to planning of load time histories for flight simulation tests. Anyway judgement choices on the load history have to be made and then it is helpful to know and to understand physical mechanism of trends observed.

## **The born of our idea, first concepts**

Considering that, results coming out from damage tolerance analysis, whose steps has been introduced at the beginning of this thesis, are strictly dependant on the considered load spectrum, is clear that it must be as much as possible similar to what is expected to obtain on the structure in service, related with manoeuvres and environment in which the airplane to be designed is expected to operate.

Now, standardized load sequences, introduced in the previous paragraph, are currently used in aeronautical design, representing a good way to obtain these spectrums avoiding large experimental cost. However, at the same time, they are quite general and need to be continuously updated or modified to increase their validity or to extend their applicability. This is the key point on which our work is based.

The idea to create a load spectrum for the aircraft to be designed representing as close as possible loads that are expected on its structure and that is not as general as the standardized load spectrum has been the concept on which our work is centred. Moreover, reduction of cost in both way, economical and time, is another of the key points of our focus.

Based on this purposes, the idea has been to develop a flight dynamic model that can be used to simulate manually or automatically all the typical and also critical manoeuvres at which the airplane to be designed is expected to be subjected during its operational life. In addition, the flight simulator that has been created is also capable to simulate possible environmental conditions such as turbulence in which the airplane is expected to operate. Anyway, for the moment the question is not related with how this flight simulator has been built up, it will be described in deeper detail in the following chapter but rather here the question should be: which are the main aircraft parameters that are used to build up the previously mentioned simulator? These parameters are those like the main geometry characteristics (wingspan, chord, length, fuselage diameter etc.) that could be known also from a first design approach, but, at the same time, they are also those parameters like stability and control derivatives for which a much more deeper knowledge of the aircraft dimensions is needed to be accurately estimated using, as we will describe, the Digital Datcom software. A so deep knowledge of dimensions of an aircraft that must still be designed could be difficult to obtain. This is the reason why, in order to build up our flight simulator, which will then be used to simulate load on the structure, we will use those parameters coming from an aircraft that is extremely similar to that one that we are going to design.

In the present thesis, the developed flight dynamics model, which is the starting point to develop our idea, is based on the previous said parameter of the Boeing C-17 Globemaster III (Figure 71).



Figure 71: Boeing C-17 Globemaster III

The reason why this is the aircraft that has been considered in our case can easily be explained considering that many dimensions were available for this type of aircraft, reducing the work required to search all these data. In fact as will be clearer in the following chapter, where an introduction to the Digital Datcom program is considered, a lot of dimensions are needed about the entire airplane to find all those values that are fundamental in the development of the flight dynamic model.

Considering that, as said before, the model should provide the load spectra for an aircraft that is as much as possible similar to that one that we are going to design, our model could be used to design structure of an aircraft that, in the following of this thesis, for simplicity of notation, will be called C-18 supposing this one as a new design of the Boeing C-17 .

However, at this point, should be also clear that once the methodology has been developed and verified, the airplane considered is no longer interesting because changing the aircraft characteristic parameters present in the model, this can be used for whatever other kind of aircraft.

As said, in the following chapter we will firstly introduce the 6DOF flight dynamic model built up in Matlab/Simulink environment. Then in the remaining chapter, the developed methodology for

damage tolerance analysis and related results will be explained in deep. Simple load conditions (CA loading) will then be used to validate obtained results.

## 5 FLIGHT DYNAMIC MODEL

The intent of this chapter is to introduce the main concepts needed to understand the developed 6DOF flight dynamic model and provide a description of the layout of the model that has been created in Matlab/Simulink environment. In particular, a key point in the use of this model for our purpose is a deep understanding of how forces and moments acting on the airplane have been simulated. Particularly important will be consideration on the main parameters that we need to define in order to relate these forces and moments with each particular flight condition. For this purpose after a quick introduction of the basic concepts of flight dynamic, a description of capabilities and limitations of the Digital Datcom software (program used to estimate aerodynamic stability and control characteristic of the aircraft, the main parameter mentioned before) will be introduced.

The dynamic model has been created with the purpose to simulate all types of flights condition at which the aircraft under design could be subjected during its operational life both, manually fly the aircraft (using external Joystick inputs) or automatically (reference trajectories in this case need to be defined and provided to the model). For this reason a short description of the designed control system is also given to provide a complete overview on the capabilities of this dynamic model.

Then at the end of this chapter the main block used to makes the simulation as much as possible real will be described in detail.

In the last paragraph examples of results in term of trajectory achievable with this simulator are presented.

## Basic Flight Dynamic concepts

Motion through the earth's atmosphere entails aerodynamic forces and moments.

Some understanding of coordinate transformation is required for navigation around the earth. Coordinate transformations and the use of appropriate reference frames are vital parts of the aircraft simulation environment used in this project. In the following will be introduced the relevant parts of flight dynamics and notations used in this work

### *Coordinate frames and notations*

Terrestrial navigation of aircraft involves the use of reference frames and coordinate transformations [4]. The main reference frames for aircraft navigation and control are denoted by the following abbreviations and notations:

ECI: Earth-centered inertial reference frame. It is a nonrotating coordinate system in which Newton's laws of motion apply. The origin of the ECI is located at the centre of the earth.

ECEF: Earth-centered, Earth-fixed frame. It also has its origin fixed to the centre of the Earth but its axes rotate relative to the inertial frame ECI

NED: it is a geographic coordinate system that has its axes aligned North, East, Down where down points normal to the Earth's surface. The NED frame moves with the vehicle and has its origin is fixed in the centre of gravity of the airplane.

BODY: This reference frame represents a vehicle fixed coordinate system which has its origin coinciding with the origin of the NED frame. The origin can be choose as the vehicle centre of mass, and the coordinate axes aligned with the vehicles vehicle reference directions. A fundamental characteristic of the body axis reference frame is that once the inertial tensor of the aircraft with respect to these axes has been defined it remains constant during the evolution of the motion being the axis fixed to the body. This observation will result particularly important in the development of the equation of motion

STABILITY: it is a particular body axis frame where the x direction is directed as the longitudinal component of the velocity vector of the vehicle with respect to the atmosphere at the initial considered condition.

WIND: This reference has its origin coincident with the origin of the body frame but in a different way with respect to the body axes it is not a fixed frame and the X-axis is always directed as the velocity vector of the vehicle relative to the atmosphere.

The aircraft equation of motion that we are going to present in the following chapter, that are the base on which the model is built up, requires coordinate rotation matrices between ECI, ECEF and NED. A plane rotation around the z-axis is made between ECEF and ECI, using the following rotation matrix:

$$R_i^e = \begin{bmatrix} \cos\mu & \sin\mu & 0 \\ -\sin\mu & \cos\mu & 0 \\ 0 & 0 & 1 \end{bmatrix} \quad (eq. 59)$$

where  $R_i^e$  represents a rotation from ECI to ECEF, and  $\mu$  is the rotation angle.

After the above rotation has been made, the transformation from ECEF to NED can be achieved as shown below:

$$T_{EV} = \begin{bmatrix} -\cos\tau\sin\lambda & -\sin\tau & -\cos\tau\cos\lambda \\ -\sin\tau\sin\lambda & \cos\tau & -\sin\tau\cos\lambda \\ \cos\lambda & 0 & -\sin\lambda \end{bmatrix} \quad (eq. 60)$$

where  $\lambda$  is the latitude and  $\tau$  is the longitude.

In addition to the earth-related coordinate transformations stated above, the aerodynamic forces and moments on an aircraft are produced by relative motion with respect to the air and depends on the orientation of the aircraft with respect to the airflow. To be able to specify the aerodynamic forces and moments, two orientation angles (with respect to the relative wind) are needed. The aerodynamic angles used are the angle of attack ( $\alpha$ ) and the sideslip angle ( $\beta$ ), defined as:

$$\alpha = \text{atan}\left(\frac{w}{V_t}\right) \quad \beta = \text{atan}\left(\frac{v}{V_t}\right) \quad (eq. 61)$$

Where:

$$V_t = \sqrt{U^2 + V^2 + W^2} \quad (eq. 62)$$

is the total speed of the aircraft, consisting of the longitudinal velocity  $U$ , lateral velocity  $V$ , and vertical velocity  $W$ . Angles  $\alpha$  and  $\beta$  define the rotations necessary to transform BODY coordinates to aircraft's stability-axes and wind-axes coordinates respectively. The rotation matrices from BODY to stability and stability to wind axes are:

$$T_{SB} = \begin{bmatrix} \cos\alpha & 0 & \sin\alpha \\ 0 & 1 & 0 \\ -\sin\alpha & 0 & \cos\alpha \end{bmatrix} \quad (eq. 63)$$

$$T_{WS} = \begin{bmatrix} \cos\beta & \sin\beta & 0 \\ -\sin\beta & \cos\beta & 0 \\ 0 & 0 & 1 \end{bmatrix} \quad (eq. 64)$$

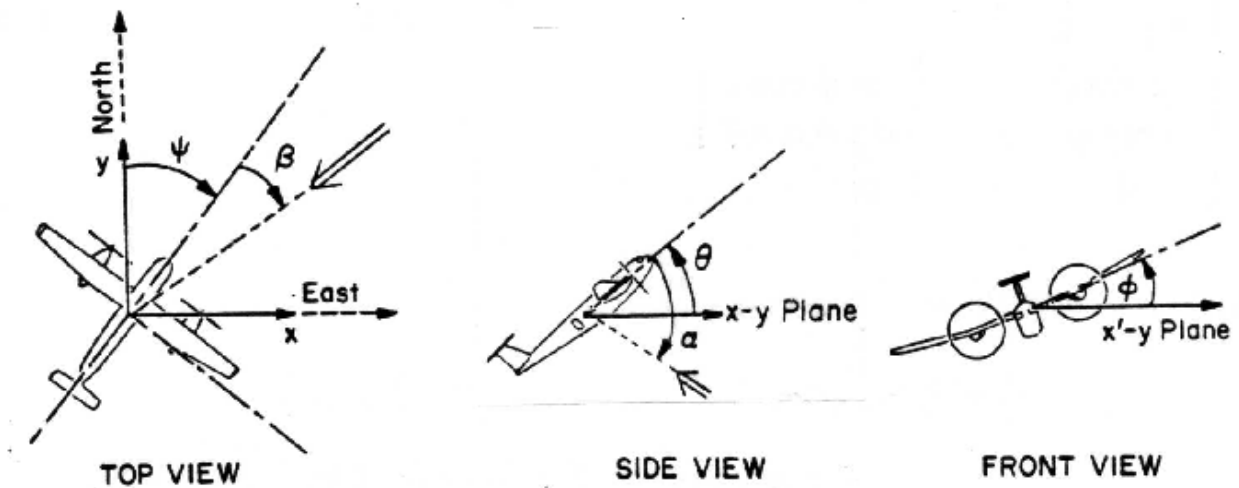


Figure 72: Euler and Aerodynamic angles

Combining these rotation matrixes, transformation from Body axis to wind axis is defined by the following matrix:

$$T_{WB} = \begin{bmatrix} \cos\alpha\cos\beta & \sin\beta & \sin\alpha\cos\beta \\ -\cos\alpha\sin\beta & \cos\beta & -\sin\alpha\sin\beta \\ -\sin\alpha & 0 & \cos\alpha \end{bmatrix} \quad (eq. 65)$$



Applying this rotational matrix to the wind axes velocity vector  $[V_t, 0, 0]^T$ , relationship between velocities in BODY and wind axes can be written:

$$U = V_t \cos\alpha \cos\beta \quad (\text{eq. 66})$$

$$V = V_t \sin\beta \quad (\text{eq. 67})$$

$$W = V_t \sin\alpha \cos\beta \quad (\text{eq. 68})$$

It is worth noting that aerodynamic forces such as lift, drag and cross-wind are naturally defined with wind-axes coordinates and therefore make calculations in the wind-axes frame is desirable. Stability-axes coordinate system on the other hand is used for analysing the effect of perturbations from study-state flight. In addition, positions of the aircraft are generally described relative to inertial reference frame while the linear and angular velocities are conveniently expressed in the body-fixed coordinate system. The need for flexibility and the convenience of calculations in different coordinate systems make the above coordinate transformations a natural part of the broad field of Guidance, Navigation and Control.

### ***Equation of motion, forces and moments***

The equations of motion can be, in principle, written in each of the previous introduced reference frame. In particular, in our model, the core is represented by a Simulink block using equations of motion in wind axis. For this reason what we are going to present now are equations of motion expressed in wind-axis. In particular, as can be expected from the observation done before on the inertial tensor, which remains constant in body axis, momentum equations will be derived here. Now, before to write down the complete set of the equations of motion, we will present separately the force equations in wind axis and the momentum equations in body axis.

### ***General equations***

The theoretical approach in the principal flight characteristic of an aircraft could be the use of an appropriate mathematical model in which can be explicit the dependence of the characteristic of motion of the vehicle itself with its inertial, propulsive and aerodynamic characteristic.

A basic mathematical model, as that one that has been built up for our purpose, can be obtained considering that aircraft behaves like a rigid body. In fact, equations coming out under this assumption are correct to evaluate a large portion of the flight characteristic of the considered airplane but they are not enough when we are in presence of elastic deformation of structural elements that are able to generate not negligible force and moment variation. Development of a model that takes into account also these phenomena can be considered as an advanced work. For this reason, for the moment, our attention will be focused in the generation of a six degree of freedom model based on the assumption of rigid body.

In case of rigid body, the first and second cardinal equation of mechanics, taking as reference an inertial frame are of the form:

$$F = m \frac{dV}{dt} \quad (eq. 69)$$

$$M = \frac{dH}{dt} \quad (eq. 70)$$

Where, with F and M we have indicated the resultant of forces and moments, with V the velocity vector of the centre of gravity and with H the moment with respect to the centre of gravity of the angular moment.

An important consideration is represented by the link between temporal derivative of a vector with respect a fixed reference and analogues temporal derivative of a vector with respect to a rotating reference with angular velocity  $\omega$ . Considering T as the general absolute vector, relation between these two temporal derivative can be written as:

$$\left(\frac{dT}{dt}\right)_{Fixed} = \left(\frac{dT}{dt}\right)_{Mobile} + \omega \times T \quad (eq. 71)$$

So, if we substitute these relations in the previous ones, we get the more general force and moment equations:

$$F = m \left[ \left(\frac{dV}{dt}\right) + \omega \times V \right] \quad (eq. 72)$$

$$M = \left(\frac{dH}{dt}\right) + \omega \times H \quad (eq. 73)$$

**Force equations in wind axis**

In order to derive a general expression for force equations in wind-axis let us consider first of all a derivation of this equation in vertical reference frame (NED) introduced before.

As previously remembered, the NED reference frame has the origin in the centre of gravity of the airplane and it moves with this: there is no relative motion between the vehicle and the reference frame, named Fv.

The angular velocity  $\omega$  of the tern Fv will be in general given by:

$$\omega = \Omega_e + \omega_v \quad (eq.74)$$

Then the absolute velocity of the centre of gravity of the vehicle will be expressed as:

$$V = \left(\frac{dR}{dt}\right)_{Fv} + (\Omega_e + \omega_v) \times R = \left(\frac{dR}{dt}\right)_{Fv} + \Omega_e \times R + \omega_v \times R \quad (eq.75)$$

Considering that, the term

$$\left(\frac{dR}{dt}\right)_{Fv} + \omega_v \times R \quad (eq.76)$$

represents the velocity of the centre of gravity relative to the Earth frame evaluated in the wind axis reference frame, and remembering (eq.72) force equation can now be written as:

$$F = m \left[ \frac{d}{dt} (V_e + \Omega_e \times R)_{Fv} + (\Omega_e + \omega_v) \times (V_e + \Omega_e \times R) \right] \quad (eq.77)$$

Then, after some algebraic manipulation using vector derivative properties, the previous equation can be written in its most general form as:

$$F = m \left[ \left(\frac{dV}{dt}\right)_{Fv} + 2\Omega_e \times V_e + \Omega_e \times (\Omega_e \times R) + \omega_v \times V_e \right] \quad (eq.78)$$

Now considering that, also the wind-axis reference frame has its origin fixed with the centre of gravity of the airplane, this equation can be extended to be applied also to this reference frame considering that ,now, the angular velocity can be expressed as:

$$\omega = \Omega_e + \omega_v + \omega_w \quad (eq.79)$$

Now, with the purpose of simplifying the equations without losing accuracy some assumptions can be introduced. The two most important are:

- Flat Earth
- No rotate Earth

Considering these simplifications the previous relation for the angular velocity  $\omega$  becomes:

$$\omega = \omega_w \quad (eq.80)$$

So that now, the general force equation derived before can be written as:

$$F = m \left[ \left( \frac{dV_e}{dt} \right)_{Fv} + \omega_w \times V_e \right] \quad (eq.81)$$

In particular this equation, explicating the gravitational force can be written in a compact matrix form as:

$$\{X\}_{FW} = m(\{\dot{V}_e\}_{FW} + \{\tilde{\omega}\}_{FW}\{V_e\}_{FW} - [T_{vw}]^{-1}\{g\}_{Fv}) \quad (eq.82)$$

Where:

$T_{vw}$  is the rotational matrix that allows evaluation of components expressed in NED reference frame like the weight force in wind axis considering the Euler angle between the two frames defined as:  $\Phi_w, \theta_w, \psi_w$ .

$\tilde{\omega}$  is the so called Skewness and it is expressed as:

$$\tilde{\omega} = \begin{bmatrix} 0 & -R_w & Q_w \\ R_w & 0 & -P_w \\ -Q_w & P_w & 0 \end{bmatrix} \quad (eq.83)$$

Considering the definition of wind axis reference frame the equation before can be explicit as:

$$\begin{Bmatrix} X_W \\ Y_W \\ Z_W \end{Bmatrix} = m \left( \begin{bmatrix} \dot{V}_W \\ 0 \\ 0 \end{bmatrix} + \begin{bmatrix} 0 & -R_W & Q_W \\ R_W & 0 & -P_W \\ -Q_W & P_W & 0 \end{bmatrix} \begin{bmatrix} V_W \\ 0 \\ 0 \end{bmatrix} - [T_{vw}]^{-1} \begin{Bmatrix} 0 \\ 0 \\ g \end{Bmatrix}_{Fv} \right) \quad (eq. 84)$$

And its scalar components are:

$$X_W = m(\dot{V}_W + g \sin \theta_W) \quad (eq. 85)$$

$$Y_W = m(R_W V_W - g \cos \theta_W \sin \Phi_W) \quad (eq. 86)$$

$$Z_W = m(-Q_W V_W - g \cos \theta_W \cos \Phi_W) \quad (eq. 87)$$

Now, at these equation must be added other relation that allow obtaining the Euler angles  $\Phi_W, \theta_W, \psi_W$  between the frame Fv and Fw. These equations are derived from the so called kinematic equation.

### **Kinematic equations**

The kinematics involve the aircraft motion when the mechanisms (such as forces and moments) causing the motion are not regarded. Kinematic equations are therefore primarily used for translation, rotation and attitude representation. Kinematic equations in wind coordinate system with respect to NED can be expressed in terms of the Euler angles  $\Phi_W, \theta_W, \psi_W$ .

$$\begin{bmatrix} \dot{X}_E \\ \dot{Y}_E \\ \dot{Z}_E \end{bmatrix} = \begin{bmatrix} \cos \psi_W & -\sin \psi_W & 0 \\ \sin \psi_W & \cos \psi_W & 0 \\ 0 & 0 & 1 \end{bmatrix} \begin{bmatrix} \cos \theta_W & 0 & \sin \theta_W \\ 0 & 1 & 0 \\ -\sin \theta_W & 0 & \cos \theta_W \end{bmatrix} \begin{bmatrix} 1 & 0 & 0 \\ 0 & \cos \Phi_W & -\sin \Phi_W \\ 0 & \sin \Phi_W & \cos \Phi_W \end{bmatrix} \begin{bmatrix} U \\ V \\ W \end{bmatrix} \quad (eq. 88)$$

The aircraft attitude is determined by:

$$\begin{bmatrix} P_W \\ Q_W \\ R_W \end{bmatrix} = \begin{bmatrix} \dot{\Phi} \\ 0 \\ 0 \end{bmatrix} + \begin{bmatrix} 1 & 0 & 0 \\ 0 & \cos \Phi & -\sin \Phi \\ 0 & \sin \Phi & \cos \Phi \end{bmatrix} \begin{bmatrix} \dot{\theta} \\ 0 \\ 0 \end{bmatrix} + \begin{bmatrix} 1 & 0 & 0 \\ 0 & \cos \Phi & -\sin \Phi \\ 0 & \sin \Phi & \cos \Phi \end{bmatrix} \begin{bmatrix} \cos \theta & 0 & \sin \theta \\ 0 & 1 & 0 \\ -\sin \theta & 0 & \cos \theta \end{bmatrix} \begin{bmatrix} 0 \\ 0 \\ \dot{\psi} \end{bmatrix} \quad (eq. 89)$$

This gives:

$$\begin{bmatrix} \dot{\Phi}_W \\ \dot{\Theta}_W \\ \dot{\psi}_W \end{bmatrix} = \begin{bmatrix} 1 & \sin\Phi_W \tan\Theta_W & \cos\Phi_W \tan\Theta_W \\ 0 & \cos\Phi_W & -\sin\Phi_W \\ 0 & \sin\Phi_W / \cos\Theta_W & \cos\Phi_W / \sin\Theta_W \end{bmatrix} \quad (eq. 90)$$

### Moment equation in body axis

Indicating with  $I$  the inertial tensor of the vehicle with respect to a generic reference system, the angular moment  $H$  introduced before, can be expressed as:

$$\{H\} = [I]\{\omega\} \quad (eq. 91)$$

If we substitute this relation in the general moment equation above (eq. 73), it becomes:

$$\{M\} = \frac{d[I]}{dt}\{\omega\} + [I]\frac{d\{\omega\}}{dt} + [\tilde{\omega}]( [I]\{\omega\} ) \quad (eq. 92)$$

This relation is true for a generic reference system. Considering now a Body-axis reference frame, remembering that in this way inertial tensor  $I$  remain constant in time, the previous relation can be also expressed as:

$$\{M\} = [I]\{\dot{\omega}\} + [\tilde{\omega}]( [I]\{\omega\} ) \quad (eq. 93)$$

The plane  $X_b Z_b$  can be generally, on an aircraft, considered as a longitudinal plane of symmetry so that centrifugal inertial moments  $I_{YZ}, I_{ZY}, I_{XY}, I_{YX}$  can be considered equal to zero. As a consequence, the inertial tensor  $I$  will be of the form:

$$[I] = \begin{bmatrix} I_{Xb} & 0 & -I_{XbZb} \\ 0 & I_{Yb} & 0 \\ -I_{ZbXb} & 0 & I_{Zb} \end{bmatrix} \quad (eq. 94)$$

So now indicating as  $L_B, M_B, N_B$  components of the moment  $M$  in Body reference frame in an explicit form, the equation (eq.93) can be written as:

$$\begin{bmatrix} L_b \\ M_b \\ N_b \end{bmatrix} = \begin{bmatrix} I_{Xb} & 0 & -I_{XbZb} \\ 0 & I_{Yb} & 0 \\ -I_{ZbXb} & 0 & I_{Zb} \end{bmatrix} \begin{bmatrix} \dot{P}_b \\ \dot{Q}_b \\ \dot{R}_b \end{bmatrix} + \begin{bmatrix} 0 & -R_b & Q_b \\ R_b & 0 & -P_b \\ -Q_b & P_b & 0 \end{bmatrix} \left( \begin{bmatrix} I_{Xb} & 0 & -I_{XbZb} \\ 0 & I_{Yb} & 0 \\ -I_{ZbXb} & 0 & I_{Zb} \end{bmatrix} \begin{bmatrix} P_b \\ Q_b \\ R_b \end{bmatrix} \right) \quad (eq. 95)$$

Where scalar components are:

$$\begin{aligned} L_b &= I_{Xb}\dot{P}_b - I_{XbZb}R_b\dot{\phantom{R}} - I_{Yb}Q_bR_b - I_{XbZb}P_bQ_b + I_{Zb}R_bQ_b \\ M_b &= I_{Yb}\dot{Q}_b - I_{Xb}P_bR_b - I_{Yb}R_b^2 - I_{XbZb}P_b^2 + I_{Zb}R_bP_b \\ N_b &= I_{Zb}\dot{R}_b - I_{XbZb}P_b\dot{\phantom{P}} - I_{Xb}P_bQ_b - I_{XbZb}R_bQ_b + I_{Yb}Q_bP_b \end{aligned} \quad (eq. 96)$$

Looking at these relations we can observe how, on the dynamic behaviour of the vehicle, an important rule is played by the so called *gyroscopic effects*. They produce, for example in case of an angular velocity  $R_B$  around the Z axis, a roll moment  $L_B$  of intensity  $I_YQ_BR_B$ . In an analogues way if the vehicle has an angular velocity  $Q_B$  around the Y axis.

In general, the roll moment introduced by these gyroscopic effects can be seen in the previous equations expressed by the term:

$$(I_{Zb} - I_{Yb})Q_bR_b \quad (eq. 97)$$

In the same way, relations like these, could be used to consider gyroscopic effects also in the other directions.

Putting in evidence gyroscopic effects, the previous equations can also be expressed as:

$$\begin{aligned} L_b &= I_{Xb}\dot{P}_b + (I_{Yb} - I_{Zb})Q_bR_b - I_{XbZb}(R_b\dot{\phantom{R}} + P_bQ_b) \\ M_b &= I_{Yb}\dot{Q}_b - (I_{Xb} - I_{Zb})P_bR_b + I_{Yb}(P_b^2 - R_b^2) \\ N_b &= I_{Zb}\dot{R}_b + (I_{Xb} - I_{Yb})P_bQ_b + I_{XbZb}(R_bQ_b - P_b\dot{\phantom{P}}) \end{aligned} \quad (eq. 98)$$

*Aerodynamic and Thrust forces*

Up to now only gravity force has been considered in the derivation of the equations of motion. However, in addition to the weight vector  $W$ , external forces acting on the airplane depend on the aerodynamic force vector, here named  $R$  and thrust force vector named  $E$ . In particular, for the thrust produced by the engine is assumed to be parallel to the  $X$ -axis of the Body reference frame. Under this assumption it can be expressed as:

$$\begin{aligned} E_x &= X_T = F_T \\ E_y &= Y_T = 0 \\ E_z &= Z_T = 0 \end{aligned} \quad (\text{eq. 99})$$

Where the subscript T indicates thrust effects.

On the other hand, aerodynamic forces in body axes are expressed as:

$$\begin{aligned} R_x &= X_A \\ R_y &= Y_A \\ R_z &= Z_A \end{aligned} \quad (\text{eq. 100})$$

The size of the aerodynamic force  $X_A, Y_A, Z_A$  is determined by the amount of air diverted by the aircraft in different directions. The amount of air diverted by the aircraft mainly depends on the total velocity (or Mach Number  $M$ ), density of the airflow  $\rho$ , geometry of the aircraft, orientation of the aircraft relative to the airflow (angle of attack  $\alpha$  and sideslip angle  $\beta$ ), control surface deflection  $\delta_e$ , angular rates ( $P, Q, R$ ), altitude ( $h$ ) and propulsion system effect ( $T_c$ ). Then there are also other effects related with time derivative of angles but these ones are less prominent since, as mentioned before, it is assumed that the aircraft is a rigid body. Based on the above dependencies, the aerodynamic forces can be modelled in a general schematic form as:

$$\begin{aligned} X_A &= qSC_x(\alpha, \beta, h, M, \delta_s, \dots) \\ Y_A &= qSC_y(\alpha, \beta, h, M, \delta_s, \dots) \end{aligned}$$



$$Z_A = qSC_z(\alpha, \beta, h, M, \delta_s, \dots) \quad (\text{eq. 101})$$

Where S represents the wing area and q the dynamic pressure defined by:

$$q = \frac{1}{2}\rho V^2 \quad (\text{eq. 102})$$

Coefficients  $C_x, C_y, C_z$  are the so called aerodynamic *stability and control coefficients* that can be derived in different way:

- Wind tunnel
- Flight test
- Computer software programs

These coefficients, as can be also understood looking at the previous relations, represent the basic parameters for the estimation of the aerodynamic forces acting on an airplane.

Combining force equations introduced in this paragraph, aerodynamic and propulsive forces (converting these in wind axis) in the previous obtained force equations we get:

$$\begin{aligned} m(\dot{V}_W + g\sin\theta_W) &= X_A + F_T \\ m(R_W V_W - g\cos\theta_W \sin\Phi_W) &= Y_A \\ m(-Q_W V_W - g\cos\theta_W \cos\Phi_W) &= Z_A \end{aligned} \quad (\text{eq. 103})$$

### Aerodynamic Moments

The external moments that affect the aircraft motion are those due to aerodynamics. As it has been done for aerodynamic forces, also aerodynamic moments can be expressed in a general schematic form as:

$$\begin{aligned} L &= qSbC_l(\alpha, \beta, h, M, \delta_s, \dots) \\ M &= qScC_m(\alpha, \beta, h, M, \delta_s, \dots) \\ N &= qSbC_n(\alpha, \beta, h, M, \delta_s, \dots) \end{aligned} \quad (\text{eq. 104})$$

Where  $b$  is the wingspan and  $c$  is the mean aerodynamic chord of the aircraft's wing.

**Aerodynamic coefficients**

Forces and moments acting on a complete aircraft can be defined in terms of dimensionless aerodynamic coefficients [5]. These aircraft aerodynamic coefficients are functions of aerodynamic angles ( $\alpha$  and  $\beta$ ), Mach number ( $M$ ), and altitude ( $h$ ). In addition, control surface deflections ( $\delta_s$ ) and propulsion system effects ( $T_c$ ) cause changes in these coefficients. The dependence of an aerodynamic coefficient can therefore be written as:

$$C = C(\alpha, \beta, h, M, \delta_s, T_c, \dots) \quad (\text{eq. 105})$$

To model aerodynamic effects during aircraft manoeuvres, a differential equation model of the aerodynamic force and moment is required. A linear approximation of these differential equations model can be achieved considering aerodynamic forces and moments to be linearly proportional to the angular rates producing them. The resulting coefficients of proportionality are known as the *aerodynamic derivatives*.

Rolling, pitching and yawing moments are related with their coefficients through the equations shown in the previous chapter expressed in aircraft's BODY coordinates.

The baseline rolling-moment coefficient, for example, is primarily a function of sideslip angle, angle of attack, altitude and Mach number. Hence, it can be written as  $C_l(\alpha, \beta, h, M)$ . Rolling moments are created by sideslip and control action of ailerons and rudder. In addition damping moments resisting to rolling and yawing motion must also be considered. The rolling moment model is given by:

$$C_l = C_l(\alpha, \beta, h, M) + \Delta C_{l\delta\alpha}(\alpha, \beta, h, M, \delta_\alpha) + \Delta C_{l\delta r}(\alpha, \beta, h, M, \delta_r) + \frac{b}{2V_T} [C_{lp}(\alpha, \beta, M, h)P + C_{lr}(\alpha, \beta, M, h)R] \quad (\text{eq, 106})$$

Where  $C_{lr}$  is the roll-damping derivative, and the quantities  $\frac{Pb}{2V_T}$  and  $\frac{Rb}{2V_T}$  can be thought as dimensionless roll and yaw rates respectively. Linearized versions of the rolling moment

dependence on  $\beta$  and a control surface deflection can be achieved by linearizing around the origin, yielding:

$$C_l(\alpha, \beta, h, M) \approx C_{l\beta}(\alpha, h, M) \times \beta \quad (eq. 107)$$

$$\Delta C_{l\delta_s}(\alpha, \beta, h, M, \delta_s) \approx C_{l\delta_s}(\alpha, \beta, h, M) \times \delta_s \quad (eq. 108)$$

where  $C_{l\beta}$  represents the dihedral derivative determining static stability in roll while  $C_{l\delta_s}$  consists of roll control derivatives.

Similar formulations can be expressed also for pitching and yawing moment coefficients as follows:

$$C_m = C_m(\alpha, h, M, \delta f) + \Delta C_{m\delta e}(\alpha, h, M, \delta e) + \frac{c}{2V_T} [C_{mq}Q + C_{m\dot{\alpha}}\dot{\alpha}] + \frac{x}{c} C_L \quad (eq. 109)$$

$$C_n = C_n(\alpha, \beta, h, M) + \Delta C_{n\delta r}(\alpha, \beta, h, M, \delta r) + \Delta C_{n\delta a}(\alpha, \beta, h, M, \delta a) + \frac{b}{2V_T} [C_{nr}Q + C_{nr}R] + \frac{x}{c} C_Y \quad (eq. 110)$$

The corresponding linearized coefficients for yawing moment depending on  $\beta$  and for yawing moments and pitching moment depending on control surfaces are:

$$C_n(\alpha, \beta, h, M) \approx C_{n\beta}(\alpha, h, M) \times \beta \quad (eq. 111)$$

$$\Delta C_{m\delta_s}(\alpha, h, M, \delta_s) \approx C_{m\delta_s}(\alpha, h, M) \times \delta_s \quad (eq. 112)$$

$$\Delta C_{n\delta_s}(\alpha, \beta, h, M, \delta_s) \approx C_{n\delta_s}(\alpha, \beta, h, M) \times \delta_s \quad (eq. 113)$$

In the equation above (eq.109)  $\delta f$  represents the wing-flap deflection, which can be treated as a separate increment.  $C_{mq}$  is the so called pitch damping derivative, and the purpose of the  $\frac{x C_L}{c}$  is to correct for any x-displacement of the aircraft's centre of mass from the aerodynamic data reference position. The acceleration derivative  $C_{m\dot{\alpha}}$  is used to model delay in the change in side-wash felt at the tail of the fuselage and wings.

In the yawing moment coefficient equation,  $C_{nr}$  is the yaw-damping derivative while  $C_{n\beta}$  represents the yaw stiffness derivative.

Now, in the same way as done above for aerodynamic moments, different coefficients can be also defined for aerodynamic forces.

The total lift coefficient, for example, is primarily a function of angle of attack ( $\alpha$ ), Mach number ( $M$ ), altitude ( $h$ ) and elevator deflection ( $\delta_e$ ). In a general form it can be expressed as:

$$C_L = C_L(\alpha, h, M) + \Delta C_{L\delta e}(\alpha, h, M, \delta e) + \Delta C_{L\delta f}(\alpha, h, M, \delta f) + \frac{c}{2V_T} [C_{Lq}Q + C_{L\dot{\alpha}}\dot{\alpha}] \quad (eq. 114)$$

With the meaning of each term similar to what already introduced for the previous equations.

In the same way, Drag coefficient and Cross-wind coefficient can be written in a general form as:

$$C_D = C_D(\alpha, h, M) + \Delta C_{D\delta e}(\alpha, h, M, \delta e) + \Delta C_{D\delta f}(\alpha, h, M, \delta f) \quad (eq. 115)$$

$$C_Y = C_Y(\alpha, \beta, h, M, \delta r) + \Delta C_{Y\delta r}(\alpha, \beta, h, M, \delta r) + \frac{b}{2V_T} [C_{Yp}P] \quad (eq. 116)$$

Again the meaning of each term appearing in these relations is clear from the meaning of the term in those previously introduced. Moreover, linearization of the various terms present in these relations can be carried out in the same way as done before. For this reason these relations have not been reported here.

### ***How aerodynamic derivatives can be obtained?***

First of all the needed to know the values of these coefficients appears extremely important from the previous observations considering that, aerodynamic forces and moments are strictly dependant from the values assumed by these coefficients in each flight condition. In fact, as introduced before, these coefficients are a function of many different parameters and their estimation is generally a not simple task. However, this kind of estimation for each flight condition (hence considering different Mach Number, Altitude, Angle of Attack, Control surface deflections, etc.) can be done in different way:

- Wind tunnel test
- Flight Test
- Using computer software programs

In our case, estimation of these values has been carried out using this last method, particularly using the so called Digital Datcom software.

In the following paragraph, a quick description of how these parameters can be obtain using this program and a description of which are the main assumption and limitation related with this type of estimation will be addressed.

## **DIGITAL DATCOM**

### *The purpose of the Digital Datcom program*

In preliminary design operations, rapid and economical estimations of aerodynamic stability and control characteristics are frequently required. The extensive application of complex automated procedures is often prohibitive in term of time and computer cost in such type of design. Similar inefficiencies, accompany hand calculation procedures, which can required expenditure of significant man-hours, particularly if configuration trade studies are involved or if estimates are desired over a range of flight conditions. The fundamental purpose of the USAF Stability and Control Datcom is in providing a systematic summary of methods for estimating stability and control derivatives in preliminary design applications. Consistent with this philosophy, the development of the Digital Datcom computer program is an approach to provide rapid and economical estimation of aerodynamic stability and control characteristics.

Digital Datcom in particular calculates static stability and dynamic derivative characteristics. The computer program also offers a trim option that computes control deflection aerodynamic data for vehicle trim at subsonic Mach number.

### *Input and capabilities of Digital Datcom*

In general, Datcom treats the traditional body-wing-tail geometries including control effectiveness for a large variety of high-lift/control devices. High-lift/control output is generally in terms of incremental effect due to deflection. The Digital Datcom addressable geometries include the

“basic” traditional aircraft concepts but also unique geometries which are identified as “special” configurations. The geometry characteristics of the airplane must be introduced through an input file written with a specified language in Notepad++. Information about the language that should be used to create this input data file with all information required and also the meaning of each designation can be found on the Digital Datcom user manual [6].

The important consideration that must be underlined here is that the longitudinal and lateral-directional stability characteristics provided by Datcom program are expressed in stability-axis system. This observation is of significant importance because points out that, in the flight dynamic model where outputs of this program will be used to generate force and moments, axis transformation should be present to get these forces and moments represented in the reference frame system needed to solve equations of motion.

Another important observation needed in order to correctly use the Digital Datcom software to create a flight dynamic model is in considering that it does not rigorously treat aerodynamics in transonic speed regime (above Mach 0.7) and for this reason an interpolation between subsonic and supersonic solutions is often the best way to proceed.

Datcom body aerodynamic characteristics can be, anyway, obtained at all Mach number only for bodies of revolution.

Straight-tapered and not- straight-tapered wings, including effects of sweep, taper and incidence can be treated by the program. Dihedral influences are included in lateral-directional stability derivatives. All these parameters must be introduced in the input data file specifying their dimensions using their specific designation language described in [7]. Airfoil section characteristics are also a required input, although most of these characteristics may be generated using the Airfoil Section Module. The Airfoil Section Module can be used to calculate the required geometry and aerodynamic input parameter to define airfoil section. This module substantially simplifies the user’s input preparation. In particular we can say that an airfoil section can be defined in the input data file using one of the following methods:

- An airfoil section designation
- Section upper and lower Cartesian coordinates
- Section mean line and thickness distribution

In addition, Digital Datcom then requires, as input data, parameters needed to define different flight conditions. In particular this requirement can be satisfied by defining a combination of two

of the following parameters: Mach number, Reynolds number, velocity, altitude, pressure and temperature. In our case, reference inputs are Mach number and altitude. They are then used to calculate Reynolds number and the other parameters needed.

### *Limitation in the use of Datcom program*

Several operational limitations exist in Digital Datcom. These limitations are listed below without extensive discussions or justification.

- The forward lifting surface is always input as the wing and the aft lifting surface as the horizontal tail. This convention is used regardless of the nature of the configuration of the considered airplane.
- If airfoil sections are simultaneously specified for the same aerodynamic surface by a NACA designation and by coordinates, the coordinate's information will take precedence.
- Ground effect methods are only applicable to longitudinal stability parameters at subsonic speed
- Only one high lift or control surface can be analysed at a time. However, the effect of high lift and control devices on downwash is not calculated.
- Outputs related with rudder control surface are not provided.

For all the reason listed here, limitations on the use of Datcom method has probably been expected but should be remembered that it is just a good and economical solution to get aerodynamic control and stability characteristic of the aircraft for a preliminary design.

### *Digital Datcom outputs*

Digital Datcom outputs allow the aircraft coefficients to be plotted. In particular, they are used to run a six-degree of freedom flight dynamics model such as our flight simulator from which execution of standard flight manoeuvres are possible. The flight dynamic model has been built up using Matlab/Simulink environment as will be described in the following paragraph. However, should be noted here that outputs of this program is not only a list of all aerodynamic stability and control characteristic of the considered airplane. In fact, an additional output from this software is

a 3D representation of the model of the airplane, as it has been defined in the input data file. This 3D representation is very helpful in identifying errors in the input file. This 3D representation is so useful to get an idea about the model of the real aircraft that we are going to considering. Of course this should be as much as possible similar to the real one.

As introduced at the end of the previous chapter, the aircraft considered in our case, to develop the previously basically explained methodology, is a Boeing C-17 Globemaster III (Figure 72). The 3D representation of the model that we have obtained as output from the Digital Datcom program, once the input data file has been correctly created is reported in figure (Figure 73).

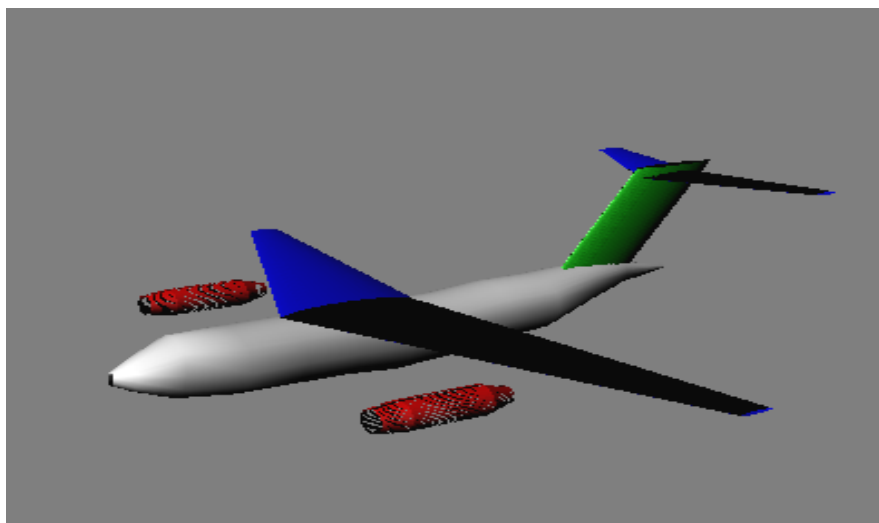


Figure 73: 3D Digital Datcom output

Of course the most important type of outputs of the program remains tables containing all the aerodynamic control and stability characteristic for all flight conditions. However as mentioned in a previous paragraph, Datcom is able to calculate characteristics only for one high-lift device and control surface at time and so for this reason many different tables, not only in term of flight condition (attitude, altitude, Mach) but also in term of considered high-lift/control surface will be obtained. In the figure below Figure 74, an example showing only a portion of one of these tables is reported. In particular here are shown results for some aircraft parameters for a flight condition characterized by an altitude of 19500 feet and a Mach Number  $M=0.5$ .



FLIGHT CONDITIONS								REFERENCE DIMENSIONS				
MACH NUMBER	ALTIITUDE	VELOCITY	PRESSURE	TEMPERATURE	REYNOLDS NUMBER	REF. AREA	REFERENCE LENGTH	MOMENT	REF. CENTER			
	FT	FT/SEC	LB/FT**2	DEG R	1/FT	FT**2	FT	FT	FT	FT	FT	
) .500	19500.00	519.44	9.9379E+02	449.194	1.0235E+08	3800.000	22.400	169.900	65.000	.000		
-----DERIVATIVE (PER RADIAN)-----												
ALPHA	CD	CL	CM	CN	CA	XCP	CLA	CMA	CYB	CNB	CLB	
)												
-16.0	.109	-1.408	.7763	-1.383	-.283	-.561	3.249E+00	-7.723E-01	-1.075E+00	1.883E-01	-7.500E-02	
-8.0	.041	-.781	.4366	-.780	-.068	-.560	5.428E+00	-3.170E+00			-9.421E-02	
-6.0	.028	-.580	.3250	-.580	-.033	-.561	5.742E+00	-3.324E+00			-1.034E-01	
-4.0	.019	-.374	.2133	-.375	-.007	-.569	5.788E+00	-3.341E+00			-1.129E-01	
-2.0	.014	-.170	.1006	-.170	.008	-.592	5.749E+00	-3.365E+00			-1.223E-01	
.0	.012	.033	-.0127	.033	.012	-.383	5.723E+00	-3.415E+00			-1.314E-01	
2.0	.015	.236	-.1289	.237	.007	-.545	5.742E+00	-3.514E+00			-1.404E-01	
4.0	.022	.440	-.2492	.441	-.009	-.565	5.807E+00	-3.665E+00			-1.494E-01	
8.0	.048	.859	-.5092	.858	-.072	-.594	5.972E+00	-4.029E+00			-1.684E-01	
9.0	.058	.965	-.5781	.962	-.094	-.601	5.979E+00	-4.093E+00			-1.732E-01	
10.0	.069	1.071	-.6477	1.067	-.118	-.607	5.633E+00	-4.100E+00			-1.781E-01	
12.0	.092	1.247	-.7855	1.239	-.170	-.634	4.529E+00	-4.141E+00			-1.838E-01	
14.0	.115	1.393	-.9281	1.380	-.225	-.673	3.602E+00	-4.199E+00			-1.857E-01	
16.0	.140	1.505	-1.0702	1.485	-.280	-.721	3.037E+00	-4.227E+00			-1.835E-01	
18.0	.169	1.611	-1.2148	1.585	-.337	-.767	2.530E+00	-4.299E+00			-1.803E-01	
19.0	.183	1.653	.0414	1.623	-.365	.026	8.226E-01	NA			-1.774E-01	
20.0	.192	1.643	.0435	1.610	-.381	.027	-9.494E-01	NA			-1.694E-01	
21.0	.202	1.623	.0455	1.587	-.394	.029	-5.426E-01	NA			-1.604E-01	
22.0	.215	1.627	.0475	1.589	-.410	.030	1.268E-01	NA			-1.538E-01	
24.0	.245	1.633	.0516	1.591	-.440	.032	3.341E-02	NA			-1.399E-01	
)			ALPHA	Q/QINF	EPSLON	D(EPSLON)/D(ALPHA)						

Figure 74: Typical outputs of Digital Datcom software

Another important limitation between those reported before must be here underlined because it has led to additional work. This is the fact that with the Digital Datcom program we are not able to get as output, aerodynamic characteristic related with rudder control surface. Being this control surface one of the most important parameters needed, being their values extremely important to build up the flight dynamic model. In order to overcome this problem, aerodynamic characteristic related with rudder control surface has been calculated by hand [7]. These parameters are:

$C_{Y\delta r}$ : it is the portion of the aerodynamic coefficient of the cross-wind force related with the rudder deflection

$C_{l\delta r}$ : it is the portion of the aerodynamic coefficient of the roll moment related with the rudder deflection

$C_{n\delta r}$ : It is the portion of the aerodynamic coefficient of the yaw moment related with the rudder deflection.

## Navigation and Control system

### Control system

A navigation and control system for our model is of extremely importance to achieve our purposes. For this reason, one of the key points in the development of our flight dynamic model

has been the design of a control system to stabilize the aircraft but also capable to guide it as required by the user. Then, the development of a navigation system was also needed to track reference trajectory simulating possible characteristic flights of the operational life of the airplane to be designed.

In the previous paragraph, the non-linear dynamic system describing the complete six degree of freedom (6DOF) motion of the aircraft has been introduced. Now, for a linear controller design, as that one chooses to be implemented in our model, these non-linear equations must be trimmed and linearized.

Considering the non-linear system introduced before represented as:

$$\begin{aligned} \dot{X}(t) &= F(X(t), U(t)) \\ Y(t) &= G(X(t), U(t)) \end{aligned} \quad (eq. 117)$$

A trim condition is defined as a constant vector  $X_0$  for which exist a constant input vector  $U_0$  that provide:

$$\begin{aligned} \dot{X}(t) &= 0 = F(X_0(t), U_0(t)) \\ Y_0(t) &= G(X_0(t), U_0(t)) \end{aligned} \quad (eq. 118)$$

The turn  $(X_0, U_0, Y_0)$  that satisfy the previous system is called *trim condition*. Then, with the assumption that the motion of the aircraft remains confined around this trimmed condition:

$$\begin{aligned} X(t) &\in (X_0 - x(t), X_0 + x(t)) \quad \forall t \in [t_0, t_f] \\ U(t) &\in (U_0 - u(t), U_0 + u(t)) \quad \forall t \in [t_0, t_f] \\ Y(t) &\in (Y_0 - y(t), Y_0 + y(t)) \quad \forall t \in [t_0, t_f] \end{aligned}$$

Where  $x(t), u(t), y(t)$  represent infinitesimal variation around the trimmed condition.

Substituting these conditions in the previous non-linear equation model we get:

$$\begin{aligned}
 \dot{X}_0 + x(t) &= F(X_0 + x(t), U_0 + u(t)) \\
 &= F(X_0, U_0) + F_x(X_0, U_0)x(t) + F_u(X_0, U_0)u(t) + o_F(x(t), u(t)) \\
 Y_0 + y(t) &= G(X_0 + x(t), U_0 + u(t)) \\
 &= G(X_0, U_0) + G_x(X_0, U_0)x(t) + G_u(X_0, U_0)u(t) + o_G(x(t), u(t)) \quad (eq. 119)
 \end{aligned}$$

This is the so called *dynamic of the infinitesimal variation around the trim condition*. At this point it can be model as a linear system expressed as:

$$\begin{aligned}
 \dot{x}(t) &= F_x(X_0, U_0)x(t) + F_u(X_0, U_0)u(t) \\
 y(t) &= G_x(X_0, U_0)x(t) + G_u(X_0, U_0)u(t) \quad (eq. 120)
 \end{aligned}$$

Where:

$$\begin{aligned}
 F_x &= \begin{bmatrix} \frac{\delta F_{x1}}{\delta x_1} & \dots & \frac{\delta F_{x1}}{\delta x_n} \\ \vdots & \dots & \vdots \\ \frac{\delta F_{xn}}{\delta x_1} & \dots & \frac{\delta F_{xn}}{\delta x_n} \end{bmatrix} & G_x &= \begin{bmatrix} \frac{\delta G_{x1}}{\delta x_1} & \dots & \frac{\delta G_{x1}}{\delta x_n} \\ \vdots & \dots & \vdots \\ \frac{\delta G_{xn}}{\delta x_1} & \dots & \frac{\delta G_{xn}}{\delta x_n} \end{bmatrix} \\
 F_u &= \begin{bmatrix} \frac{\delta F_{u1}}{\delta u_1} & \dots & \frac{\delta F_{u1}}{\delta u_n} \\ \vdots & \dots & \vdots \\ \frac{\delta F_{un}}{\delta u_1} & \dots & \frac{\delta F_{un}}{\delta u_n} \end{bmatrix} & G_u &= \begin{bmatrix} \frac{\delta G_{u1}}{\delta u_1} & \dots & \frac{\delta G_{u1}}{\delta u_n} \\ \vdots & \dots & \vdots \\ \frac{\delta G_{un}}{\delta u_1} & \dots & \frac{\delta G_{un}}{\delta u_n} \end{bmatrix} \quad (eq. 121)
 \end{aligned}$$

They are the Jacobian matrices of the function F and G with respect to X (state) and U (control input) at the equilibrium point. This system of equation represents the linearized system that we were looking for.

In particular, using the notation:

$$\begin{aligned}
 A &= F_x & B &= F_u \\
 C &= G_x & D &= G_u \quad (eq. 122)
 \end{aligned}$$

The linearized system can also be presented as:

$$\begin{aligned}\dot{x}(t) &= Ax(t) + Bu(t) \\ y(t) &= Cx(t) + Du(t)\end{aligned}\quad (\text{eq. 123})$$

Here  $A$  is the so called *State Matrix* while  $B$  is generally named as *Control Matrix*. These matrices are extremely important in order to study the stability of the aircraft. In particular, information in this sense can be obtained looking at the eigenvalues of the matrix  $A$ . In fact, as known, if these eigenvalues are negative the system is stable while on the other hand if they are positive the system will be unstable. The main purpose of a control system is in moving these points so that the behaviour of the airplane will result to be more stable with respect its natural condition.

The state of the non-linear system can then be obtained by summing the outputs of this linear system, which are the variations around the trim condition, to the trim condition itself.

As mentioned, linearization of the system is particularly important when designing a linear control system. In fact, designed autopilot will be based on the linearized system. In particular these autopilots will estimate the variation of the state producing a variation of the output variable  $u(t)$  to be added to the trimmed value  $U_0$ .

In particular in our case the airplane has been trimmed and linearized at cruise condition described by:

- Mach Number: 0.67
- Altitude: 26000 ft
- Flight path angle equal to zero
- Level wing

The trim values of the nine states  $u, v, w, p, q, r, \Phi, \Theta, \psi$  and the four control inputs  $\delta_e, \delta_t, \delta_r, \delta_a$  were returned. These values were used to linearize the complete non-linear system as described above.

### *Linearized equation of motion*

Here the linearized equation of motion will be presented without their derivation considering that it is just a mathematical application of the previous description. However, should be underlined is that these linearized equations are expressed in Stability axis that, as introduced before, is a particular choice of body axis. In this way, the inertial matrix  $I$  of the airplane once defined will

remain constant. Based on its definition, this reference frame has at the initial condition the longitudinal axis coincident with the trim speed direction. It allows simplifying the velocity vector as:

$$V_T = \begin{bmatrix} U_0 \\ 0 \\ 0 \end{bmatrix} \quad (\text{eq. 124})$$

Another consideration, even more important of that one before, is that, considering the initial condition as an arbitrary choice, it can be choose in a completely arbitrary way. So the linearized equation of motion can be extremely simplified if we consider a straight flight with level wing. Under these considerations we have:

$$\begin{aligned} V_{B0} = \psi_{B0} = \Phi_{B0} = 0 \\ P_{B0} = Q_{B0} = R_{B0} = 0 \end{aligned} \quad (\text{eq. 125})$$

Where V represents lateral speed.

Writing the linearized equation of motion under this condition, the fundamental consequence from a control system design point of view is that, equations of the longitudinal plane and those of the lateral-directional plane are without any relation. In other words it means that the complete system of linear equation of motion can be divided in two subsystems, one describing the longitudinal motion and the other describing the lateral-directional motion. As further consequence the state vector can be divided in two state vectors with 4 state variables each:

$$\begin{aligned} X_{long} &= [u, w, q, \theta] \\ X_{lat} &= [v, p, r, \Phi] \end{aligned}$$

Based on these assumptions and considering the way to proceed introduced before the two systems of linearized equation of motion can be written as follow.

1. Longitudinal linearized equation of motion

$$\begin{aligned}
 \dot{u} &= -g\theta + X_u u + X_w w + X_{\delta t} \delta_t \\
 \dot{w} &= U_0 q + Z_u u + Z_w w + Z_q q + Z_{\delta e} \delta_e \\
 \dot{q} &= M_u u + M_w w + M_{\dot{w}} \dot{w} + M_q q + M_{\delta e} \delta_e \\
 \dot{\theta} &= q
 \end{aligned}
 \tag{eq. 126}$$

2. Lateral-Directional linearized equation of motion

$$\begin{aligned}
 \dot{v} &= Y_v v + Y_p p + (Y_r - U_0)r + g\Phi + Y_{\delta a} \delta_a + Y_{\delta r} \delta_r \\
 \dot{p} - \frac{I_{xz}}{I_z} \dot{r} &= L_v v + L_p p + L_r r + L_{\delta a} \delta_a + L_{\delta r} \delta_r \\
 \dot{r} - \frac{I_{xz}}{I_z} \dot{p} &= N_v v + N_p p + N_r r + N_{\delta a} \delta_a + N_{\delta r} \delta_r \\
 \dot{\Phi} &= p
 \end{aligned}
 \tag{eq. 127}$$

Where the  $K_i$  parameters (like for example  $X_u$ ) are the so called *aerodynamic derivatives*. These parameters can be obtained deriving the corresponding force equation with respect to the variable indicated by the pedix. Just to make an example of the meaning of each of these parameters let us consider the first aerodynamic derivative  $X_u$ .

First of all the external force acting on an airplane in the X direction is composed by the aerodynamic Drag force and the Thrust force produced by the engine:

$$X = -D + T = -\frac{1}{2} C_D \rho U^2 S + T
 \tag{eq. 128}$$

Then, considering that as said the pedix represent the derivation variable we have:

$$X_u = \left( \frac{\partial X}{\partial U} \right)_{U=U_0} = -\rho S U_0 C_{De} - \frac{1}{2} \rho S U^2 \left( \frac{\partial C_D}{\partial U} \right)
 \tag{eq. 129}$$

In other words  $X_u$  represents the variation of the force along the X direction due to velocity variation  $u$ .

The meaning of all the others aerodynamic stability can be obtained proceeding in the same way.

### *Linear quadratic regulator (LQR) control system*

Now that the linearized equations have been obtained the design of the linear control system can be considered. In particular, a linear dynamic controller to provide trajectory tracking has been developed. The Feedback control systems are widely used. In response to demands for increased efficiency and reliability, these control systems are being required to deliver more accurate and better overall performance in face of difficult and changing operating conditions. In order to design control systems to meet the demands of improved performance and robustness when controlling complicated processes, new design tools and better underlying theory are required. In particular, a standard method of improving the performance of a control system is to add extra sensors and actuators. This necessarily leads to a multi-input multi-output control system (MIMO). Thus, it is a requirement for any modern feedback control system design methodology that is able to handle the case of multiple actuators and sensors. This is the reason why for our purpose a MIMO control system has been chosen to be the best solution and it has been preferred to an oldest single input single output (SISO) control system.

There are two main different approaches to build up a linear multi-input multi-output control system:

1. *Pole placement*: in this approach appropriate poles are *a priori* assigned to the system. However is not so simple determining a priori which are the exact pole values that impose to the airplane the desired behaviour but they can be chosen only on the basis of the handling qualities.
2. *Linear quadratic regulator*: in this approach the solution of the control is found by minimizing a specified performance index (PI) so that an optimal control gain can be obtained. Optimal control gain means a gain able to provide the best trade-off between the percentage of throttle required and control surface deflection needed. For this reason this type of control design is also called *Optimal Control* [9]

The selected choice to develop the control system for our model is fundamentally based on the second approach even if in a deeper detail the design method can be seen as a hybrid method

between the two previously introduced linear MIMO approaches. The reason why this type of approach has been selected will be explained in the following paragraph.

**LQR overview**

Let us consider the following linear system already introduced in eq.123:

$$\begin{aligned} \dot{x}(t) &= Ax(t) + Bu(t) \\ y(t) &= Cx(t) + Du(t) \end{aligned}$$

Then define a cost function J, that represents the performance index introduced before, as:

$$J = x^T(t_f)S_f x(t_f) + \int_{t_0}^{t_f} (y^T(t)Qy(t) + u^T(t)Ru(t))dt \quad (eq. 130)$$

Where the weighting matrices Sf, Q and R must be:  $S_f \geq 0$   $Q \geq 0$  and  $R > 0$ .

The elements on the diagonal of these matrices have a quite clear meaning. These elements are weighting the square of the single components of the vectors  $x(t_f), y(t), u(t)$ .

The solution of the optimal control problem is defined as a function  $u^0(t)$  for which  $\forall t \in [t_0, t_f]$  represents a minimum of the performance index J.

Without reporting here all the derivation of the control law (for more information [5]) the solution of standard LQR problem can be seen as: find a controller  $u(t) = Kx(t)$  such that the feedback system is internally stable and J is minimized. It turns out that such controller uses a constant gain K. In particular, as can be demonstrated, using the famous Riccati equation, the constant gain is defined as:

$$K = -R^{-1}B^T S \quad (eq. 131)$$

Where S is the solution of the Algebraic Riccati equation:

$$A^T S + SA - PBR^{-1}B^T P + Q = 0 \quad (eq. 132)$$



Once the weighting matrices has been defined, depending on the purpose for which the control has been designed, the solution of the optimal control problem can be found using a Matlab library function named “*lqry*”. This function takes as inputs the state space matrices A,B,C,D and weighting matrices Q and R providing as outputs poles of the system (Eigenvalue of the state matrix A), the solution matrix of the Riccati equation S and the gain matrix K that is the term on which we are particularly interesting.

Once the gain K has been obtained the control law is given by:

$$u(t) = Kx(t) \quad (\text{eq. 133})$$

So substituting this expression into the linear system (eq.123) we can rewrite this one as:

$$\begin{aligned} \dot{x} &= (A + BK)x(t) \\ y &= (C + DK)x(t) \end{aligned} \quad (\text{eq. 134})$$

Now, the state matrix A is substituted with a new state matrix defined as (A+BK) that, if the gain matrix K has been correctly determined, allows to improve the stability of the system moving toward the left direction in the complex plane its poles.

### *Design procedure*

Design procedure, carried out to get the optimal K matrix has been developed using an iterative process that as mentioned before can be seen as a hybrid method between the LQR and the Pole Placement approach. This procedure allows to link the choice of the matrices Q and R, that are fundamental in the definition of the gain matrix K as it is clear looking at the previous introduction of LQR technique, to a certain parameter k so that the root locus will depend on this one and the weight inside the matrices Q and R can be choose as a function of the position of the poles of the system. The method used can be summarized with the following list of points:

1. The weight matrix R on the input is choosing. There are different ways in which it can be done. One of this is the so called *Control Authority* for which the weighting elements

are selected as a function of the maximum scale value of the relative parameter. This leads to a definition of the matrix R as:

$$R = \begin{bmatrix} 1 & 0 \\ 0 & \frac{\delta_{c1,max}^2}{\delta_{c2,max}^2} \end{bmatrix}$$

2. The matrix Q is selected. In particular it is expressed in a parametric form with a parameter  $k > 0$  and where the value  $q$  is a just first trial that can be tuned in subsequent loops if the motion of the poles on the complex plane does not meet the required characteristics (handling qualities)

$$Q = \begin{bmatrix} kq & 0 \\ 0 & q \end{bmatrix}$$

3. The Algebraic Riccati equation ARE is numerically solved using the Matlab function "lqry" introduced before. In particular, with this choice of the matrix Q we will get a parametrized solution of the matrix S so that  $S = S(k)$ . From this parametrized matrix the gain matrix K will be also parametrized by the parameter k:

$$K(k) = -R^{-1}B^T S(k)$$

4. The Eigenvalues of the controlled system are then determined. These values as said before are another output of the Matlab function "lqry". As can be expected, considering how the state matrix changes when a control action is present (eq.134) also these values will be parametrized by the parameter k.

$$\lambda_i(k) = \lambda_i(A + BK(k))$$

5. The root locus is drawn as a function of this parameter k. From this plot a value of k can be choose considering that value of k placing poles of the system in a region where the hand qualities and the required design characteristics are satisfied.
6. With this choose value of the parameter k the matrix Q is now fixed and in particular the definition of this matrix has been directly related with the position of the poles on the root locus. This is why, as previously mentioned, the actual method used in designing our control system can be seen as an hybrid method.

7. However, if the restriction imposed by the handling qualities or the design requirements cannot be satisfied by any  $k$  values we have to go back at the first point changing the value of  $q$  in the matrix  $Q$  or modifying the elements in the matrix  $R$ . This procedure explains why the adopted methodology is an iterative solution.

An example of how the root locus comes out applying the methodology described is presented by following figure (Figure 75):

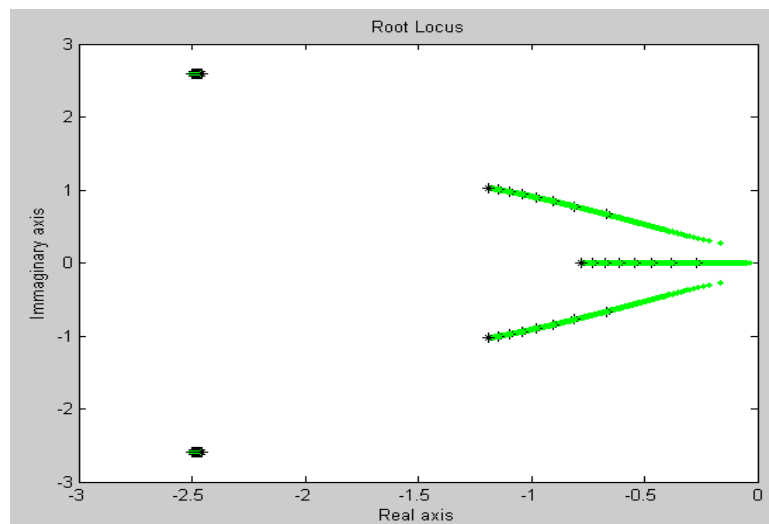


Figure 75: Root locus coming from design procedure used

The Matlab code developed for control system design and using the previous described methodology is reported here below.

```
%Weighting matrices definition

R=diag([1 4]);
sys_C17=ss(Along_5a,Blong_5a,C_5a,D_5a); %linear system definition
q=1;
q1=1;
q2=1;
i=1;
disp('thinking...')
for k=0.01:0.01:3
    Q=diag([k k*q k*q1 k*q2]);
    [Kott,S,E(:,i)]=lqry(sys_C17,Q,R);
    plot(E(:,i),'g.')
    i=i+1;
end

% plot Root locus

m=1;
for j=1:i-1
    if j==10*m
        m=m+1;
        plot(E(:,j),'k.')
        pause(0.1)
    else
```

```

        plot(E(:,j), 'g.')
        pause(0.1)
        hold on

    end
end

%Evaluate solution

disp('Enter the selected value')
k_select=input('k select=')
Q_a_scelta=diag([k_select q*k_select q1*k_select q2*k_select]);
[K_LQ,S,Eigenvalue_selected]=lqry(sys_C17,Q_a_scelta,R);
disp('Eigenvalue of the feedback system')
Eigenvalue_selected_altitude
plot(Eigenvalue_selected_altitude, 'b*')
disp('Eigenvalue of the system without feedback')
Eigenvalue_Along=eig(Along_5a)
disp('Evaluate the improvement')

```

In our case the principal autopilots that have been developed to manually or automatically fly the aircrafts are:

- Pitch attitude control system → Pitch angle is the controlled variable
- Roll angle control system → Roll angle is the controlled variable
- Climb rate/airspeed hold → Airspeed is one of the controlled variables. The other is the pitch angle that in this case is controlled as a function of the required rate of climb/descent considering the following linearized link relation:

$$\dot{h} = -w + U_0 \square$$

- Altitude/airspeed hold → Altitude and Airspeed are the two controlled variable
- Track hold → Heading and distance with respect the reference trajectory are here controlled

The details of the design of each of these control systems are not here reported because it is not the real focus of this thesis and also considering that the general iterative way to proceed has been described before.

## Navigation system

A navigation system has also been defined to have the possibility to track the required trajectory accurately. In fact, making test trying to track some reference trajectories provided by the flight plan stored in the flight management system in terms of reference Altitude, speed, pitch angle,

bank angle, Heading angle and time just with the developed control systems using code above, the needed of an outer navigation control system came was clear especially in order to bring back the airplane on the reference trajectory in case of external input acting during the flight such as those due to wind. For this reason, the main purpose of the developed navigation system is to reduce the so called flight technical errors (FTE) [10] defined as:

- Cross track error: Distance between the aircraft current position and the closest point on the reference trajectory.
- Along Track error: Distance between aircraft current position and the desired position at that time on the reference path.
- Altitude error: Difference between actual altitude and desired altitude.

The navigation system has been developed so that these flight technical errors are estimated in real-time during the simulation. To make this real-time estimation the definition of *Euclidean errors* (EE), defined as the 3D distance between the actual aircraft position and the nominal position for each point in time, and the definition of *Relative Bearing* between two points have been used. Doing in this way the EE is then projected along-track and perpendicular to the nominal track in the horizontal and vertical plane [11].

Once these flight technical errors were available at each time, a navigation control system based on these parameters and considering geometrical relations has been developed. The main task of this navigation system is in providing an additional variation of the reference guidance parameters. This variation is needed to bring back the airplane its prescribed reference trajectory. In particular, proportional gains are also used to reach this result in a short time maintaining smooth variations of flight parameters like speed, bank angle, etc.

The concept of Required Navigation Performance (RNP) and saturation of each control surfaces and engine thrust was then considered to validate the designed guidance and control system.

Flight dynamic model: main components

Now, the most important basic concepts on which our flight dynamic simulator is based have already been introduced so, the layout of this model can be described.

First of all should be remembered that this model is a full six-degree of freedom model (6DOF) developed in a Matlab/Simulink environment. The complete model can be seen as composed by four different main subsystems where inside each of them, the most important parts of the model are present (Figure 76). These four most important subsystems are so called:

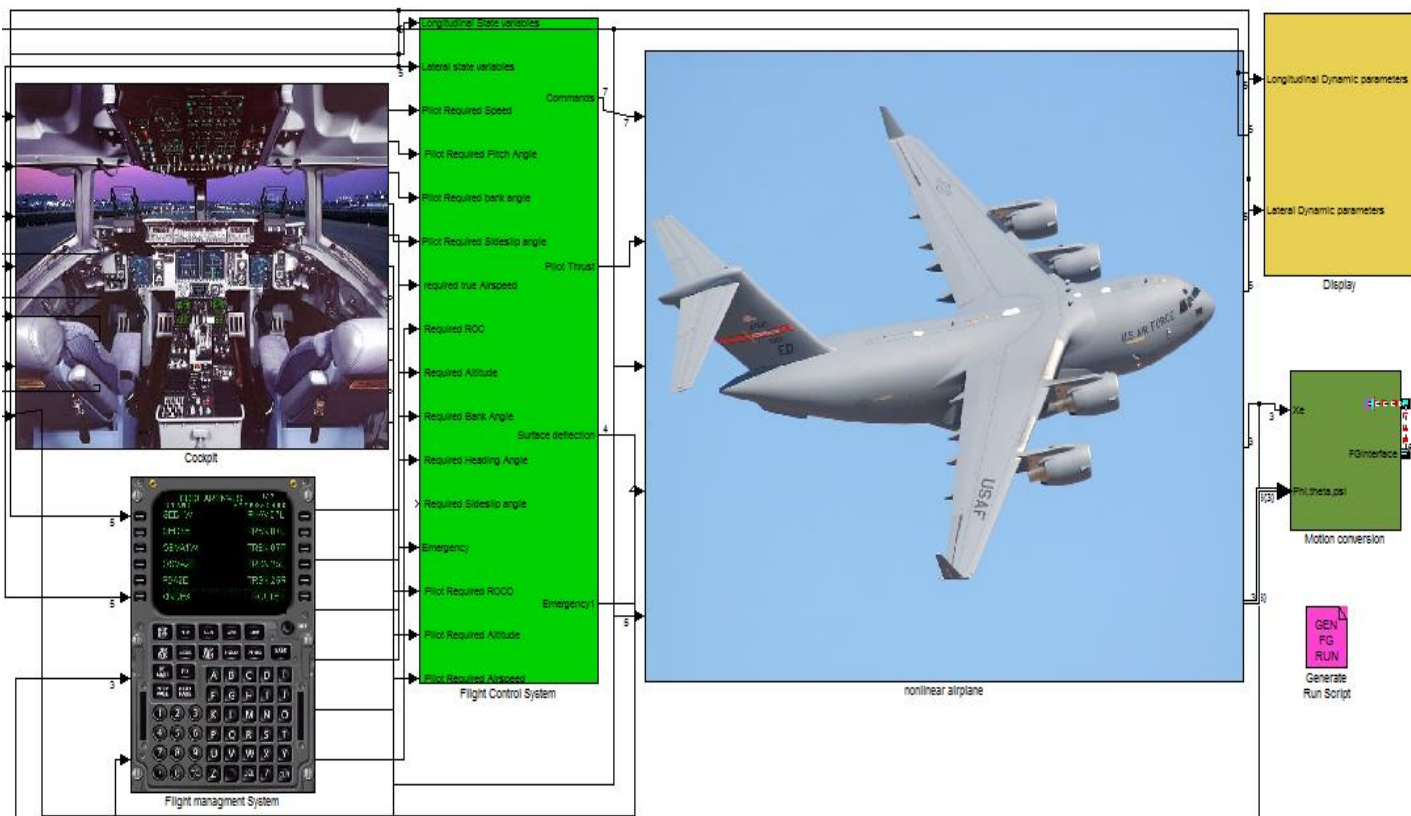


Figure 76: General overview of the 6DOF flight dynamic model in Simulink environment

- **Non-linear equation of motion:** inside this block there is the core of the model with the integration of the non-linear equation of motion as described in the previous paragraphs, under the important assumption of constant mass
- **Cockpit:** here inside we have a display representation of the most important flight parameters and control surfaces deflection. This block is particularly important in case of Pilot in command (joystick) when a flight gear interface or other visual outputs program are not activated to take under control flight parameters.

- **Flight control system:** inside this block we have both longitudinal and lateral-directional control designed using with the previously introduced Linear Quadratic Regulator (LQR) technique.
- **Flight management system:** it represents the outer loop of the guidance and control system. Inside this block the flight plan is also stored and the calculation of the flight technical error in real time is computed to modify reference guidance parameter to accurately track reference trajectory

1. Non-linear equation of motion subsystem

Inside this block many other important sub-blocks are present (Figure 77)

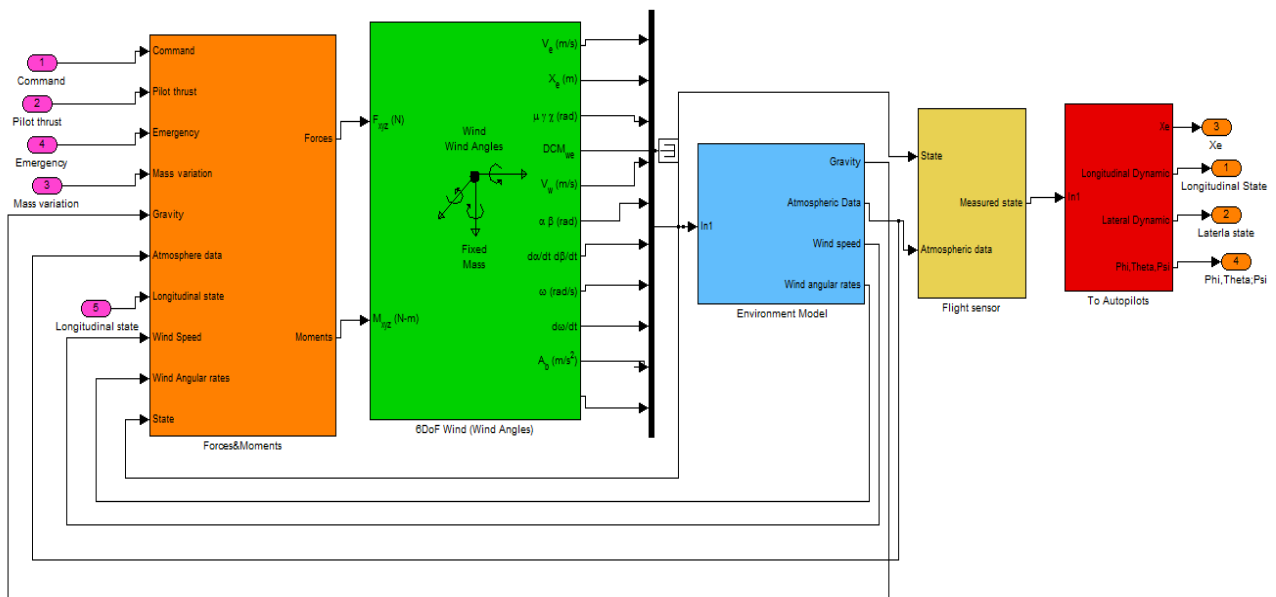


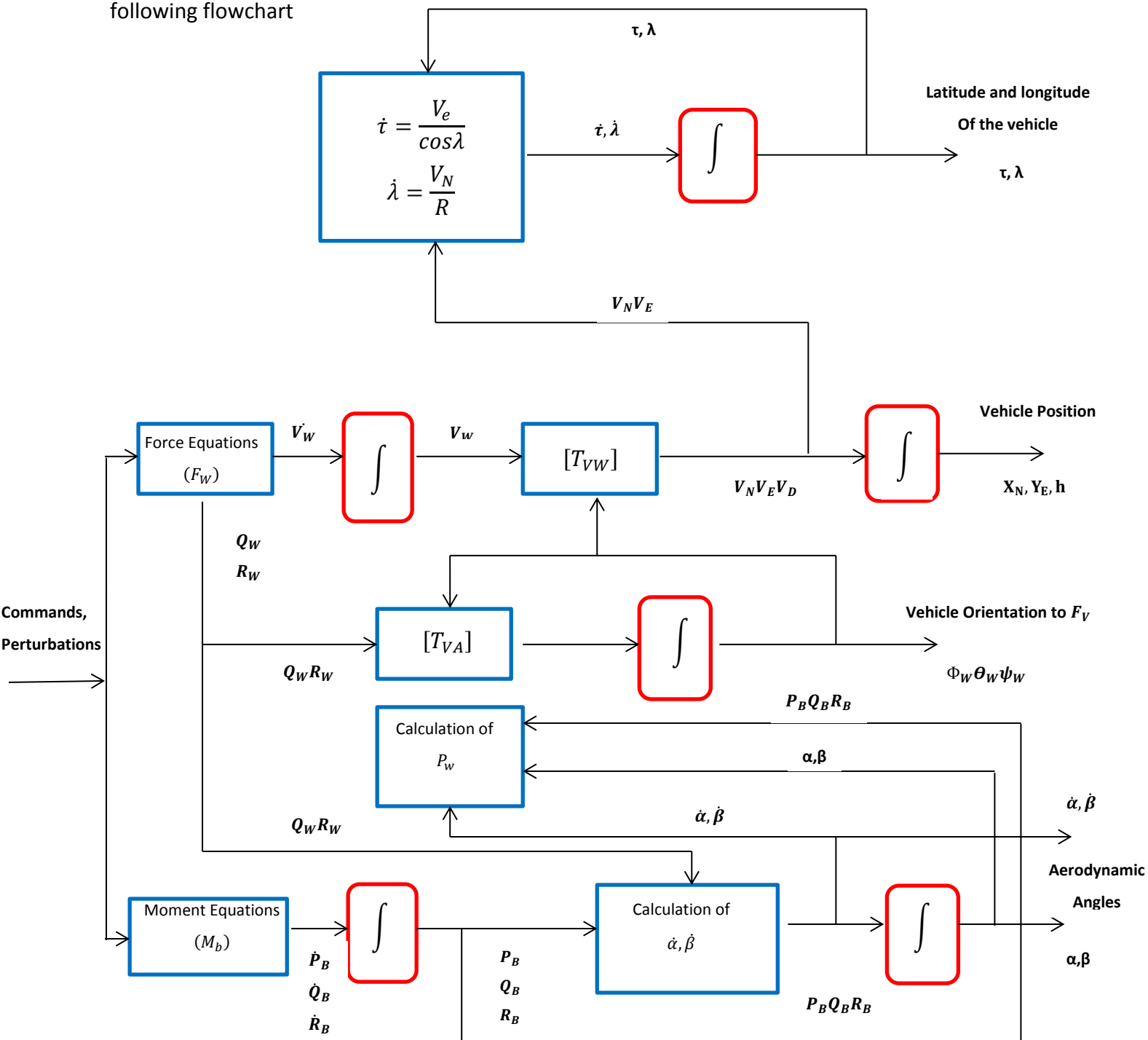
Figure 77: Non-linear equation of motion subsystem

Starting from the left of this figure and going to right each of the blocks present are here below described.

**Force&Moments:** Inside this block the calculation of all forces and moments acting on the airplane during the simulation as a function of the flight condition, are time by time calculated. As has been previously introduced the most important parameters in the determination of these forces and moments are the so called aerodynamic stability and control coefficients that has been estimated using the Digital Datcom program already introduced before. In particular, as seen there are a lot of these parameters coming out from this software and each of them is dependent on the particular considered flight condition. For this reason all these data have been stored in a Matlab

code called "DYNAMIC\_DATA.m". Then all these values can be used in Simulink to generate forces and moments for each flight condition using *look-up table* that has a function of (Altitude, angle of attack and Mach number) take the right coefficient needed for that condition from the Matlab script for each force and moment component.

6DOF Wind: This is a Simulink block that integrates the non-linear equation of motion in wind axis introduced before starting from the knowledge of forces in wind axis and moments in body axis. In particular how outputs are obtained from inputs (forces and moments) can be seen looking at the following flowchart





Environmental model: The environmental model is composed by three different subsystems:

1. **Wind model:** Here wind has been considered as decomposed in two different parts:

- *Discrete wind:* The mathematical representation that I used to model discrete gust is:

$$V_{wind} = \begin{cases} 0 & x < 0 \\ \frac{V_m}{2} \left( 1 - \cos\left(\frac{\pi x}{d_m}\right) \right) & 0 \leq x \leq d_m \\ V_m & x > d_m \end{cases} \quad (eq. 135)$$

Where:  $V_m$  gust amplitude,  $d_m$  gust length,  $V_{wind}$  wind speed and  $x$  is the distance travelled

- *Random wind:* This part of the wind has been modelled using a first order Gauss-Markov process [12] described by the following differential stochastic equation:

$$\dot{x} + \beta x = w \quad (eq. 136)$$

Where :  $x$  is the sthocstic component of the wind speed to be estimated,  $\beta$  inverse of the time constant and  $w$  is a random white Gaussian noise that is the input of this differential equation.

2. **Atmospheric model:** The atmospheric model has been created using the ISA Atmospheric model Simulink block (Figure 78). This block compute international standard atmospheric parameters considering as input the geopotential altitude in a range between 0Km and 20Km. The outputs of this block are: Temperature, Speed of sound, Density and Pressure. The most important assumption used to compute these outputs with this model is for Speed of Sound and Density that are calculated using a perfect gas relationship.

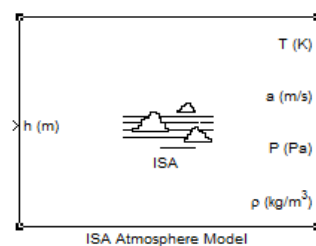
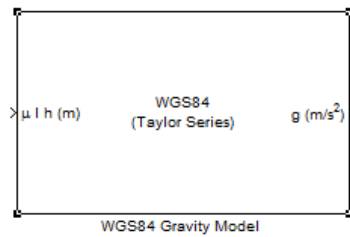


Figure 78: ISA atmospheric model Simulink block

3. **Gravity model:** The gravity model has been created using the 1984 World Geodetic System (WGS84) representation of Earth’s gravity model (Figure 79). The Simulink block used to compute

this value assumes a geocentric equipotential ellipsoid of revolution. The inputs of the block are the geodetic altitude, latitude and longitude



**Figure 79: Gravity model Simulink block**

Flight sensor&Air data model: This part has been added to simulate errors provided by on board instrument on flight parameters to pilot or autopilot. Also here, to model errors a First order Gauss-Markov process which creates a random with Gaussian noise at which sensor measurement could be subjected has been considered. In particular barometric altimeter and Pitot tube for altitude and airspeed measurement have been simulated by replacing the actual values of altitude and speed coming out from the 6DOF Wind Simulink block with values coming out from consideration about static pressure and dynamic pressure, adding also pressure noise. The flow charts representing how these sensors have been simulated are reported below.

- Pitot-tube simulation

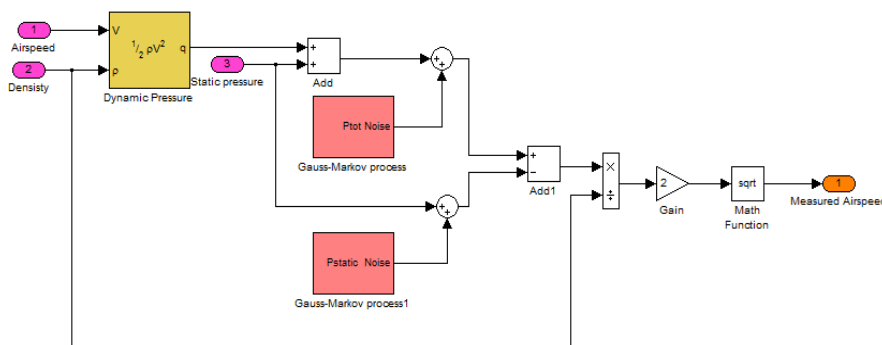


**Figure 80: Pitot tube representation for airspeed measurements**

- Barometric altimeter simulation

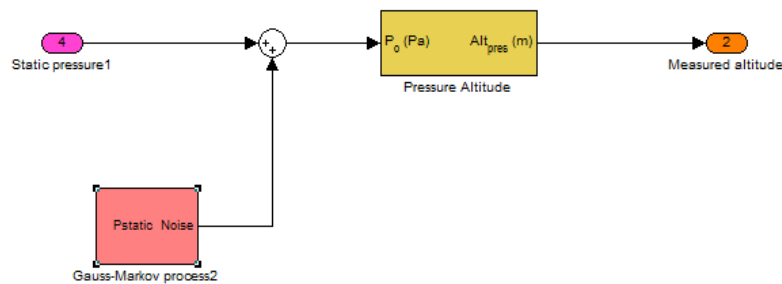


Figure 81: Barometric altimeter simulation for altitude measurements

## 2. Flight control system

Inside this main block other two blocks are present: in one of these there are all the longitudinal developed control systems while in the other one all the lateral-directional developed control systems are present. In fact as already pointed out before the assumption used to get the linearized equation of motion on which the control systems are based allows considering separately lateral and longitudinal dynamic. Inside this block there is also a part related with a complex logic selection of the controller (autopilot) to be used as a function of pilot requirements in case of pilot in command configuration. In fact, the model has been developed so that, pressing one of the buttons on the joystick, a certain type of autopilot can be engaged as required by the pilot. For example, setting a certain altitude in the cockpit subsystem and pressing the relative button to engage an altitude hold autopilot on the joystick the airplane will be stabilized and maintained at the required altitude. The same procedure can be carried out for each of the other developed autopilot.

## 3. Flight Management system

Inside this main block, the reference trajectories, stored in Matlab as vectors containing the values of the most important flight parameters (Altitude, Speed, Pitch angle, Bank angle, Flight path angle, Heading angle) where each element of the vector represents the value of a certain variable at a given time are load inside the simulation interpolating this data as a function of simulation time using look-up table. These values are then provided to the guidance and navigation system that, comparing these values with the actual airplane location is able to calculate real-time flight

technical error and provide correction of the reference parameters used by the inner loop control system to bring back the airplane on the reference trajectories.

### *Typical trajectory results*

Now before to conclude this chapter related with the design of the flight dynamics model and starting in describing how it has been used to develop our methodology for damage tolerance analysis some results coming out from this model can be presented. In particular, even if they are not the parameters on which we will be focused in the following, important confirmation about the functionality of the developed 6DOF flight dynamic model can be obtained looking at some example considering typical trajectories that we are able to simulate. In particular to do this should be remembered that the model has been developed to work in two different configurations:

1. *Pilot in command*: In this configuration the user can manually flight the aircraft using external input provided by a joystick to simulate particular trajectories.
2. *Automatic flight*: In this configuration, reference trajectories need to be loaded and then they will be automatically tracked by the airplane from take-off to landing.

So in the following, results of two different flights, one for each configuration, in term of altitude, speed and trajectory tracked will be presented.

#### **Example 1:** Pilot in command

- *Speed variation during the flight commanded by pilot engine throttle input*

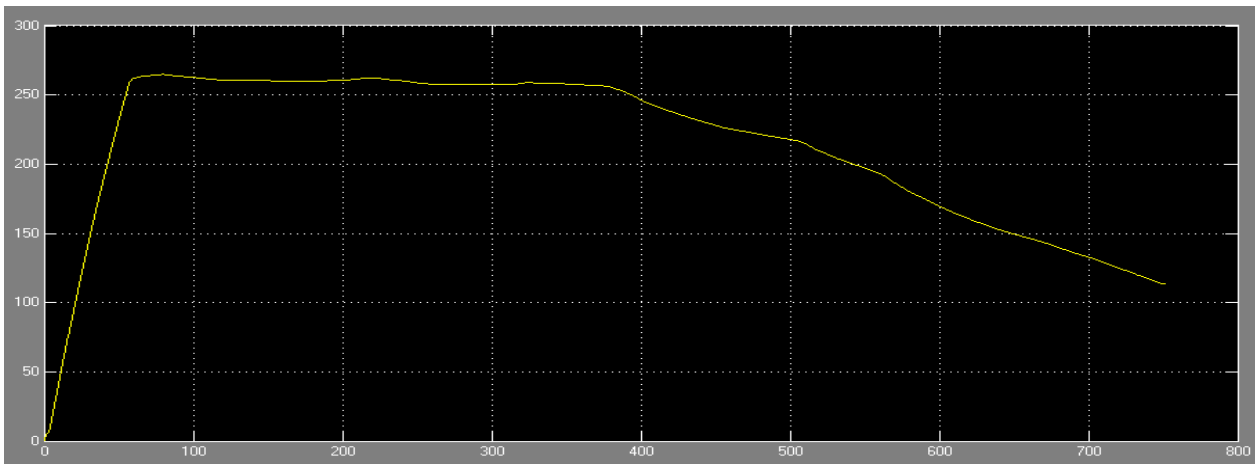


Figure 82: Speed Variation

➤ *Altitude variation:*

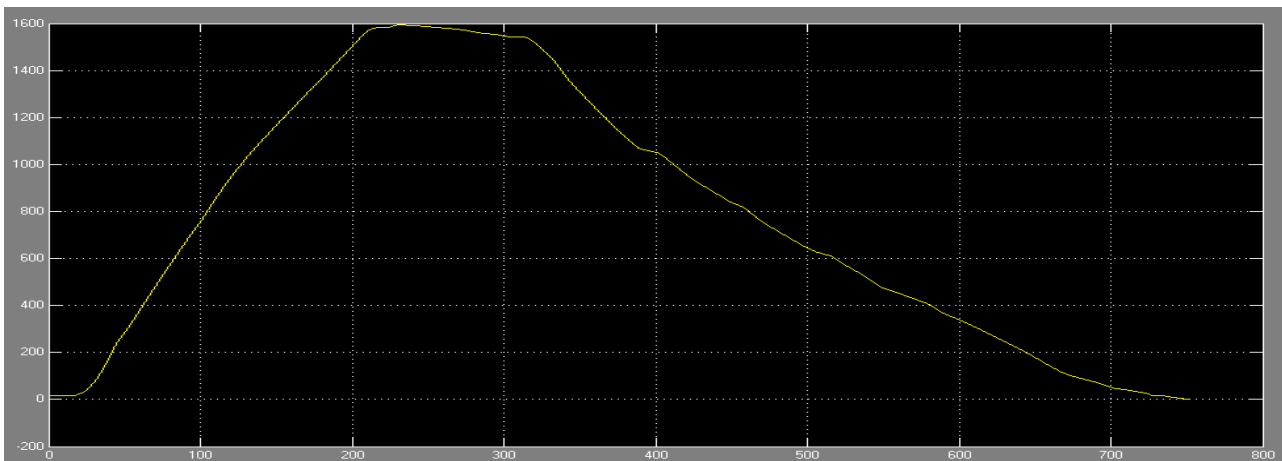


Figure 83: Altitude variation

➤ *Comparison between Pitch angle required by the pilot and available Pitch angle*

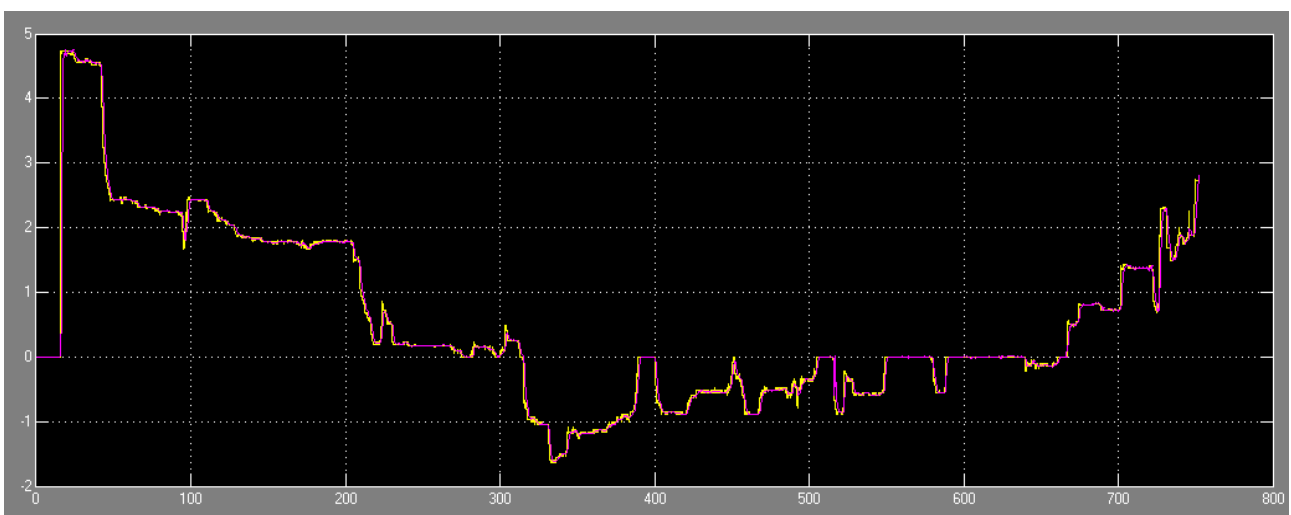


Figure 84: Pitch angle comparison

➤ *Comparison between Bank angle required by the pilot and available Bank angle:*

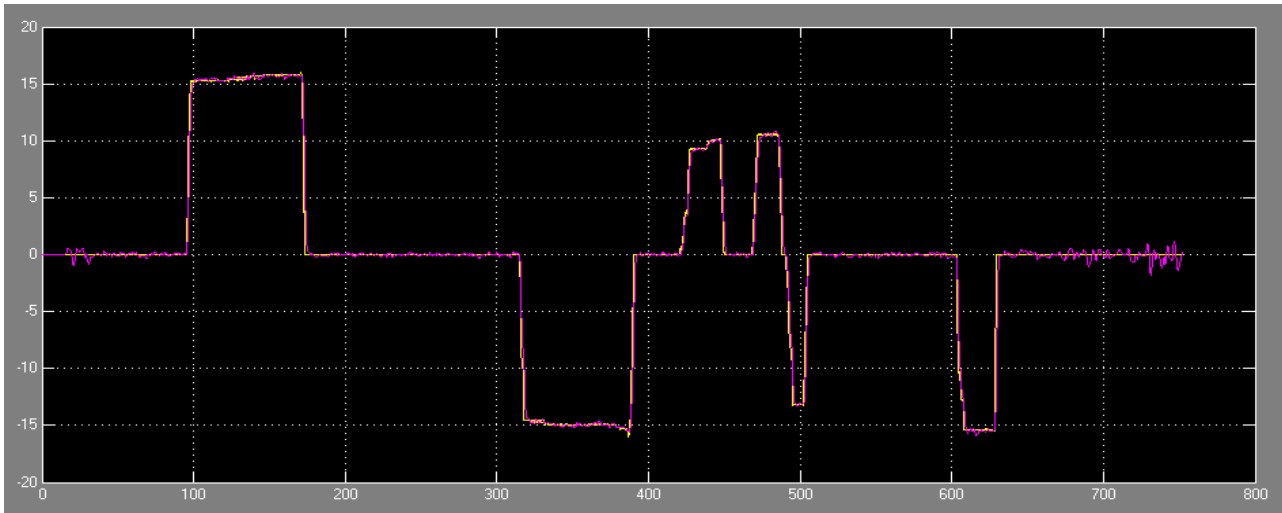


Figure 85: Bank angle comparison

➤ 2D trajectory tracked

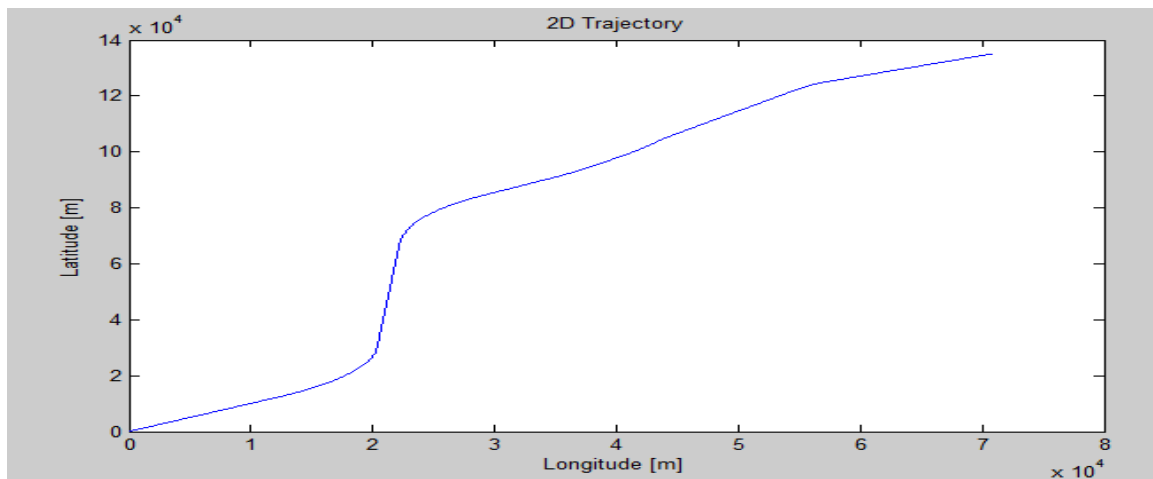


Figure 86: 2D trajectory tracked

➤ 3D trajectory tracked

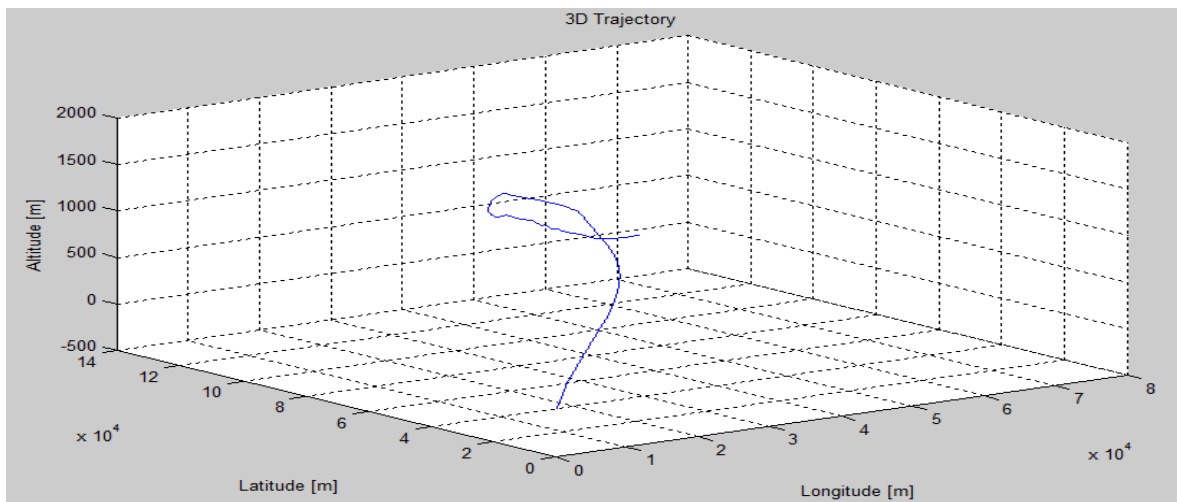


Figure 87: 3D trajectory tracked

**Example 2:** Automatic flight

The case of study considered to obtain these results was:

- *Flight*: Paris-Amsterdam,
- *Flight plan*: Noise configuration
- Average windy day (maximum wind considered 40 km/h)

Note that algorithms developed to obtain this kind of results are not detailed described here with the intent to summarize the report to just a general overview of the main steps carried out and main results obtained

➤ 2D & 3D Trajectory tracked

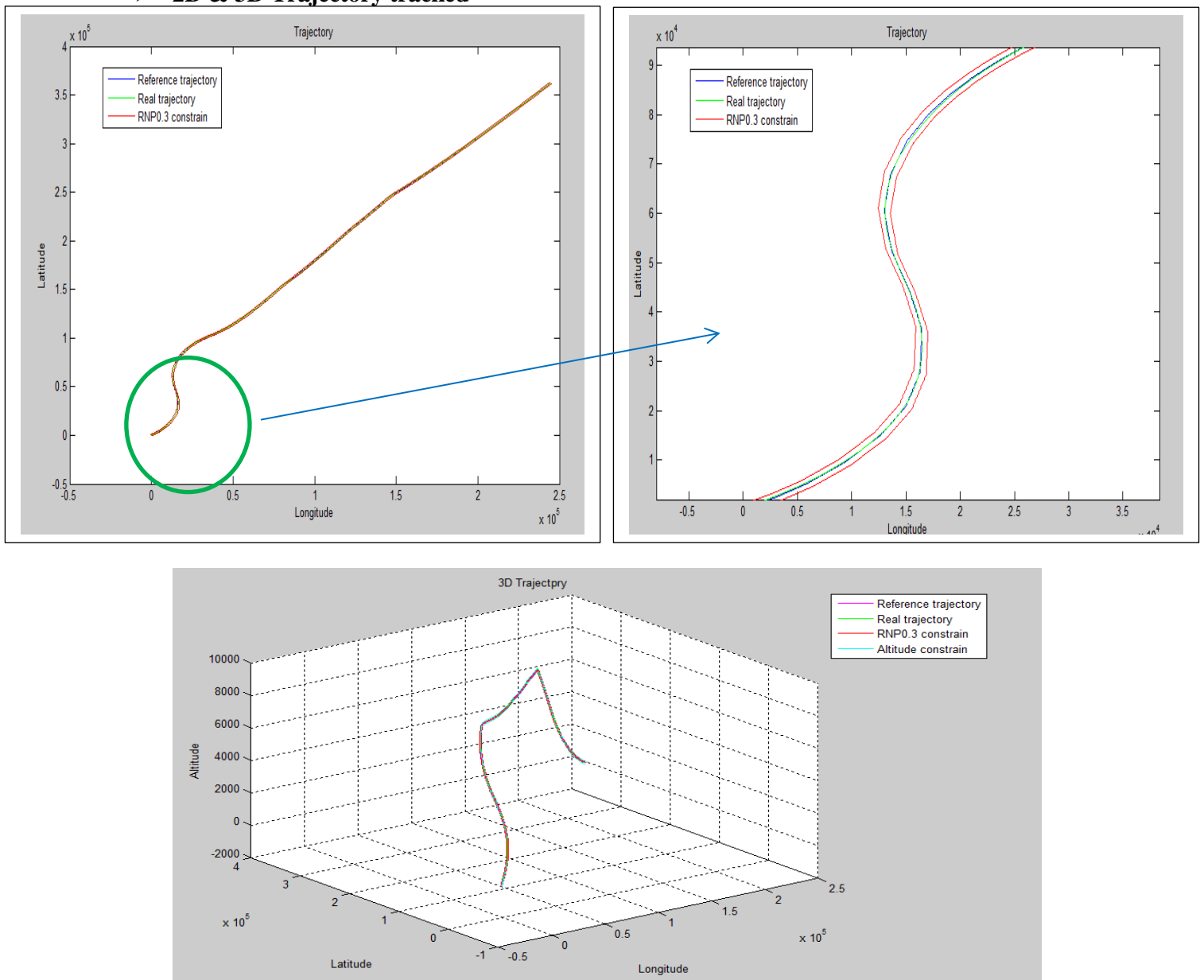


Figure 90: 3D Trajectory tracked with RNP constrains

➤ Flight technical errors

- Cross track error

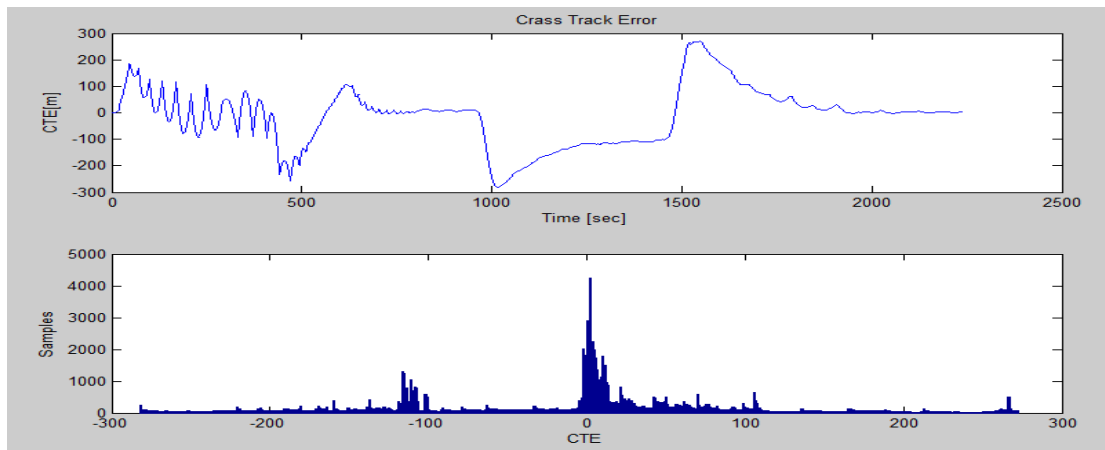


Figure 91: Cross track errors

- Along track error

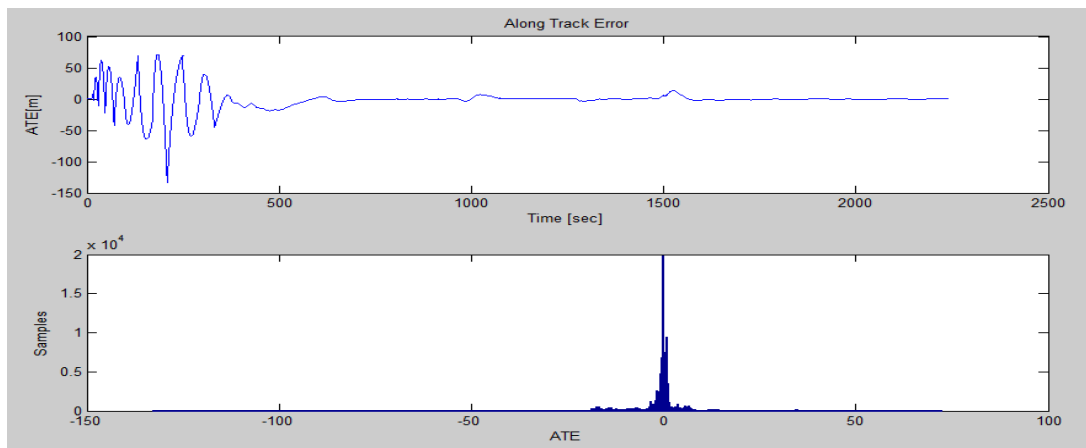


Figure 92: Along track errors

- Altitude error

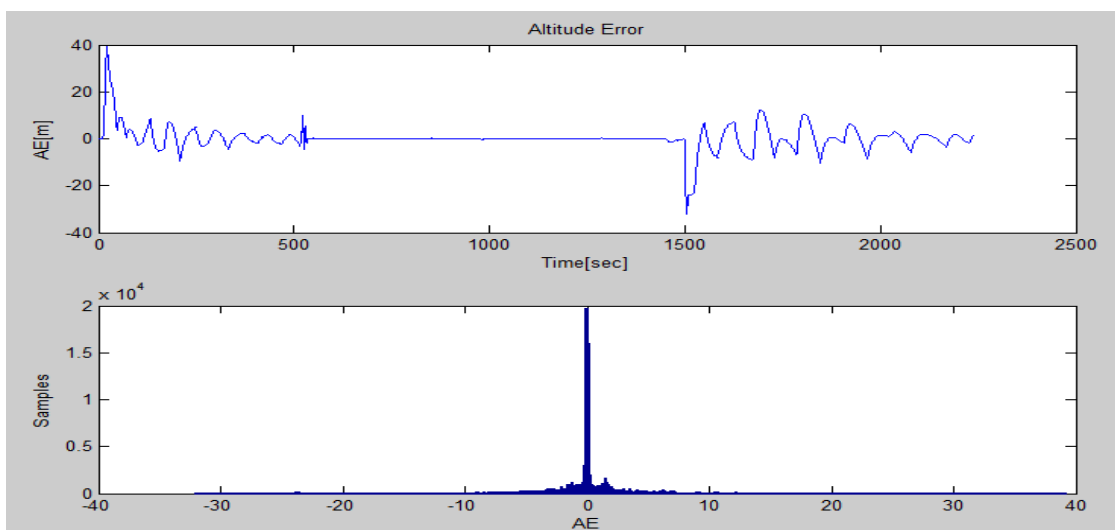


Figure 93: Altitude error



What is important to note here is that they are only few of the parameters that can be obtained running the simulation. In particular, in the following of thesis, we will be particularly interesting in accelerations, forces and moments acting on the structure of the airplane. In fact, as will be described in deep and how can be understood from the previous chapter, they will be the basic parameters needed to start our methodology for damage tolerance analysis.

## 6 NUMERICAL METHODOLOGY FOR DAMAGE TOLERANCE

### DESIGN ANALYSIS

#### Objective of the developed methodology

In the first chapters of this thesis all the basic concepts of fracture mechanism analysis for design against fatigue failure were introduced, pointing out the main aspects that should be considered in developing a numerical methodology for this purpose. These bases are fundamental in the understanding of the developed algorithms that will be presented in this chapter. Moreover, in Chapter 5, the 6DOF flight dynamic model has also been widely described in all its capacities and limitations introducing the basic flight dynamic and automatic control concepts used. In addition, the main blocks created have been described in detail. As mentioned, this model represents an important starting point for our work. In fact, inputs for crack growth analysis are derived from here. In particular, the main outputs of the dynamic model used that will be used as inputs for fatigue analysis are: aerodynamic forces (principally lift) and accelerations.

What must be pointed out in this introduction at this chapter is that, the main focus of our work is just a development of the basis of numerical methodology that, starting from the said inputs, allows getting the two main objectives of the fracture mechanism analysis:

- Residual strength diagram
- Crack growth diagram

Once this methodology has been developed and tested, step by step, all the strong assumptions introduced can be removed to get an even more realistic result.

Of course, outputs of this numerical crack growth analysis, will be obtained considering all the previously observation done about crack growth under variable amplitude loads. In other words it means that the principal focus will be the development of the primary structure of a methodology that, based on very simple initial assumptions, introduced in the next paragraph, provides the two said main results taking into account all the principal aspects that influence crack growth in a structural component subjected to a real load spectrum (VA irregular load spectrum). Hence, the

developed algorithm can be seen as a flow chart with many “white blocks” where for the moment very simple considerations are present in many of them. Then once the methodology has been developed and tested, these simple assumptions could be modified to make more real but also complex this numerical analysis. As we will see, the main assumptions considered in this first code generation are related with loads and type of structural element considered. To verify the obtained results, simple CA loading sequences have been used as will be described in the following.

To conclude this first introduction, should be also pointed out how, with the purpose to reduce computational time, in this first design approach, only few flights, flying manually and automatically the aircraft, have been considered.

**Main assumptions and inputs determination for crack growth analysis**

The first important assumption introduced to get a very simple basic model on which our methodology can be developed in a simpler way, has been to consider the airplane as a rigid body, as done to develop the equation of motion in Chapter 5, but with only one degree of freedom (1DOF). In particular, the only motion allowable is represented by translations along the Z direction in body axis (Figure 94).

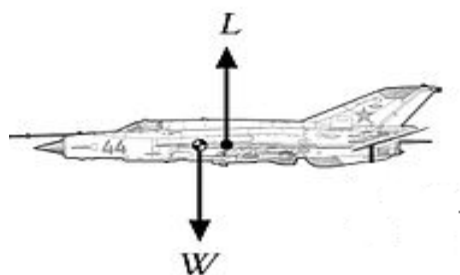


Figure 94: Aircraft 1DOF force schematization

We know that it is a strong assumption but, at the same time, it is needed to create a first clear way to proceed.

The crack growth analysis has then been considered just for one of the most critical airplane component from a fatigue point of view: wings.

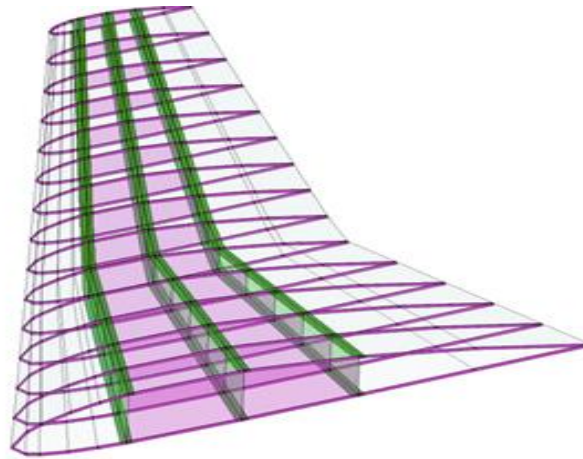


Figure 95: Schematic wing representation

Here in figure (Figure 95), a typical transport aircraft wing is represented. The main components of the wing can be quickly described as:

- **Spars**: They are beams that cross longitudinally the entire wing from the root to the tip. Of course, if more spars are present higher load can be sustained. The typical section of these beams is a full double T.
- **Centring**: They are elements placed normally to the wing span, hence normally placed with respects spars. Their principal function is to provide the aerodynamic shape at the wing but, they also must guarantee not local deformation on the structure. In addition, they also link the various elements present in the wing (spars, currents, skins)
- **Currents**: They are small section beam with the main purpose to contribute to the bending stiffness of the wing together with the spars that, anyway, remain the principal elements for this purpose. Another function of these elements is to increase the stiffness of the skin of the wing
- **Skin**: It creates a barrier between the fluid that flows on the upper side of the wing, with low pressure, and that one flowing on the lower side of the wing characterized by an higher pressure, to create the resultant aerodynamic force that is the so called Lift. They are cult with sheet of small thickness.

Looking at the figure above and considering these short descriptions of the main wing components, can be understood how a good assumption to further simplify the model that, in any case is not as strong as the assumption introduced before, is in modelling the aircraft's wing as an framed beam. In particular, considering that as said, the spars are the principal elements that provide bending stiffness to the wing and that are generally characterized by a double T section,

the following schematization for the wing, is used to calculate stresses (Figure 96). As can be expected, the critical location from a fatigue (but also static) point of view will be at the root of the wing where the highest stress values are expected.

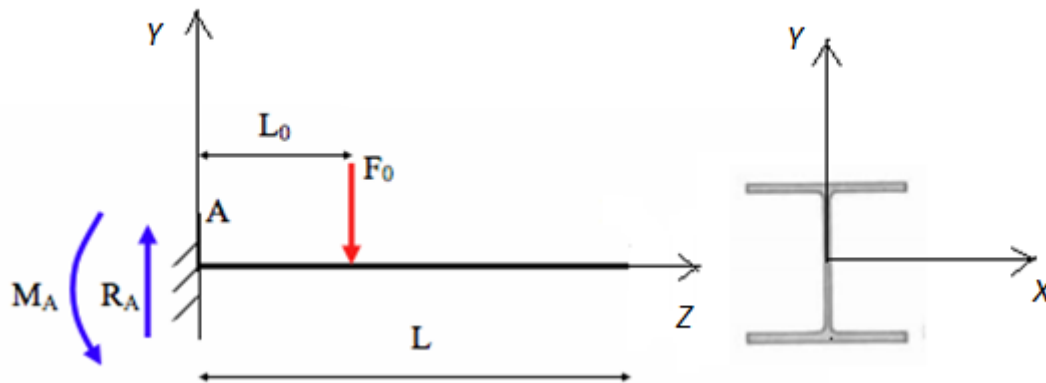


**Figure 96: Simple wing schematization**

An important observation can be done looking at this figure. The axis orientation is different with respect that one defined for Body axis reference frame. In fact, here, the orientation reported in Figure 95 is the typical one used, for convention, in structural analysis. This observation will result particularly important in the following in order to avoid trivial mistakes.

The characteristics of this beam section in term of dimensions have been obtained from handbooks.

Now considering the first strong assumption introduced before (airplane with 1DOF), the main force acting on the wing are simply:

- Weight force
- Aerodynamic force (Lift)

In reality these forces interact also due to aeroelastic effects but, considering the second assumption introduced above (rigid body) they can be neglected.

Under all these assumptions, the only outputs of the 6DOF model used as inputs for our analysis are:

- Acceleration time history along the Z direction in body axis (Y-direction in reference frame expressed in Figure (96))
- Lift time history in body axis.

Considering that as shown in relation derived in Chapter 3, crack growth analysis is carried out considering stress, these values are then used in order to determine the stress history at which the wing is subjected. The first step in doing this will be derivation of *inertial force* considering the acceleration time history obtained from the flight dynamic model and using this in the second Newton’s law as follow:

$$F_y(t) = ma_z(t) \quad (eq. 137)$$

Here, nomenclature of the derived inertial force is expressed in the reference frame defined in Figure 96 while that one of the acceleration is referred to Body axis reference frame. To avoid trivial mistake previously mentioned, from this point all force and moments will be considered in the reference frame conventionally used for structural analysis. Doing this, equation 137 will become:

$$F_y(t) = ma_y(t) \quad (eq. 138)$$

Then, m is the mass of the wing that can be considered to be

$$m = \rho V \quad (eq. 139)$$

Using this relation to determine the mass of the wing in eq.138 the inertial force time history can be derived. An example of the spectrum of this force, resulting from the dynamics model run out for a certain number of simulated flights (manually and automatically with different trajectories and weather conditions), is reported in figure (Figure 97).

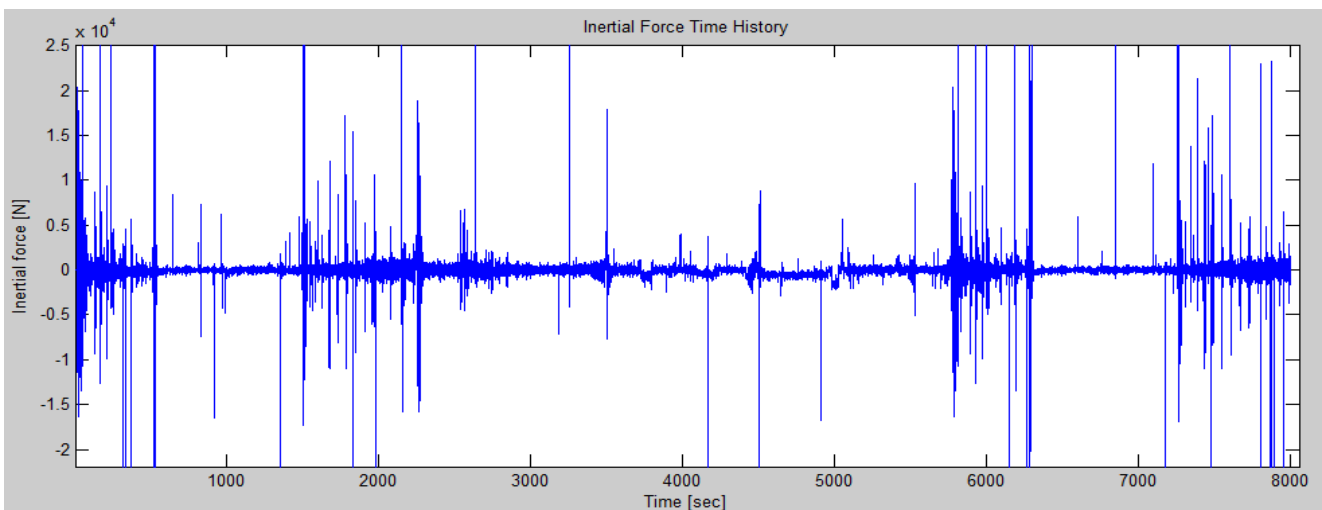


**Figure 97: Inertial force time history**

On the other hand, lift spectrum can be directly derived from the dynamic model after that the simulation is run out without any additional calculation. An example of the Lift force spectrum, obtained considering the same simulations used to derive the previous one, is reported in figure (Figure98) :

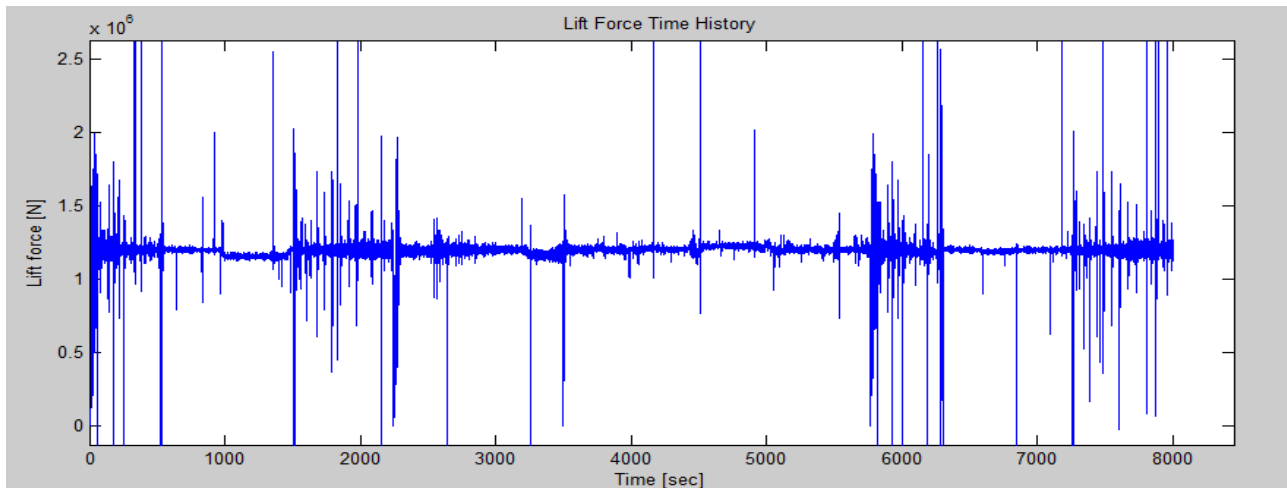


Figure 98: Lift force spectrum

However, as mentioned, in crack growth analyses we are more interesting in stress that in loads. For this reason, the next step is concerning the determination of the stress history starting from these force spectrums as inputs.

## Stress history generation

The only type of stress that has been considered acting on the wing is that related with the bending moment. Our interest now, is to determine the stress distribution along the beam and, in particular, the stress distribution on each section of the beam, especially the critical one (root section).

Now, before to introduce the simplified beam model of *De Saint Venant* used, the basic concepts of the Cauchy stress tensor and the equilibrium equations must be firstly introduced.

To derive equilibrium equations, definition of Power is needed. In a simple way Power can be defined as the product between force done and the speed obtained. However, in order to get a definition much more useful in defining equilibrium equations, let us consider an arbitrary body  $B_a$  and then, let's take a part  $ba$  of this one as it is represented in figure (Figure 99).

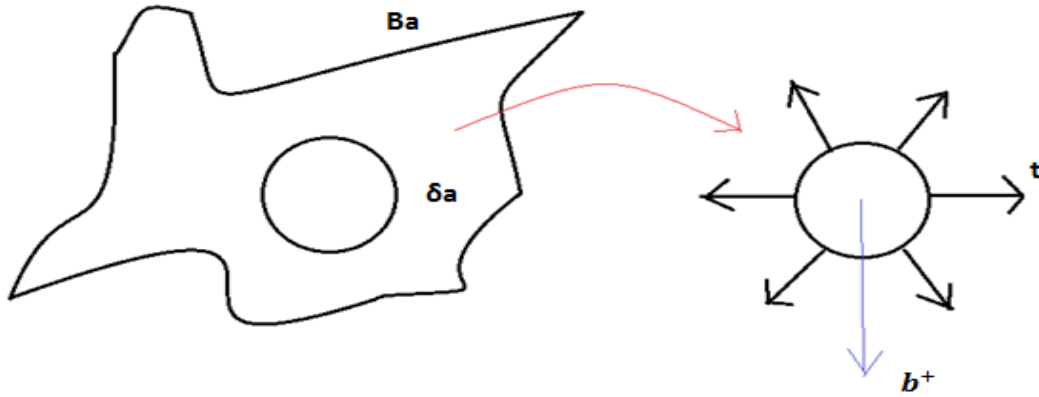


Figure 99: Volume and contact forces on a generic body

When considering a generic body like this, we have also take into account the fact that the considered body is always immersed in a certain environment. For this reason, there will be some interactions between this environment and the body itself. These interactions are generally divided in:

- Volume → named as  $b^+$ , are the interactions of the body with the environment
- Contact → named as  $t$ , are the interaction at the contact between part 1 and 2 as in the previous figure

The Power is a scalar quantity and the external power acting on the part  $ba$ , can be defined as:

$$P_{\partial ba}^{ext} = \int_{ba} b^+ v dy + \int_{\partial ba} t v dy \quad (eq. 140)$$

Here  $\partial ba$  is the border of the part  $ba$ .

The important consequence of the fact that the power is defined as a scalar quantity is that its value does not change changing the reference frame. It is one of the basic concepts that allow to obtained equilibrium equations that we are looking for. However, to obtain equilibrium equations, we need to transform what has been said up to now in words in mathematical relations. With this purpose let us consider two different observer named  $o$  and  $o'$ . One observer  $o'$  rotate and translate with respect the other one  $o$ . In view of this roto-traslacion, a variable  $y$  in  $o$  becomes a variable  $y'$  in  $o'$  defined as:

$$y' = w(t) + Q(t)(y - y_0) \quad (eq. 141)$$



Where the quantities  $w$  and  $Q$  are both function only of time.

This relation defines a rigid attitude change leading to no length variation of the body between the two observers. In mathematical terms it means:

$$|y_1 - y_2|^2 = |y'_1 - y'_2|^2 \quad (eq. 142)$$

The speeds, obtained deriving  $y$  measured by the observers can be simply expressed as:

$$v = \dot{y} \quad (eq. 143)$$

$$v' = \dot{y}' = \dot{w} + \dot{Q}(y - y_0) + Q\dot{y} \quad (eq. 144)$$

In order to compare these two speeds,  $\dot{y}'$  should be expressed in the reference frame of the observer  $o'$ . Considering that the matrix  $Q$  is orthogonal, i.e.  $Q^T = Q^{-1}$  and indicating  $v'$  in the reference frame of the observer  $o$  as  $v^*$  we can write:

$$v^* = Q^{-1}\dot{y}' = Q^T\dot{v}' = Q^T\dot{w} + Q^T\dot{Q}(y - y_0) + Q^TQ\dot{y} \quad (eq. 145)$$

The first term:  $Q^T\dot{w} = C(t)$  represents the relative translation. The term  $Q^TQ\dot{y}$  is generally named  $v(t)$ .

Then, for the property of the orthogonal matrices, we also know that  $Q^TQ = I$ . Deriving this expression with respect time we get:

$$Q^T\dot{Q} + \dot{Q}^TQ = 0 \quad (eq. 146)$$

With some algebraic manipulations, is simple to obtain:

$$Q^T\dot{Q} = -(Q^T\dot{Q})^T \quad (eq. 147)$$

In words this relation means that the matrix  $Q$  is antisymmetric. Formally can be written:

$$Q^T\dot{Q} := W \text{ so that } \nabla q \in R^3 \quad W(y - y_0) = q \times (y - y_0)$$

Finally the velocity of  $o'$  in  $o$  can be expressed as:

$$v^* = C(t) + q(t) \times (y - y_0) + v(t) \quad (eq. 148)$$

Remembering that, as defined before, the external power is independent from the considered reference frame being this one a scalar quantities and considering relations found up to now, the equilibrium equations can be derived. In fact:

$$P_{ba}^{ext}(v) = P_{ba}^{ext}(v^*) \quad (eq. 149)$$

Substituting equation eq.148:

$$P_{ba}^{ext}(v) = P_{ba}^{ext}(C + q \times (y - y_0) + v) = P_{ba}^{ext}(v) + P_{ba}^{ext}(C + q \times (y - y_0)) \quad (eq. 150)$$

This implies:

$$P_{ba}^{ext}(C + q \times (y - y_0)) = 0 \quad \nabla C, q, ba \quad (eq. 151)$$

It means that power, calculated over whatever kind of rigid motion, must be equal to zero.

Remembering the definition of external power given before, this relation can also be expressed as:

$$\begin{aligned} \int_{ba} b^+(C + q \times (y - y_0))dV + \int_{\partial ba} t(C + q \times (y - y_0))da = 0 = C \int_{ba} b^+dV \\ + \int_{\partial ba} tda + q \left( \int_{ba} (y - y_0) \times b^+dV + \int_{\partial ba} (y - y_0) \times tda \right) = 0 \quad (eq. 152) \end{aligned}$$

Where to obtain this result the property of mixed product has been used.

Being the value of the sum of these terms equal to zero  $\nabla C, q, ba$  the only possibility is that:

$$\int_{ba} b^+ dV + \int_{\partial ba} t da = 0$$

$$\int_{ba} (y - y_0) \times b^+ dV + \int_{\partial ba} (y - y_0) \times t da = 0 \quad (eq.153)$$

These are the so called *Balance Equations*. In particular, the first one express the balance of forces while, on the other hand, the second express the balance of moments.

Starting from this balance equation, the equilibrium equation in which we are interesting in order to define a relation allowing to obtain stress distribution on each section of a beam can be derived. However, stress tensor of Cauchy should be firstly introduced.

Let us now consider the following figure (Figure 100) representing a certain cut section at a certain point:

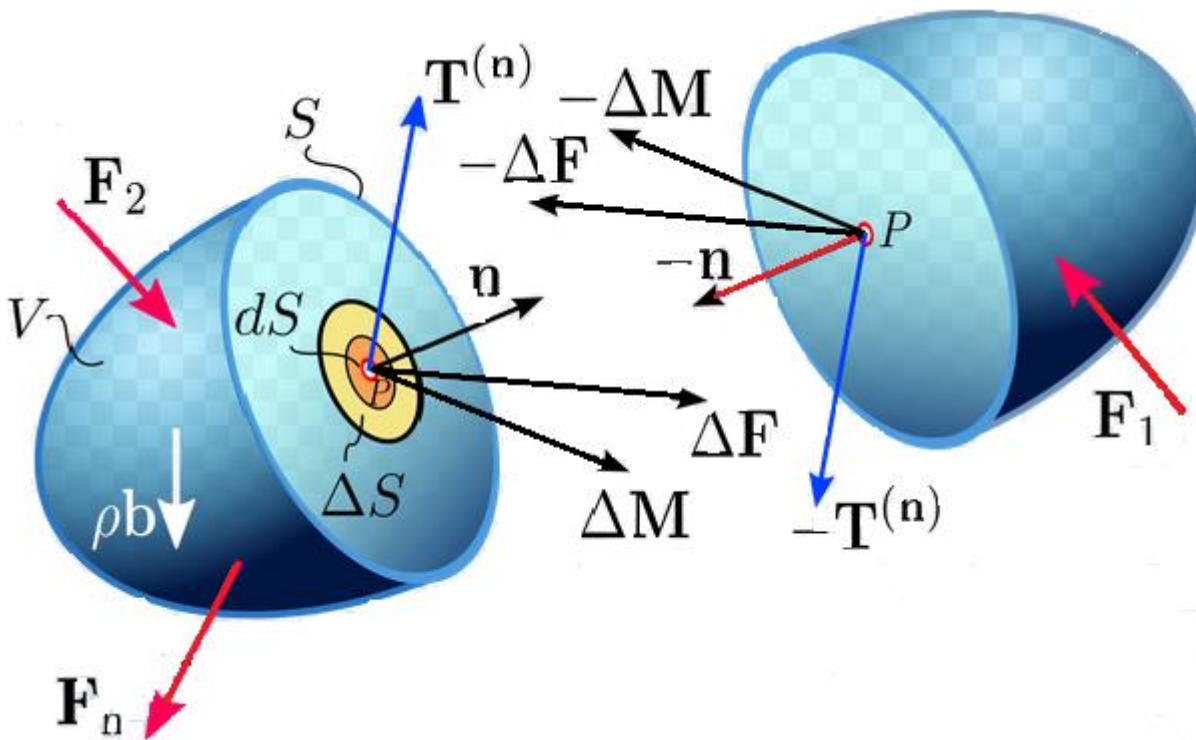


Figure 100: Body interactions

At the cut surface, interactions between molecules of the two cut parts can now be represented by forces F and moments M. F and M represents the resultants of forces and moments

respectively. In particular we are interesting to know what happen in a point of the cut section. For this reason, what should be considered is the limit for the section that tends to zero. Now, to make this we cannot consider the area of the section that tends to zero ( $A \rightarrow 0$ ) because, for example, also the area of a segment tends to zeros. To avoid this problem what should be considered is that, instead of the area, the diameter of the section, named  $diamA$ , tends to zero. The diameter is defined as the maximum distance between two points on the considered section area. Making this diameter tends to zero all the area of the section tend to zero but in this way we are sure that it tends to zero in a point. With these considerations, the following two limits can be write down:

$$\lim_{diamA \rightarrow 0} \frac{F}{A} = t \quad (eq. 154)$$

$$\lim_{diamA \rightarrow 0} \frac{M}{A} = 0 \quad (eq. 155)$$

The existence of these two limits is guaranteed by Cauchy. In other words, the meaning of the existence of these two limits is that we have always force type interaction.

In general, the vector  $t$  depends on the choose point  $x$  and on the orientation of the cut named  $n$ .

In the 3D space  $t$  will be described by 9 components:

- 3 coordinate are needed to define the point  $x$
- 3 coordinate are needed to define the orientation  $n$
- 3 coordinate are needed to define the vector  $t$

Now that meaning of the  $t$  vector has been introduced, let us consider an infinitesimal material part with a tetrahedral shape as represented in figure (Figure 101).

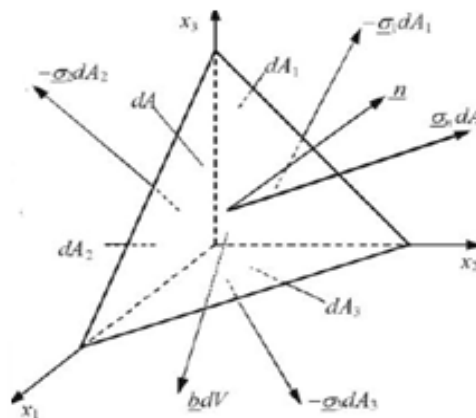
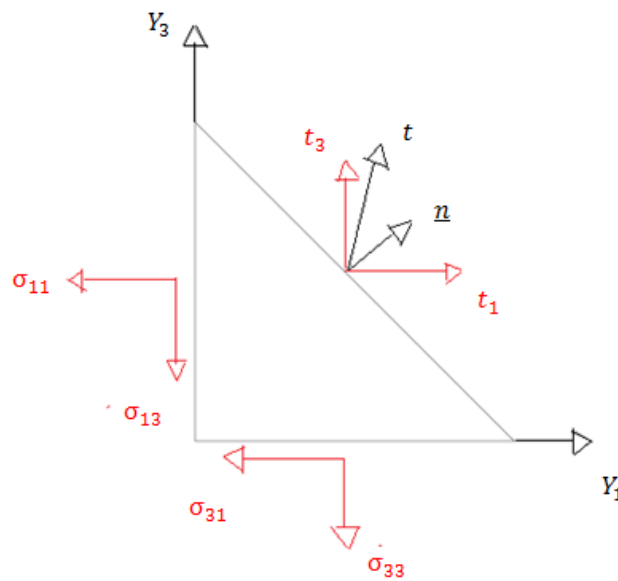


Figure 101: Infinitesimal 3D material portion of tetrahedral shape

Where with  $dA_i$  we refer to the face normally placed with respect  $y_i$  that in a mathematical way can be expressed as:

$$dA_i = n_i dA \quad (eq. 156)$$

Over the overall face  $dA$  will be present a certain stress. Hence, the body to be in equilibrium needs reactions on the other faces whose sum is equal to the applied stress on the surface  $dA$ . For simplicity we can consider a 2D representation as shown in figure (Figure 102).



**Figure 102: 2D infinitesimal material portion of tetraedical shape**

For example, on the face 1 that has as normal  $y_1$  will act a reaction of components:  $\sigma_{11}, \sigma_{12}, \sigma_{13}$ . To make equilibrium, we have to sum each of these components present on each surface. For hypothesis, we have considered an infinitesimal tetrahedral portion of material so that, the vector  $t$  defined before can be considered constant on the face  $dA$ . However, in general, on a finite surface, it could change point by point. Now, the equilibrium equation, with all the considerations done about the notation used, can be written explicitly in the three directions as:

$$\begin{aligned} t_1 dA &= \sigma_{11} dA_1 + \sigma_{12} dA_2 + \sigma_{13} dA_3 \\ t_2 dA &= \sigma_{21} dA_1 + \sigma_{22} dA_2 + \sigma_{23} dA_3 \\ t_3 dA &= \sigma_{31} dA_1 + \sigma_{32} dA_2 + \sigma_{33} dA_3 \end{aligned} \quad (eq. 157)$$

And remembering the geometry property represented in eq.153, we can also write:

$$\begin{aligned}
 t_1 dA &= \sigma_{11} n_1 dA + \sigma_{12} n_2 dA + \sigma_{13} n_3 dA \\
 t_2 dA &= \sigma_{21} n_1 dA + \sigma_{22} n_2 dA + \sigma_{23} n_3 dA \\
 t_3 dA &= \sigma_{31} n_1 dA + \sigma_{32} n_2 dA + \sigma_{33} n_3 dA
 \end{aligned}
 \tag{eq. 158}$$

So simplifying terms dA in both sides of equations we find at the end a point by point property. Dividing everything for dA and using a compact notation we can write:

$$\begin{Bmatrix} t_1 \\ t_2 \\ t_3 \end{Bmatrix} = \begin{pmatrix} \sigma_{11} & \sigma_{12} & \sigma_{13} \\ \sigma_{21} & \sigma_{22} & \sigma_{23} \\ \sigma_{31} & \sigma_{32} & \sigma_{33} \end{pmatrix} \begin{Bmatrix} n_1 \\ n_2 \\ n_3 \end{Bmatrix}
 \tag{eq. 159}$$

Or in an even more compact form:

$$t = \sigma n
 \tag{eq. 160}$$

This last equation is what is referred as *Theorem of Cauchy*. Here  $\sigma$  is the previously mentioned Stress Tensor of Cauchy.

At this point, considering the Gauss theorem for which:

$$\int_{\partial ba} A n da = \int_{ba} div(A) dV
 \tag{eq. 161}$$

and using this one in the previous obtained forces balance equation with together the Theorem of Cauchy, avoiding here the trivial mathematical steps, we are able to obtain the following relation:

$$\int_{ba} (b^+ + div(\sigma)) dV = 0
 \tag{eq. 162}$$

Being the integrand continuous, this relation can be written as:

$$b^+ + \text{div}(\sigma) = 0 \quad (\text{eq. 163})$$

This is the so called *Balance Equation of Cauchy*. This equation becomes much clearer if it is explicit in three partial differential equations as:

$$\begin{aligned} b_1^+ + \frac{\partial \sigma_{11}}{\partial x_1} + \frac{\partial \sigma_{12}}{\partial x_2} + \frac{\partial \sigma_{13}}{\partial x_3} &= 0 \\ b_2^+ + \frac{\partial \sigma_{21}}{\partial x_1} + \frac{\partial \sigma_{22}}{\partial x_2} + \frac{\partial \sigma_{23}}{\partial x_3} &= 0 \\ b_3^+ + \frac{\partial \sigma_{31}}{\partial x_1} + \frac{\partial \sigma_{32}}{\partial x_2} + \frac{\partial \sigma_{33}}{\partial x_3} &= 0 \end{aligned} \quad (\text{eq. 164})$$

Of course this is just the balance equation related with the balance of forces. Another balance equation, related with moments, can be obtained but it is not meaningful for our purpose.

Now, after this introduction of basic concepts, the relation to find stress distribution on each section of the beam can be obtained. As mentioned above, to get this stress distribution, the double T beam used to model the wing, is considered as a beam of *De Saint Venant*. Considering the beam in this way, means considering a further simplified beam model that allows to find the solution of the elastic solid. De Saint Venant considers a series of hypothesis on the geometry, load distribution and stress distribution on the beam itself. These hypotheses on the beam can be summarized with the following list of points:

- Homogeneous and Istropic solid
- Prismatic solid with a finite number of angles
- The length of the axis is much more long with respect the diameter
- Volume force and reaction force are zero
- The body is loaded only on the bases
- The stress tensor is characterized by the following form:

$$\sigma = \begin{pmatrix} 0 & 0 & \sigma_{13} \\ 0 & 0 & \sigma_{23} \\ \sigma_{31} & \sigma_{32} & \sigma_{33} \end{pmatrix}$$

Even if the assumption introduced by De Saint Venant seems to be far from what is expected on a real beam, especially considering the fourth one, has been shown that also in condition far from those described by these hypothesis the stress distribution obtained is really close to that one predicted by this model.

In particular, remembering the balance equation obtained before and considering the assumptions introduced by De Saint Venant they will be:

$$\begin{aligned} \frac{\partial \sigma_{13}}{\partial x_3} &= 0 \\ \frac{\partial \sigma_{23}}{\partial x_3} &= 0 \\ \frac{\partial \sigma_{31}}{\partial x_1} + \frac{\partial \sigma_{32}}{\partial x_2} + \frac{\partial \sigma_{33}}{\partial x_3} &= 0 \end{aligned} \quad (eq. 165)$$

What come out from this system of equations is that, the tangential stress on each section of the beam normal to the Z axis are independent on the location of the considered section along the Z axis. In other words, it means that if they are equal to zero on the bases they will be equal to zero everywhere. In this case, also the normal stress component is independent from Z. What should be pointed out at this point is that, load characteristics can be defined considering the action acting on the bases (z=L) and named  $\sigma_{ij,0}$ , as:

- Normal force

$$N_0 = \int_A \sigma_{zz,0} dA \quad (eq. 166)$$

- Cut force

$$T_{x,0} = \int_A \sigma_{zx,0} dA \quad (eq. 167)$$

$$T_{y,0} = \int_A \sigma_{zy,0} dA \quad (eq. 168)$$

- Torque Moment



$$M_{T,0} = \int_A (\sigma_{zy,0}x - \sigma_{zx,0}y) dA \quad (eq. 169)$$

- Bending Moment

$$M_{x,0} = \int_A \sigma_{zz,0}y dA \quad (eq. 170)$$

$$M_{y,0} = - \int_A \sigma_{zz,0}x dA \quad (eq. 171)$$

For each other section normal to the Z axis the load characteristics can be obtained considering the *Principle of Euler* which says that, if a body is in equilibrium, each part of this must be in equilibrium. Following this principle, must be:

$$\begin{aligned} N &= N_0 \\ T_x &= T_{x,0} \\ T_y &= T_{y0} \\ M_x &= M_{x,0} - zT_{y0} \\ M_y &= M_{y,0} + zT_{x0} \\ M_T &= M_{T,0} \end{aligned}$$

An important observation is that, each case of loading can be solved separately applying then the superposition principle to the four characteristic loads defined before. The consequence of this is that, the De Saint Venant problem can be simply defined as: searching for each of these cases the load stress distribution in each section. This is the reason why to develop our methodology, without any loss of generality, we have considered only stress distribution related with bending moment due to vertical forces (forces acting along the y direction of the beam). In fact, with the consideration done, is then possible in the future to consider also different load in addition to those considered here developing this methodology to make more complete the overall analysis without invalidate the numerical methodology itself. This will result clearer when the key relation to get stress distribution on each section will be derived in the following.

Particularly interesting for our purpose is to consider that, how has been demonstrated the solution of the normal stress distribution on each section normal to the z axis, can be expressed in the following form:

$$\sigma_{zz} = a + bx + cy - z(a_1 + b_1x + c_1y) \quad (eq.172)$$

Now, the derivation of each of the coefficient of this equation must be determined in order to get a useful relation. These information introduced up to now will be used. In particular the coefficient  $a_1$  will be assumed to be equal to zero without any demonstration because in a different way with respect the other coefficient its derivation requires a deeper detailed analysis that is not in the purpose of this thesis.

1. Coefficient a

$$N = \int_A \sigma_{zz} dA = \int_A a + bx + cy - z(b_1x + c_1y) dA \quad (eq.173)$$

Remembering that  $S_x = \int_A x dA$  and  $S_y = \int_A y dA$  are the so called static moment. They are zero if the reference frame considered is a barycentre reference frame. Being our reference of this type as can be seen looking at Figure 95, coefficient a can be written as:

$$a = \frac{N}{A} \quad (eq.174)$$

2. Coefficient b

The relation that must be considered in this is case is:

$$\begin{aligned} M_y &= \int_A \sigma_{zz} x dA = \\ &= \int_A \left( \frac{N}{A} + bx + cy - z(b_1x + c_1y) \right) x dA = \end{aligned}$$

$$= \int_A \left( \frac{N}{A} y + bx^2 + cyx - z(b_1x^2 + c_1yx) \right) ydA \quad (eq. 175)$$

Where  $I_{xy} = \int_A xydA$  is the centrifugal moment and it is zero if the considered reference frame is a principal reference frame. Then considering also the definition given before for Static moment and the section for  $z = 0$ , we get:

$$b = -\frac{M_{y,0}}{I_y} \quad (eq. 176)$$

3. Coefficient  $c$

It can be obtained exactly in the same way as for the coefficient  $b$  but considering as starting equation that one for  $M_x$ . It will be expressed as:

$$c = \frac{M_{x,0}}{I_x} \quad (eq. 177)$$

4. Coefficient  $c_1$

$$M_{ox} = M_x - zT_{y,0} \quad --> \quad zT_{y,0} = M_x - M_{ox}$$

$$M_x - M_{x,ox} = \int_A \sigma_{zz} ydA - \int_A \left( \frac{N}{A} - \frac{M_{y,0}}{I_y} x + \frac{M_{x,0}}{I_x} y \right) ydA \quad (eq. 178)$$

From here remembering the choice of the reference system we obtain:

$$c_1 = -\frac{T_{y,0}}{I_x} \quad (eq. 179)$$

5. Coefficient  $b_1$

The way to proceed here, is the same followed for coefficient  $c_1$  but now the starting point is  $M_y - M_{y,0}$ . Then we obtain:

$$b_1 = -\frac{T_{x,0}}{I_y} \quad (eq. 180)$$

Substituting all these coefficients in the previous relation and making simple algebraic manipulations we are able to obtain the following important relation:

$$\sigma_{zz} = \frac{N}{A} - \frac{M_y}{I_y}x + \frac{M_x}{I_y} \quad (eq. 181)$$

This relation is the so called *Trinomial of Navier*.

This one is the key relation that, once defined the characteristic loads (Normal force N and bending moments  $M_x, M_y$ ) in the section at which we are interesting, allows us to determine the normal stress distribution in that section.

Once, from outputs of the flight dynamic model, forces time history are obtained (their results has been already shown before) it is the first relation that must be used to transform force in stress, more useful for crack growth prediction analysis.

In order to use this relation, load characteristics acting on each section (Normal force, cut force, bending moment) must be determined. To make this, relations introduced before for a generic section will be used (eq.166-171). In particular, a schematization of the force acting on the beam is needed to get these values. Again, with the idea to simplify as much as possible the basic structure of our methodology, inertial force and lift force can be considered acting in the middle of the beam. In this way schematization and the load characteristics due to these forces can be simply considered. These are as shown in figure (Figure 103):

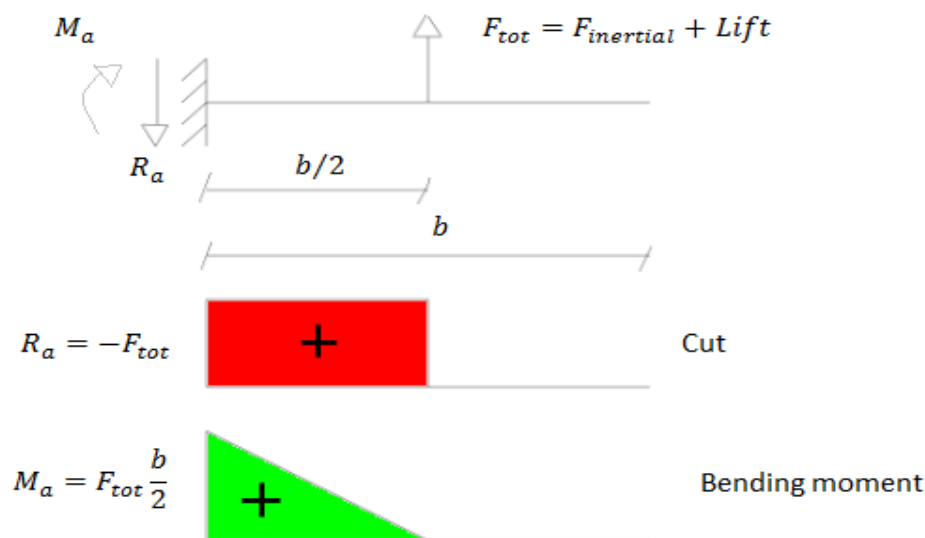


Figure 103: Beam loads characteristic distributions

This schematization could be then improved considering a more real distribution of forces. For example, a uniform or triangular distribution of inertial force and an elliptical distribution of the lift force along the wing span could be considered.

Looking at the previous figure (Figure 103) where diagrams of load characteristics are reported we can observe how under our schematization (1DOF model), normal forces are zero in each section. Of course it will not be true in reality and it is just an assumption introduced here to make simpler the model. Anyway, can be also understood that, once the methodology has been completely developed and tested, adding a lateral force on the previous beam schematization, only lead to a normal force distribution along the beam different from zero that can be simply determined and added to the Trinomial of Navier. In other words it means that our method to proceed, for the purpose of this moment can be considered natural. In fact, it creates a very simple schematization of the reality but, at the same time it can be modified in a very simple way once the entire numerical model has been developed.

On the other hand, regarding to the cut force distribution, its load diagram has also been determined in the previous figure (Figure 103). In fact, it is something that must be taken into account to determine bending moment acting on the beam (eq.170-171) and moreover, it is also important to be considered for a complete analysis. However the cut forces do not produce normal stress and for this reason they are not considered in the Trinomial of Navier.

The only term remaining are those related with the bending moments. In particular, considering again our assumption of 1DOF, force are only oriented along the y direction so that the only bending moment component is  $M_x$ . The Trinomial of Navier becomes:

$$\sigma_{zz}(y) = \frac{M_x}{I_y} y \quad (\text{eq. 182})$$

At this point, the only thing left to get stress distribution on each section is the determination of bending moment and Inertial moment.

With regard to bending moment, it can be determined using the relation above. In particular in this simple beam schematization it can be simply calculated as:

$$M_x = F_i z + Lift z \quad (eq. 183)$$

Where,  $F_i$  the inertial force and  $z$  is the distance along the beam from section and force considered. In our case, considering the simple schematization before (Figure 96) and the fact that we are interesting in the knowledge of the stress distribution at the root of the wing being this one the critical location, it becomes:

$$M_x = F_i \frac{L}{2} + Lift \frac{L}{2} = (F_i + Lift) \frac{L}{2} \quad (eq. 184)$$

Where,  $L$  is the length of the beam that is equal to half the wingspan of the airplane considered. With regard to the inertial moment, it can be calculated using relation coming out from handbooks making use of dimensions of the considered section beam. The principal dimensions for a double T beam are reported in figure (Figure 104):

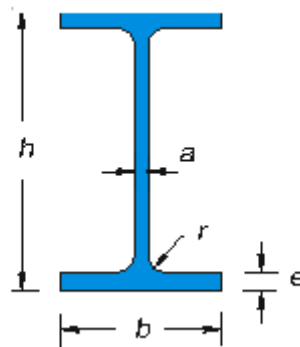


**Figure 104: Double T section dimensions**

Considering these dimensions, the inertial moment can be obtained from the following relation

$$I_x = \frac{BH^3 - bh^3}{12} \quad (eq. 185)$$

$$I_y = \frac{(H - h)B^3}{12} + \frac{h(B - b)^3}{12} \quad (eq. 186)$$

Dimension considered in our case are reported in table:

B	220mm
L	25500mm
H	600mm
h	540mm
a	12mm
e	19mm

As can be seen from the Trinomial of Navier, stress distribution on each section under this schematization of forces has a typical butterfly shape.

From here we can understand how the critical location will be present at the upper and lower top of the beam. In particular on an aircraft wing, considering the action of the lift force, the lower top of the beam is the most critical location. In fact, it is loaded with a positive mean stress that is the most critical type of load from a fatigue point of view (cracks tend to be opened).

At this point, applying the previous relation time by time for all the force history a stress time history spectrum at the root of the beam can be obtained. It looks like as it is shown in figure (Figure 105).

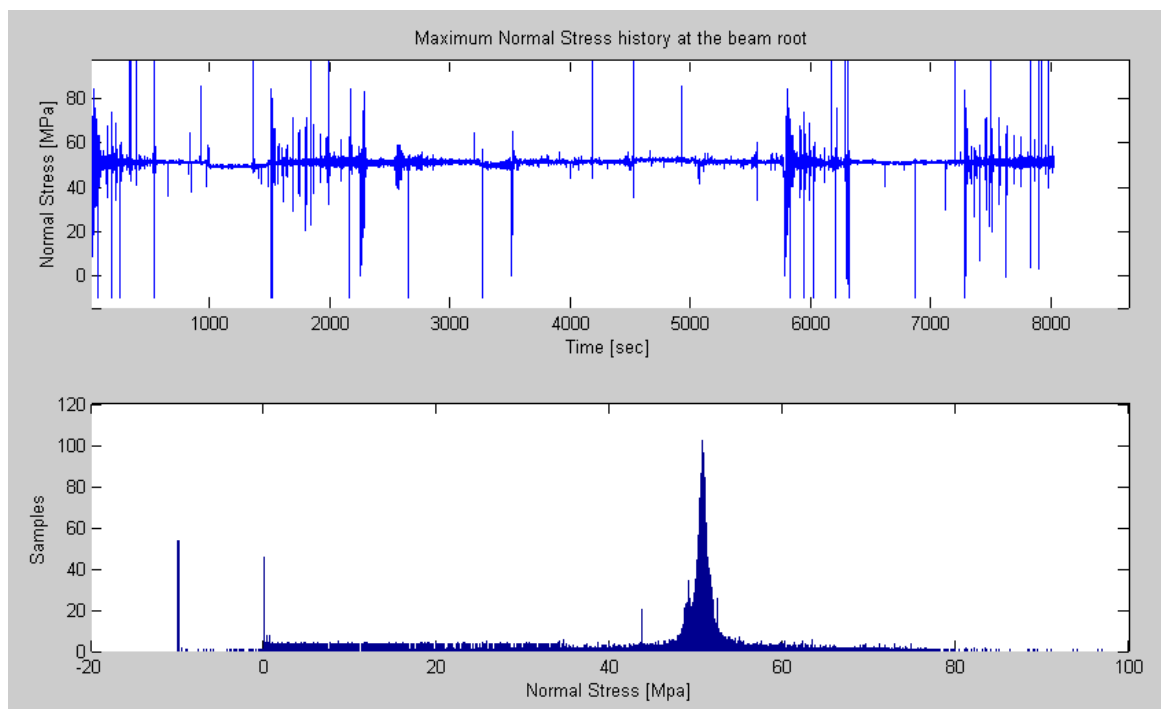


**Figure 105: Generated stress history**

Looking at this figure (Figure 105) we can understand how a real case load spectrum is much more complex than the simple constant amplitude load case.

The Matlab code used to obtain stress at the critical location at each time using value coming from the simulation is reported here below:

```
load Acc
load Lift

y=[-H/2:100:H/2];
first=0;
for i=1:length(timel)
    az(i)=Acc(i);
    M(i)=m.*az(i).*b/2+Lift(i)*b/12;
    Sigma_zz_max(i)=M(i).*H./(2*Ix);
for k=1:length(y)
    M1(k)=m*az(i)*b/2;
    Sigma_zz(k)=M1(k)*y(k)/(2*Ix);
end
Sigma_history(:,i)=Sigma_zz;
first(i)=Sigma_zz_max(i);

end

figure(2)
subplot(2,1,1)
plot(timel,Sigma_zz_max)
xlabel('Time [sec]')
ylabel('Normal Stress [MPa]')
title('Maximum Normal Stress history at the beam root')
subplot(2,1,2)
hist(Sigma_zz_max,length(Sigma_zz_max))
xlabel('Normal Stress [Mpa]')
ylabel('Samples')
```

Where the vector named “*Sigma\_zz\_max*” represents the vector that interpolating its point provide the load spectrum shown before.

Summarizing, what we need to know to obtain a spectrum like this is:

- $N(t), M_x(t), M_y(t)$
- $I_x, I_y, L$



### Process of load spectrum generation

At this point an important consideration must be pointed out. As said, introducing the purpose of our work, what we want to realize is an algorithm performing a damage tolerance analysis for a new structure. This structure will be generally different with respect that one used to obtain these values, at least in term of dimensions. Instead, in terms of loads acting, they can be considered the same because they have been obtained simulating typical mission using an aircraft as much as possible similar to that one to be designed. For this reason, while the force acting on the structure can be considered the same, stresses will be different between the Boeing C-17, used to run the flight dynamic simulation, and the new airplane named for simplicity of notation C-18. It means that a transition between this stress history to that of the C-18 will be needed. In particular, looking at the parameters needed to obtain the spectrum of the C-17 (Figure 104) those that could be different between the two structures are:  $I_x, I_y, L$ . Changing these values with those of the new structure a different stress spectrum will be obtained. In order to reduce as much as possible computational time, that is one of the biggest problem when treating airplane load history due to the amount of data, this transition between these two spectrums has been done in terms of stress levels whose meaning was already introduced in the previous chapter (Chapter 4) dealing with load spectrum.

At this point, taking into account considerations done, the logical next step is in dividing the obtained spectrum in levels. First of all, the right number of levels must be determined. As already mentioned in previous chapters, this choice is a trade-off between accuracy and computational time cost but, as demonstrated, a good choice is placed in a range between 10-12 levels (Figure 67). In our case the number of selected levels was 12 (note that it will means a 2D range matrix of 144 cells!). The division of the spectrum in levels has been simply done as follow:

1. Take the maximum stress value of the entire load spectrum
2. Take the minimum stress value of the entire load spectrum
3. Determine the difference between the two previous values and divide for the selected number of levels. In this way, the range amplitude for each level is:

$$\Delta = \frac{\sigma_{max} - \sigma_{min}}{N}$$

In this way a number of intervals equal to the number of levels minus one can be also determined. Each of these intervals, considering how they have been defined, are characterized by the same amplitude. In particular, the value of this amplitude determines the accuracy achievable. In our case the amplitude of each interval is equal to 11MPa that referring to what is reported in literature about these types of considerations should provide a good accuracy. In the following figure an example of the spectrum divided in level is shown (Figure 106).

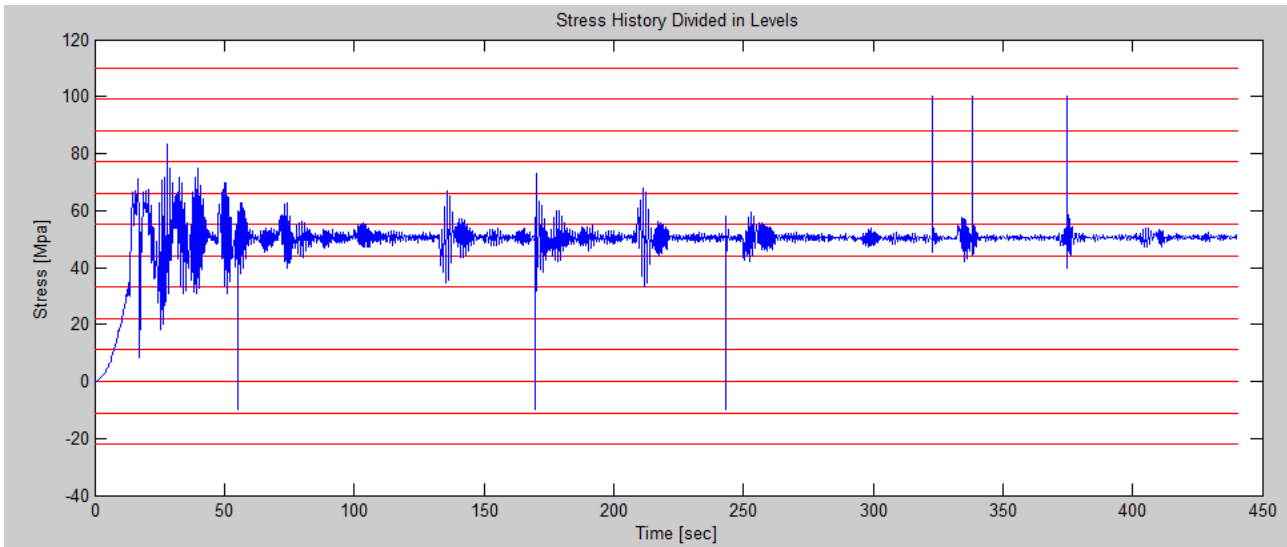


Figure 106: Stress history generated divided in levels

Note that here, only a small portion of the entire spectrum has been considered. In fact, in order to analyse the entire spectrum, it had to be divided in small portion, otherwise the computational time was too much high. This problem can be improved using a much more performance computer.

In order to determine the transition between the load spectrum of C-17 to that of C-18 using levels as described before, a load correction factor (LCI) has been introduced as follow:

$$LCI = \frac{bHL}{b_1H_1L_1} \frac{I_{x1}}{I_x} \quad (eq. 187)$$

Here the parameters with pedix 1 represent those of the new structure. Defining this parameter, we are able to simply determine the stress level amplitude (SLA) for the new structure starting from the known stress level amplitude of the C-17 considering the following simple relation:

$$SLA_1 = \frac{SLA}{LCI} \quad (eq. 188)$$

The definition of the level correction factor as before, in other words means that if LCI is smaller than 1 the load spectrum of the C-18 is characterized by a highest value of the maximum and/or a lowest value of the minimum stress amplitude.

At this point, algorithms to extract and represent in a useful way the main characteristics of the load spectrum are needed to develop a crack growth analysis and must be here described. The main load spectrum characteristic for a crack growth analysis using the fracture mechanism concepts as previously introduced are: peaks, valleys and ranges.

In view of this, an algorithm to determine all peaks and valleys has been created. This algorithm is simply based on the mathematical definition of relative maximum and minimum so that it can be described with the following steps:

- Consider the vector containing all the stress value in time
- If  $\sigma_{zz}(i) < \sigma_{zz}(i + 1)$  and  $\sigma_{zz}(i + 1) > \sigma_{zz}(i + 2)$  the value of  $\sigma_{zz}(i + 1)$  is considered as a peak and it is stored in a vector named "Peak\_history".
- Else if  $\sigma_{zz}(i) > \sigma_{zz}(i + 1)$  and  $\sigma_{zz}(i + 1) < \sigma_{zz}(i + 2)$  the value of  $\sigma_{zz}(i + 1)$  is considered as a vally and it is stored in a vector named "Valley\_history".
- Else the value of  $\sigma_{zz}(i + 1)$  is a middle value and it is not considered because it is not of primary importance in crack growth analysis

To validate results, which are expressed as two vectors, should be verified that the total number of peaks is equal to the total number of valleys. It can be easily done comparing the length of the two vectors provided by the algorithm and named respectively *Peak* and *Vally*. Here below, the Matlab code of this algorithm is reported.

```

Sigma1=[Sigma_zz_max, Sigma_zz_max(end)];
for i=2:length(Sigma_zz_max)
    if Sigma_zz_max(i)>Sigma_zz_max(i-1) && Sigma_zz_max(i)>Sigma1(i+1)
        Peak(i)=Sigma_zz_max(i);
    else if Sigma_zz_max(i)<Sigma_zz_max(i-1) && Sigma_zz_max(i)<Sigma1(i+1)
        Valley(i)=Sigma_zz_max(i);
    else Middle(i)=Sigma_zz_max(i);
    end
end
end
Sigma(i)=Sigma_zz_max(i);
end

```

Looking at the load spectrum obtained, as could be expected, it is irregular. A representation of this one on the exceedance diagram is not so meaningful but, anyway, can still be useful to get an idea about the severity of the obtained spectrum, especially to compare this one with others spectrum like, for example, the standardized ones previously described and currently used in aeronautical industry.

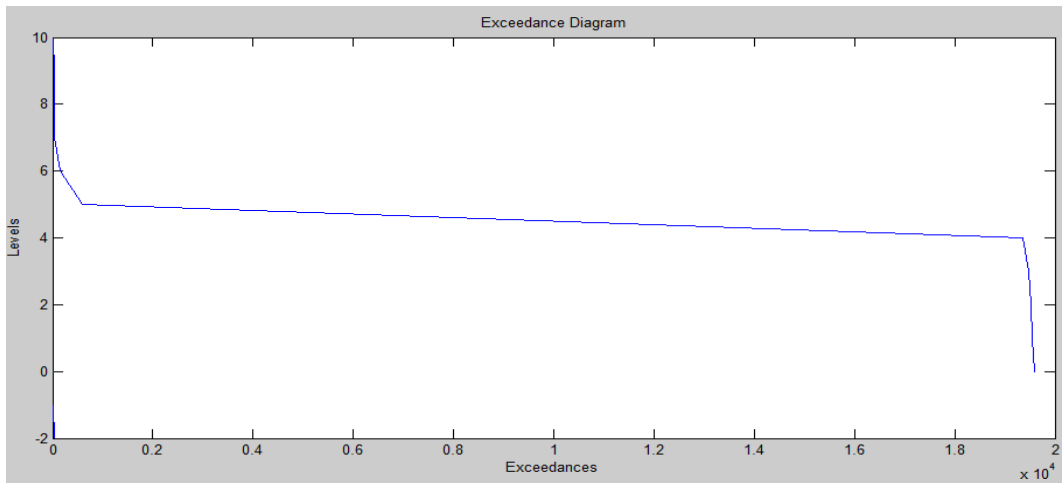


Figure 107: Exceedance diagram of the obtained stress history

This diagram as described in Chapter 4 is expressed as number of peaks above each level. Starting from here, the number of peaks in each level can be also determined. In fact, it can be simply obtained by differentiating the number of peak above one level and the number of peak above the lower one. Hence, in addition to this plot, a histogram representing the number of peaks for each interval has been also plot out just to have a clearer statistical vision of the spectrum severity. In the figure below (Figure 108), a typical representation of this histogram in terms of number of peak per positive interval (interval above reference level taken equal to zero) is shown.

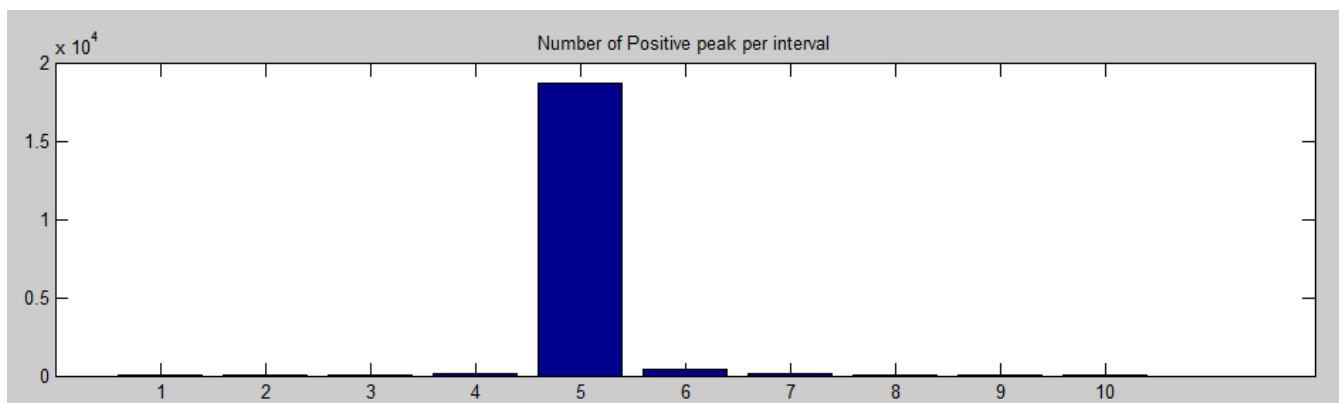


Figure 108: Histogram representing number of peaks per interval

The Matlab code of the algorithm used to derive both these plots is reported here below:

```

for i=1:length(Sigma_level_pos)
    EX=Positive_peak(find(Positive_peak>Sigma_level_pos(i)));
    NEX(i)=length(EX);
    NEX1=fliplr(NEX);
    NEX2=[0,NEX];
end
for i=1:length(Sigma_level_neg)
    EXN=Negative_valley(find(Negative_valley<Sigma_level_neg(i)));
    NEXN1(i)=length(EXN);
    NEXN=fliplr(NEXN1);
    NEXN2=[0,NEXN];
end

NEX1=[NEXN,NEX];
U_neg=length(Sigma_level2);
U_pos=length(Sigma_level1);
Level_neg=[-U_neg:1:-1];
Level_neg=fliplr(Level_neg);
Level_neg1=[0,Level_neg];
Level_pos=[0:1:U_pos];
LEVELS=[Level_neg,Level_pos];

figure(4)
Z=zeros(length(NEXN1));
plot(NEX,Level_pos)
hold on
plot(NEXN1,Level_neg1)
hold on
plot(NEXN1,Z)
xlabel('Exceedances')
ylabel('Levels')
title('Exceedance Diagram')
N1=[NEX,0];
for i=1:length(NEX)
    figure(5)
    PPI1(i)=N1(i)-N1(i+1);
end
PPI=PPI1(1:(end-1));
N2=[NEXN1,0];
for i=1:length(NEXN1)
    NPI1(i)=N2(i)-N2(i+1);
end
NPI=NPI1(1:(end-1));
Positive_interval=[1:N_livelli_pos];
Negative_interval=[1:N_livelli_neg];
figure(5)
subplot(2,1,1)
bar(Positive_interval,PPI)
title('Number of Positive peak per interval')
subplot(2,1,2)
bar(Negative_interval,NPI)
title('Number of Negative peak per interval')

```

Where, the vector named “*Sigma\_level\_pos*”, contains the stresses values of each positive level and the vector named “*Sigma\_level\_neg*” contains the stresses values of each negative level. In fact, as has been pointed out in Chapter 4 when a not symmetric load spectrum is treated, the

exceedance diagram must be developed separately for both the upper and lower side with respect the reference level. The reference level, in our case, has been considered to be coincident with a stress equal to zero.

Finally to summarize all these results that, as mentioned, can be used just to obtain information about the severity of the spectrum, an algorithm summarizing all these results automatically in a table has also been developed. The needed of an algorithm that automatically fill in a table like that is of extremely importance because in this way, when a new simulated flight is performed, the table will be automatically updated. An example of this table is shown.

	Levels	Counts	Negative_Exceedances	Positive_Exceedances
1	-2	0	0	0
2	-1	41	0	0
3	0	44	41	19586
4	1	24	0	19542
5	2	42	0	19518
6	3	116	0	19476
7	4	18773	0	19360
8	5	426	0	587
9	6	118	0	161
10	7	12	0	43
11	8	3	0	31
12	9	28	0	28
13	10	0	0	0

**Figure 109: Summary table of the processed load spectrum**

This table has been also useful also to verify that the previous developed algorithms provide correct values.

As described in Chapter 4, useful methods to process the spectrum and store data are those called “range counting method” where, instead of information about peak and valley, we are able to get information about load amplitude. In particular more interesting are those methods, of this type, named “2D methods” that allow to get information not only on the amplitude but also on the mean value or R-ratio of each cycle. Using these methods load spectrum information are stored in a matrix like that one reported in Figure 58. Different way to fill in this matrix has been already described before:

- Simple 2D range counting method
- Rainflow counting method

As already pointed out, the Rainflow counting method is much more conservative if used to predict crack growth. This is the reason why it has been the chosen method to develop our methodology. As seen, there are two different algorithms that can be used to apply the concept on which this method of processing load spectrum is based. However, that one providing the simpler way in terms of numerical calculation is the so-called ATSM algorithm. This is the reason why it is the one that we preferred to use. The general form of this algorithm was already introduced and described before so that here only how it has been really applied is described. However, for the moment, with data available, the Rainflow algorithm cannot directly be applied. In fact, before to proceed we need to determine the interval in which each peak and valley (whose values are known from a previous code) is located.

To make this, the following Matlab code has been developed:

```
o=0.*E;
A=find(Sigma_zz_max);
B=Sigma_zz_max(A(1));
if B>0
o=ordina(Peak_history,Valley_history);
else if B<0
o=ordinal(Peak_history,Valley_history);
end
end
for i=1:length(o)
yu=1;
for k=1:(length(Sigma_level_plot11)-1)
if o(i)>Sigma_level_plot11(k) && o(i)<Sigma_level_plot11(k+1)
N_level(i)=yu;
yu=yu+1;
else yu=yu+1;
end
end
end
```

In this algorithm, the variable B has been used to know if the first stored value of the load spectrum is a peak or a valley. Then, a vector named “o” containing all peaks and valley alternatively has been created. The function that is called in this algorithm named “ordina” (or “ordina1” depending if the first is a peak or a valley) has been created to build up the previously defined vector composed of alternate peak and valley values. To carry out this algorithm two “for” cycles were needed: the external one is used to move step by step in each element of the defined vector “o” while the inner loop, on the other hand, is used to evaluate the considered element of the vector “o” at which interval belongs. The output of this algorithm is a vector named “N\_level” in which the location for each element of the vector “o”, in terms of interval, is

stored. Now that the vector “N\_level” has been determined, the Rainflow counting method can be applied. The developed Matlab code for the Rainflow counting method is reported here below:

```
x1=N_level; x=[N_level,0,0,0]; D=1;
for i=1:length(x1)
    if x(D)<x(D+1)
        if x(D)<=x(D+2) && x(D+1)<=x(D+3)
            y(i)=x(D+3);
            y1=x(D+3);
            y_peak(i)=x(D+1); %Neglected peak
            y_valley(i)=x(D+2); %Neglected valley
            D=D+3;
        else y(i)=x(D+1);
            y1=x(D+1);
            D=D+1;
        end
    else if x(D)>x(D+1)
        if x(D)>=x(D+2) && x(D+1)>=x(D+3)
            y(i)=x(D+3);
            y1=x(D+3);
            y_peak(i)=x(D+2); %Neglected Peak
            y_valley(i)=x(D+1); %Neglected valley
            D=D+3;
        else y(i)=x(D+1);
            y1=x(D+1);
            D=D+1;
        end
    else if x(D)==x(D+1)
        y(i)=x(D+1);
        D=D+1;
    end
end
    if (D)>=(length(x1))
        break
    end
end
N_rainflow=[x(1),y];
N_peak_rainflow_negletted=y_peak;
A121=find(y_peak);
for i=1:length(A121)
    N_peak_rainflow_negletted(i)=y_peak(A121(i));
end
B11=find(y_valley);
for i=1:length(B11)
    N_valley_rainflow_negletted(i)=y_valley(B11(i));
end
Nlevel_rainflow=N_rainflow(1:(end-1));
N_peak_rainflow_negletted=N_peak_rainflow_negletted(1:length(A121));
N_valley_rainflow_negletted=N_valley_rainflow_negletted(1:length(N_peak_rainflow_neglette
d));
%larger ranges
for i=1:length(Nlevel_rainflow)
    CL1(i)=N_rainflow(i);
    RO1(i)=N_rainflow(i+1);
end
%Smaller ranges
for i=1:length(N_peak_rainflow_negletted)
    CL11(i)=N_valley_rainflow_negletted(i);
    RO12(i)=N_peak_rainflow_negletted(i);
end
for i=1:length(N_peak_rainflow_negletted)
    CL111(i)=N_peak_rainflow_negletted(i);
    RO121(i)=N_valley_rainflow_negletted(i);
end
CL_rainflow=[CL1,CL11,CL111]; RO_rainflow=[RO1,RO12,RO121];
```



As can be seen from here, the application of the very simple rainflow algorithm, as introduced in Chapter 4, is quite complex when applied to a real load spectrum. Here, the variable D has been used to change the considered element inside the vector “N\_level”. In fact it cannot be done considering a simple “for” cycle (for each loop it would move forward one steps) because depending on the current tern of range considered, at the next step, we should move forward one or three steps. It is clear from the logic on which this algorithm is based. The variable “CL\_rainflow” (CL is for column) and “RO\_rainflow” (RO is for row) need to be defined because they are fundamental to fill in the matrix with the outputs of the Rainflow counting method. Based on these two vectors, an algorithm automatically fill in a matrix, as that in Figure 58 but characterized by 144 cells (12 intervals) has been created. It is quite long but does not need particular clarification. For this reason, it has not been reported here. However, how the filled in matrix appears when running the algorithm is shown in figure.

	From 1	From 2	From 3	From 4	From 5	From 6	From 7	From 8	From 9	From 10	From 11	From 12
To 1	0	0	0	0	0	0	0	0	0	0	0	0
To 2	0	0	0	0	5	2	15	17	6	2	0	0
To 3	0	0	126	0	0	0	4	0	0	0	0	0
To 4	0	0	6	60	0	1	2	7	15	6	3	0
To 5	0	0	0	8	96	9	11	6	26	5	0	0
To 6	0	0	0	0	7	236	129	210	52	0	0	15
To 7	0	4	0	5	8	147	40670	217	31	1	0	19
To 8	0	19	0	10	19	198	213	288	14	0	0	0
To 9	0	18	4	14	20	54	16	18	64	0	0	0
To 10	0	6	0	1	6	0	1	0	0	0	0	0
To 11	0	0	0	2	0	1	0	0	0	0	0	0
To 12	0	0	0	0	0	2	32	0	0	0	0	0

**Figure 110: 2D Rainflow counting matrix**

The developed Rainflow algorithm, has been resulted quite complex when applied to the real load spectrum like can be considered that one coming out from our flight dynamic model. For this reason, before to move on, verification of results provided by this algorithm is necessary. This test has been carried out considering two very simple load sequences appositely created. Anyway, it has been also a test for all the other algorithms developed and introduced up to now. The two simplified load sequence considered are:

- Constant amplitude load sequence (Figure 111)
- Simple variable amplitude load sequence (Figure 112)

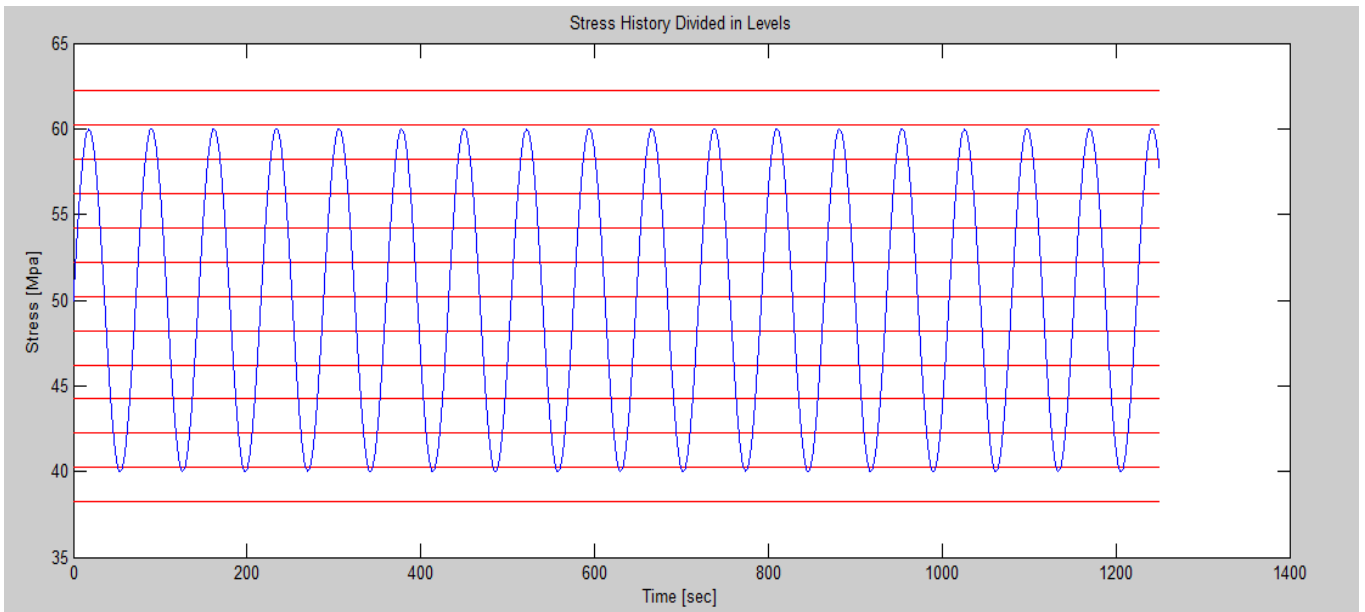


Figure 111: Testing constant amplitude load sequence

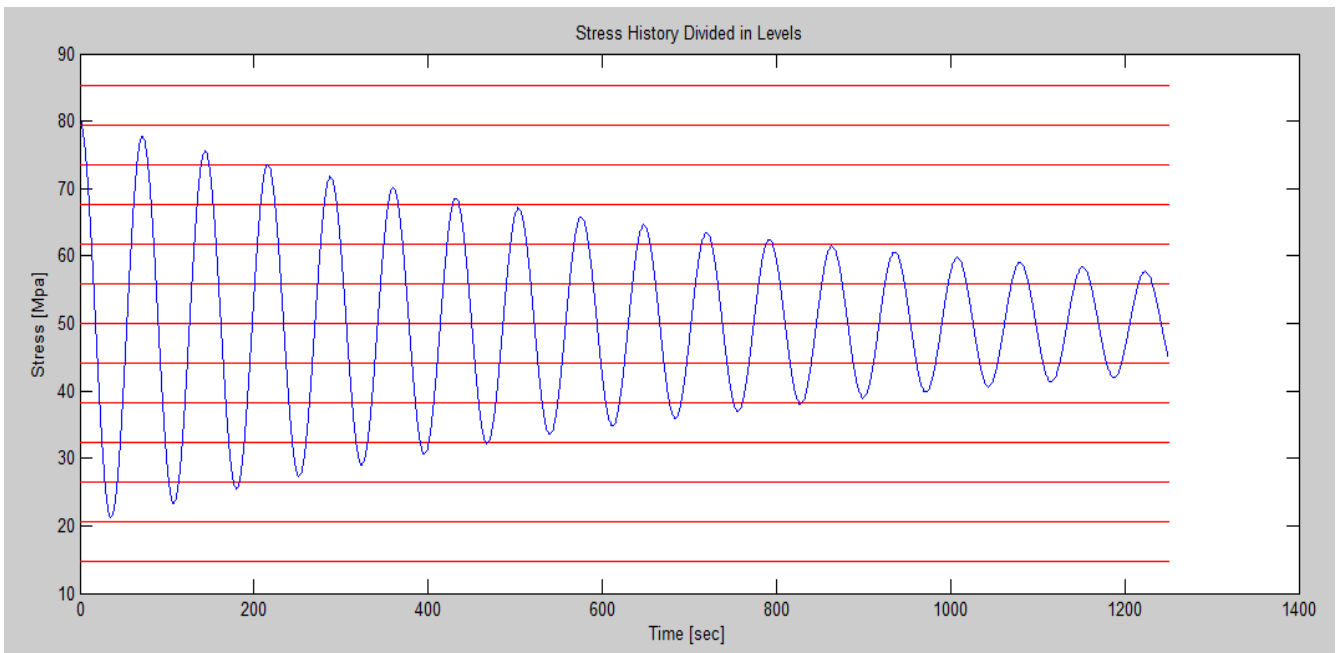


Figure 112: Testing damping load sequence

In these figures they are already divided in levels so that, even without numerical calculation, the load matrix can be simply determined by hand. This allows verifying the presence of possible errors introduced by the Rainflow algorithm above. Results expressed in matrix form for both these simple cases are reported here below.

	From 1	From 2	From 3	From 4	From 5	From 6	From 7	From 8	From 9	From 10	From 11	From 12
To 1	0	0	0	0	0	0	0	0	0	0	17	0
To 2	0	0	0	0	0	0	0	0	0	0	0	0
To 3	0	0	0	0	0	0	0	0	0	0	0	0
To 4	0	0	0	0	0	0	0	0	0	0	0	0
To 5	0	0	0	0	0	0	0	0	0	0	0	0
To 6	0	0	0	0	0	0	0	0	0	0	0	0
To 7	0	0	0	0	0	0	0	0	0	0	0	0
To 8	0	0	0	0	0	0	0	0	0	0	0	0
To 9	0	0	0	0	0	0	0	0	0	0	0	0
To 10	0	0	0	0	0	0	0	0	0	0	0	0
To 11	16	0	0	0	0	0	0	0	0	0	0	0
To 12	0	0	0	0	0	0	0	0	0	0	0	0

Figure 113: 2D Rainflow 2D counting matrix for CA testing loading sequence

	From 1	From 2	From 3	From 4	From 5	From 6	From 7	From 8	From 9	From 10	From 11	From 12
To 1	0	0	0	0	0	0	0	0	0	0	0	0
To 2	0	0	0	0	0	0	0	0	0	0	3	0
To 3	0	0	0	0	0	0	0	0	1	3	0	0
To 4	0	0	0	0	0	0	0	1	4	0	0	0
To 5	0	0	0	0	0	0	0	4	0	0	0	0
To 6	0	0	0	0	0	0	0	0	0	0	0	0
To 7	0	0	0	0	0	0	0	0	0	0	0	0
To 8	0	0	0	2	4	0	0	0	0	0	0	0
To 9	0	0	2	3	0	0	0	0	0	0	0	0
To 10	0	1	2	0	0	0	0	0	0	0	0	0
To 11	0	2	0	0	0	0	0	0	0	0	0	0
To 12	0	0	0	0	0	0	0	0	0	0	0	0

Figure 114: Rainflow 2D counting matrix for damping testing load sequence

They are the confirmation that the developed algorithm provides correct results. In fact, even if these are extremely simple load sequences, they are enough to validate our code.

The matrix coming out from this algorithm is the fundamental input for crack growth analysis using all the fracture mechanism concepts introduced in Chapter 3. Generally speaking, this matrix can be divided in two parts:

- Upper triangle: here are present all the positive range
- Lower triangle: here are present all the negative range

The positive range are those that tend to open the crack and for this reason are those that are dangerous from a fatigue point of view. In other words it means that load ranges stored in the upper portion of the matrix are those used in the subsequent crack growth analysis.

Before to go on with the application of these results in crack growth analysis process, what should be pointed out is that, all the results presented here, are only related with a small portion of the load spectrum and not with the entire one. In fact, as already mentioned, has been necessary to split the load sequence of each simulated flight in more than one part to reduce computational time. In fact, the idea has been to develop a general Matlab code in which the main algorithms are

those described before. Then these are applied at each portion in which the complete load spectrum has been divided. Results of these algorithms are essentially load ranges represented in the upper triangle of the obtained matrices from the Rainflow counting method used to process the spectrum. All these load ranges coming from each flight portion for each considered flight will be then processed and used in the following crack growth prediction analysis. In particular, referring to only one flight (then procedure can be repeated for other different simulated flight), once the process described by the previously introduced algorithm for each portion of the simulated flight have been used, main results for the following crack growth analysis are stored in vectors. As it is clear from observations carried out in Chapter 3 , the two main parameters needed for each simulated flight are: load cycles vector (vector containing a sequence of each load cycle as derived from the 2D Rainflow resultant matrix) and R-ratio vector (vector containing the characteristic R-ratio of each of the load cycle of the previous vector). In particular, the elements of these vectors need to be randomly placed accurately in order to maintain for each load cycle the corresponding R-ratio. This can be automatically done using the following developed algorithm.

```

%Load main parameters for each flight portion considered
load Parameters_part_1
load Parameters_part_2
load Parameters_part_3
load Parameters_part_4
load Parameters_part_5
%Generate random load sequence for each flight
DS1=[DS1_C18_rainflow1,DS1_C18_rainflow2,DS1_C18_rainflow3,DS1_C18_rainflow4,DS1_C18_rainflow5];
R1=[R_C18_rainflow1,R_C18_rainflow2,R_C18_rainflow3,R_C18_rainflow4,R_C18_rainflow5];
DS1_pos=[1:1:length(DS1)];
n=length(DS1_pos);
DS1_pos_rand=DS1_pos(randperm(n));
for i=1:length(DS1_pos_rand)
    JJ=DS1_pos_rand(i);
    DS1_rand(i)=DS1(JJ);
    R1_rand(i)=R1(JJ);
end
LDS_noise=length(DS1_rand);
DS_noise=DS1_rand;
R_noise=R1_rand;
%Save parameters for subsequent complete crack growth analysis
save('Flight_Noise','DS_noise','R_noise','LDS_noise')

```

As can be seen, at the beginning of this algorithm, the main parameters coming from the application of the previously described algorithm (processing spectrum algorithm), for each flight

portion considered are loaded. In particular, the algorithm above, used as example, refers to the simulated automatic flight with flight plan Noise. Outputs of this algorithm are:

1. *DS\_noise*: it is a vector containing all the load cycles coming from the Rainflow counting method relative to the considered flight and placed randomly
2. *R\_noise*: it is a vector containing all the R-ratio (Chapter 3) for each load cycle respectively. Being the load cycles placed randomly, this algorithm guarantee that also in this new configuration, independent from its element position each load cycle is characterized by its own R-ratio.
3. *LDS\_noise*: it simply a number equal to the length of the *DS\_noise* vector. This parameter is not needed for crack growth analysis but as will be shown in the following it is essential to create a semi-random load sequence.

## Crack growth analysis algorithm

The crack growth prediction algorithms, which have the objective to determine the residual strength diagram and the crack growth diagram, will be described in the following. In fact, before to do this, must be observed that the crack growth analysis prediction is not developed separately for each portion of the complete flight spectrum but, a database of the main results obtained running the Matlab code for each portion is created so that, it can be carried out uniquely in a Matlab script named “*crack\_growth.m*”. With these main results stored, we are able to perform not only the crack growth analysis prediction, presenting results in the previous remembered diagram but in the same code we can also present the total exceedance diagram, the histogram plot representing the number of peak per interval and the Rainflow 2D counting method matrix.

Now, the last step is to present the crack growth analysis prediction algorithms which have been developed to be used for damage tolerance design approach.

Here, first of all, the importance of the load sequence, whose effects have been explained in chapter 3, must be considered. As already known, when the Rainflow counting method is applied the load sequence is lost. Here, important observations on the advantages achievable with our methodology based on load sequences belonging to a flight characterized by a certain severity specified by the user must be introduced.

Generally speaking, there are an infinite number of ways in which the load cycles obtained from the previous described Rainflow algorithm can be applied. However, practically, only two of them are really applicable when the load sequence characteristics are presented in term of exceedance diagram and/or 2D matrix. They could be:

- Completely random load sequence: In these case the only information needed are those provided by the 2D matrix resulting from the Rainflow algorithm as previously described. A vector composed by randomly distributed load cycles can be generated in Matlab simply using the following general code based on the Matlab function *randperm*:

```
load DS1_C18_rainflow_tot
n=length(DS1_C18_rainflow_tot);
DS1_C18_rainflow_tot_random=a(randperm(n))
```

- Semi-random load sequence: In this case, the general way to proceed has been explained in chapter 4. It is based on information provided by the total exceedance diagram. Results achievable in term of crack growth using a semi-random load sequence are more realistic than those achievable using a simple completely random load sequence. It can be explained considering interaction effects phenomena introduced in Chapter 3. What should be remembered here is that, a semi-random load sequences is characterized by periods of different severity (each of these periods is defined with the process described in Chapter 4) applied randomly with cycles in each period even randomly applied. This should represent in a more realistic way loads at which an airplane could be subjected during its operational life. However, as can be understood considering the general way to proceed to get a semi-random load sequence, a numerical algorithm providing such result could be not so easy to be defined.

One of the main advantages of our methodology, where load sequences are appositely created by the user using designed flight simulator described in Chapter 5, is that, we are able to get the more realistic semi-random load sequence without needed to apply the commonly used process in aeronautical field based on exceedance diagram and described in Chapter 4. This allows avoiding the development of complex algorithms and even strong assumption on the shape of the exceedance diagram. In fact, in our case, with the algorithms previously described, load spectrum of each predefined flight can be treated separately and then results applied randomly to generate a complete semi-random load sequence for subsequent crack growth analysis. Hence, the main effort of our methodology is not only related with the fact that a less general complete load

spectrum can be derived with respect standardized load sequence, being the aircraft considered in the simulator very similar to that one to be designed, but, at the same time, we are also able to provide to the user the possibility of selecting the severity of each flight (environment, manoeuvres, etc.) and process each of them separately so that a real semi-random sequence can be defined.

The way to proceed to get a semi-random load sequence applying our methodology can be described with the following list of points:

1. User defines flight plan, not only in term of trajectory and aircraft mass but also considering expected flight severity due to for example turbulence.
2. Running the simulation (manually or automatically) the load history and then the stress history at the selected critical location can be defined as described in the first part of this chapter.
3. The load spectrum obtained with this run simulation can be processed separately using the Rainflow counting method described and developed in the previous part of this chapter. The result of this method will be a vector containing all load cycles useful for subsequent crack growth analysis. These cycles come out from the 2D matrix and their real sequence is lost. For this reason the previously mentioned vector is created in a random way using the already introduced "*randperm*" Matlab function.
4. This way to proceed will be repeated for many different user defined and simulated flight plans. They need to be built up in order to represent as much as possible real complete load spectrum representing the entire operational life of the airplane considered.
5. Once all the user defined flight plans have been simulated and processed as defined at point 3, we will get many different load vectors with randomly applied elements. Each of these vectors can be then considered as an element of another vector representing the load vector of the entire aircraft life considered with simulations.
6. At this point to create a semi-random load sequence as it has been defined, each of these elements that in reality are random vectors representing a certain flight period, must be randomly applied. In this way, the searched semi-random load sequence can be created. It will be useful in the following crack growth analysis.

Here below, the Matlab algorithm developed to load all together the load vectors for each flight period considered and generate a semi-random load sequence is reported:

```

load Flight_noise load Flight_noise1
load Flight_departure load Flight_manual
DS1_C18=[DS_noise,DS_noise1,DS_departure,DS_manual];
R_C18=[R_noise,R_noise1,R_departure,R_manual];
LDS_tot=[LDS_noise,LDS_noise1,LDS_departure,LDS_manual];
V=DS1_C18;
V_length=LDS_tot;
V_pos=0.*ones(1,length(V_length));
k=0;
for i=2:length(V_length)
    V_pos(i)=k+V_length(i);
    k=V_pos(i);
end
V_position=0.*ones(1,length(V_length));
V_position(1)=1;
V_position(2:end)=V_pos(2:end);
n=length(V_position);
V_pos_rand=V_position(randperm(n));
DS_semi_random=0.*ones(1,length(V));
R_semi_random=0.*ones(1,length(R_C18));
g=0;
for i=1:length(V_pos_rand)
    JJ=V_pos_rand(i);
    index=find(V_position==JJ);
    L=V_length(index);
    DS_semi_random((g+1):(g+L))=V((JJ+1):(JJ+L));
    R_semi_random((g+1):(g+L))=R_C18((JJ+1):(JJ+L));
    g=L+g;
end
DS1_C18_rainflow_tot=DS_semi_random;
R_C18_rainflow_tot=R_semi_random;

```

At the beginning, vectors output from the last introduced algorithm for each flight are load. Of course Matlab is not able to see each of these vectors inside the complete one as an element but only as a normal vector characterized by a length equal to the sum of the length of each loaded vectors. For this reason, this algorithm is needed to process this vector to obtain the searched semi-random load sequence. In order to obtain a more useful vector for our purpose, at each of these “load vector elements” has been assigned a certain number representing the position of its first element in the complete vector. This has been useful to get a simple vector where each element is characterized by a single number at which the “*randperm*” Matlab function can be applied. Once the random location of the associated simpler elements vector to those in which we are really interested has been generated, the correspondent complete random vector can be obtained making use of the meaning of each of these assigned numbers and knowing the length of each “load vector element” of the initial complete load vector (this is the reason why is essential to store in memory also the length of each load cycle for each flight). At this point the searched semi-random load sequence can be obtained. Probably this algorithm is much more difficult to say than to make or use.



However, that one described up to now, is an important step linking the phase in which the load spectrum is processed and that where the real damage tolerance analysis, described in the following of this thesis, is considered.

Now, this generated semi-random load sequence will be used to determine the two main plots in which we are interesting in damage tolerance analysis. In developing these algorithms, other inputs, in addition to those already described are needed. In particular these inputs are:

- material data that can be derived from handbooks, they are a function only of the material
- empirical coefficient that will be used in crack growth model as described in the relation derived in Chapter 3

. However the most important one are:

- Fracture Toughness
- Yield strength
- Geometry factor  $\beta$
- $m$ , coefficient needed in Yield zone model
- $A, B$  coefficient needed in crack closure model

In our case, always considering as focus, the development of the methodology more that the results coming out from here, the material considered is: *Al 2024 T3 – 51*. It is an aluminium alloy where the prevalent alloyed element is Copper (Cu). With together the alloy 7075 it is the most used on the airplane airframe. Then the designation T3-51 refers to an alloy that has been heat treated and quenched.

In the following table, the values considered for each of the previous mentioned parameters are reported. How these values have been used is described in the following.

Fracture Toughness: $K_I$	$73.7 \text{ MPa}\sqrt{\text{m}}$
Yield strength: $\sigma_{02}$	$324 \text{ N/mm}^2$
Yield zone model coefficient: $m$	1
Crack closure model coefficient: A	0.4
Crack closure model coefficient: B	0.6

In addition to this parameter, a geometry factor  $\beta$ , which is used in the Paris relation to take into account the effect of the finite width of the structure, is also needed. As already introduced, this parameter  $\beta$  being a dimensionless parameter is generally expressed as a function of the ratio between the crack length  $a$  and the width of the structure  $W$ . Moreover, the shape of this function depends on the type of crack (centre crack, edge crack, etc.). In our case, remembering that the section of the beam considered is a double T and taking into account the previous observation about stress concentration factor  $K_t$  (Chapter 3), in particular its meaning in representing the inhomogeneous distribution of stresses, we expect that the more probable location for crack development, is one of the corners shown in figure (Figure 115).

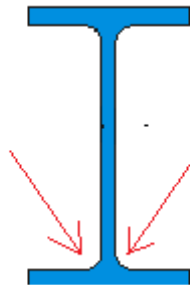


**Figure 115: Critical locations for crack development**

Then the most critical corners are those in the lower part being in this portion the structure subjected to a positive mean stress.

Considering these observations, the function to describe the geometry factor  $\beta$  is assumed to be the empirical function provided by a double crack edge. This relation can be expressed as:

$$\beta(a) = \frac{1.222 - 1.222 \left(\frac{a}{W}\right) - 0.060 \left(\frac{a}{W}\right)^2 + 0.728 \left(\frac{a}{W}\right)^3}{\sqrt{1 - 2 \frac{a}{W}}} \quad (eq. 189)$$

Now, that all the parameters needed to use equations introduced in Chapter 3 are introduced, the developed algorithms can be described.

First of all, based on material data the total residual strength of the considered material can be obtained. As explained, the real residual strength diagram is a combination of the residual

strength reduction due to crack growth and the residual strength before collapse. For this reason Feddersen interpolation (Chapter 3), has been used to create the total residual strength diagram of the material. The total strength diagram obtained is shown in figure:

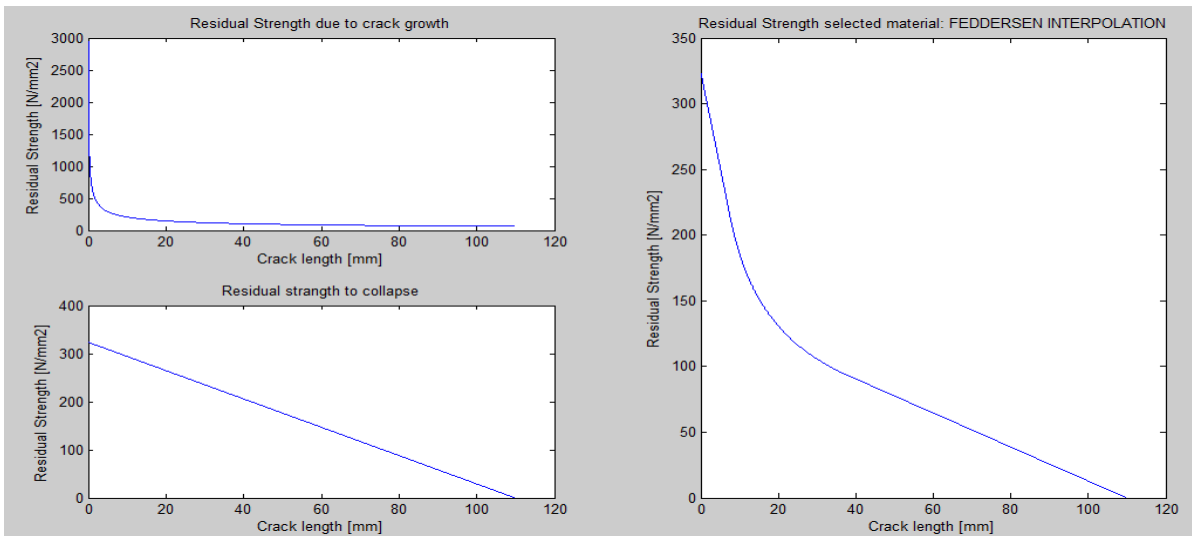


Figure 116: Residual strength diagram with Feddersen interpolation

Here, the total plot, representing the Feddersen interpolation and coming from the combination of the other two, as described in Chapter 3, is shown on the right and side. On the left hand side, the plots of the residual strength reduction related with fracture toughness and collapse strength are singularly reported. This plot could be useful for instance to compare two different materials in the designing phase. The Matlab code used to derive this plot is that one here below:

```
%FEDDERSEN INTERPOLATION residual strength
Beta1=(1.122-1.122*(W/(6*W))-0.060*(W/(6*W))^2+0.728*(W/(6*W))^3)/(sqrt(1-2*(W/(6*W))));
S1=KI/(Beta1*sqrt(pi*W/6));
for i=1:length(a11)
Beta(i)=(1.122-1.122*(a11(i)/W)-0.060*(a11(i)/W)^2+0.728*(a11(i)/W)^3)/(sqrt(1-2*(a11(i)/W)));
Sigma_res1(i)=Sigma02-((1/3*Sigma02)/a23)*a11(i);
Sigma_res(i)=KI/(Beta(i)*sqrt(pi*a11(i)));
Sigma_res3(i)=S1-(S1/(W/2-W/6))*(a11(i)-W/6);
if a11(i)<a23
Sigma_res_tot(i)=Sigma_res1(i);
else if a11(i)>a23 && a11(i)<=W/6
Sigma_res_tot(i)=Sigma_res(i);
else if a11(i)>W/6
Sigma_res_tot(i)=Sigma_res3(i);
end
end
end
end
figure(2)
subplot(2,2,1)
plot(a,Sigma_residual)
subplot(2,2,3)
plot(a,Sigma_res_col)
subplot(2,2,[2,4])
plot(a11,Sigma_res_tot)
```

Now, our objective, is in drawing on this plot the amount of strength reduction associated with a certain structure usage so that, it can be seen, load sequence after load sequence (or simulated flight after simulated flight), how it has been reduced due to crack growth. In order to make this, the first thing has been the development of an algorithm that, considering one of the crack growth models introduced before (No-interaction model, Yield zone model, crack closure model, Strip Yield model, etc.), provide the crack length after a certain number of cycles. Then this value of the crack length is used to derive the residual strength reduction related with this increment in crack length itself. In chapter 3 many different crack growth model were introduced. Each of them is characterized by more or less accuracy in predicting crack growth. However, a general rule valid for each of them is that, higher is the accuracy of a certain model and much more complex is the model itself. Also in view of this observation, in our case three different methods has been applied:

1. Simple crack growth method without consideration about interaction effect
2. Yield zone model where interaction effect are considered even if in a simple way
3. Crack closure model.

In the following, developed algorithms and how results are presented for each of them is shown. Comparing these results will be useful to get a feedback about the validity of the results provided. In fact, as can be expected by considerations in Chapter 3, the crack growth rate will be smaller in model where interaction effects are considered or in other words we expect that the no-interaction model are much more conservative.

Before introducing the developed algorithms for each of the said models, another important consideration should be pointed out. One of the main objectives of an analysis like that we are going to develop is the determination of the critical crack length starting from a provided minimum allowable residual strength. Knowing these parameters is then possible to determine the number of cycles (hours, flight, years...) at which critical crack has been reached. In doing this, the parameter which complicates the determination of this critical crack length is represented by the geometry factor  $\beta$ . In fact, as it has been introduced before, it is a function of the crack length itself. Considering the relation to determine the critical crack length:

$$a_{critc} = \frac{1}{\pi} \left( \frac{K_c}{\beta \sigma_{res}} \right)^2$$

the needed of an iterative process to determine this values comes out. This type of iterative process has been carried out developing the following Matlab code:

```

Sigma_p=input('Insert the Permissible Minimum Residual Strength: ');
a11=[0.001:0.001:(W/2)];
Beta1=(1.122-1.122*(W/(6*W))-0.060*(W/(6*W))^2+0.728*(W/(6*W))^3)/(sqrt(1-2*(W/(6*W))));
S1=KI/(Beta1*sqrt(pi*W/6));
%iterative process to determine the critical crack length
for i=1:length(a11)
Beta(i)=(1.122-1.122*(a11(i)/W)-0.060*(a11(i)/W)^2+0.728*(a11(i)/W)^3)/(sqrt(1-2*(a11(i)/W)));
ap(i)=1/pi*(KI/(Beta(i)*Sigma_p))^2;
if abs(ap(i)-a11(i))<0.001
    break
else if abs(ap(i)-a11(i))>0
    i=i+1;
end
end
end
ap=ap(end);
    
```

At the beginning this algorithm requires at the user the introduction of the minimum allowable value of the residual strength (design parameter) so that, the corresponding critical crack length can be found. On the other hand, fracture toughness, is a material characteristic that, once the material has been choose it is a fixed quantity stored as material data information.

The parameter named a11 in the previous code, containing all the crack lengths, is a vector introduced just to create the loop of the iterative process. On the other hand, at each loop, the parameter  $a_p$  represents a trial of the critical crack length that we are looking for running this algorithm. Then, to determine if this trial is the real critical crack length, the difference with respect to the current considered value a11(i), used to determine the geometry factor  $\beta$ , is carried out:  $a_p$  will be the critical crack length only if the two crack lengths values are the same or, in other words, if the difference between these two parameters is zero.

The first developed algorithm use the basic (and unrealistic) no-interaction model. Here crack growth is supposed to be a function only of the current load cycle and so independent from the load history up to that point. Below the algorithm is reported.

```

%Crack growth with simple non-interaction model
a=0.1;
for i=1:length(DS1_C18_rainflow_tot)
    Beta(i)=(1.122-1.122*(a/W)-0.060*(a/W)^2+0.728*(a/W)^3)/(sqrt(1-2*(a/W)));
    if R_C18_rainflow_tot(i)<=0
        da_dN(i)=C*(Beta(i)*DS1_C18_rainflow_tot(i)*sqrt(pi*a))^m;
    else if R_C18_rainflow_tot(i)>0
        da_dN(i)=C*(Beta(i)*DS1_C18_rainflow_tot(i)*sqrt(pi*a)/(1-
R_C18_rainflow_tot(i))^(1-gamma))^m;
    end
    end
    a1_rainflow(i)=da_dN(i)+a;
    a=da_dN(i)+a;
    Sigma_res1(i)=Sigma02-((1/3*Sigma02)/a23)*a1_rainflow(i);
    Sigma_res(i)=KI/(Beta(i)*sqrt(pi*a1_rainflow(i)));
    Sigma_res3(i)=S1-(S1/(W/2-W/6))*(a1_rainflow(i)-W/6);
if a1_rainflow(i)<a23
    Sigma_res_tot1(i)=Sigma_res1(i);
else if a1_rainflow(i)>a23 && a1_rainflow(i)<=W/6
    Sigma_res_tot1(i)=Sigma_res(i);
else if a1_rainflow(i)>W/6
    Sigma_res_tot1(i)=Sigma_res3(i);
    end
end
end
Sigma_residual(i)=KI/(sqrt(pi*a1_rainflow(i)));
end
figure(4)
subplot(2,2,[1:2])
N=[1:1:length(DS1_C18_rainflow_tot)];
plot(N,a1_rainflow)
xlabel('Number of cycle')
ylabel('Crack length [mm]')
title('Crack growth Rainflow counting method')
subplot(2,2,3)
plot(a1_rainflow,Sigma_res_tot1)
xlabel('Crack length [mm]')
ylabel('Residual Stress [N/mm2]');
title('Residual strength variation with crack growth')
subplot(2,2,4)
plot(a1_rainflow,Sigma_res_tot1,'r*')
hold on
plot(a11,Sigma_res_tot)
hold on
plot(ap,Sigma_res_tot,'g')
xlabel('Crack length [mm]')
ylabel('Residual Stress [N/mm2]');
title('Residual strength variation with crack growth general view')
legend('Actual Residual Strength','Residual Strength','Critical Crack Length')

```

Results coming out from this code and used for damage tolerance analysis are reported in figure (Figure 117)

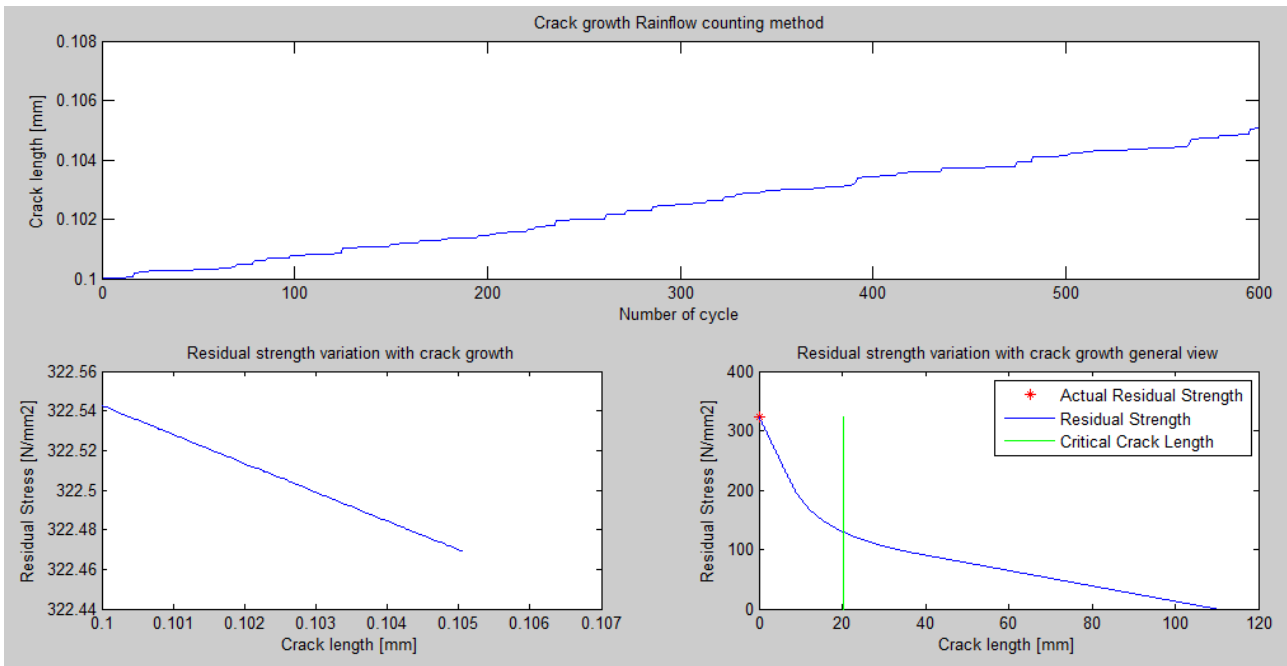


Figure 117: Crack growth results from non-interaction model

The diagram on the top in figure (Figure 116) represents the crack length as a function of the number of cycle. It is the previously called a-N diagram.

The plots below represent residual strength reduction due to crack growth. In particular, the plot on the left hand side represents the actual residual strength reduction after the considered load sequence and its influence on the total residual strength diagram is reported in the right hand side. Here the red portion (it seems a point in figure due to the small reduction of residual strength related with the short load sequence considered) represents where the actual residual strength is in the total plot. In addition, on this plot, with the green line, the location of the critical crack length corresponding to the provide input of minimum allowable residual strength is shown.

A second algorithm, where the same results will be shown, is here below reported. The important difference is that now the obtained results come out using the so called Yield zone model. Even if in a very simple and inaccurate way, retardation effect is here considered and the final crack growth obtained considering the same load sequence is expected to be shorter than before.

```

% Crack growth: Yield zone model
a=0.1;
rp=0;
for i=1:length(DS1_C18_rainflow_tot)
    Beta(i)=(1.122-1.122*(a/W)-0.060*(a/W)^2+0.728*(a/W)^3)/(sqrt(1-2*(a/W)));
    DK(i)=Beta(i)*DS1_C18_rainflow_tot(i)*sqrt(pi*a);
    r(i)=1/pi*(DK(i)/Sigma02)^2;
    lambda(i)=rp+a0-a;
if lambda(i)>r(i)
    CP(i)=(r(i)/rp);
    rp=rp;
else if lambda(i)<r(i)
    rp=r(i);
    CP(i)=1;
end
end
if R_C18_rainflow_tot(i)<=0
    da_dN(i)=CP(i)*C*(Beta(i)*DS1_C18_rainflow_tot(i)*sqrt(pi*a))^m;
else if R_C18_rainflow_tot(i)>0
    da_dN(i)=CP(i)*C*(Beta(i)*DS1_C18_rainflow_tot(i)*sqrt(pi*a)/(1-
R_C18_rainflow_tot(i))^(1-gamma))^m;
end
end
al_rainflow(i)=da_dN(i)+a;
a=da_dN(i)+a;
Sigma_res1(i)=Sigma02-((1/3*Sigma02)/a23)*al_rainflow(i);
Sigma_res(i)=KI/(Beta(i)*sqrt(pi*a1_rainflow(i)));
Sigma_res3(i)=S1-(S1/(W/2-W/6))*(al_rainflow(i)-W/6);
if al_rainflow(i)<a23
    Sigma_res_tot1(i)=Sigma_res1(i);
else if al_rainflow(i)>a23 && al_rainflow(i)<=W/6
    Sigma_res_tot1(i)=Sigma_res(i);
else if al_rainflow(i)>W/6
    Sigma_res_tot1(i)=Sigma_res3(i);
end
end
end
Sigma_residual(i)=KI/(sqrt(pi*a1_rainflow(i)));
end
figure(5)
subplot(2,2,[1:2])
N=[1:1:length(DS1_C18_rainflow_tot)];
plot(N,al_rainflow)
xlabel('Number of cycle')
ylabel('Crack length [mm]')
title('Crack growth Yield Zone model')
subplot(2,2,3)
plot(al_rainflow,Sigma_res_tot1)
xlabel('Crack length [mm]')
ylabel('Residual Stress [N/mm2]');
title('Residual strength variation with crack growth')
subplot(2,2,4)
plot(al_rainflow,Sigma_res_tot1,'r*')
hold on
plot(a11,Sigma_res_tot)
hold on
plot(ap,Sigma_res_tot,'g')
xlabel('Crack length [mm]')
ylabel('Residual Stress [N/mm2]');
title('Residual strength variation with crack growth general view')
legend('Actual Residual Strength','Residual Strength','Critical Crack Length')

```



As said, concepts of crack tip plasticity are here taken into account with the consequence that, crack growth in the current cycle is related with previous loads.

Developing this algorithm, the parameter  $m$ , defined in chapter 3, results particularly important in affecting obtained results. This coefficient is an empirical coefficient depending, not only on the material used, but also on the type of load sequence. For this reason, an empirical determination of this value is needed to improve results. In any case accurate value of this parameter is generally difficult to be obtained. It is an additional drawback in the use of this model. In our case, for simplicity and without any loss of generality, this coefficient has been considered to be equal to 1. Results coming out from here are presented in figure (Figure 118).

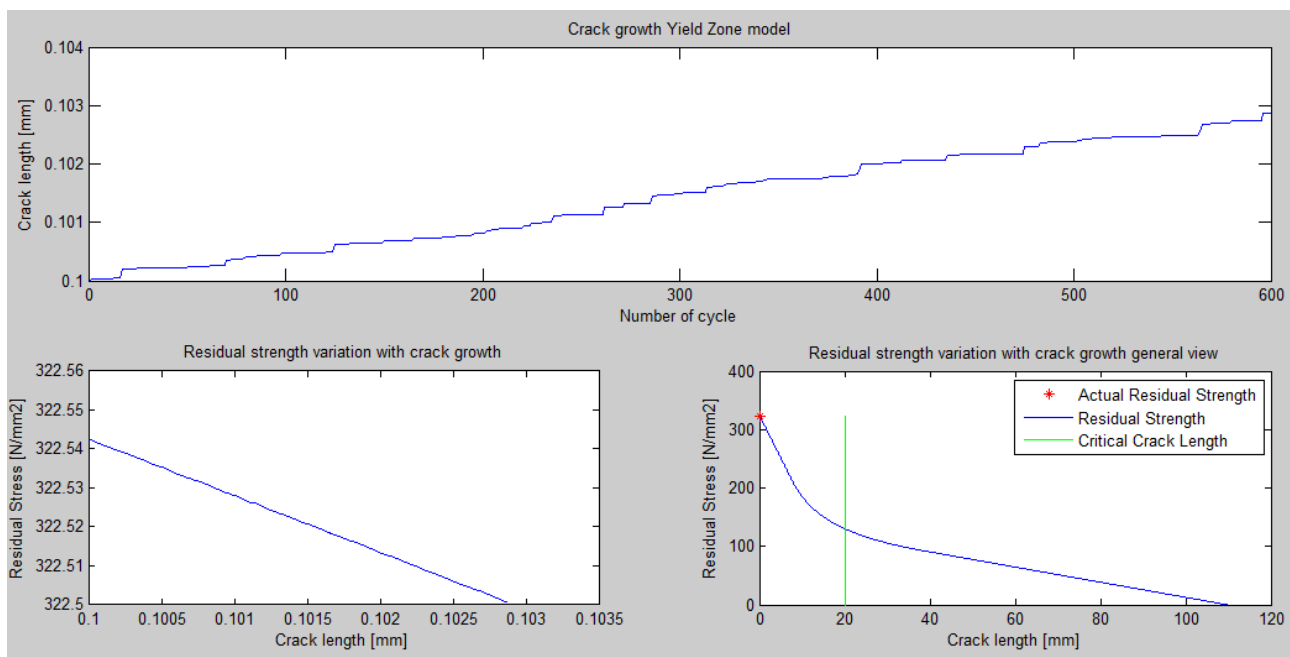


Figure 118: Crack growth results from Yield zone model

The meaning of each of this plot is the same as explained before. What could be interesting here is a comparison of the crack growth with the previous case. As can be expected, remembering the retardation phenomena due to crack tip plasticity, for the same load spectrum, the final crack length predicted by this model is shorter with respect what is predicted by the previous one.

To conclude this chapter, the third developed algorithm, based on crack closure model, a more accurate model with respect to those before, is presented here. As seen in chapter 3, there are three different crack closure models. That one developed here is the so called PREFASS model which requires, in a different way with respect to the model introduced before, information on previous load that must be stored in memory. In fact, the basic concept of this model is that, the

opening stress  $S_{op}$ , is calculated at each cycle, as a function of the previous maximum and minimum absolute loads. The algorithm is presented here:

```
%Crack growth: CRACK CLOSURE model
a=0.1;
for i=1:length(DS1_C18_rainflow_tot)
    Beta(i)=(1.122-1.122*(a/W)-0.060*(a/W)^2+0.728*(a/W)^3)/(sqrt(1-2*(a/W)));
    Smax(i)=DS1_C18_rainflow_tot(i)/(1-R_C18_rainflow_tot(i));
    Smin(i)=Smax(i)-DS1_C18_rainflow_tot(i);
    Kmax(i)=Beta(i)*Smax(i)*sqrt(pi*a);
    Kmin(i)=Beta(i)*Smin(i)*sqrt(pi*a);
    Kmaxa=max(Kmax);
    Kmina=min(Kmin);
    R(i)=Kmina/Kmaxa;
    U(i)=A1+B1*R(i);
    DK(i)=Beta(i)*DS1_C18_rainflow_tot(i)*sqrt(pi*a);
    DKeff(i)=U(i)*DK(i);
    if R_C18_rainflow_tot(i)<=0
        da_dN(i)=C*DKeff(i)^m;
    else if R_C18_rainflow_tot(i)>0
        da_dN(i)=C*(DKeff(i)/(1-R_C18_rainflow_tot(i))^(1-gamma))^m;
    end
end
a1_rainflow(i)=da_dN(i)+a;
a=da_dN(i)+a;
    Sigma_res1(i)=Sigma02-((1/3*Sigma02)/a23)*a1_rainflow(i);
    Sigma_res(i)=KI/(Beta(i)*sqrt(pi*a1_rainflow(i)));
    Sigma_res3(i)=S1-(S1/(W/2-W/6))*(a1_rainflow(i)-W/6);
if a1_rainflow(i)<a23
    Sigma_res_tot1(i)=Sigma_res1(i);
else if a1_rainflow(i)>a23 && a1_rainflow(i)<=W/6
    Sigma_res_tot1(i)=Sigma_res(i);
else if a1_rainflow(i)>W/6
    Sigma_res_tot1(i)=Sigma_res3(i);
end
end
end
Sigma_residual(i)=KI/(sqrt(pi*a1_rainflow(i)));
Sigma_res_col(i)=((2*e*B)+(W-a1_rainflow(i))*h)/((2*e*B)+(W)*h)*Sigma02;
end
figure(6)
subplot(2,2,[1:2])
N=[1:1:length(DS1_C18_rainflow_tot)];
plot(N,a1_rainflow)
xlabel('Number of cycle')
ylabel('Crack length [mm]')
title('Crack growth CRACK CLOSURE model')
subplot(2,2,3)
plot(a1_rainflow,Sigma_res_tot1)
xlabel('Crack length [mm]')
ylabel('Residual Stress [N/mm2]');
title('Residual strength variation with crack growth')
subplot(2,2,4)
plot(a1_rainflow,Sigma_res_tot1,'r*')
hold on
plot(a11,Sigma_res_tot)
hold on
plot(ap,Sigma_res_tot,'g')
xlabel('Crack length [mm]')
ylabel('Residual Stress [N/mm2]');
```

Results are present as in the previous considered case (Figure 119)

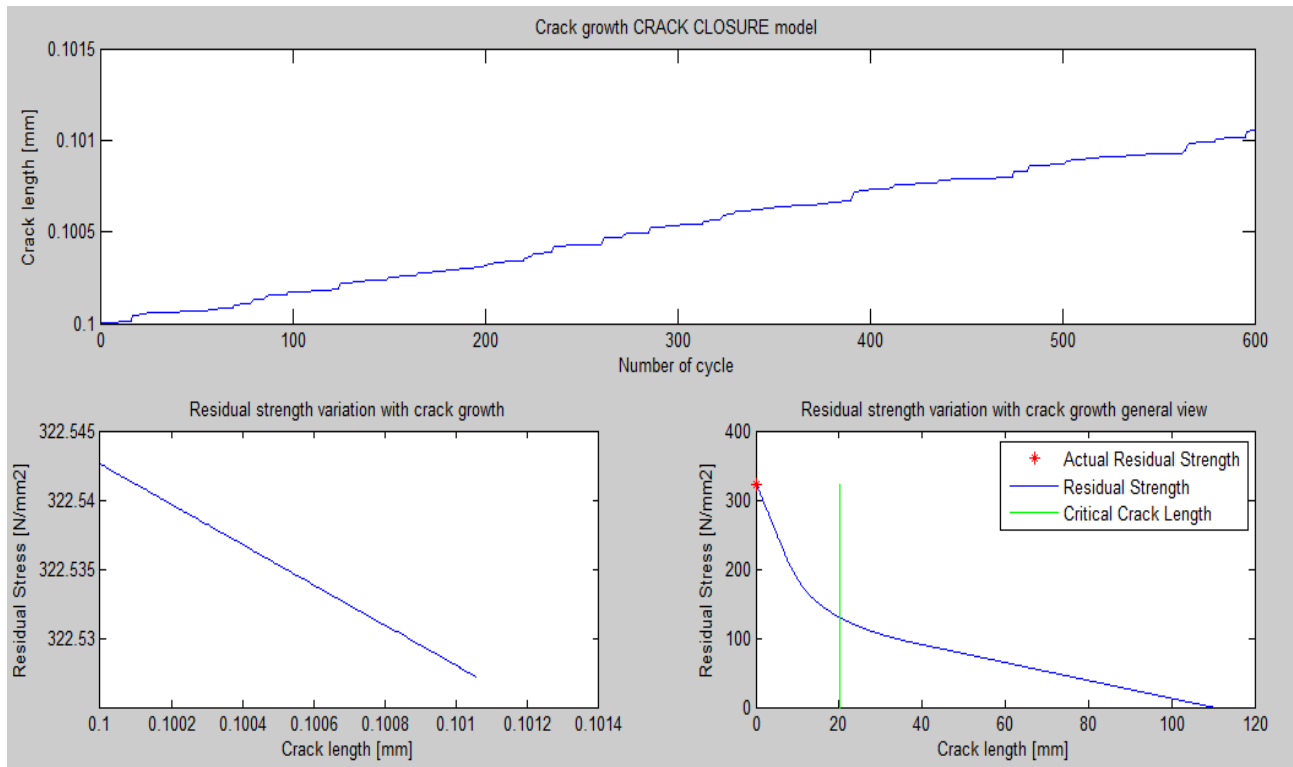


Figure 119: Crack growth results from crack closure model

Again, could be quite interesting to compare these results with the previous obtained ones especially those in terms of crack growth. Being this one a more complete model, taking into account interference effect in a deeper detail with respect Yield zone model, a further reduction in crack length for the same load sequence is expected. Results reported in these plots confirm this expectation providing that obtained results are correct.

Concluding, should be also remembered the important role played by the initial crack length in the fatigue life. In particular, as pointed out in chapter 3, if a small crack length is considered as the initial value  $a_0$  to develop analysis, a larger crack growth life will be obtained. It could lead to possible unconservative results. This observation is important to be taken into account by the future user of this developed methodology for damage tolerance design. Particular attention should be placed in the definition of this initial crack length before to run the model. Moreover, also an accurate definition of all the empirical coefficients, used and introduced in each of these models, should be considered. It must be done not only with the purpose to avoid unconservative

results but also to limit too much conservative results. This is especially true aircraft design where design on the edge of failure, as already introduced in Chapter 2 (Figure 5), is always the best solution.

## Fracture control

Now that the main results of damage tolerance analysis have been derived in the previous paragraph the question is: how these results can be used in designing against fatigue? In this paragraph we are going to introduce the principal consideration that must follow the determination of the previous results. In particular, their importance, especially from an economical point of view will be pointed out.

The main purpose of a damage tolerance analysis is to establish inspection procedures determining inspection intervals. At this moment the structural strength as a function of the crack size has been calculated using fracture mechanism concepts. As seen, a condition on the lowest acceptable strength in case of presence of crack is generally needed to be set. Then, when the residual strength diagram as that in Figure 116 has been calculated, the maximum permissible crack size, named  $a_p$ , can be derived.

The other information needed from analysis is the crack propagation curve (ex. top of Figure 118). As said it shows how a crack develops by fatigue as a function of time.

Once these diagrams are available, the reduction of strength associated with a certain operational period can be determined and visualized on plots like that in the lower portion of Figure 118.

In the next step, these information are used to exercise the so called *fracture control*. It can be defined as the operation in which designer, based on some statistical considerations, prescribe the number of inspections needed to maintain a certain level of safety.

There are several ways in which statistical information can be used to exercise fracture control procedure. Anyway, in all cases, the time period (H) to reach the maximum permissible crack size  $a_p$  is the essential information (Figure 120). In fact, because of no crack is allowed to grow beyond this size, repair or replacement of the considered structural component is dictated by H.

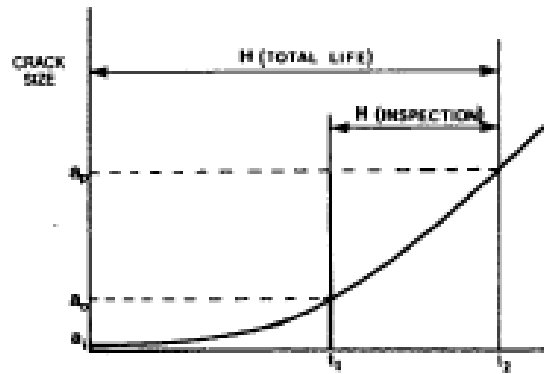


Figure 120: Time period H to reach critical crack length

Damage tolerance design philosophy for transport aircraft generally prescribes the two following control procedures:

- Periodic inspections: repair upon crack detection.

Safety is insured when cracks are eliminated before they impair the strength more than acceptable. In other words it means that they must be repaired before reaching the crack size  $a_p$ . Many inspections methods can be used but whatever it is, there is a certain crack of size  $a_0$  before which detection is questionable being crack unlike to be detected. This implies that discovery and repair must occur in the time interval H between  $a_0$  and  $a_p$ . The length of the crack  $a_0$  depends on the prescribed inspection method.

Safety is maintained by providing a sufficient number of inspections during H to ensure that crack is detected before  $a_p$ . Generally two inspections prescribed inside the time interval H between  $a_0$  and  $a_p$  are a good option. To explain this let us consider the previous Figure 120. If an inspection takes place at time  $t_1$  the crack will be missed (high probability due to the crack length smaller or equal to the minimum detectable size) and the next inspection should be performed at time  $t_2$ , after an interval H. Here the crack would already be too long. Hence inspection interval must be shorter than H. Inspection scheduled at  $H/2$  does not matter at which time the crack initiate but it will always give two opportunities for detection.

- Fail safe design: repair upon occurrence of partial failure

Providing fail safety by means of crack arresters or multiple load paths is essentially a variation of the previous introduced method based on inspections. Also in this case cracks

or failed members must be detected and repaired. As already pointed out in chapter 2, the only difference applying this type of design approach instead of a pure damage tolerance analysis is that, here the structure will be designed to tolerate a larger damage which is more readily apparent. In this case, no special inspections are necessarily other than frequent check. When properly designed, a structure can still sustain  $\sigma_p$  when one member fails.

However if we consider now the previous obtained damage tolerance results, calculation of time interval H and prescription of an inspection interval program is what is needed at this point. In doing this a first important assumption is regarding the detectable crack size and realizing that, detection of cracks larger than the “detectable size” is not a certainty. In fact, there are many factors that can influence this. As can be imagining generally the probability of crack detection depends upon crack size. In particular, has been experimentally determined that this probability of detection as a function of the crack length can be expressed as a mathematical relation of this shape:

$$p = 1 - e^{-\{(a-a_0)/(\lambda-a_0)\}^\alpha} \quad (eq. 190)$$

Where a is the actual crack size considered,  $a_0$  is the minimum detectable crack size while  $\alpha$  and  $\lambda$  are parameters determining the shape of the curve p-a.

If we plot this relation on a plot p-a for different values of  $a_0, \alpha, \lambda$  we get what is reported in figure (Figure 120)

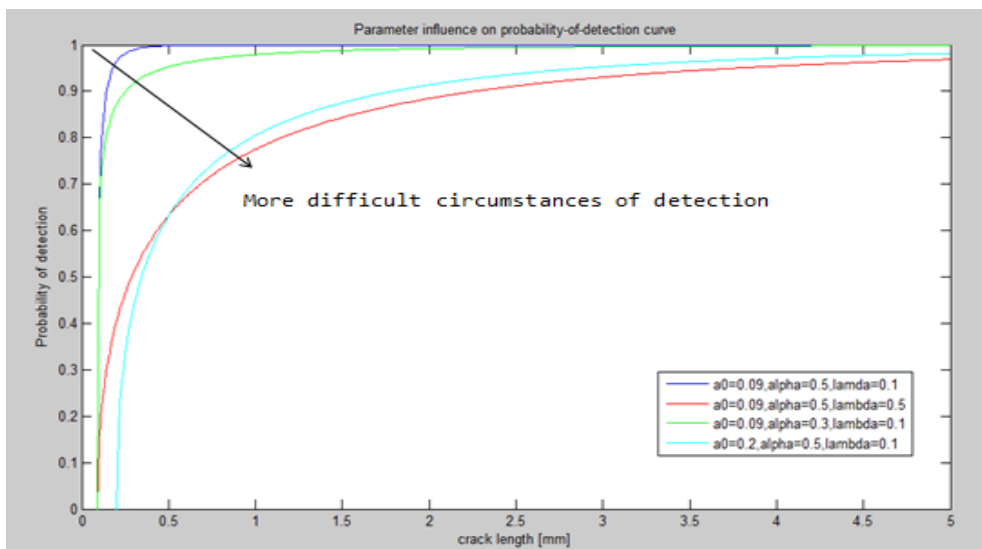


Figure 121: Probability of detection curve

Looking at this plot (Figure 121) should be realized how the definition of the previous parameters  $\alpha, \lambda$  influence the shape of the so called *probability-of-detection* curve. In particular, working on these values, depending on the specific analysed situation, difficulty of detection can be set up. As will be shown in the following, it is probably the key point in prescribing an inspection program.

Again, looking at Figure 121, can be seen as there is a certain crack size, named  $a_0$ , below which detection is physically impossible. Again this value depends upon the detection method used and it will be different in case of visual detection and X-ray detection. Moreover, as appear also from the plot above, probability of crack detection is never equal to 1 even for large cracks.

A consequence of this is that, the probability of non-detection of a crack given by  $1 - p$ , will be never equal to zero.

What follows from these observations is that at each inspection there is chances that crack will be missed. However, at successive inspections, the crack will be longer and the probability of detection will be higher as prescribed by eq.190. In any case, there will be always a chance that it goes to be undetected. The cumulative probability of detection can be expressed as:

$$P = 1 - \prod_{i=1}^n (1 - p_i) \quad (eq. 191)$$

Coming back to consider the detectable crack size  $a_0$  and its influence in the definition of the inspection interval what should be considered is that, even if the definition of  $a_0$  (value in eq.190) is generally choose arbitrarily this value, in order to define the inspection window H, could be defined as that crack with a probability of detection equal to 50%. This assumption on the minimum detectable crack size reduces the length of the interval H ( $H = N_p - N_d$ ) allowing a much more conservative definition of the inspection interval lengths. Proceeding in this way, different probability curve, i.e. different  $\alpha, \lambda$  values, defined by equation (eq.190), lead to different minimum detectable crack size. At the end it leads to different inspection interval. To get a clear understanding of this influence of the probability-of-detection curve in prescribed inspection interval, the following figure (Figure 121) could be useful.

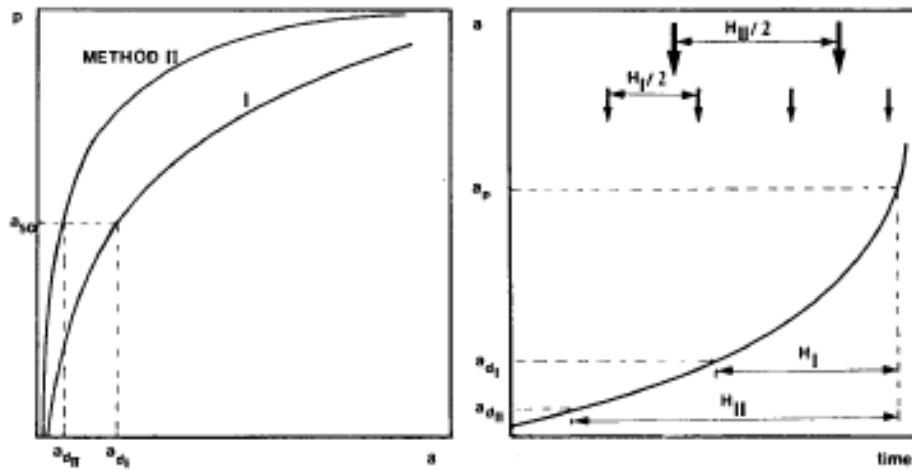


Figure 122: Different fracture control procedure

The crack would be inspected the first time when they still have a size smaller than  $a_{50}$ . At this first inspection, in fact, probability of detection however not zero unless  $a < a_0$ .

The probability-of-detection curves are different for the two procedures but either method would be satisfactory on the basis of the criterion  $I = H/2$ , where  $I$  is the inspection interval. The method II is generally used for ultrasonic inspection and it is more convenient due a longer inspection interval. It is based on a higher probability-of-detection curve. On the other hand method I could be used for example in case of visual inspection (less probability of crack detection for the same crack size).

These two inspection intervals have been obtained considering a different  $a_{50}$  for the same crack growth process because different values of  $\alpha$  and  $\lambda$  have been set up. However, they are both acceptable but the level of safety of course is not the same. The effect of the length of inspection interval in providing safety is even more evident if we consider two different processes, characterized by two different crack growth rates but where the same  $a_{50}$  and  $a_p$  are considered. Consequently, both cracks will be inspected equally often. Now looking at the two different crack growth rate reported in Figure 123, can be understood that crack 1 would have a much better chance of being detected than crack 2. In this second case in fact, the crack will be much shorter in both inspections. Here, even if the same criterion of prescribing inspection interval was applied for both cracks, not the same level of safety is achieved.



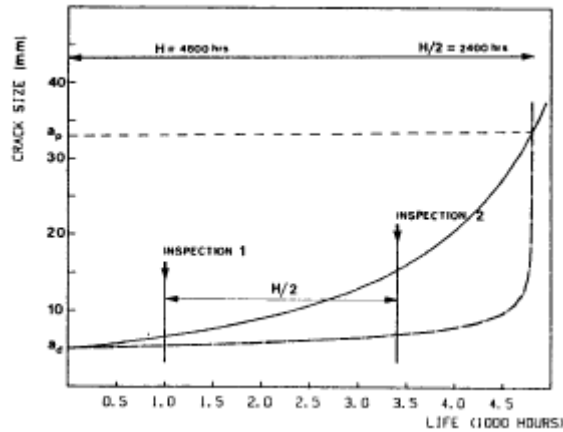


Figure 123: Fracture control for different crack growth process

All the observations done up to now are important to underline how the prescribed length of the inspection interval should be established such as a key parameter in providing a consistent safety level (generally expressed as cumulative probability of detection), independent from the shape of the crack growth curve. The aimed for cumulative probability of detection could be set for example at 95 or 98% and be specified as a damage tolerance requirements. Then, given the calculated crack growth curve, permissible crack size and the probability-of-detection considered for the present case (depend on the specificity and accessibility) the cumulative probability of detection  $P$  can be calculated for different length of the inspection interval using eq.191. Then, from this iterative process, the interval length to get the desired cumulative probability of detection can be obtained. This interval will be different for different inspection methods, different crack growth curves, accessibility and specificity as can be expected from the previous reported examples but, in any cases, under this way of proceeding, the cumulative probability of detection will be always the same (equal safety). A computer program developed for this purpose can perform this calculation iteratively to determine the inspection interval length needed to maintain the prescribed level of safety ( $P=95-98\%$ ). This program should consider the calculation for different interval lengths based on the provided crack growth curve coming out from all the previous introduced algorithms.

The developed algorithm for this purpose is reported in the following. The basic concept on which it is based is that, for a certain defined inspection interval, crack size at which inspection takes place is determined from the crack propagation curve ( $a-N$ ). At each inspection, probability of detection follows from the application of eq.190 where the parameters needed to use this relation must be choose considering inspection method, specificity and accessibility of the present case as

already pointed out before. Then these results are applied to obtain the cumulative probability function  $P$  with eq.191. If this value with the selected number of inspection intervals is larger than 95% then this is the number of inspections needed to maintain the desired level of safety.

The following code is the Matlab code developed to execute fracture control operation at the end of our numerical analysis making use of the previously obtained results.

```

%Algorithm to determine inspection interval

%Input variables

a0=0.09;
lambda=0.1;
alpha=0.5;
Sigma_p=60;

%Critical crack length

a11=[0.001:0.001:(W/2)];
for i=1:length(a11)
Beta(i)=(1.122-1.122*(a11(i)/W)-0.060*(a11(i)/W)^2+0.728*(a11(i)/W)^3)/(sqrt(1-2*(a11(i)/W)));
ap(i)=1/pi*(KI/(Beta(i)*Sigma_p))^2;
if abs(ap(i)-a11(i))<0.001
    break
else if abs(ap(i)-a11(i))>0
    i=i+1;
end
end
end
ap=ap(end); %Critical crack length. Determined from the minimum allowable residual strength set

%Minimum detectable crack length

ad=a0+(lambda-a0)*(log(1/(1-0.5))^(1/alpha)); %crack with 50% of probability of detection

%Definition of Nd: Number of cycle for detectable crack, Np: Number of cycle before critical crack
err=0.0001;
for i=1:length(al_rainflow)
    delta=abs(al_rainflow(i)-ap);
    if delta<err
        err=delta;
        break
        index=i;
    end
end
ap1=al_rainflow(i);
err=0.0001;
for i=1:length(al_rainflow)
    delta=abs(al_rainflow(i)-ad);
    if delta<err
        err=delta;
        break
    end
end

```

```

        index=i;

    end
end
ad1=a1_rainflow(i);
N=[1:1:length(DS1_C18_rainflow_tot)];
Nd=N(find(a1_rainflow==ad1));           %Number of cycles for detectable crack
Np=N(find(a1_rainflow==ap1));         %Number of cycles before reaching
critical crack length
H=Np-Nd;
%Number of Inspection intervals needed, iterative cycle

KK=[1:1:10];                          %Maximum number of interval.

for i=2:10
    n=KK(i);
    for i=2:n
        L=H/n;
        L2=L;
        for i=2:n
            L1(i)=L2;
            L2=L2+L;
        end
        for i=2:n
            err=10;
        for k=1:length(N)
            delta=abs(N(k)-L1(i));
            if delta<err
                err=delta;
                break
                index=k;
            end
            N1(i)=N(k);
        end
        end
        for i=2:n
            a1(i)=a1_rainflow(find(N==N1(i)));
        end
        p=1-exp(-((a1-a0)./(lambda-a0)).^alpha);
        for i=1:length(p)
            if real(p(i))>1
                p(i)=0;
            else p(i)=p(i);
            end
        end
        P1=1-p;
        P(i)=1-prod(P1);
        if P>=0.95
            break
        else i=i+1;
        end
    end
    if P>=0.95
        break
    end
end
end
ni=find(P>=0.95);
ni=ni(1);
disp('Number of detection intervals required')
n_interval=ni

```

```

disp('Number of cycles between inspections')
N_cycles=H/n_interval
A=[1:1:50];
N_cycles=N_cycles.*A(1:n_interval)

for i=1:N_cycles
    p11=1-exp(-((a1_rainflow-a0)./(lambda-a0)).^alpha));
figure(1)
subplot(1,2,1)
plot(a1_rainflow,p11)
xlabel('crack length [mm]')
ylabel('Probability of detection')
title('Probability curve')
subplot(1,2,2)
plot(N,a1_rainflow)
hold on
plot(N_cycles(i),a1_rainflow)
xlabel('Number of cycles')
ylabel('Crack length [mm]')
title('Crack growth')
end

```

As can be seen in this algorithm, vector resulting from damage tolerance analysis  $a1\_rainflow$  is used. In particular, it is used to determine the number of cycles to reach a detectable crack ( $a_d$  defined at that one with 50% of probability of detection) and the critical crack ( $a_p$  determined from the defined minimum allowable residual strength). These two values have been respectively named  $N_d$  and  $N_p$ . As mentioned, the additional inputs introduced here are represented by parameters providing the shape of the probability-of-detection curve ( $a_0, \lambda, \alpha$ ). They have been selected arbitrarily (user definition) taking into account inspection methods, specificity and inspectability generally referring to coefficients already considered in other developed analysis. However, the arbitrary choice of these coefficients is allowed. In fact, relation above (eq.190) does not come out from statistical results but it is just a fitting curve. For this reason, in principle, all relations having approximately the same behaviour can be considered.

On the other hand, the main output of this algorithm are represented by the number of inspections needed to maintain the desired level of safety ( $P > 95\%$ ). This result is the so called  $n\_interval$  in the above code and it is also associated with a certain number of cycles between each prescribed inspection represented by the vector named  $N\_cycles$ . To get a clearer idea about the prescribed inspection program obtained using this methodology, a visual representation of the inspection interval has also been considered. It has been done using the crack growth plot (a-N). This is the most useful plot for this purpose because it allows a visual representation of the crack length expected at each inspection and the number of cycles at which this inspection should be

performed. In addition on this final visual representation, probability of detection curve coming out from the choice of the selected parameters before is also represented.

Figure below (Figure 124) shows visually results of the algorithm above.

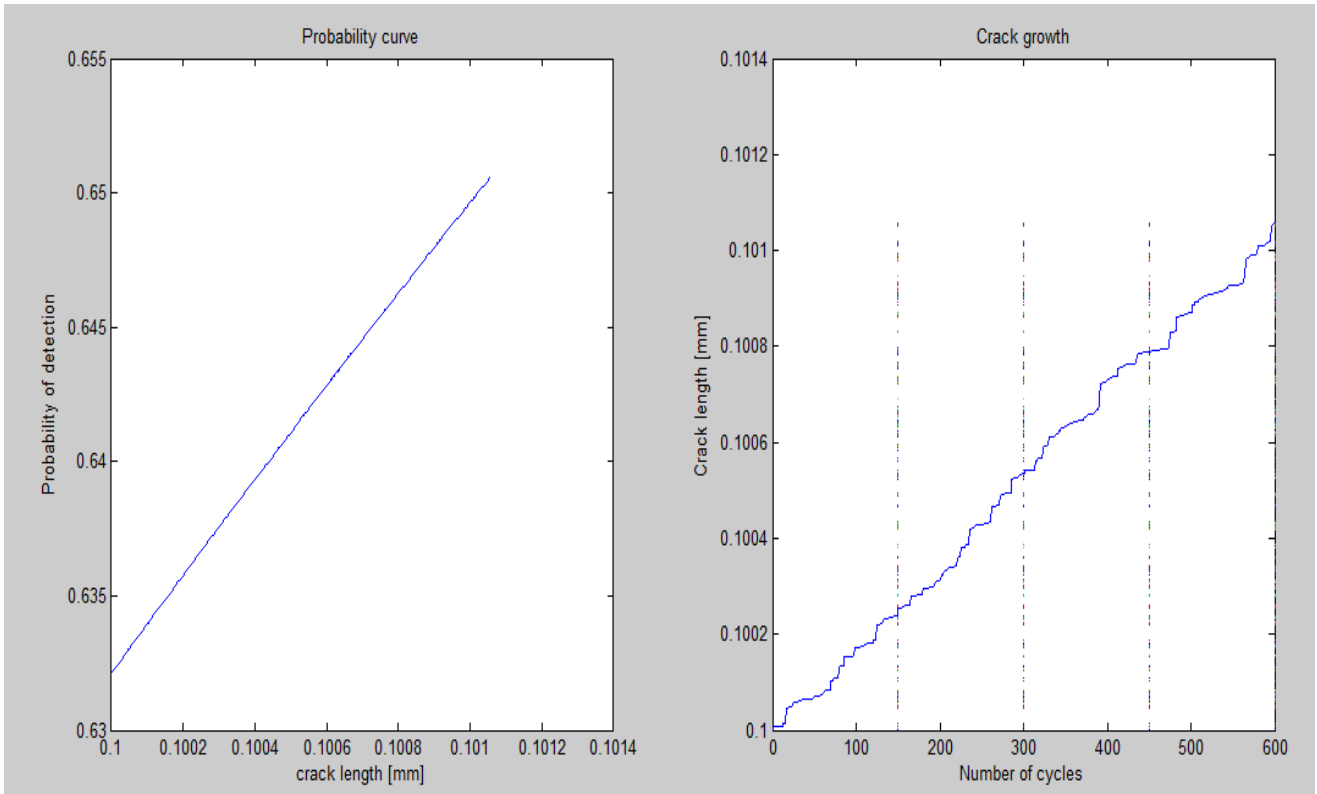


**Figure 124: Fracture control inspection interval prescribed**

The optimum fracture control plan depends upon the consequences of a fracture. If the number of fracture experienced is considered to be at an acceptable level with a certain fracture control plan at acceptable costs, then the plan is close to be optimum. Before implementation of a fracture control program, the objective must be identified. Before defining the permissible residual strength or permissible crack size, the desired level of safety should be established, even if only qualitatively. In general, every component of a structure sets different fracture control requirements. Just to make an example, the following figure (Figure 125) shows a comparison between two different fracture plan obtained in our case considering two different probability-of-detection curve (plots on the left hand side make use of the red curve in figure 121 while plots on the right and side make use of the blue one).

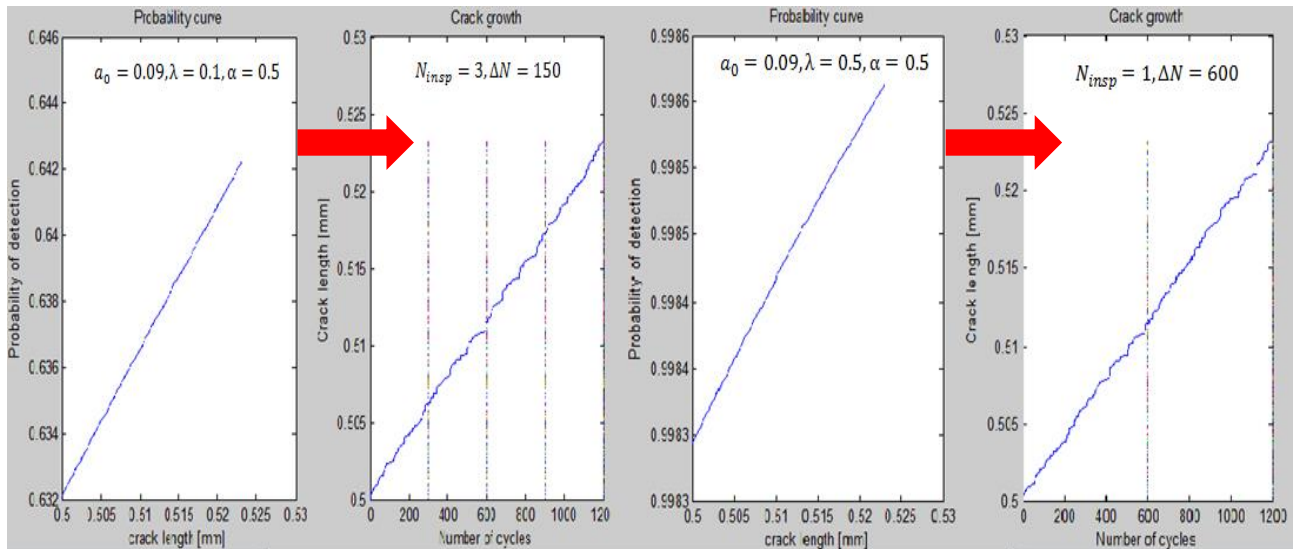


Figure 125: Different fracture control plan

Then the optimal control plan, as mentioned above, will depend on the consequence of fracture and on the cost needed to perform that type of plan.

The acceptable consequences of failure form the basis for the fracture control philosophy. However, establishing the acceptable consequence of fracture is an economic as well as an ethical problem. In fact the cost of fracture control, from a technical point of view must be compared with the consequences of failure in term of economic, ecological and human lost. Of course it is morally difficult to assign a cost to a human life but it is practically what is done.

The potential cost of *fracture*, based on the previous observations, includes:

- Loss of human lives
- Impact on environment
- Damage to building and surrounding structures

On the other hand, the costs of *fracture control* include:

- Damage tolerance analysis (many man hours)
- Coupon tests and verification tests
- Inspections
- Repairs or periodic replacements

Here inspections costs appear. This explains why a fracture control plan as described before is needed. However, all these costs are quite easily determined but those of fracture are more difficult: some items can be estimated while others can be “gaussed” only.

As a general rule, if the cost of a single fracture is called  $S$  and the probability of fracture is called  $P$ , then the total cost can be considered to be  $PS$ . Of course when the probability of failure is small could be wise to use a fracture control measures with a low cost. Anyway, if we consider a qualitative Fracture Control Index (FCI) where an higher FCI means a more extensive fracture control measures and a decreasing possibility of failures all the previous observation can be summarized with the following common plots.

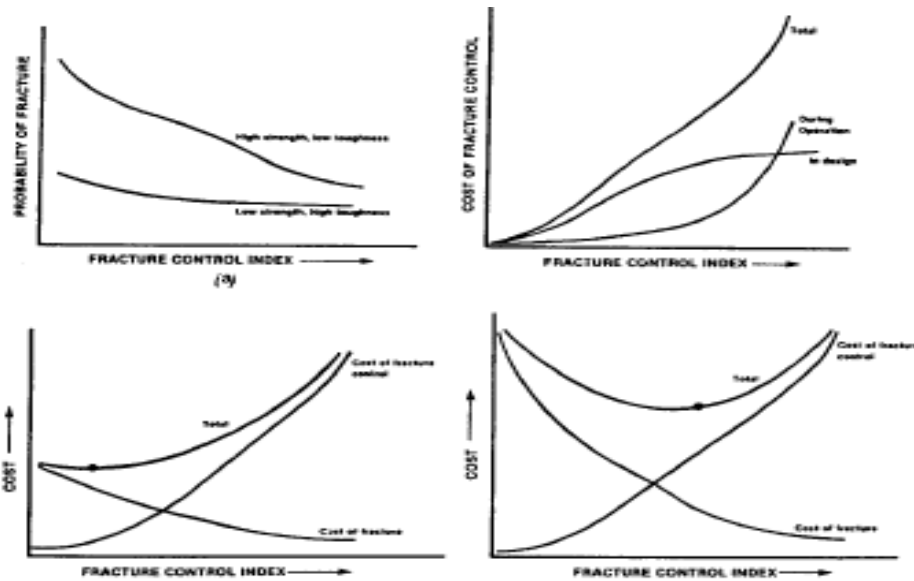


Figure 126: Cost of fracture control

Of course, the minimum of the total cost curve indicates the most economic fracture control.

Now, coming back to the time available for fracture control  $H$ , we have already seen how it is dependent on the residual strength and crack growth curve. However, in essence, fracture safety is not affected by the length of  $H$  as mentioned before. In fact, if  $H$  is short, frequent inspections must be scheduled or, on the other hand, component must be replaced soon. Long inspection intervals or replacement times are desirable from an economic point of view. So at this point, to conclude the argument related with fracture control in designing phase, the question could be: how we can improve the situation when  $H$  is too small to be economically acceptable. The following parameters could be taken into account:

- Use material with better properties: it can be done for example using a material with higher toughness because in this way we are able to increase the value of  $a_p$ . However it has only a limited influence in the increment of  $H$ . In fact, remembering what has been

pointed out in the quick introduction of the fatigue process carried out in Chapter 1 most of the life is in the early phase of crack growth. Modifying the value of  $a_p$  we only affect the steeper part of the crack growth curve.

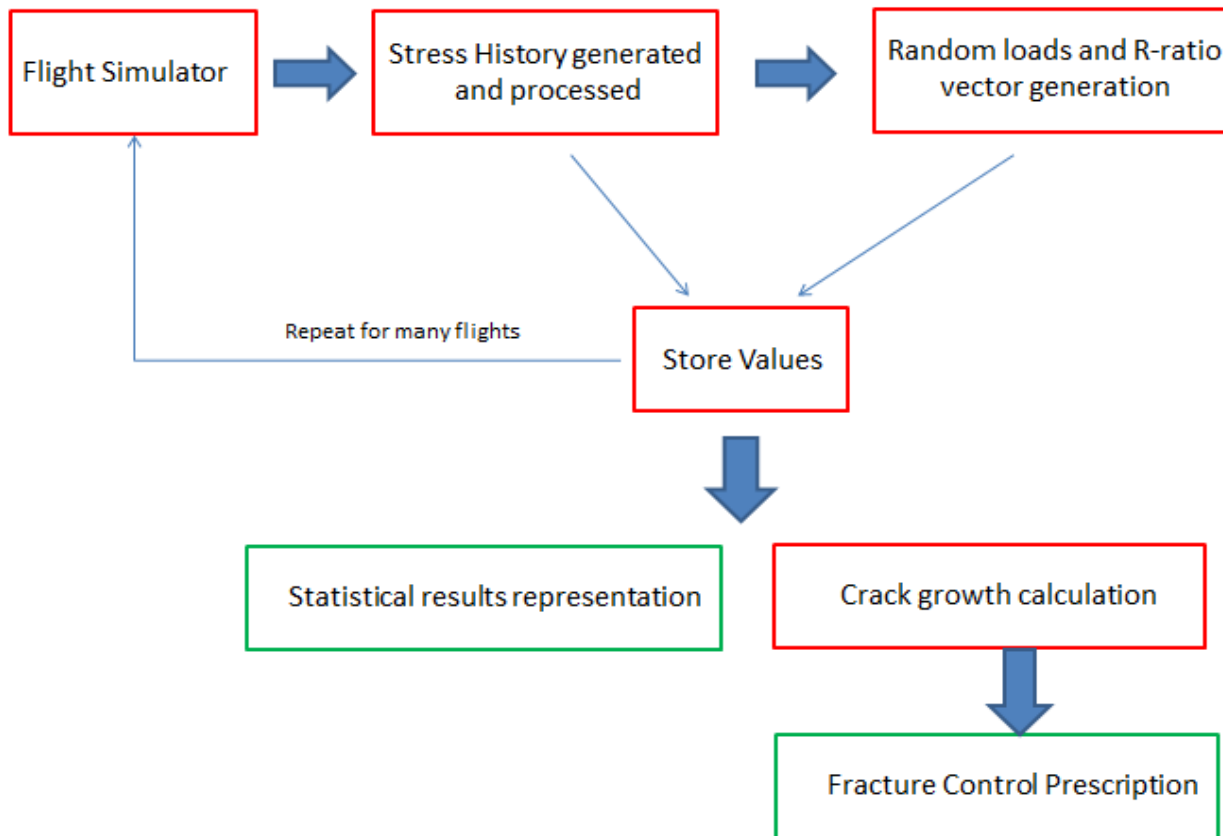
- Selection of a better inspection procedure: It can be done improving the detection technique adopted. In fact as mentioned before it allows the reduction of the value of the minimum detectable crack length leading to a larger H especially considering the small slope of the crack growth curve in the first portion. The penalty in this case will be a more difficult inspection.
- Redesign or lower stress: Crack growth curve is governed by stress intensity factor. In particular remembering the Paris relation introduced in Chapter 3 it is proportional to  $\Delta K^m$  where m is a material data. Considering for example  $m=4$ , a 15% reduction in K lead to an increment in H of about  $1.15^4 = 1.75$ . The reduction in K can be obtained both with a reduction in  $\sigma$  or a reduction in  $\beta$

The main consequence resulting from these observations makes crucial that damage tolerance assessments starts in the early design phase when modifications are still possible. In fact, on the other hand, once the design is already finished, the options for improvement are drastically reduced. In this case only the second option between those described above still remains possible.



Summary of the developed methodology

This paragraph has been introduced just to get a compact visualization of the developed algorithm for damage tolerance analysis making use of a flight simulator to get load spectrum. This can be done considering the following flow-chart diagram where the main steps are simply summarized. Then for each of this block, inputs and outputs will be listed below.



1. Flight Simulation

Inputs:

- Aircraft parameters: Dimensions, Stability and control derivatives, aircraft limitations
- Flight plan: Manual (Joystick is needed), Automatic (Trajectories need to be defined)
- Environment

Outputs:

- ✓ Forces
- ✓ Moments
- ✓ Accelerations

**2. Stress history generation and processing**

Inputs:

- Vertical acceleration
- Lift force
- Wing parameters: Dimensions, Material

Outputs:

- ✓ Stress History
- ✓ 2D Load counting matrix with 12 levels (Rainflow)
- ✓ Number of level exceedance
- ✓ Number of peaks per interval

*Useful for statistical purposes*

**3. Random Load and R-ratio sequence generation**

Inputs:

- 2D Loading matrix (Rainflow)

Outputs:

- ✓ Random Load and R-ratio vector (consistently defined)

**4. Final results presentation**

Inputs:

- Random Load and R-ratio vector
- Minimum permissible Residual strength
- Number of level exceedance
- Number of peaks per interval
- Material data ( $K_I, F_{ty}, F_{col}$ )
- Parameters determining probability-of-detection curve

Outputs:

- ✓ Total exceedance diagram
- ✓ Exceedance table
- ✓ Total 2D load matrix
- ✓ Crack Growth Curve
- ✓ Residual strength diagram
- ✓ Fracture control strategy prediction

*Obtained applying different methodology*

## 7 COMMENTS AND FUTURE WORK

In this last chapter of this thesis, conclusion regarding the main results achieved with our developed methodology and principal source of errors affecting these results will be pointed out. In the development of this work, the key point is represented by fracture mechanism concepts and relative methods for crack growth analysis. All these considerations have been introduced in Chapter 3. However, the short-comings of fracture mechanism are not the important error drivers. In fact, rather than these, data inputs and assumptions done are the prevalent sources of errors. In the following paragraph the principal ones will be considered in deeper detail. Then in the next paragraphs, future work needed to improve our developed methodology, remembering that it just represents a first feasibility study of load spectrum and damage tolerance analysis by means of flight simulator, will be introduced.

### Principal sources of errors

First of all, as already pointed out in Chapter 3, errors due to the use of Linear Elastic Fracture Mechanis (LEFM) for the residual strength analysis occurs mainly at small and large crack sizes, where plastic deformation plays an important rule, making the derived important residual strength diagram affected by errors. However, quite acceptable results can be obtained introducing the so called Feddersen interpolation taking into account possibility of fracture by collapse in addition to fracture by crack extension. In any case, should be considered that LEFM concepts that are based on the assumption of linear-elastic behaviour for the material, can be used in fracture analysis accurately only as long as a limited plastic deformation occurs at or near the tip of the crack. In case where is not true anymore, and so plastic deformation is large, EPFM concepts should be considered [13]. These concepts are still based on elastic behaviour but it assumes that the stress-strain curve is non-linear. However, the question following these observations is: how much small should be plastic zone to consider enough accurate LEFM? Plastic zone, should be so small that its size is determined using the toughness  $K$  and only  $K$ . This occur if

the plastic zone, does not extend beyond a value  $r$  at which the first term of the following relation is still much larger than all the other terms:

$$\sigma_{i,j} = \frac{K_I}{\sqrt{2\pi r}} f_{ij}(\theta) + C_1 r^0 + C_2 r^{1/2} + \dots \quad (eq.192)$$

This relation is just the general and complete equation of those in eq.8 obtained considering only the first term and neglecting the others being these ones very small in condition where LEFM is applicable. In case where the condition above is not verified, i.e.  $r$  is large, the constant terms  $C_1$ ,  $C_2$  and so on in eq. will become significant. As a general rule can be said that this condition does not occur until  $K_I/\sigma_{ys} > 2$ .

However, must be considered that in general, plastic deformation involved in cracking is very small. For this reason, crack growth analysis generally use LEFM concepts. An extension is creep cracking for which EPFM concepts must be used.

Crack growth model are not ideal even if, those well calibrated, provide results in which the error in calculated life is generally only about 10%. These errors are those intrinsically present inside these models, i.e. those expected when all the principal parameters involved like  $\beta, da/dN$  and load history are accurately known.

In any case, the larger errors, as already mentioned in this thesis are those due to data input. It is especially true for material data being this one generally averaged to account for all possible environments in which the airplane is supposed to operate.

Moreover, principal data stored from load history processing algorithms (peaks, valleys, ranges), represent just an approximation of the real load history. In fact, as described in Chapter 4, each load range used for crack growth analysis is associated with a certain transition between two intervals defined by the levels in which the spectrum has been divided. Larger is the amplitude of each of this interval and larger will be the approximation introduced. Then, additional errors introduced by load history are those associated with an improper sequence. In particular, randomizing the sequences, even if in reality they are only semi-random, could introduce a great difference between achievable results and real process. The algorithm developed to reduce as much as possible these types of error sources, analysing the load sequence with our methodology, has been introduced in Chapter 6.

Of intermedia importance are also error introduced by not accurate stress intensity factor. In fact, Paris relation, that is the most important one, on which most of the crack growth models are based, prescribe for metals that the crack growth is proportional to about the 4<sup>th</sup> of the stress intensity factor. In other words it means that a 10% of error in  $\beta$  and  $\sigma$  leads to a 1.4 factor of error in the predicted life.

Remembering also what has been pointed out in Chapter 3 about initial crack length considered in crack growth prediction analysis, its influenced in the obtained results is of extremely importance. Conservative results can be obtained if an initial large crack is considered. Moreover, regarding the initial defect considered, also the shape of this one is of particular importance. In particular if a flaw defect is considered and the conservative assumption of initial circular flaw instead of elliptical is introduced, an error factor of 2 or 3 could be also obtained. This value is much larger than that one related with error associated with inaccurate stress or geometry factor. However these latter observations refer with a more accurate 3D analysis. In our case, a simple through crack with a straight crack front perpendicular to the plate surface has been considered.

Finally there are errors due to specific computer modelling that may be related with: integration scheme, rounding error, etc. However with regard to errors introduced by the integration scheme they are only possible if a constant load sequence is to be analysed. In fact, as discussed in Chapter 3 in this case, step integration can be considered while in case of variable amplitude load sequence, integration is performed cycle-by-cycle. Particular attention should be placed on accuracy used when applying numerical calculation to perform analysis as those described in the previous chapters of this thesis. Of particular importance is the use of a *double precision* instead of a *single* one. It is particularly interesting in case of variable amplitude loads where the crack length increment ( $da$ ) per cycle could be very small. By default Matlab works with a double precision so it has not been a problem in our case but should be something that must be taken into account working with other types of calculators.

All the parameters introduced here and many others introduce error in results of fracture mechanism analysis but, in spite of this, fracture mechanism remains a good engineering tool for damage tolerance analysis. In fact, almost no engineering method is ideal but generally speaking, if this method provides needed answer than it is useful. Today, as reported in literature, fracture mechanism concepts can be used to predict failure strength of a structure in most cases within about 10%. However, even if in the future better fracture theory can be presented, the main problem will be always related with scatter in material data.

All these consideration must be observed when results provided by our algorithms are analysed to prescribe inspection intervals following the procedure described at the end of Chapter 6.

However, in this conclusive chapter should be remembered that being this one a first work having the purpose of developing the basic algorithm needed to develop a damage tolerance analysis starting from simulated load spectrum, results presented in Chapter 6 are not really meaningful. They have been plotted just to show how the developed methodology promises that good results can be achievable. Of course in order to get meaningful results, first of all, much more flights need to be simulated then, secondly, some of the strong assumptions introduced should be substituted by others. These new assumptions must lead to a lower difference between simulated and real case. In the following paragraph some consideration in this direction will be considered.

## Future Work

In this last paragraph the main points where strong assumptions have been introduced in the developing of this work, whose need to be substituted by more realistic considerations will be addressed one by one.

### 1. Wing mass

First of all, the inertial force (eq. 138) has been calculated considering the mass of the wing simply given as the mass of the double T beam (eq.139). In other words, the assumption behind this mass representation is in neglecting all the other wing components contributing in the increment of mass but that are necessary as explained in Chapter 6. A more realist equation for the wing's mass can be found in literature. For example a well-used equation for this purpose is the following empirical relation [14]:

$$W_w = W_{zf} 0.0017 n_{ult}^{0.55} t_{r,max}^{-0.3} \left( \frac{b}{\cos(\lambda_{c/2})} \right)^{1.05} \left( 1 + \sqrt{\frac{6.25 \cos(\lambda_{c/2})}{b}} \right) \left( \frac{W_{zf}}{S} \right)^{-0.3} \quad (eq. 193)$$

Where:  $W_{zf}$  is the zero-fuel weight of the airplane,  $n_{ult}$  is the ultimate load factor that is equal to  $n_{ult} = 1.5n_{lim}$ ,  $t_{r,max}$  is the maximum thickness of the root of the wing,  $b$  is the wing span,  $S$  is the wing area and  $\lambda_{c/2}$  is the swept angle of the wing.

2. Load distribution

Following consideration above, also the very simple load distribution considered (Figure 102) should be revised and substituted with a much more real distribution over the beam for both considered forces: Inertial and lift force. For example, considering a tapered wing like that of the Boeing C-17 Globemaster III used in our model (Figure 70) a good wing weight distribution can be supposed to be triangular (Figure 127). On the other hand, regarding to lift force distribution, as known from aerodynamic considerations, it is strictly related with the 3D shape of the wing. In particular as shown both, analytically and experimentally, an elliptical distribution of lift is that producing the lower induced drag. Hence, at least for the airplane mentioned before and used in our model, which also represents one of the most advanced airplane in aerodynamic terms (data provided estimate an Oswald efficiency factor greater than one, 1.01), a simple but not so strong assumption is in considering this one as an elliptical distribution (Figure 127).

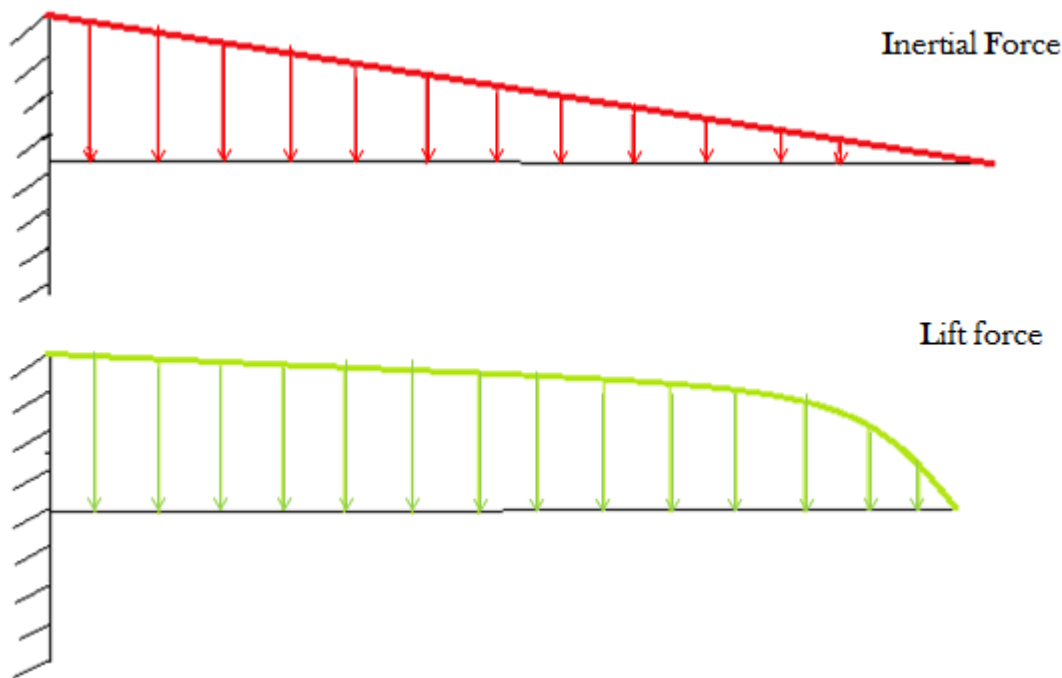


Figure 127: More detailed Inertial force and Lift distribution

Of course, force distributions like those represented in figure complicate the subsequent determination of stresses at the root of the wing. In particular the shape of the load characteristics (Cut, Bending moment) associated with these force distributions will be much more complex than the simplest one considered in Figure 102. The shape of these distributions can be found applying

concepts of the *Theory of bending beams*. Here for simplicity this argument is not treated in detail but just the fundamental relations coming out and useful for our purpose are considered. They can be obtained applying relation introduced in Chapter 6 (eq. 166-171) to an infinitesimal portion of the beam. In particular, calling  $q$  the distributed load,  $T$  cut load and  $M$  the bending moment the following important relations can be obtained:

$$\frac{dT}{dx} = -q \quad (\text{eq. 194})$$

$$\frac{dM}{dx} = T \quad (\text{eq. 195})$$

$$\frac{d^2M}{dx^2} = -q \quad (\text{eq. 196})$$

The following consideration can be derived from these equations:

1. In portion of the beam where  $q = 0$  the cut load  $T$  is constant and the bending moment changes with linear law
2. In portion of the beam where  $q \neq 0$  the cut load and bending moment change with continuity. In particular, if the distributed load  $q$  is uniformly distributed, the cut load change with a linear law itself while bending moment change with a second order parabolic law. On the other hand, if the distributed load  $q$  change with linear law, the cut load will be represented by a parabolic second order law while the bending moment will be characterized by a third order law
3. In portion of the beam where  $T = 0$ , bending moment is constant and viceversa in portion where the bending moment is constant the cut load  $T = 0$ . However everywhere the cut load  $T \neq 0$  the bending moment is variable.

These are the important considerations needed to determine the shape of the load characteristics in this more complex case. However, these are also those used indirectly to get the simple distribution in Figure 102. Just to introduce in deeper detail this concept related with load distribution considered for future improvement of the developed methodology, algorithms calculating these load characteristics associated with force distributions previously introduced has been developed in our work. The two following figures (Figure 128,129) represent for lift and inertial force distributions of Figure 127 the relative load characteristics (cut and bending moments) distribution. Of course they are reported here just to represent the difference with



respect the case considered before. In fact, as it is clear from discussion in Chapter 6 the specific values represented in these plots will change time-by-time depending on the applied loads.

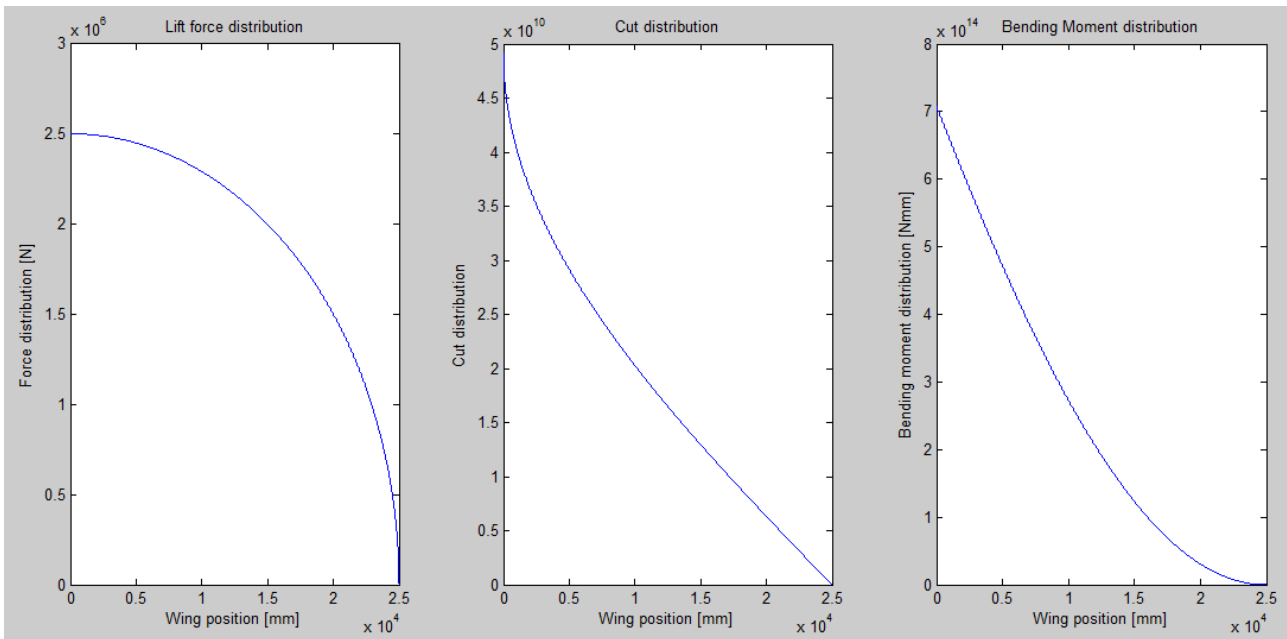


Figure 128: Load characteristics related with elliptical lift distribution

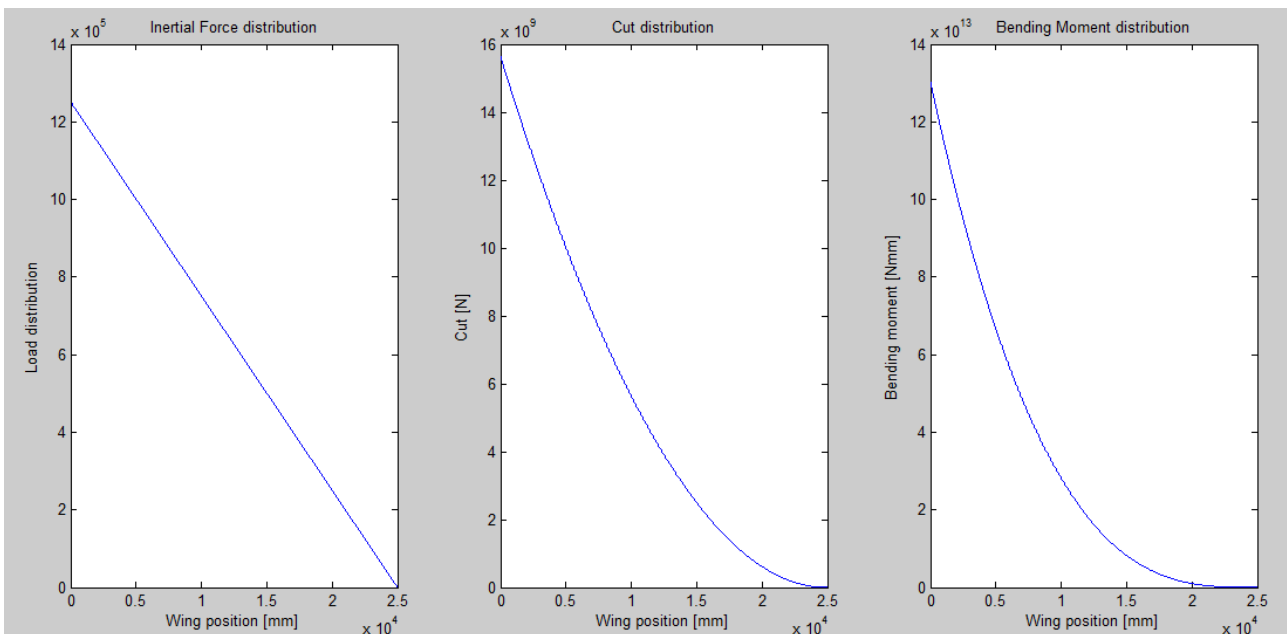


Figure 129: Load characteristics related with triangular inertial force distribution

All these value should be summed together to find the complete load characteristic distribution needed for stress determination at the root of the wing. To make this, detailed assumptions on how forces are shared between the spars of the wing should be considered. Then, once these new

load characteristic will be introduced in the previous developed algorithm, results coming out should represents, with a higher fidelity, real behaviour of crack growth.

**4. Two different types of crack**

Even if these concepts has not been introduced in Chapter 3 where the basic consideration of fracture mechanism analysis was treated, doing crack growth prediction analysis must be considered that there are two different types of cracks that should be considered in predictions:

1. Part through crack: It is a crack that is nucleated on the surface and it is expanding in the material but it has not already influenced the entire thickness of the considered structure.
2. Through crack: It is a crack that has already reached the material thickness and it is beginning to develop in the transversal direction of the material.

The following figure (Figure 130) provides a good example to show the principal difference between these two types of crack introduced.

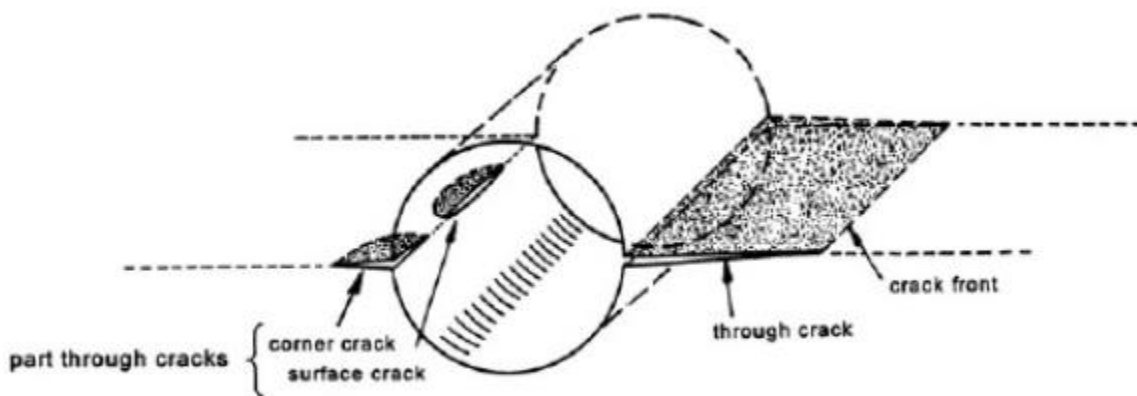


Figure 130: Part through crack and through crack

Generally speaking can be said that a through crack is the continue of a part through crack representing on the other hand the initial shape of a surface crack. In particular, when the part through crack reaches the thickness of the material it is considered to transform in a through crack and starts to expand in the remaining W direction. A well-known example of part through crack having also a technically relevant interest is a semi-elliptical initial flaw. The process of expansion of this initial cack in the material is schematically represented by the following figure (Figure 131).

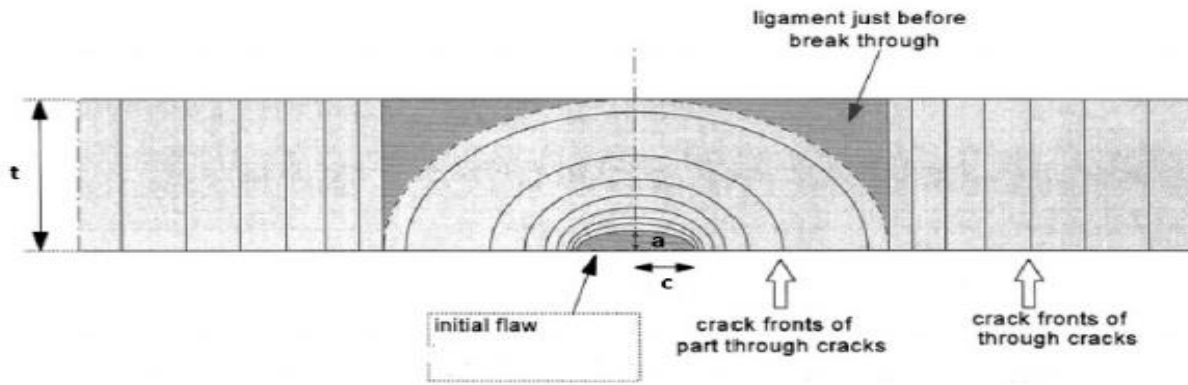


Figure 131: Semi-elliptical initial flaw extension

Prediction crack growth of a part through crack is much more complex than that of a simple through crack because stress intensity factor varies along the crack front. In other words it means that the crack growth rate  $da/dN$  varies along the crack front.

For a geometric description of the elliptical crack the ratio between its two semi axis  $a/c$  and the angle position  $\Phi$  are generally considered ( $\Phi = 0$  surface position,  $\Phi = \frac{\pi}{2}$  deepest point).

An assumption that can be used to study crack growth in this condition is that the shape of the crack when it is expanding remain always elliptical but the ratio  $a/c$  varies becoming closer to 1 (circular crack front).

The two most famous methods that could be used to determine the stress intensity factor at each position of the crack front are [16]:

1. Irwin Method:

It assumes that K at each location can be determined as:

$$K = \frac{S\sqrt{\pi a}}{\Phi} \left( \frac{a^2}{c^2} \cos^2 \varphi + \sin^2 \varphi \right)^{1/4} \quad (\text{eq. 197})$$

Where  $\Phi$  is generally substituted by  $\sqrt{Q}$ :

$$\left. \begin{aligned} Q &= 1 + 1.464 \left( \frac{a}{c} \right)^{1.65} && \text{if } \frac{a}{c} \leq 1 \\ Q &= 1 + 1.464 \left( \frac{c}{a} \right)^{1.65} && \text{if } \frac{a}{c} > 1 \end{aligned} \right\} \quad (\text{eq. 198})$$

2. Newman-Raju method:

It is a modern method based on finite element analysis results where even the crack thickness  $t$  and the structure dimension  $W$  is considered. Simply this method introduces a correction factor  $F$  to the previous relation provided by Irwin:

$$F = \left[ M_1 + M_2 \frac{a^2}{t} + M_3 \frac{a^4}{t} \right] g f_\varphi f_w \quad (\text{eq. 199})$$

Where different expression for terms appearing in this relation must be considered depending on the *crack aspect ratio*:

$M_1 = 1.13 - 0.09(a/c)$	}	if $a/c \leq 1$
$M_2 = -0.54 + \frac{0.89}{[0.2 + (a/c)]}$		
$M_3 = 0.5 - \left[ \frac{1}{0.65 + (a/c)} \right] + 14(1 - (a/c)^{24})$		
$g = 1 + [0.1 + 0.35(a/t)^2](1 - \sin\varphi)^2$		
$f_\varphi = [(a/c)^2 \cos^2\varphi + \sin^2\varphi]^2$		
$f_w = [\sec(\pi c/2W \sqrt{a/t})]^{0.5}$		
$M_1 = \sqrt{\frac{c}{a}} \left( 1 + \frac{0.04c}{a} \right)$	}	if $a/c > 1$
$M_2 = 0.2(c/a)^2$		
$M_3 = -0.11(c/a)^4$		
$g = 1 + [0.1 + 0.35\left(\frac{c}{a}\right)(a/t)^2](1 - \sin\varphi)^2$		
$f_\varphi = [(a/c)^2 \cos^2\varphi + \sin^2\varphi]^2$		
$f_w = [\sec(\pi c/2W \sqrt{a/t})]^{0.5}$		

Here just as introduction for future development of our model taking into account this concepts the variation of the stress intensity factor on the crack front for a simple case of CA loading with  $S_{max} = 100 \text{ N/mm}^2$  has been considered. The plots resulting from the developed Matlab code considering the simpler Irwin model are reported here below:

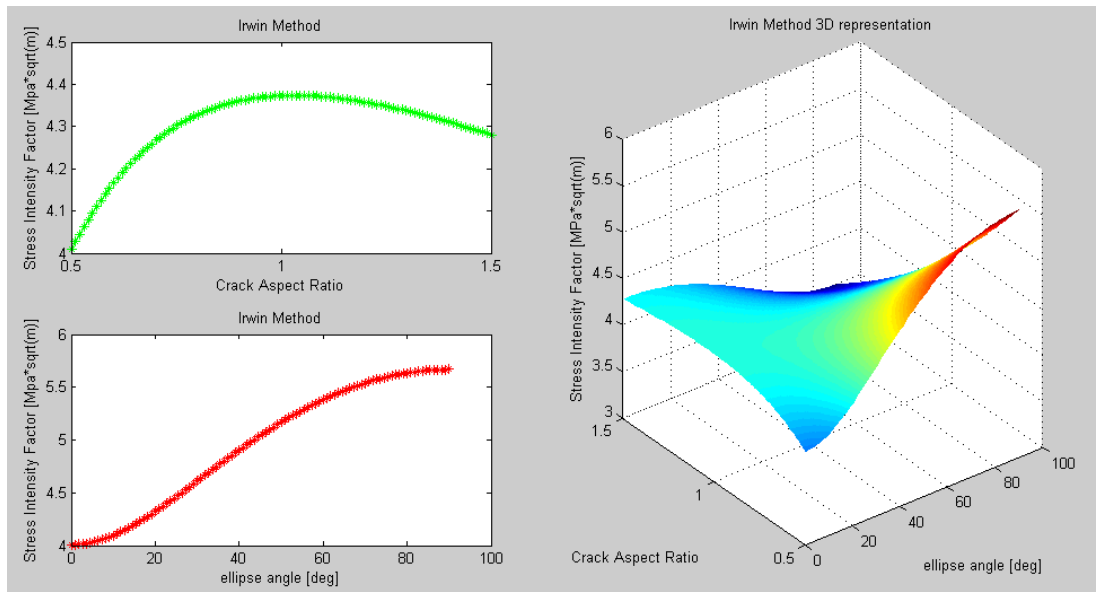


Figure 132: Stress intensity factor variation on the crack front of a semi-elliptical crack

From these results relative to a general case, a qualitative dependence of  $K$  from the other dimensions can be obtained. It results clear that whatever the elliptical shape of the initial crack is, it always tend to grow toward a circle shape.

The developed Matlab code to get these results is reported here:

```
S=100;
t=0.002;
ratio=linspace(0.5,1.5);
phi=linspace(0,pi/2);
a=0.0015;
c=0.005;
if ratio>1
Q=1+1.464*(1/ratio).^1.65;
else
Q=1+1.464*ratio.^1.65;
end
for i=1:100
for j=1:100
K(i,j)=S*sqrt(pi*a./Q(i))*(ratio(i)^2*(cos(phi(j))).^2+(sin(phi(j))).^2).^0.25;
end
end
phi=phi.*180./pi;
figure(2)
subplot(2,2,1)
plot(ratio,K(:,1),'*g-')
xlabel('Crack Aspect Ratio')
ylabel('Stress Intensity Factor [Mpa*sqrt(m)]')
title('Irwin Method')
subplot(2,2,3)
plot(phi,K(1,:), '*r-')
xlabel('ellipse angle [deg]')
ylabel('Stress Intensity Factor [Mpa*sqrt(m)]')
title('Irwin Method')
subplot(2,2,[2,4])
surf(phi,ratio,K)
shading interp
colormap('jet')
ylabel('Crack Aspect Ratio')
xlabel('ellipse angle [deg]')
zlabel('Stress Intensity Factor [MPa*sqrt(m)]')
```

As can be observed from the previously introduced model, stress distribution on the crack front is strongly influenced by the *crack shape*. In particular consideration on how the crack growth ratio changes when the crack is expanding is extremely important for a future development of this concept in crack growth prediction. In fact, it allows determining the crack length in the direction of the span of the structure. This dimension, when the through crack will be formed, represents its initial dimension. The crack shape can be determined solving the following equation:

$$\left. \begin{aligned} \frac{da}{dN} &= \left[ 0.9 \sqrt{\frac{a}{c}} \left( 1.11 + 0.35 \frac{a^2}{t} \right)^{-m} \right] && \text{if } a/c \leq 1 \\ \frac{da}{dN} &= \left[ 0.9 \sqrt{\frac{a}{c}} \left( 1.11 + 0.35 \frac{a^2}{t} \frac{a}{c} \right)^{-m} \right] && \text{if } a/c > 1 \end{aligned} \right\} \text{(eq. 200)}$$

The following plot (Figure133), represents how the crack shape changes during crack extension, considering for different initial shapes.

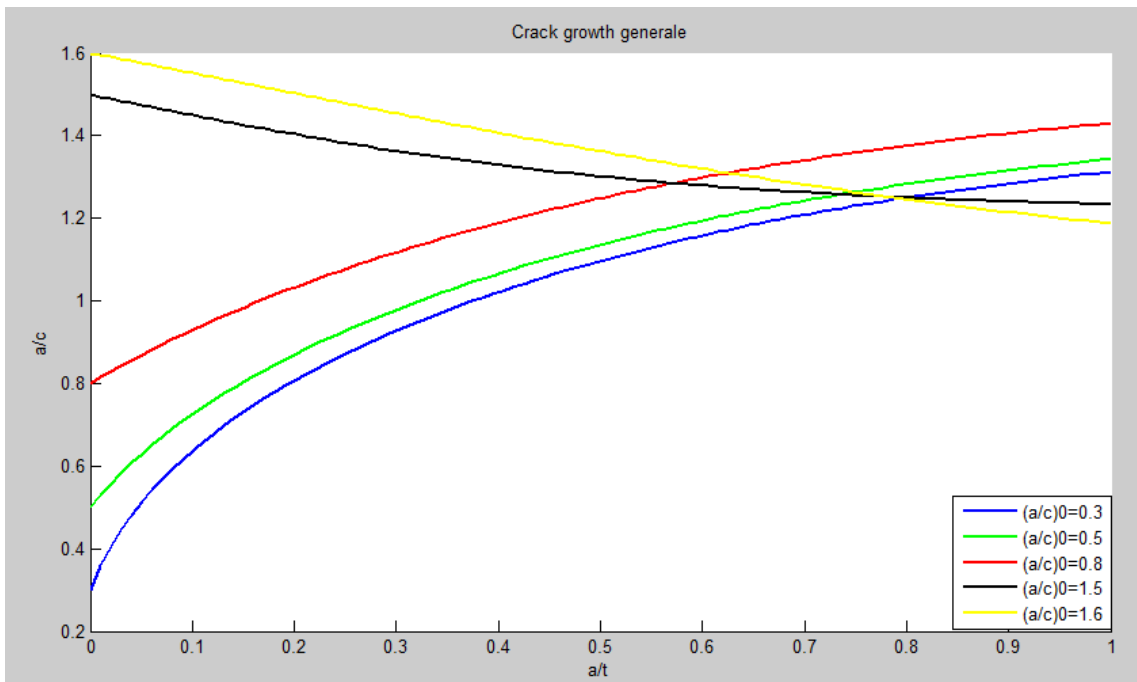


Figure 133: Part through crack shape variation during crack extension

The Matlab code used to get these results is reported below:

```

for caso=1:5
switch caso
case 1
ratio=1.5/5;
case 2
ratio=0.5;
case 3
ratio=0.8;
case 4
ratio=1.5;
case 5
ratio=1.6;
end
t=0.002;
depth=linspace(0,1);
m=3.353;
z=zeros(1,100);
for j=1:10
if ratio>1
da_dc=-(0.9*ratio.^0.5.*(1.1+0.35*depth.^2.*ratio)).^-m;
else
da_dc=(0.9*ratio.^0.5.*(1.1+0.35*depth.^2)).^-m;
end
for i=1:length(depth)
if i==1
z(i)=ratio(i);
else
z(i)=z(i-1)+da_dc(i)*(depth(i)-depth(i-1));
end
end
ratio=z;
end
figure(8)
hold on
plot(depth,ratio,col(caso),'linewidth',2)
xlabel('a/t')
ylabel('a/c')
title('Crack growth generale')
legend(' (a/c)0=0.3', '(a/c)0=0.5', '(a/c)0=0.8', '(a/c)0=1.5', '(a/c)0=1.6', 'location', 'best'
)
end

```

With all the consideration done up to now we are able to improve our current methodology where only the simpler through crack is considered. The following steps summarize the complete procedure that should be followed to improve results obtained and described in Chapter 6.

1. Let us consider a certain crack variation in the deep direction
2. Taking the shape model developed above let us insert the previous value of  $a$  and obtain the correspondent variation of  $c$
3. Use these new values inside the Irwin or the more complete Newman-Rojia model to get:
  - New  $\Delta K$
  - New  $K_{max}$ , i.e. the maximum stress intensity factor obtained when the load is at its maximum peak and crack has the geometry obtained at point 2
4. Let use this value to calculate  $da/dN$

5. Adding the obtained increment of  $a, c, N$  to their initial value we can start a new iteration.
6. This procedure will be stopped when a through crack is obtained ( $a = t$ )
7. Starting from this algorithm already developed for crack growth can be used again. The geometry factor  $\beta$  will be that already derived for embedded cracks.

This procedure can really improve achieved results providing a much more complete methodology. Of course it must be modified to take into account the more complex VA loading case. In addition, information on the initial crack shape ratio are needed

**5. Shortcomings of Paris Relation**

Considering plot in Figure representing the experimental behaviour between crack growth rate  $da/dN$  and stress intensity factor range  $\Delta K$ , Paris relation (eq.4) represents a good approximation only in the central region but it does not consider the asintotical behaviour in the others two regions. In addition, the simple Paris relation alone does not take into account R-ratio effect in crack growth rate. For both these reasons, as mentioned in Chapter 3 others relations have been developed. The most famous ones are:

- Walker relation:

$$\frac{da}{dN} = \frac{C \Delta K^m}{(1 - R)^{m(1-\lambda)}} \quad (eq. 201)$$

- Forman relation:

$$\frac{da}{dN} = \frac{C \Delta K^m}{(1 - R)(K_c - K_{max})} \quad (eq. 202)$$

- Priddle relation:

$$\frac{da}{dN} = C \left[ \frac{\Delta K - \Delta K_{th}}{\Delta K_c - \Delta K_{th}} \right]^m \quad (eq. 203)$$

- Nasgro relation:

$$\frac{da}{dN} = C \left[ \frac{1 - f}{1 - R} \Delta K \right]^m \frac{\left( 1 - \frac{\Delta K_{th}}{\Delta K} \right)^p}{\left( 1 - \frac{\Delta K_{max}}{\Delta K_c} \right)^q} \quad (eq. 204)$$

Where:

$$f = \begin{cases} \max(R, A_0 + A_1 R + A_2 R^2 + A_3 R^3) & \text{if } R \geq 0 \\ A_0 + A_1 R & \text{if } -2 \leq R < 0 \\ A_0 - 2A_1 & \text{if } R < -2 \end{cases}$$



And coefficients are:

$$A_0 = (0.825 - 0.34\alpha + 0.05\alpha^2) \left[ \cos\left(\frac{\pi}{2} \frac{S_{max}}{\sigma_0}\right) \right]^{1/4}$$

$$A_1 = (0.415 - 0.071\alpha) S_{max}/\sigma_0$$

$$A_2 = 1 - A_0 - A_1 - A_3$$

$$A_3 = 2A_0 + A_1 - 1$$

In particular the threshold value  $\Delta K_{th}$  has been calculated for the following comparison using relation:

$$\Delta K_{th} = \Delta K_0 \frac{\sqrt{\frac{a}{a+a_0}}}{\left(\frac{1-f}{(1-A_0)(1-R)}\right)^{1+C_{th}R}} \quad (eq. 205)$$

All these parameters introduced are empirically determined [17] and their value can be found on apposite handbook. A quick description of each of them is reported:

- $\alpha$ : plane stress constrain factor
- $\frac{S_{max}}{\sigma_0}$ : ratio between maximum stress applied and stress for plastic deformation
- $a_0$ : value of  $3.81 \cdot 10^{-5}m$  for both part through crack and through crack
- $C_{th}$ : Threshold value
- $K_{max}$ : maximum stress intensity factor of a certain cycle

Here in this Chapter just to get an idea about the different predicted crack growth rate for different  $\Delta K$  by each of these relation, a simple algorithm has been developed.

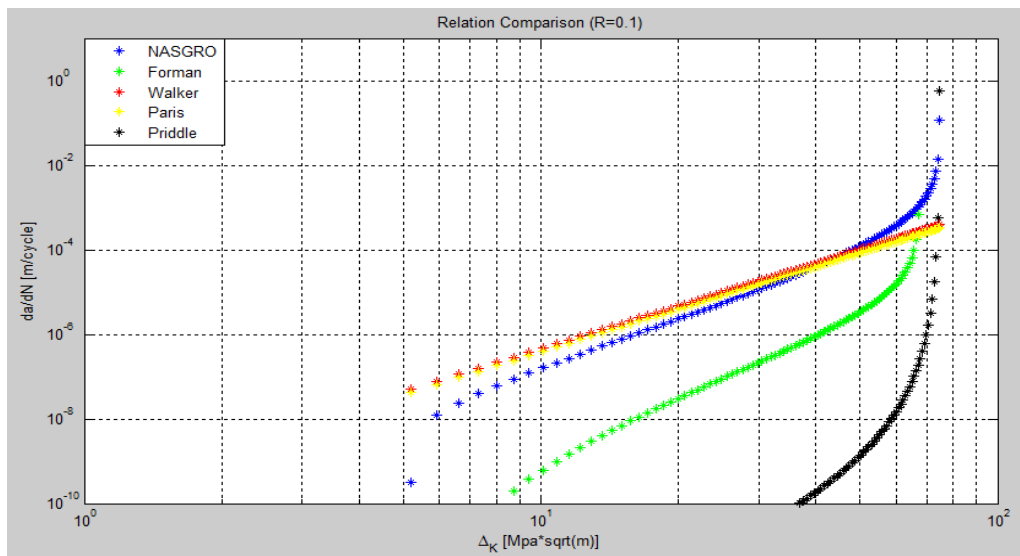


Figure 134: Different crack growth prediction model

The Matlab code used to get this visual result is reported here below. It makes use of the relation introduced above, considering material data provided by handbook and an R-ratio equal to 0.1 of a very simple constant amplitude load sequence.

```

K_crit=74.722;
A_k=1;
B_k=1;
C=1.7073e-10;
n=3.353;
p=0.5;
q=1;
delta_K_0=2.857;
C_th=1.5;
alpha=1.5;
S_max_sigma_0=0.3;
a=0.005;
a_0=0.0000381;
R=0.1;
K_max=linspace(7,K_crit-0.1);
A_0=(0.825-0.34*alpha+0.05*alpha^2)*(cos(pi/2*S_max_sigma_0))^1/alpha;
A_1=(0.415-0.071*alpha)*S_max_sigma_0;
A_3=2*A_0+A_1-1;
A_2=1-A_0-A_1-A_3;
lambda=0.5;
if R>=0
f=max(R, A_0+A_1*R+A_2*R^2+A_3*R^3);
elseif -2<=R<0
f=A_0+A_1*R;
else
f=A_0-2*A_1;
end
delta_K_th=delta_K_0*sqrt(a/(a+a_0))/(1-f/((1-A_0)*(1-R)))^(1+C_th*R);
delta_K=linspace(delta_K_th+0.001,K_crit-0.001);
da_dN_nasgro=C*((1-f)/(1-R))*delta_K.^n.*(1-delta_K_th./delta_K).^p./(1-
K_max/K_crit).^q;
figure(1)
R=0.1;
loglog(delta_K,da_dN_nasgro,'*b')
axis([1 100 10^(-10) 10])
xlabel('\Delta_K [Mpa*sqrt(m)]')
ylabel('da/dN [m/cycle]')
title('Relation Comparison (R=0.1)')
grid on
da_dN_forman=C*(delta_K-delta_K_th).^n./((1-R)*K_crit-delta_K);
hold on
loglog(delta_K,da_dN_forman,'*g')
da_dN_walker=C*delta_K.^n/(1-R)^(n*(1-lambda));
loglog(delta_K,da_dN_walker,'*r')
da_dN_paris=C*delta_K.^n;
loglog(delta_K,da_dN_paris,'*y')
da_dN_priddle=C*((delta_K-delta_K_th)./(K_crit-K_max)).^n;
loglog(delta_K,da_dN_priddle,'*k')
legend('NASGRO','Forman','Walker','Paris','Priddle')

```

6. Mixed mode behaviour

As seen the purpose of damage tolerance analysis is to ensure safety of the component scheduling inspections. As can be observed in Chapter 6, in doing this, accurate calculation of stress intensity factor and understanding of the fatigue crack behaviour are required. To get these results, as explained in the previous paragraph, Linear Elastic Fracture Mechanism (LEFM) concepts and relative equations represent a good solution. However, analysis performed with our methodology is limited to a simple loading case such as bending. Then the normal stress distribution is determined using the Trinomial of Navier. In practise however, engineering components or structures are often subjected to combine loading (tension, bending, torsion) which in turn causes mixed mode fracture (remembering mode introduced Mode I, II, III). Of course in these cases, calculation of stress intensity factor and evaluation of fatigue crack growth become more complex. Interesting research topics are available in literature, they should be considered to introduce these concepts in our model. In view of these observations and as already mentioned in the previous chapter, the assumption introduced of considering the wing with only one degree of freedom (Chapter 6) is a strong assumption. In fact, aircraft wing, that is the case of study of our work, is always subjected to some torsional moment producing shear stresses that must be taken into account in addition to the normal one.

Also in this case, just to introduce these concepts to future developer, a quick discussion can be carried out. First of all, stress intensity factor associated with the other opening mode should be considered. The following relations explain the main difference between each of them:

$$K_I = \sigma_{zz}\sqrt{\pi a} \quad (eq. 206)$$

$$K_{II} = \sigma_{zx}\sqrt{\pi a} \quad (eq. 207)$$

$$K_{III} = \sigma_{zy}\sqrt{\pi a} \quad (eq. 208)$$

Here the reference frame considered is one as that in Figure

Hence, as can be seen also from these relations, the only knowledge of normal stress  $\sigma_{zz}$  as derived above is not anymore enough. In fact at this point knowledge of the shear stress due to torsional moment are needed. They can be obtained for example using the so called *Bredt Theory*. Again, for the introduction purpose of this paragraph, concepts behind this theory are not here

introduced but just the main relation coming out is showed. However it has its basic concept in the equilibrium equation derived in Chapter 6. The fundamental relation coming out is:

$$\tau = \frac{M_t}{2\Omega t} \quad (eq.209)$$

Where  $M_t$  represents the torsion moment that must be estimated,  $\Omega$  represents the area under the isoline considered and  $t$  is the thickness of the portion where uniform tangential distribution are considered. However this equation cannot be applied directly to determine tangential stress distribution in a double T beam as that one considered. In fact, it is derived only for closed section while it is an open one. To overcome this inconvenient our section can be decomposed in three rectangular portions and the applied torsional moment will be absorbed by each of them. As a consequence the total torsional moment can be written as  $M_t = \sum_i M(i)_t$ . Then from consistent considerations the torsional moment acting on each of this portion can be calculated as:

$$M(i)_t = M_t \frac{I(i)_t}{\sum_i I(i)_t} \quad (eq.210)$$

Torsional moment so calculated can be used to determine shear stress in each portion of the beam with relation above (eq.199)

In general, torsion load will contribute to the  $K_{II}$  and  $K_{III}$  values. However, tension and torsion loads will interact producing a maximum principal stress that determines the crack path. In particular this interaction will contribute to the effective stress intensity factor (it should not be confused with that of eq.39) defined in [15] as:

$$K_{eff} = \sqrt{(K_I + |K_{II}|)^2 + 2K_{II}^2} \quad (eq.212)$$

Then comparing this value with that of  $K_I$ , the importance of torsional moment in crack growth propagation can be derived.

Introducing all the consideration done in this paragraph in the previously derived and described methodology could drastically improve achievable results.

**Comments on achieved results**

Now that our work has been explained and future possible needed improvements introduced, conclusions related with achieved results can be considered.

With the achieved results, our initial objectives have been successfully completed. In fact, as described through the chapters of this thesis, starting from a user defined airplane, using the developed flight dynamic simulator and all the algorithms in Chapter 6, useful results from load spectrum processing analysis cannot only be obtained but they can also be used for a complete damage tolerance analysis. In fact, remembering the main purposes of this type of analysis (Chapter 2) each of these can be successfully achieved following the previously described process. Even if, results shown, come out from a primitive methodology only, due to strong assumptions introduced, they cannot be considered as real values but at the same time they are the demonstration of how this defined way to proceed is correct. In particular, this developed methodology, once completed with concepts introduced in this last chapter, could be used in aeronautical field to design against fatigue typical critical components such as wing. In particular, wing spar has been our case of study but, however, this approach is not limited only at this type of application, but, in principle, it can be used for whatever other kind of critical components. In fact, while assumptions on load distributions, type of crack, material, type of inspectability, etc. must be redefined, the basic structure of the developed methodology remains always the same.

To conclude, this developed methodology open new scenarios in aeronautical field to design against fatigue, not only promising a cost reduction avoiding a large use of physical measurements but it also allows a much more specific analysis with respect what is actually done using standardized load sequences introduced in Chapter 4.

## References

1. *"The practical use of fracture mechanism"*, David Broek, Galena, OH, USA
2. *"Fatigue of structures and materials"*, Jaap Schijve, Delft University of Technology
3. *"Fatigue Crack Growth Prediction under Variable Amplitude Loading"*, S.U.Khan, J.Schjve, Delft University
4. *"The engineering analysis and design of the aircraft flight dynamics model"*, M.Peters, M.A.Konyac, October 2012
5. *"Fundamentals of Airplane Flight Mechanics"*, David G.Hull
6. *"Datcom plus User manual"*, Holy Cows, Orlando, September 2011
7. *"The USAF stability and control Datcom"*, McDonnell Douglas Astronautics Company, St. Louis Division
8. *"Airplane flight dynamics and automatic flight controls"*, Jan Roskam
9. *"Optimal control theory: An introduction"*, Donald E.Kirk, April 30, 2004
10. *"Performance Based Navigation Operational Approved Handbook"*, ICAO, August 2010
11. *"High accuracy four-dimensional trajectory prediction for civil aircraft"*, W. Shuster, M.Poretta, W. Ochieng, Centre for Transport studies, Imperial college of London Gauss
12. *"Gaussian Markov process"*, C.E. Rasmussen, Massachusetts Institute of Technology, 2006
13. *"Failure analysis and Fracture mechanism"*, David Broek
14. *"Commercial Airplane design principle"*, P.M. Sforza, University of Florida
15. *"Fatigue crack growth of a corner crack in a square prismatic bar under combined cyclic tension-cyclic torsion"*, Judha Purbolaksono, Ramesh Singh, International journal of fatigue, July 2014
16. *"Stress intensity factor equations for cracks in three dimensional bodies subjected to tension and bending loads"*, Newman J.C., Raju I.S., Langely Research Laboratory, 1984
17. *"User guide and technical manual"*, Air Force Research Laboratory, 2000